



**University of
Nottingham**

UK | CHINA | MALAYSIA

Glutamine Metabolism and DNA Repair in Breast Cancer

Thesis submitted to the University of Nottingham for the degree of Doctor of
Philosophy.

May 2025

Ali Abdulsalam Ali Fakroun

BSc, MSc.

School of Medicine
University of Nottingham

Abstract

Metabolic reprogramming and genomic instability are two key cancer hallmarks. The link between these two hallmarks in different types of cancer has yet to be fully explored. Cancer cells alter their metabolic pathways to meet their necessary energy and cellular block demands. They also modulate the expression of their DNA repair proteins to encounter the DNA damage caused by exogenous and endogenous factors, such as reactive oxygen species. This thesis investigates the association between glutamine metabolism and the DNA repair pathway in breast cancer, focusing on Solute Carrier Family 7 Member 5 (SLC7A5) and two DNA repair proteins, Flap endonuclease 1 (FEN1) and Exonuclease 1 (EXO1). These genes were selected based on their moderate positive correlation at the mRNA level, as identified through Breast Cancer Gene-Expression Miner v5.1 (bc-GenExMiner v5.1) dataset, and due to their established biological relevance in previous cancer studies. SLC7A5 functions as an amino acid exchanger, mediating the uptake of essential large neutral amino acids, particularly leucine, in exchange for intracellular glutamine. This activity supports glutamine-dependent mammalian target of rapamycin complex 1 (mTORC1) signalling, which fuels cell growth and biosynthesis. Meanwhile, FEN1 and EXO1 are structure-specific nucleases involved in distinct DNA repair pathways, base excision repair and mismatch repair, respectively, both play critical roles in preserving genomic stability under oxidative stress.

The biological and clinical outcome of SLC7A5 co-expression with either FEN1 or EXO1 was assessed in large, annotated cohorts of breast cancer at the mRNA and protein levels. In vitro, functional assay experiments were conducted to find the role of SLC7A5/FEN1 high expression in tumour behaviour, and further proteomic analysis was carried out to find common interacting proteins between the two pathways.

The high expression of SLC7A5 and either FEN1 or EXO1 at the mRNA and protein level was associated with poor prognosis, while the high expression of SLC7A5/FEN1 was linked to

adverse outcomes in ER-positive tumours, and the high expression of SLC7A5/EXO1 was associated with poor outcomes in ER-negative tumours. Assay experiments demonstrated that double knockdown of SLC7A5 and FEN1 impaired proliferation, reduced breast cancer cell migration and invasion ability, caused S phase cell cycle arrest, and induced apoptosis. Furthermore, the dual knockdown of SLC7A5 and FEN1 disrupted mitochondrial function, marked by reduced ATP production and respiratory capacity, reinforcing their role in maintaining metabolic fitness. Proteomic analysis identified shared interacting proteins enriched in pathways related to DNA repair, RNA metabolism, and mitochondrial function, supporting a functional link between these biological systems.

Collectively, this thesis explored a novel association between glutamine metabolism and DNA repair pathways in breast cancer. The findings position SLC7A5/FEN1 and SLC7A5/EXO1 high expression as clinically relevant prognostic biomarkers and lay the foundation for therapeutic strategies that co-target metabolic and DNA repair vulnerabilities in breast cancer.

Publications

1. The amino acid transporter SLC7A11 expression in breast cancer

Preyanka Nath, Lutfi H. Alfarsi, Rokaya El-Ansari, Brendah K. Masisi, Busra Erkan, **Ali Fakroun**, Ian O. Ellis, b, Emad A. Rakha, and Andrew R. Green

Cancer biology & therapy, 2023

2. Tripartite Motif-Containing 2, a Glutamine Metabolism-Associated Protein, Predicts Poor Patient Outcome in Triple-Negative Breast Cancer Treated with Chemotherapy

Brendah K. Masisi, Rokaya El Ansari, Lutfi Alfarsi, **Ali Fakroun**, Busra Erkan, Asmaa Ibrahim, Michael Toss, Ian O. Ellis, Emad A. Rakha and Andrew R. Green

Cancers, 2024

3. ATF4 as a Prognostic Marker and Modulator of Glutamine Metabolism in Oestrogen Receptor-Positive Breast Cancer

Roshni Patel, Lutfi H. Alfarsi, Rokaya El-Ansari, Brendah K. Masisi, Busra Erkan, **Ali Fakroun**, Ian O. Ellis, b Emad A. Rakha, b Andrew R. Green

Pathobiology: journal of immunopathology, molecular and cellular biology, 2024

4. Hydroxyacid Oxidase 1, a Glutamine Metabolism-Associated Protein, Predicts Poor Patient Outcomes in Luminal Breast Cancer

Busra Erkan, Skye MacIntyre, Charlotte Brown, **Ali Fakroun**, Ayat G. Lashen, Nigel P. Mongan, Ian O. Ellis, Emad A. Rakha and Andrew R. Green

International journal of molecular sciences, 2024

5. SLC1A5 is a key regulator of glutamine metabolism and a prognostic marker for aggressive luminal breast cancer.

Lutfi H. Alfarsi, Rokaya ElAnsari, Busra Erkan, **Ali Fakroun**, Madeleine L. Craze, Mohammed A. Aleskandarany, Kiu Wai Cheng, Ian O. Ellis, Emad A. Rakha & Andrew R. Green

Scientific Reports, 2025

Conference posters and presentations

Poster presentation

Glutamine Metabolism and DNA Repair in Breast Cancer.

Ali Fakroun, Rokaya Elansari, Srinivasan Madhusudan, Emad Rakha and Andy Green.

Pathological Society Conference, 27-29 June 2023, Liverpool, United Kingdom.

Oral presentation

Glutamine Metabolism and DNA Repair in Breast Cancer.

Ali Fakroun, Rokaya Elansari, Srinivasan Madhusudan, Emad Rakha and Andy Green.

Pathological Society Conference, 18-20 June 2024, Sheffield, United Kingdom.

Acknowledgements

First and foremost, I am deeply grateful to Almighty Allah for granting me the strength, patience, and perseverance to undertake and complete this research journey.

I would like to express my sincere appreciation to my supervisor, Dr Andy Green, for his exceptional guidance, support, and encouragement throughout the course of this project. His knowledge, insight, and patience have been invaluable, and I am truly thankful for the opportunity to conduct this research under his supervision.

I am also thankful to Prof Emad Rakha for his thoughtful input and valuable suggestions, which played a significant role in shaping the direction of this work.

My appreciation also goes to all the members of the Breast Pathology Research Group for their support, technical assistance, and helpful discussions along the way. Also, I would like to extend my thanks to all my lab mates in the BDI.

Finally, I would like to thank my mother for her prayers and unwavering support, as well as my father and my siblings for standing by me throughout this journey.

Abbreviations

BC	Breast Cancer
BCSS	Breast Cancer-Specific Survival
BER	Base Excision Repair
DMFS	Distant Metastasis Free Survival
EMT	Epithelial-to-Mesenchymal Transition
ER	Oestrogen Receptor
EXO1	Exonuclease 1
FEN1	Flap Endonuclease 1
GLS	Glutaminase
GLUD1	Glutamate Dehydrogenase 1
GSH	Glutathione
HER2	Human Epidermal Growth Factor Receptor 2
H-score	Histochemical Score
HR	Homologous Recombination
IHC	Immunohistochemistry
IDH1	Isocitrate Dehydrogenase 1
KM-plotter	Kaplan Meier-Plotter
MAPK	Mitogen-Activated Protein Kinase
METABRIC	Molecular Taxonomy of Breast Cancer International Consortium
MMR	Mismatch Repair
mTORC1	mammalian Target of Rapamycin Complex 1

NER	Nucleotide Excision Repair
NHEJ	Non-Homologous End-Joining
NPI	Nottingham Prognostic Index
PAM50	Prediction Analysis of Microarray 50
PBS	Phosphate Buffered Saline
PI3K	Phosphoinositide 3-Kinase
PPP	Pentose Phosphate Pathway
PR	Progesterone Receptor
PRPP	Phosphoribosyl-Pyrophosphate
R5P	Ribose-5-Phosphate
RFS	Recurrence Free Survival
ROS	Reactive Oxygen Species
siRNA	Small Interfering RNA
SLC7A5	Solute Carrier Family 7 Member 5
TBS	Tri-Buffered Saline
TCA	Tricarboxylic Acid Cycle
TMA	Tissue Microarray
TNBC	Triple Negative Breast Cancer
TP53	Tumour Protein p53
W.B	Western Blotting
2HG	2-Hydroxyglutarate

Table of Contents

Chapter 1 General Introduction	1
1.1 Cancer hallmarks	2
1.1.1 Sustaining proliferative signalling	2
1.1.2 Evading growth suppressors	2
1.1.3 Resisting cell death	3
1.1.4 Enabling replicative immortality	3
1.1.5 Inducing angiogenesis.....	4
1.1.6 Activating invasion and metastasis.....	4
1.1.7 Deregulating cellular energetics	5
1.1.8 Avoiding immune destruction.....	5
1.1.9 Genome instability and mutations	6
1.1.10 Tumour-Promoting Inflammation.....	6
1.2 Prognostic and Predictive Biomarker Factors in Breast Cancer	8
1.2.1 Tumour grade.....	9
1.2.2 Tumour size	9
1.2.3 Lymph node stage	10
1.2.4 Receptors.....	10
1.3 The nature and importance of ER, PR, and HER2 in breast cancer	11
1.4 Molecular subtypes of breast cancer.....	13
1.4.1 The Luminal Subtypes	13
1.4.2 HER2-enriched (Erb-B2) Subtype.....	14
1.4.3 Basal-like subtype.....	14
1.5 Glutamine metabolism in breast cancer	16
1.6 The origin of DNA damage in breast cancer	19
1.6.1 Endogenous sources.....	19
1.6.2 Exogenous sources.....	23
1.7 DNA replication.....	24
1.8 Nucleotide biosynthesis in breast cancer	27
1.8.1 Purine and pyrimidine de novo pathway	27
1.8.2 Purine and pyrimidine salvage pathway	28
1.8.3 Targeting Purine and Pyrimidine Synthesis Pathways	29
1.9 DNA repair mechanisms.....	31
1.9.1 Base excision repair	31
1.9.2 Mismatch repair	32

1.9.3 Nucleotide excision repair	32
1.9.4 DNA double-strand breaks repair	33
1.10 Upregulation of DNA repair in cancer: driving therapy resistance and tumour progression.....	33
1.11 The potential association between SLC7A5 and DNA repair in breast cancer	36
1.12 Hypothesis.....	39
1.13 Aims.....	39
Chapter 2 General materials and methods	40
2.1 Patient cohort	41
2.1.1 Molecular Taxonomy of Breast Cancer International Consortium (METABRIC) cohort	41
2.1.2 External cohort.....	42
2.1.3 Patients' protein expression cohorts	43
2.1.4 Patient's clinical outcome and events definition	45
2.2 Immunohistochemistry (IHC) and antibody optimisation	45
2.2.1 IHC staining	45
2.2.2 Evaluation of Staining.....	47
2.3 Cell lines	49
2.3.1 Thawing of cell lines.....	49
2.3.2 Passaging of cell lines	50
2.3.3 Cryopreservation of cell lines	50
2.3.4 Cell lysate.....	51
2.3.5 Protein quantification.....	53
2.4 Western blotting (WB).....	53
2.4.1 Sample preparation and gel electrophoresis	53
2.4.2 Transfer of proteins and staining	54
2.4.3 Detection Method.....	55
2.4.4 Western blotting using Enhanced Chemiluminescence (ECL).....	55
2.5 Transient knockdown.....	55
2.6 CellTitre 96 Aqueous One Solution Cell Proliferation Assay (MTS assay)	56
2.7 Cell count.....	57
2.8 Wound healing assay	57
2.9 Transwell invasion assay	58
2.10 Cell Cycle.....	59
2.11 Apoptosis	61
2.12 Cell Mito Stress assay.....	63
2.13 Co-Immunoprecipitation and mass spectrometry	64

2.14 Statistical Analysis.....	66
Chapter 3 The prognostic significant of SLC7A5/FEN1 high expression in breast cancer	67
3.1 Introduction.....	68
3.1.1 Hypothesis.....	70
3.1.2 Aims.....	70
3.2 Methods.....	71
3.2.1 SLC7A5 and FEN1 genomic and transcriptomic analysis in breast cancer	71
3.2.2 SLC7A5/FEN1 protein expression in breast cancer	71
3.2.3 Statistical analysis.....	72
3.3 Results.....	73
3.3.1 FEN1 expression in breast cancer.....	73
3.3.2 SLC7A5/FEN1 association with clinicopathological parameters in breast cancer	76
3.3.3 SLC7A5/FEN1 high expression association with breast cancer biomarkers.....	76
3.3.4 Prognostic value of high SLC7A5/ high FEN1 expression	79
3.4 Discussion.....	90
Chapter 4 Assessing the functional impact of SLC7A5 and FEN1 knockdown on breast cancer cell behaviour	93
4.1 Introduction.....	94
4.1.1 Hypothesis.....	95
4.1.2 Aims.....	95
4.2 Methods.....	96
4.2.1 FEN1 and SLC7A5 cell transfection with small interfering RNA (siRNA)	96
4.2.2 Cell proliferation and count	96
4.2.3 Wound healing assay and invasion assay	96
4.2.4 Cell Cycle and Apoptosis.....	97
4.2.5 Statistics	97
4.3 Results.....	98
4.3.1 The effect of FEN1 and SLC7A5 knockdown on breast cancer cell proliferation.	98
4.3.2 Effect of FEN1 and SLC7A5 knockdown on cell migration and invasion in breast cancer cells.....	105
4.3.3 Impact of FEN1 and SLC7A5 knockdown on cell cycle progression and apoptosis in BC cell lines.....	109
4.4 Discussion.....	116
Chapter 5 Functional interdependence of SLC7A5 and FEN1: Impact on mitochondrial function in breast cancer cells.....	120
5.1 Introduction.....	121
5.1.1 Hypothesis.....	122
5.1.2 Aims.....	122

5.2 Methods.....	123
5.2.1 Transient siRNA knockdown of SLC7A5 and FEN1.....	123
5.2.2 Western blotting.....	123
5.2.3 Metabolic Flux Analysis.....	123
5.2.4 Co-immunoprecipitation and mass spectrometry.....	123
5.2.5 Data analysis.....	124
5.2.6 Transcriptomic analysis of co-immunoprecipitant candidates in breast cancer cohorts.....	125
5.2.7 Statistical analysis.....	125
5.3 Results.....	126
5.3.1 Impact of FEN1 knockdown on SLC7A5 expression and reciprocal effects in breast cancer cell lines.....	126
5.3.2 Effect of FEN1 and SLC7A5 knockdown on mitochondrial function in breast cancer cell line.....	129
5.3.3 Impact of FEN1 and SLC7A5 knockdown on the metabolic phenotype of breast cancer cell line.....	133
5.3.4 Identification of common protein partners between SLC7A5 and FEN1 in MCF-7 and MDA-MB-436 breast cancer cell line.....	135
5.3.5 Cytidine triphosphate synthase 1 (CTPS1) and nucleoporin 205 (NUP205) correlate with SLC7A5 and FEN1 in MCF-7 and MDA-MB-436 cells.....	136
5.4 Discussion.....	146
Chapter 6 Exploring EXO1 as a prognostic marker and its significant association with SLC7A5 in breast cancer.....	152
6.1 Introduction.....	153
6.1.1 Hypothesis.....	154
6.1.2 Aims.....	154
6.2 Methods.....	155
6.2.1 SLC7A5 and mismatch DNA repair genomic and transcriptomic analysis in breast cancer.....	155
6.2.2 EXO1 protein expression in breast cancer.....	156
6.2.3 Western blot.....	156
6.2.4 Tissue array and Immunohistochemistry analysis.....	156
6.2.5 Statistical analysis.....	157
6.3 Results.....	158
6.3.1 EXO1 Expression in breast cancer.....	158
6.3.2 Association of EXO1 with clinicopathological parameters.....	164
6.3.3 Association of EXO1 with patient outcome.....	168
6.3.4 Association of SLC7A5/EXO1 with clinicopathological parameters.....	182
6.3.5 Association of SLC7A5/EXO1 with patient outcome.....	185

6.4 Discussion	197
Chapter 7 General discussion.....	200
7.1 Background	201
7.2 Main findings of the study	202
7.3 Final Conclusion	207
7.4 Limitations of the study	208
7.5 Future directions	209
References.....	210

Chapter 1 General Introduction

1.1 Cancer hallmarks

The hallmarks of cancer currently consist of ten distinct biological capabilities that allow tumour growth and progression [1]. These hallmarks highlight the complex mechanisms that enable tumour development and provide a framework for understanding them [1]. They include sustaining proliferative signalling, evading growth suppressors, resisting cell death, enabling replicative immortality, inducing angiogenesis, activating invasion and metastasis, deregulating cellular energetics, avoiding immune destruction, genome instability and tumour-promoting inflammation (Figure 1.1) [2]. In the context of breast cancer, these hallmarks manifest through specific molecular and cellular alterations that support the tumour initiation, progression and treatment resistance [2].

1.1.1 Sustaining proliferative signalling

Cancer cells maintain continuous proliferative signalling by evading growth suppressors and control signalling. In breast cancer cells, this is often driven by the overexpression of growth factor receptor pathways, such as receptor tyrosine kinases (RTKs), which play a key role in activating proliferative and survival signalling [2]. Another receptor is human epidermal growth factor receptor 2 (HER2). HER2 overexpression is linked to accelerated cell growth and proliferation through the activation of signalling pathways, such as Mitogen-activated protein kinase (MAPK) and Phosphatidylinositol 3-Kinase/Protein Kinase B (PI3K/AKT) pathways [2]. One common targeted therapy is trastuzumab, which inhibits HER2 signalling [3].

1.1.2 Evading growth suppressors

To maintain the high proliferation rate, cancer cells must evade programs that negatively regulate cell proliferation, which are controlled by tumour suppressors, particularly tumour protein p53 (TP53) and phosphatase and tensin homolog (PTEN) [4]. *TP53* is a gene that plays an important role in cell proliferation, DNA repair, metabolism and apoptosis [5]. *TP53* mutation is found in 25-30% of the highly aggressive subtype of triple-negative breast cancer (TNBC) [2]. *PTEN* is also a key gene that prevents cell division and prevents tumour growth.

The loss of *PTEN* promotes the PI3K/AKT pathway, which contributes to sustained proliferation signalling. *PTEN* mutations are detected in nearly 10% of breast cancer [6].

1.1.3 Resisting cell death

The ability to evade cell death is a hallmark of cancer, allowing tumour cells to overcome intrinsic mechanisms of self-destruction and maintain survival under oncogenic and therapeutic stress [1]. There are four main types of regulated cell death, including necroptosis, ferroptosis, pyroptosis and apoptosis [7]. Apoptosis is the most extensively studied type of programmed cell death [8]. Dysregulation of the apoptosis process allows tumour cells to resist immune surveillance, tolerate genotoxic stress, and accumulate mutations [9].

The B-cell lymphoma 2 (*BCL2*) protein family plays an important role in the regulation of mitochondrial-mediated apoptosis. This family composed of both pro-apoptotic proteins, such as BAX, BAK, BID, and anti-apoptotic proteins, including BCL-2, BCL-XL, and MCL-1, which interact to control mitochondrial outer membrane permeabilisation (MOMP) and cytochrome c release [8]. In breast cancer, the upregulation of anti-apoptotic protein BCL-2 is frequently observed in both oestrogen-positive (ER+) and ER- tumours, which correlates with poor prognosis [2].

1.1.4 Enabling replicative immortality

Cancer cells have the capability of unlimited proliferation due to the high expression of telomerase, an enzyme that maintains telomere length and prevents replicative senescence [10]. The telomerase reverse transcriptase (TERT) catalytic protein subunit is the core component of the enzyme telomerase, which facilitates continuous cell proliferation by extending the 3' end of the telomere, therefore preventing critical telomere shortening [10]. Telomerase activity is detectable in the majority of breast tumours, and its expression is associated with poor prognosis [11].

1.1.5 Inducing angiogenesis

Tumour cells need to satisfy their nutrient and oxygen demands and evacuate metabolic waste and carbon dioxide for continuous growth [2]. To achieve this, breast cancer cells upregulate pro-angiogenic factors, particularly vascular endothelial growth factors (VEGF), which promote angiogenesis [12]. The high expression of VEGF was associated with tumour aggressiveness and poor prognosis, specifically in HER-2 positive and TNBC subtypes [12].

1.1.6 Activating invasion and metastasis

The leading cause of mortality in breast cancer patients is the ability of tumour cells to invade surrounding tissues and spread from the primary organ to distant sites in the body [2]. This multistep process, known as the metastatic cascade, begins with the loss of epithelial characteristics and acquisition of mesenchymal traits, enhancing motility and invasiveness through a process known as epithelial-to-mesenchymal transition (EMT) [13].

During EMT, the downregulation of adhesion molecules such as E-cadherin, combined with the overexpression of matrix metalloproteinases (MMPs), enables cancer cells to degrade the extracellular matrix and penetrate surrounding tissues [14, 15]. These invasive cells can then enter nearby blood vessels or the lymphatic system in a process called intravasation [15].

Once in the circulation, tumour cells face various challenges, including shear stress and immune surveillance [16]. To evade destruction, they often travel in clusters or form aggregates with platelets and immune cells, enhancing survival [16].

Upon reaching a distant site, a subset of these circulating tumour cells (CTCs) extravasates through the vascular wall and invades the local stroma of secondary organs such as the bone, lung, liver, or brain [17].

To successfully establish secondary tumours, these disseminated cancer cells often undergo mesenchymal-to-epithelial transition (MET) to re-establish growth and proliferation in the new tissue microenvironment, contributing to disease progression, poor prognosis, and resistance to therapy [18].

1.1.7 Deregulating cellular energetics

Breast cancer cells alter their metabolism to fuel their aberrant proliferation. The Warburg effect, or aerobic glycolysis, is a characteristic found in breast cancer cells, as glycolysis is elevated in the presence of oxygen, which allows tumour cells to generate ATP rapidly and accumulate biosynthetic precursors, which are important to cancer development [19]. TNBC exhibit high glycolytic activity, contributing to its aggressive behaviour and poor prognosis [2].

Furthermore, cancer cells become addicted to glutamine to the point where they fail to proliferate in its absence [20]. Glutamine metabolism plays a key role in regulating redox balance, and it is essential in the biosynthesis of nucleotides, proteins and lipids [20]. Key cellular glutamine transporters, such as solute carrier family 1 member 5 (SLC1A5) and SLC7A5, are upregulated in breast cancer cells and associated with poor clinical outcomes [20].

1.1.8 Avoiding immune destruction

The immune system constantly checks cells and tissue for developing cancer cells and immature tumours that accidentally develop and eliminates them; however, some cancer cells can evade tumour surveillance [2].

In TNBC, high expression of programmed death-ligand 1 (PD-L1) on tumour cells enables immune evasion by binding to the PD-1 receptor on T cells [21]. This interaction transmits an inhibitory signal that suppresses T-cell activation, reducing their ability to proliferate, produce cytokines, and kill cancer cells. Consequently, the tumour evades immune-mediated destruction [21]. Moreover, elevated PD-L1 expression in TNBC has been associated with resistance to conventional therapies and poor clinical outcome [21].

1.1.9 Genome instability and mutations

The disruption of the DNA repair machinery and several components of genomic maintenance is one of the ways cancer cells increase their mutation rate, hence disrupting their genomic stability [22]. In breast cancer cells, the most common germline mutation is in Breast Cancer Susceptibility Genes 1 and 2 (*BRCA1* and *BRCA2*) [2]. Mutations in these genes result in homologous recombination deficiency, which leads to the accumulation of DNA double-strand breaks, promoting tumorigenesis [2]. Breast cancer arising from *BRCA1* mutations is most likely to be TNBC. Furthermore, breast cancer cells exhibit overexpression of several DNA repair genes, such as flap Endonuclease 1 (*FEN1*), exonuclease 1 (*EXO1*), centromere protein X (*CENPX*), FA Core Complex Associated Protein 24 (*FAAP24*), FA Complementation Group D2 (*FANCD2*), Fanconi anemia complementation group I (*FANCI*), Ubiquitin Conjugating Enzyme E2 T (*UBE2T*) and FA Complementation Group A (*FANCA*), that are associated with tumour progression and poor prognosis [23].

1.1.10 Tumour-Promoting Inflammation

Chronic inflammation plays an important role in breast cancer progression, as it provides the tumour microenvironment with pro-angiogenic factors, growth and survival factors [24]. Furthermore, tumour-associated macrophages (TAMs) are a major component of the tumour microenvironment, in particular, secrete proinflammatory cytokines, such as interleukin-6 (IL-6), tumour necrosis factor alpha (TNF α) and interleukin-1 beta (IL-1 β), that promote immune evasion, EMT and angiogenesis [25]. They are also associated with tumour progression and poor prognosis in breast cancer patients [25].

The hallmarks of cancer provide a comprehensive framework for understanding the biological processes involved in breast cancer initiation, progression and metastasis. Four additional hallmarks have been more recently proposed, including senescent cells, polymorphic microbiomes, unlocking phenotypic plasticity and nonmutational epigenetic reprogramming (Figure 1.1) [1]. The understanding of the interplay between the tumour heterogeneity and

these hallmarks will result in the development of better therapeutic approaches and improve patient outcomes.

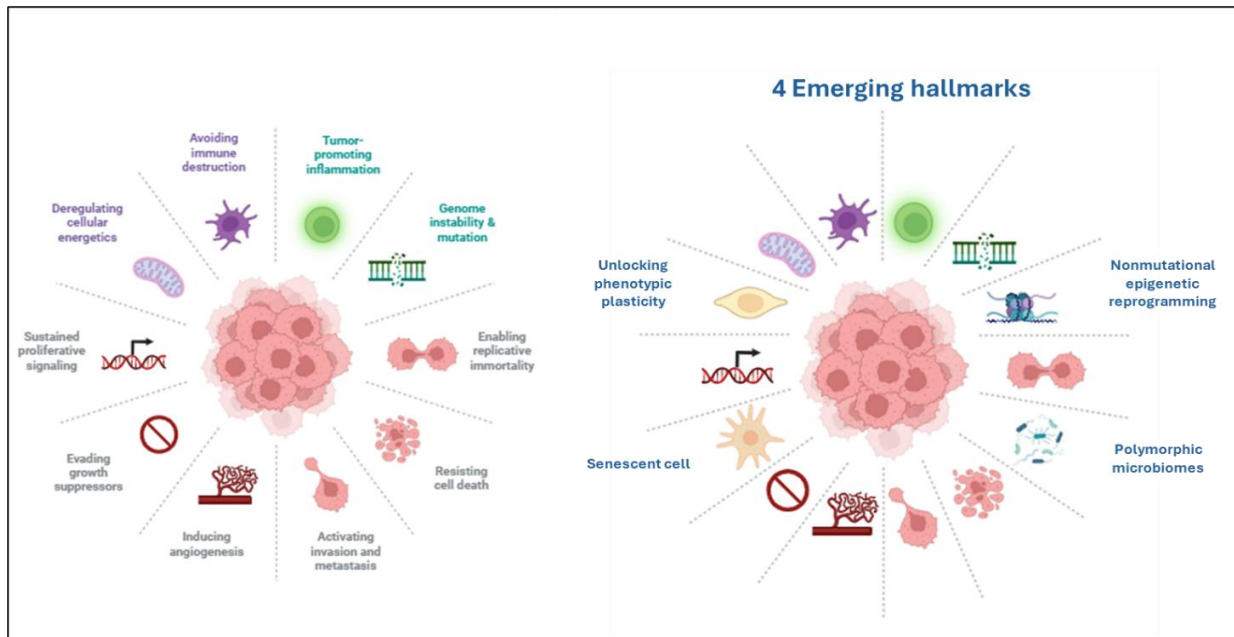


Figure 1.1. The hallmarks of cancer include the ten previously established characteristics and the four proposed hallmarks. These hallmarks collectively contribute to cancer initiation, progression and the transformation to malignancy (adapted from Hanahan et al, 2022). Figure created using BioRender.

1.2 Prognostic and Predictive Biomarker Factors in Breast Cancer

Prognostic factors are indicators that provide information about a patient's overall cancer outcome, regardless of treatment. They reflect the natural course of the disease and help in estimating the risk of survival or recurrence without considering treatment interventions [26].

Traditional prognostic factors in breast cancer include tumour size, histological grade, lymph node involvement, and patient age. Molecular biomarkers such as oestrogen receptor (ER), progesterone receptor (PR), HER2, and triple-negative (TN) status are also widely recognised as prognostic indicators [27, 28]. Understanding how these factors interact is important for assessing disease aggressiveness and patient outcomes [29].

In contrast, predictive biomarkers are used to predict patients' response to specific treatments. These biomarkers guide therapeutic decisions by identifying patients who are more likely to respond or not respond to targeted therapies [30]. For example, ER and PR positivity predict responsiveness to endocrine therapy, while HER2 amplification predicts benefit from HER2-targeted therapies, such as trastuzumab [31]. Predictive markers are thus critical for optimising treatment selection and minimising unnecessary toxicity, allowing more personalised and effective cancer management [31].

Importantly, some biomarkers serve dual roles. For example, ER and HER2 can both function as prognostic and predictive markers [32], depending on the clinical context and treatment approaches. Stratifying breast cancer patients based on these markers is essential not only for prognosis but also to ensure an appropriate therapeutic approach [32].

1.2.1 Tumour grade

Tumour grade serves as a crucial prognostic indicator in breast cancer, as it evaluates the degree of differentiation of breast cancer cells in comparison to normal breast cells, reflecting the biological aggressiveness of the tumour. The Nottingham grading system of breast cancer involves the evaluation of three distinct components: tubule formation, nuclear pleomorphism, and mitotic count [33, 34]. The first in the system is tubule formation which indicates to the extent of glandular structure within the tumour and is scored as follows, score 1 given when the gland formation is found in more than 75% of the tumour area, score 2 for 10-75%, and score 3 for tumours with less than 10% tubular formation [33, 34]. The second in the system is nuclear pleomorphism, which evaluates the shape, size and uniformity of the nucleus in the tumour cell, score 1 represents small and regular nuclei, score 2 indicates a moderate increase in size and variability, while score 3 reflects marked variability. The final component of the system is mitotic count, which measures the number of mitoses in a given area of the tumour using high-power microscopy. Importantly, the threshold for scoring mitotic count depends on the microscope's field diameter, making it lens-dependent. Therefore, mitotic figures are typically assessed per 10 high-power fields (HPFs), with scoring criteria adjusted according to the specific field area. The three components of the system are summed and assigned to an overall tumour grade. Grade 1 tumour represents well well-differentiated tumour and is associated with a good prognosis (total score 3-5). Grade 2 tumours indicate moderately differentiated tumours and are associated with an intermediate prognosis (total score 6-7). Grade 3 tumours show poorly differentiated tumours and are associated with poor prognosis (total score 8-9) [33, 34].

1.2.2 Tumour size

Tumour size is a critical prognostic indicator, as patients with larger tumours show a higher risk of metastasis, recurrence and poor patient outcomes, while patients with smaller lesions show a lower risk of metastasis and recurrence; also, smaller tumour size is associated with better patient outcomes [35].

1.2.3 Lymph node stage

Lymph node status is considered a critical prognostic factor in breast cancer; for example, the axillary lymph nodes (LN) are often the first site where breast cancer spreads, so the absence and the presence of LN are significant indicators for early-stage breast cancer patients [36].

Generally, breast cancer patients with lower LN stage have a more favourable prognosis, in comparison to patients with higher LN stage. Furthermore, the number of involved lymph nodes is associated with poor prognosis [37]. The LN stage system consists of three different categories: LN stage 1 indicates no LN involved; LN stage 2 represents 1-3 LNs are involved; finally, LN stage 3 indicates more than 3 LNs are involved [38].

1.2.4 Receptors

ER, PR and HER2 are routinely assessed by immunohistochemistry (IHC) on paraffin-embedded sections in all breast cancer patients [39]. The recommended cutoff for positive ER and PR expression in invasive breast cancer is 1% [40], while HER2 positivity is defined as an IHC score of 3+, if HER2 expression results were equivocal (IHC score 2+), then HER2 gene amplification is confirmed using Fluorescence in situ hybridisation (FISH) assay [40]. TNBC is defined by the absence of ER, PR, and HER2 expression [41], and is assessed by using IHC, where ER and PR expression are considered negative when it is <1%, while HER2 is determined negative if the IHC score is 0 or 1+, if HER2 IHC is 2+, FISH is used to confirm its status [40, 42].

1.3 The nature and importance of ER, PR, and HER2 in breast cancer

ER, PR, and HER2 are pivotal molecular biomarkers that are used for the classification, prognosis, and therapeutic stratification of breast cancer [43]. ER and PR are members of the nuclear hormone receptor family, and function as ligand-activated transcription factors [44, 45]. Upon binding to their respective ligands, oestrogen or progesterone, these receptors translocate to the nucleus, and bind to specific DNA sequences and regulate the transcriptional activity of the targeted genes, including oestrogen receptor 1 (*Esr1*), oestrogen receptor 2 (*Esr2*), and Progesterone Receptor (*PGR*), which encode the oestrogen and progesterone receptors, respectively [44, 45]. These transcriptional events control the expression of genes involved in key cellular processes such as proliferation, differentiation, and survival. While these pathways are essential for maintaining normal breast tissue homeostasis, their dysregulation in cancer leads to uncontrolled cellular growth and tumour development [46].

HER2, encoded by the erythroblastic oncogene 2 (*ERBB2*) gene, is a transmembrane receptor tyrosine kinase and a member of the ERBB family. Under normal physiological conditions, HER2 plays a role in regulating cell growth, survival, and repair in mammary epithelial cells [47]. Unlike hormone receptors, HER2 does not require a ligand to initiate signalling; instead, it initiates signalling through a process called dimerisation. In breast cancer, the *ERBB2* gene becomes amplified, resulting in the overproduction of HER2 protein on the cell surface [48]. This gene amplification and subsequent receptor overexpression lead to aberrant activation of downstream signalling pathways, independent of ligand binding [48]. This persistent activation stimulates oncogenic pathways, particularly the PI3K/AKT and MAPK cascades, which are involved in promoting oncogenic processes such as uncontrolled cell proliferation, enhanced survival, angiogenesis, and increased metastatic potential [49].

Clinically, the expression of ER, PR, and HER2 is essential for breast cancer classification and directly influences therapeutic choices. Tumours expressing ER and/or PR are typically hormone-positive and are highly responsive to endocrine therapies [50]. These treatments

include selective oestrogen receptor modulators such as tamoxifen, which competitively inhibits oestrogen from binding to its receptor, and aromatase inhibitors such as anastrozole, which works by blocking an enzyme called aromatase, stopping the conversion of androgens to oestrogen in postmenopausal women, therefore, inhibiting tumour cell proliferation and reducing the risk of recurrence [51, 52].

HER2-positive tumours, while biologically aggressive, are highly amenable to targeted therapies [53]. Trastuzumab, also called Herceptin, is a monoclonal antibody that binds to the extracellular domain of the HER2 receptor, which prevents it from dimerising and triggering signalling pathways that promote tumour progression. Additional HER2-targeted agents, for example, the antibody-drug conjugate trastuzumab emtansine (T-DM1), Pertuzumab, and small molecule tyrosine kinase inhibitors such as neratinib and lapatinib [53]. These treatments work to improve the patient outcome and are used in various settings depending on the tumour stage [54, 55]. In the case of triple-positive tumours, a combined treatment approach is taken, by using both endocrine and HER2-targeted therapies, which showed promising results in terms of patient outcome and managing tumour progression [56]. Conversely, tumours lacking expression of ER, PR, and HER2, known as TNBC, do not benefit from endocrine therapy or HER2-targeted agents, which makes cytotoxic chemotherapies the main therapeutic approach available [57]. Standard chemotherapeutic agents include platinum agents, anthracyclines and taxanes, which induce cell death by disrupting DNA synthesis [57]. Emerging therapeutic approaches, including immunotherapies and targeted therapies, have been introduced specifically for TNBC. Immune checkpoint inhibitors, such as pembrolizumab and atezolizumab, which work by blocking the PD-L1/PD-1 axis, restore T-cell activation and tumour immune surveillance [58]. Additionally, PARP inhibitors such as talazoparib and Olaparib exploit defects in homologous recombination DNA repair pathways, specifically in TNBC with BRCA1/2 mutation, resulting in synthetic lethality and selective tumour cell death [59, 60].

1.4 Molecular subtypes of breast cancer

Based on gene expression patterns, BC can be classified into four main molecular subtypes: luminal-like tumours (including luminal-A and luminal-B), HER2 enriched tumours and basal-like [61-64](Table. 1.1). These subtypes were initially defined using a 50-gene molecular classifier known as prediction analysis of microarray 50 (PAM50), which enables accurate distinction between the subtypes without compromising diagnostic precision [65].

1.4.1 The Luminal Subtypes

The most common type of BC is the luminal subtype, as it represents 60% to 70% of all tumours. The name luminal is derived from the similarity between genes that are expressed by these tumours and those expressed by the epithelial cells that line the lumen of the terminal duct lobular unit (TDLU) [61]. The distinguishing feature of this subtype is the high expression of the ER. In addition to high ER expression, the majority of luminal tumours express PR and different genes that are linked to ER function such as solute carrier family 39 zinc transporter member 6 (*SLC39A6*), X-box binding protein 1 (*XBP1*), GATA binding protein 3 (*GATA3*) and B cell lymphoma 2 (*BCL2*) [66]. The luminal subtype is divided into two different subgroups, luminal A and luminal B. Luminal A subtype is more frequent than luminal B, as it represents almost 40% of all breast cancers, while luminal B comprises roughly 20% (Table. 1.1) [61].

Luminal B tumours have lower expression of PR and higher expression of cell cycle and proliferative genes compared to luminal A tumours. Moreover, proliferating cell nuclear antigen (PCNA) and Ki-67, which are immunohistochemical markers of cell proliferation, are expressed at high levels in luminal B compared to luminal A subtype. The high frequency of p53 mutations is linked to luminal B but not luminal A tumours [61]. However, luminal A subtypes have a high level of ER and PR expression in comparison to luminal B subtypes [65]. Morphologically, luminal B tumours are less well-differentiated, while luminal A tumours are well-differentiated [61]. Patients who are diagnosed with luminal A tumours have significantly better disease-free survival (DFS) and overall survival (OS) in comparison to patients with

luminal B subtype [61]. Therefore, the luminal A subtype has a better prognosis, and generally, they respond well to hormone/endocrine therapy [65]. There is a subset of the luminal B subtype that expresses high levels of HER2, due to its gene amplification. This subset confers a worse overall outcome than luminal B tumours that do not express HER2 [65].

1.4.2 HER2-enriched (Erb-B2) Subtype

HER2, which is known as HER2/neu and Erb-B2, accounts for around 12% to 20% of all breast cancer (Table 1.1) [61]. HER2 is an oncogenic tyrosine kinase receptor, which in turn activates oncogenic pathways related to increased angiogenesis, proliferation, and invasiveness [67]. HER2-enriched tumours generally exhibit low levels of ER and high levels of HER2 expression [65]. Interestingly, HER2-enriched subtypes are not distinguished by *Ki-67* expression, as all tend to exhibit high proliferative activity. However, these tumours have a worse prognosis in comparison to luminal subtypes, and they are associated with shortened OS and DFS, which indicates the high impact of the oncogene HER2 [61].

1.4.3 Basal-like subtype

Basal-like breast cancer (BLBC) represents around 15% of all invasive breast cancer (Table 1.1) [61]. This subtype fails to express hormone receptors (HRs) and HER2 genes, and they frequently show a mutation in the p53 [65]. At the time of diagnosis, these tumours are characterised by high grade, large tumour size and a high rate of recurrence locally and distantly. BLBCs account for 70% to 80% of TNBC. Based on gene expression profiling (GEP), the other 20% to 30% of TNBC is categorised into at least six subgroups, for example, mesenchymal stem-like, immunomodulatory, luminal androgen, basal-like 1 and basal-like 2 subtypes [61]. Basal-like TNBC is associated with poor prognosis and is considered the most aggressive subtype of breast cancer [64].

Table 1.1. Summary of the intrinsic molecular subtypes of breast cancer and their immunohistochemistry (IHC) status.

Intrinsic Subtype	IHC status	Outcome	Prevalence
Luminal A	[ER+] [PR+] [HER2-] [Ki67-]	Good	40%
Luminal B	[ER+] [PR+/-] [HER2-/+] [Ki67+]	Intermediate/Poor	20%
Her2-enriched	[ER-] [PR-] [HER2+] [Ki67-]	Poor	12%-20%
Basal-like	[ER-] [PR-] [HER2-]	Poor	15%

1.5 Glutamine metabolism in breast cancer

Glutamine is a water-soluble amino acid that plays an important role in protein synthesis in mammalian cells, however, its biological function is far beyond protein synthesis, where its carbon skeleton is incorporated into fatty acids and glucose, while its nitrogen is used in the biosynthesis of non-essential amino acids and nucleotides [68]. Fourteen amino acid solute carriers have been identified to accept glutamine as a substrate. Nevertheless, none are solely selective for glutamine or associated with its influx. These transporters belong to four different gene families: The solute carrier family 1 (SLC1), SLC6, SLC7 and SLC38 [68].

Breast cancer cells can become addicted to glutamine, and the lack of its availability can lead to failure in growth and proliferation [69]. Alterations in glutamine metabolism in breast cancer are controlled by the activation of oncogenes, such as *MYC*, which regulates the expression of SLC7A5 [70]. It also inhibits the expression of miR23a/b, which is responsible for repressing the expression of glutaminase (*GLS*), subsequently increasing the expression of *GLS* [69]. Furthermore, *MYC*-driven ER-negative tumours show 2-hydroxyglutarate (2-HG) and *GLS* overexpression [69]. The loss of tumour suppressors is also responsible for the alteration in glutamine metabolism; one example is retinoblastoma (*Rb*), which is involved in the regulation of SLC1A5 expression [70].

Glutamine is first transported into cells through plasma membrane solute carriers, mainly via SLC1A5, where it can be used for the biosynthesis of nucleotides, as glutamine is an important source for nitrogen (Figure 1.2) [71]. Next, cytosolic glutamine is transported by mitochondrial-bound solute carriers through the inner mitochondrial membrane, where it is converted into glutamate via *GLS* (Figure. 1.2) [71]. Glutamate is a precursor for glutathione (GSH), which is used by cells to maintain their redox balance and reinforce the antioxidant response (Figure. 1.2) [19].

Alternatively, glutamate replenishes the mitochondrial tricarboxylic acid cycle (TCA) via its conversion into alpha-ketoglutarate (α -KG), which occurs with the aid of glutamate dehydrogenase 1 (GLUD1) (Figure 1.2) [69]. Under stress conditions, such as hypoxia, α -KG undergoes reductive carboxylation, which helps in the synthesis of citrate and fatty acids. Furthermore, α -KG is an important cofactor for enzymes that take part in the epigenetic modification process [71]. Tumour cells that harbour mutations in isocitrate dehydrogenase 1 (*IDH1*) or *IDH2*, for example, cholangiocarcinoma and glioma, show oncogenic activity by expressing high levels of 2-HG, which is the result of glutamine-derived α -KG conversion. 2-HG competitively inhibits DNA modifications and α -K-dependent histone enzymes [69]. Another function of glutamine is facilitating the import of essential amino acids, such as leucine, which is transported into the cancer cell via SLC7A5 in exchange for glutamine (Figure. 1.2). Leucine is considered as the rate-determining step that maintains the activation of mammalian target of rapamycin complex 1 (mTORC1), which then regulates protein translation and prevents apoptosis in cancer cells (Figure. 1.2) [70].

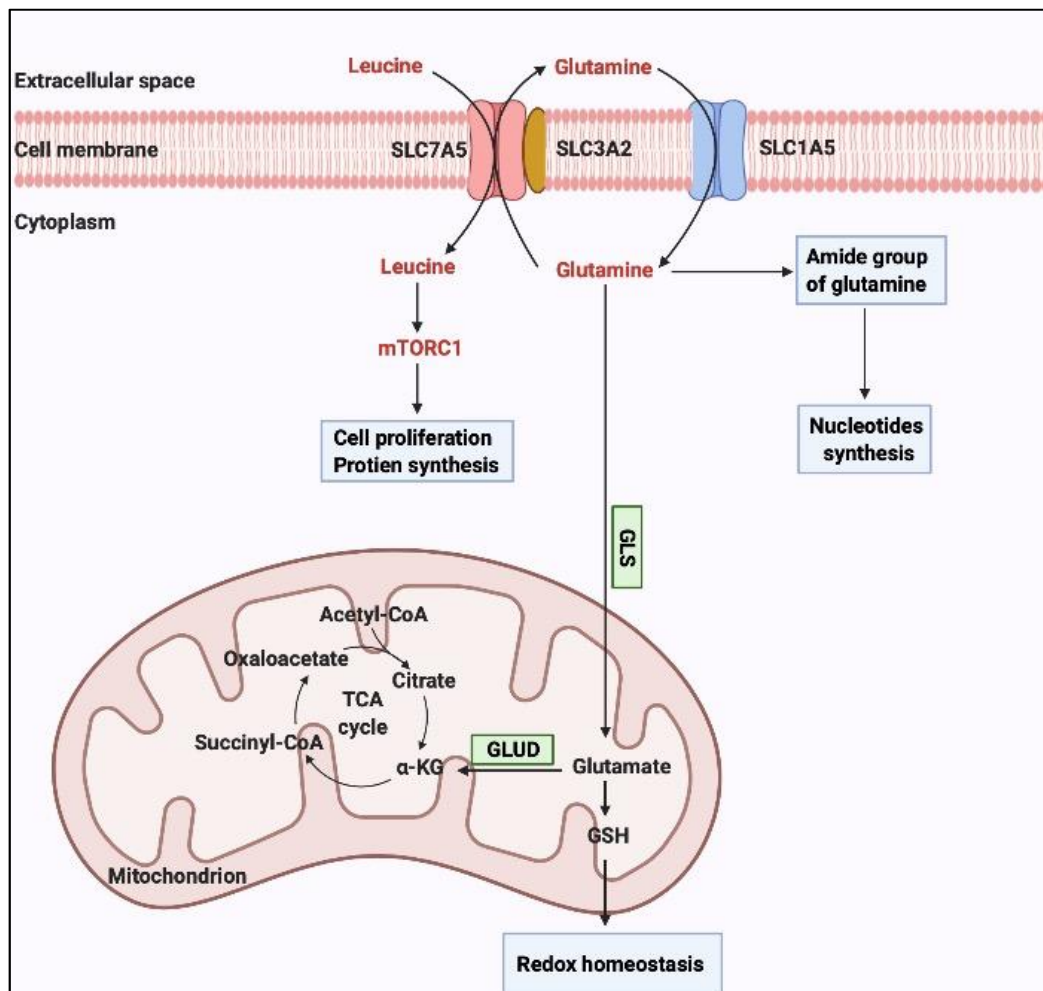


Figure 1.2. Glutamine metabolism in tumour cells. Glutamine is transported into tumour cells by solute carrier family 1 member 5 (SLC1A5), where it provides the nitrogen base for nucleotide biosynthesis. Cytosolic glutamine is transported into mitochondria via glutaminase (GLS), which converts glutamine into glutamate. This helps tumour cells in maintaining their redox homeostasis, as a result of the production of glutathione (GSH) with the help of glutamate. Alternatively, glutamate dehydrogenase 1 (GLUD1) catalyses the conversion of glutamate into alpha-ketoglutarate (α -KG), which is a part of the tricarboxylic acid cycle (TCA). SLC7A5, with the aid of SLC3A2, import leucine into the tumour cells in exchange for intracellular glutamine. Leucine activates mammalian target of rapamycin complex 1 (mTORC1), which plays a role in cell proliferation and protein synthesis. Figure created using BioRender.

1.6 The origin of DNA damage in breast cancer

Breast cancer is caused by the accumulation of genetic mutations that disrupt the function of normal cells [72]. DNA damage is the key driver of these mutations, which affect the genome integrity and enhance tumourigenesis [72]. The origin of DNA damage in breast cancer is linked to both endogenous and exogenous sources, which cause epigenetic modifications and mutations leading to genomic instability [73], one of the cancer hallmarks [1]. The sources of endogenous DNA damage mainly result from intrinsic cellular processes, including spontaneous replication stress, hydrolytic reactions and oxidative metabolism [74]. During the process of DNA replication single strand breaks (SSBs) and double-strand breaks (DSBs) are generated due to polymerase errors, replication fork stalling and collision with transcription machinery [74].

Oxidative stress is a key driver for the progression of breast cancer, and it is defined as the imbalance between the production of antioxidant defence mechanisms and the generation of reactive oxygen species (ROS), which includes hydrogen peroxide (H_2O_2), hydroxyl radical ($\text{HO}\cdot$) and superoxide anion (O_2^-), are generated by the partial reduction of oxygen [75]. The high levels of ROS are responsible for lipid peroxidation, protein oxidation and DNA damage, leading to genomic instability [76]. Breast cancer subtypes, particularly HER2-positive and TNBC, show high levels of oxidative stress, as a result of endogenous and exogenous factors. Endogenous sources, such as mitochondrial dysfunction and oestrogen metabolism, while exogenous sources include environmental pollutants and lifestyle factors [77].

1.6.1 Endogenous sources

Mitochondria play a key role in the redox balance, cellular energy metabolism and apoptosis regulation. The activity of mitochondria is the main source of ROS, particularly H_2O_2 and O_2^- , furthermore, the production of mitochondrial ROS in normal cells is regulated by the antioxidant defence system, such as catalase (CAT), glutathione peroxidase (GSH) and superoxide dismutase (SOD) [78]. Nevertheless, in breast cancer cells, impaired

mitochondrial function leads to high levels of ROS generation, which contributes to metabolic reprogramming, genomic instability and tumour progression [79].

The dysfunction of the electron transport chain (ETC) in mitochondria is one of the causes of ROS overexpression. ETC is in the inner membrane of mitochondria, and consists of four protein complexes (I-IV) and ATP synthase (Complex V) [78]. In normal cells, electrons Flavin adenine dinucleotide (FADH₂) and Nicotinamide-adenine dinucleotide (NADH) deliver electrons, that pass through ETC, causing the synthesis of ATP via oxidative phosphorylation [78], however, in breast cancer cells, this function is impaired, as it is common for breast tumours to have a dysfunctional complex I, which cause the electrons to leak prematurely, reacting with oxygen and forming O₂⁻, hence elevating the levels of oxidative stress [80]. Mitochondrial DNA (mtDNA) is very susceptible to oxidative damage as it lacks protective histones. Damaged mtDNA caused by ROS further impairs the function of ETC, which creates a vicious cycle of high ROS generation, leading to impaired OXPHOS and ATP depletion [79]. Mutations in mtDNA are common in breast cancer, a previous study identified mutations in cytochrome c oxidase (COX) genes and deletions in NADH dehydrogenase, which cause the increase in genomic instability by promoting nuclear DNA damage as a result of ROS generation, and enhances tumour survival by modulating metabolism and shifting it towards glycolysis [81]. Moreover, breast cancers with BRCA1 and BRCA2 deficiency exhibit high levels of mtDNA mutations, which indicates the association between mitochondrial dysfunction and DNA repair [82].

Oestrogen metabolism is one of the main inducers of oxidative stress, while oestrogen is important for the development of normal breast tissue, its metabolic byproducts promote the production of ROS, which leads to DNA damage and metabolic instability [83]. Oestrogen metabolism is a complex process that involves the interplay of phase I and phase II enzymatic reactions, which are mostly catalysed by cytochrome P450 enzymes (CYP), including CYP3A4, CYP1A1/2 and CYP1B1. In the first phase of metabolism, oestrone (E1) is reduced to oestradiol (E2) via the enzyme 17 β -hydroxysteroid dehydrogenase type 1 (17 β -HSD1),

while 17β -HSD2 catalyses the reverse reaction of E2 to E1 [84]. E2 then undergoes hydroxylation at positions C2, C4 and C16, to produce three primary metabolites, including 2-hydroxyestradiol (2-OHE2), 4-hydroxyestradiol (4-OHE2), 16-alpha-hydroxyestradiol (16 α -OHE2) (Figure 1.3) [84]. Both of 4-OHE2 and 16 α -OHE1 exhibit oncogenic potential. For instance, 4-OHE2 undergoes redox cycling, which results in the production of hydroxyl radicals (OH), H₂O₂ and O₂⁻ increasing the oxidative stress [84]. These ROS lead to the formation of 8-Oxo-2'-deoxyguanosine (8-oxo-dG), which causes oxidative DNA damage, hence promoting the genomic instability of the cell [85]. 16 α -OHE2 exhibits a strong oestrogenic activity, unlike 2-OHE2, which represents a weak oestrogenic activity. 16 α -OHE2 has a similar property to E2 as it binds to the oestrogen receptor, and keeps a sustained ER activation, enhancing cell proliferation, it is also known as estriol (E3). Furthermore, 16 α -OHE2 interfere with DNA replication via forming stable DNA adducts, which increases the mutation rate and cause genomic instability [86]. It was indicated that high levels of 16 α -OHE2 was associated with the increased risk of breast cancer, especially in postmenopausal women [86].

Phase II represents the elimination of oestrogen and prevents the accumulation of oestrogenic and genotoxic metabolites that contribute to the development of breast cancer [84]. The main enzymes that are involved in the second phase are sulfotransferase (SULT), catechol-O-methyltransferase (COMT) and glucuronosyltransferases (UGTs), these enzymes facilitate the excretion and detoxification of oestrogen metabolites, as they convert 2-OHE2, 4-OHE2 and 16 α -OHE2 into sulphated, methylated and glucuronidated forms (Figure 1.3) [87]. The impaired function of phase II metabolism leads to the accumulation of toxic metabolites that increase oxidative stress, hence elevating DNA damage [84]. For example, the alteration in the expression or the function of SULTs [88, 89] and UGTs disrupts the oestrogen homeostasis, hence promoting tumour progression in breast cancer [90].

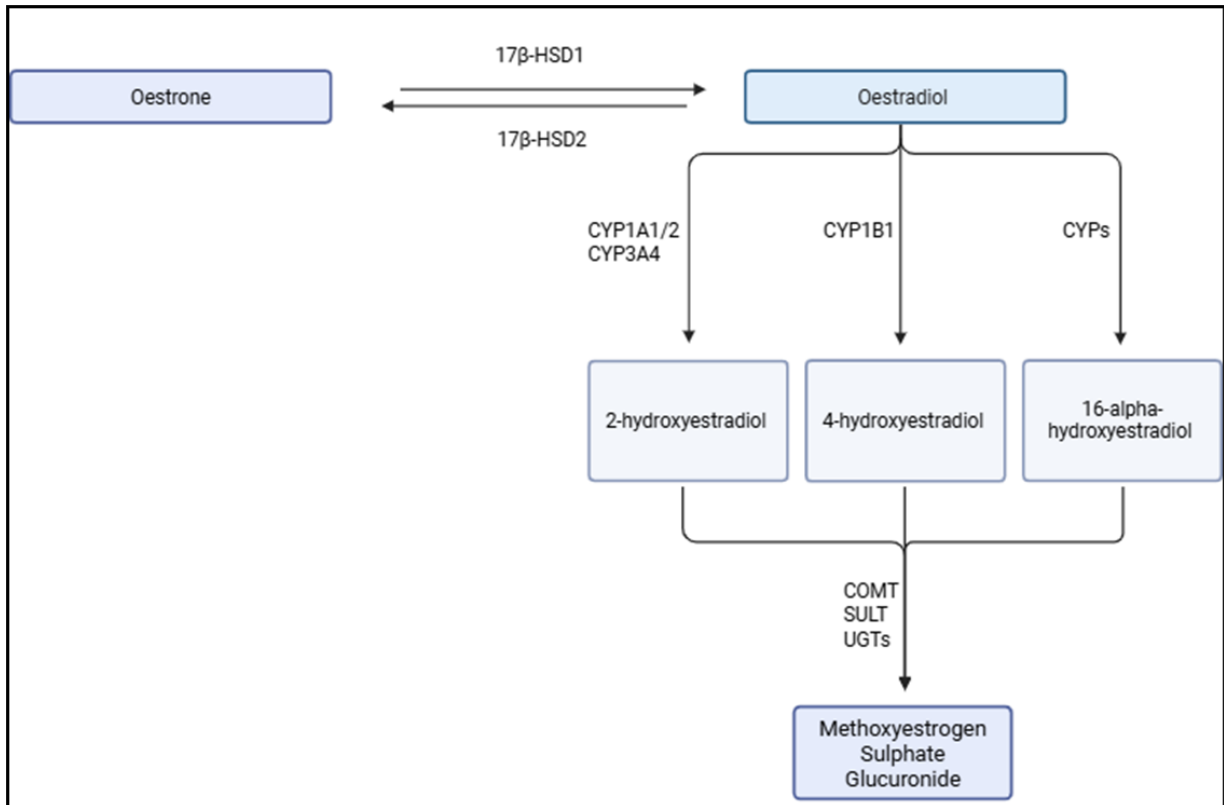


Figure 1.3. Endogenous oestrogen metabolism. The diagram shows the metabolic pathways of endogenous oestrogen metabolism, highlighting the interconversion between oestrone (E1) and oestradiol (E2) through 17β-hydroxysteroid dehydrogenases (17β-HSD1 and 17β-HSD2). In phase I metabolism, oestradiol is metabolised through cytochrome P450 enzymes (CYP), including CYP3A4, CYP1A1/2 and CYP1B1, leading to the formation of 2-hydroxyestradiol, 4-hydroxyestradiol, and 16-alpha-hydroxyestradiol, which have varying biological activities and implications in oestrogen metabolism and carcinogenesis. In phase II, these hydroxylated oestrogens are further metabolised via the following enzymes: catechol-O-methyltransferase (COMT), sulfotransferase (SULT) and glucuronosyltransferases (UGTs), converting them to methoxyestrogen, sulphate, and glucuronide, which are considered water-soluble products, facilitating oestrogen detoxification and absorption. Figure created using BioRender.

1.6.2 Exogenous sources

Environmental pollutants are an exogenous source that influences oxidative stress and DNA damage. Several environmental pollutants affect oxidative stress and increased the risk of breast cancer, including polycyclic aromatic hydrocarbons (PAHs) and heavy metals such as cadmium. PAHs are usually found in industrial emissions and cigarettes, and they are metabolised via CYP enzymes, generating ROS metabolites that lead to the formation of DNA adducts and oxidative damage [91], which increases the risks of breast cancer development [92]. Cadmium is an example of a heavy metal that contaminates water and food, it causes the depletion of GSH, which leads to the disruption of antioxidant defence and increases lipid peroxidation, hence elevating the levels of oxidative stress [93], promoting the development of breast cancer [94].

DNA damage is also affected by dietary habits that influence oxidative stress levels, including excessive alcohol consumption, high-fat diet and processed foods. These are associated with the generation of ROS and oxidative stress [95-97]. Acetaldehyde, which is a carcinogen that is generated via alcohol metabolism, causes antioxidant depletion and ROS production, leading to an increase in DNA damage and breast cancer risk [98]. Obesity is considered another factor that increases the risk of breast cancer, because of the increased oestrogen biosynthesis and lipid peroxidation, which increases oxidative stress and DNA damage [99]. On the other hand, diets that are rich in antioxidants, such as polyphenols, flavonoids, vitamins C and E, decrease the levels of oxidative stress and DNA damage, hence reducing the risk of breast cancer [100].

Collectively, oxidative stress is a major contributor to DNA damage and the initiation of breast cancer development and progression, arising from both endogenous metabolic processes and exogenous environmental factors. The persistent DNA damage caused by oxidative stress leads to genomic instability, tumour progression and therapy resistance, indicating the importance of exploring and targeting ROS-mediated pathways for cancer prevention and treatment.

1.7 DNA replication

DNA replication is a fundamental cellular process in which the entire genome is duplicated during cell division [101]. In eukaryotic cells, this mechanism is tightly regulated and occurs during the S phase of the cell cycle. It is essential for the accurate transmission of genetic information through successive generations of cells [101]. The replication process is initiated from numerous genomic loci, known as origins of replication, which are recognised by the origin recognition complex (ORC) [102]. Upon activation, these origins give rise to replication forks, where the parental DNA strands are unwound and serve as templates for the simultaneous synthesis of two complementary daughter strands [102].

This process is coordinated by the replisome, a dynamic multi-protein machinery composed of key components, such as DNA helicases, DNA polymerases, and DNA topoisomerase [103]. Other important factors include DNA ligase and enzymes that remove RNA primers, for example, FEN1 (Figure. 1.4) [104]. The helicase unwinds the DNA template, allowing DNA polymerase to synthesise nascent DNA strands, continuously on the leading strand and discontinuously on the lagging strand (Figure. 1.4) [102]. DNA replication proceeds in a semi-conservative manner, meaning each new DNA molecule contains one parental and one newly synthesised strand [102].

Replication is finalised during the termination phase, which involves the convergence of opposing replication forks, the disassembly of the replisome, and the resolution of DNA molecules [105]. This precisely coordinated process is important for preserving the genomic integrity, as errors during termination lead to incomplete replication fork collapse, or chromosomal rearrangements, ultimately contributing to genomic instability [106].

Replication fork stalling occurs when the replisome encounters physical obstacles or DNA structural aberrations that impede its progression [101]. This leads to the exposure of regions of single-stranded DNA (ssDNA), which are rapidly coated by Replication Protein A (RPA) to stabilise the fork and prevent collapse [101]. The accumulation of RPA-coated ssDNA serves as a signal for the activation of the ATR-CHK1 signalling pathway, a key component of DNA

damage response (DDR), that induces cell cycle arrest and facilitates fork stabilisation and repair [107, 108]. Once replication stress is resolved, the stalled fork can restart through coordinated actions of DNA helicases, such as the RECQ family, and structure-specific nucleases, including FEN1 and EXO1 [109]. However, prolonged stress or failure to restart results in the replication fork collapsing, leading to DNA double-strand breaks (DSBs), necessitating repair through high-fidelity mechanisms such as homologous recombination [106].

A major source of replication stress is transcription–replication conflicts (TRCs), which arise when the replication machinery encounters the transcription complex operating on the same DNA template [110]. These encounters happen in either a co-directional or head-on manner, with head-on collisions being particularly disruptive, often inducing higher levels of fork stalling and collapse [111]. Even co-directional conflicts, although less severe, still disrupt replication dynamics [111]. One of the key consequences of TRCs is the formation of R-loops, which are RNA-DNA hybrids with displaced non-template strands, that act as physical barriers to fork progression and can promote genomic instability if unresolved [111].

To maintain genomic integrity, cells deploy several mechanisms to resolve TRCs and prevent R-loop accumulation [112]. These include RNase H enzymes that degrade RNA within hybrids, helicases that unwind DNA, and topoisomerases, which alleviate DNA supercoiling [112]. However, in cancer cells, elevated transcriptional activity and uncontrolled proliferation, increase the incidence of TRC frequency and replication stress [113]. In response, tumour cells often rely on upregulation of DNA repair and fork processing enzymes, for example, FEN1 and EXO1 to rescue stalled forks and repair DSBs, especially when homologous recombination pathways are compromised [114].

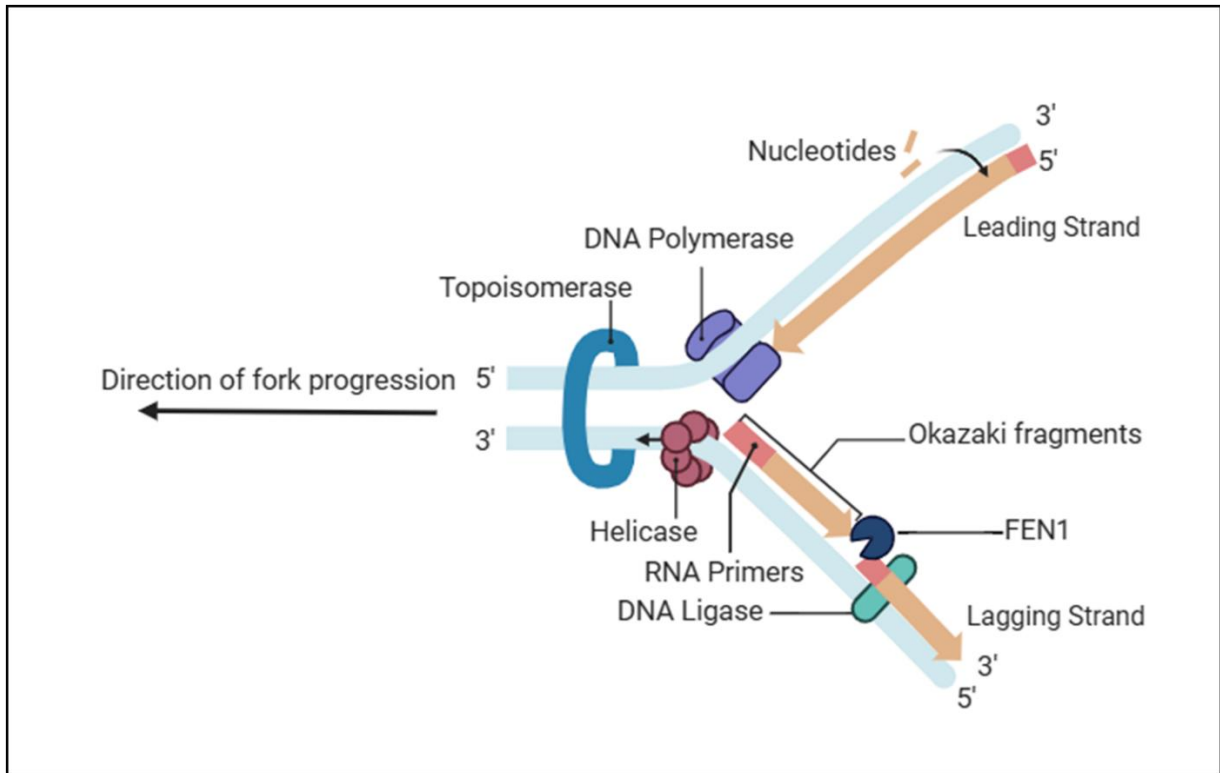


Figure 1.4. Representation of the DNA replication fork. As the replication fork advances, DNA helicase unwinds the parental double-stranded DNA, producing two single-stranded templates. Topoisomerase relieves tensional stress generated ahead of the fork. On the leading strand, replication occurs continuously in the 5' to 3' direction, mediated by DNA polymerase, which incorporates nucleotides complementary to the template strand. On the lagging strand, synthesis occurs discontinuously as short DNA fragments known as Okazaki fragments, each initiated by RNA primers. These fragments are extended by DNA polymerase and subsequently processed by FEN1, which removes RNA primers or flaps. Finally, DNA ligase seals the nicks between fragments to form a continuous DNA strand. The diagram indicates the overall direction of replication fork progression. Figure created using BioRender.

1.8 Nucleotide biosynthesis in breast cancer

Nucleotides are the main building blocks of genetic materials, and consist of purines (guanine and adenine) and pyrimidines (thymine and cytosine). Two pathways are involved in nucleotide biosynthesis, the de novo pathway and the salvage pathway [115].

The dysregulation of purine and pyrimidine synthesis pathways is observed in breast cancer, contributing to tumour progression and metastasis [116].

1.8.1 Purine and pyrimidine de novo pathway

The biosynthesis of purine requires amino acids, carbon dioxide and formyl groups. The purine biosynthesis pathway starts with the conversion of ribose-5-phosphate (R5P) from the pentose phosphate pathway (PPP) into phosphoribosyl-pyrophosphate (PRPP), catalysed by the enzyme PRPP synthetase. The rate-limiting step of this pathway is controlled by the enzyme glutamine PRPP aminotransferase, which catalyses the binding of PRPP with glutamine, resulting in the production of 5-phosphoribosylamine and the release of phosphate [117]. The pathway culminates in the synthesis of inosine monophosphate (IMP), which is a precursor of guanine and adenine nucleotides [117].

The de novo pyrimidine synthesis pathway requires glucose, the amino acid glutamine and aspartate [117]. The first step in the pyrimidine synthesis pathway is the formation of the pyrimidine ring, which is catalysed by the enzyme carbamoyl-phosphate synthetase 2, aspartate transcarbamoylase, and dihydroorotase (CAD), which converts glutamine and aspartate into dihydroorotate (DHOA) and N-carbamoyl-aspartate [118]. Then, orotate (OA) is produced via the conversion of DHOA by the mitochondrial membrane enzyme dihydroorotate dehydrogenase (DHODH). OA is transformed into orotidine monophosphate (OMP) upon the addition of PRPP. This leads to the formation of the main pyrimidine precursor uridine monophosphate (UMP), which is catalysed by UMP synthase (UMPS) [118].

For Deoxycytidine triphosphate (dCTP) synthesis, both nucleoside diphosphate kinase (NDPK) and cytidine monophosphate kinase (CMPK) cause the phosphorylation of UMP into

uridine triphosphate (UTP), then the bidirectional CTP synthase (CTPS) causes the formation of CTP. CDP is then formed as a result of the dephosphorylation of CTP by nucleoside diphosphate kinases (NDPK). After that, the enzyme ribonucleotide reductase (RNR) catalyses the reduction of CDP into deoxycytidine diphosphate (dCDP), NDPK then catalyses the synthesis of dCTP, which is incorporated into the DNA [118].

The synthesis of deoxythymidine triphosphate (dTTP) starts with the generation of deoxyuridine triphosphate (dUTP), which is catalysed by dUTPase. dUTP is then dephosphorylated to dUMP. Furthermore, the production of dUMP is catalysed by deoxycytidylate deaminase (DCTD), which converts dCMP to dUMP. After that, dTMP and dTDP are formed via Thymidylate synthase (TS), as well as deoxythymidine monophosphate (dTMP) kinase. Finally, dTTP is produced via the phosphorylation of dTDP and incorporated into the DNA [118].

1.8.2 Purine and pyrimidine salvage pathway

The salvage pathway is essential for recycling nucleobases and nucleosides, which allows the cells to maintain nucleotide pools efficiently, as this pathway uses less energy in comparison to the de novo synthesis pathway [117].

Purine salvage pathway maintains intracellular purine nucleotide pools by recovering the purine bases, for example, hypoxanthine, guanine and adenine, which are all converted back to their respective nucleotides. There are key enzymes that facilitate this process, including adenine phosphoribosyltransferase (APRT), which catalyse the conversion of adenine to adenosine monophosphate (AMP), and hypoxanthine-guanine phosphoribosyltransferase (HGPRT), which converts guanine to guanosine monophosphate (GMP), and hypoxanthine to IMP [119].

Similarly, the pyrimidine salvage pathway allows the reutilisation of nucleosides, such as thymidine, uridine and cytidine, as well as pyrimidine bases including thymine, uracil and cytosine. This process is facilitated by important enzymes, such as uridine-cytidine kinase

(UCK), which phosphorylates uridine and cytidine to UMP and cytidine monophosphate (CMP), respectively, while thymidine kinase (TK) phosphorylates thymidine to thymidine monophosphate (TMP) [118].

1.8.3 Targeting Purine and Pyrimidine Synthesis Pathways

Targeting the nucleotide metabolism in cancer is a promising therapeutic approach that can inhibit tumour progression and activate the immune system [115].

Increased purine synthesis supports the rapid proliferation of breast cancer cells, making this pathway a potential therapeutic target. One of the important intermediates in the purine *de novo* pathway is IMP, which is converted to either AMP or GMP [115]. Mycophenolic acid (MPA) is a non-competitive inhibitor that targets Inosine Monophosphate Dehydrogenase (IMPDH), which is responsible for converting IMP to XMP, which is a key step in the production of guanine. Although MPA showed promising antitumour activity in animal models, it did not show clinical efficacy in cancer patients [120]. Moreover, cancer cells use the salvage pathway for purine production. APRT is one of the key enzymes, which is targeted by 6-mercaptopurine (6-MP), a competitive inhibitor of APRT. 6-MP causes cell cycle arrest in kidney cancer [121]; however, in breast cancer, only a small group of patients seemed to benefit, particularly patients with BRCA-defective tumours [121].

For several decades, targeting the pyrimidine synthesis pathway, particularly the *de novo* pathway, has remained the backbone of cancer therapy [118]. The most essential enzymes in this pathway are CAD and DHODH, as they represent the rate-limiting step of this pathway, and they facilitate the formation of OA, which is a key intermediate in pyrimidine synthesis [117]. The overexpression of DHODH is linked to the increased production of pyrimidine, which enhances resistance to genotoxic therapies and tumour progression [118]. There are several DHODH inhibitors, such as brequinar (BRQ) and leflunomide, that reached market approval as immunosuppressive agents in rheumatoid arthritis and multiple sclerosis [118]. Although the DHODH inhibitor BRQ showed promising antitumour activity in *in vitro* and *in vivo* studies, it

could not be reproduced in phase II clinical trials [118]. Another example is 5-Fluorouracil anti-cancer therapy, which targets thymidine synthase (TS). This drug is used for breast cancer, it causes the depletion of pyrimidine and cancer cell death. However, it comes with several limitations, such as resistance in cancer patients and a low response rate [118]. Furthermore, cancer cells rely on the pyrimidine salvage pathway as well, one of the key enzymes is TK, and an aberration in this enzyme was reported in breast cancer [118]. High expression of TK was associated with poor prognosis in breast cancer patients [118]. Azidothymidine (AZT) is a TK inhibitor [122], which inhibits tumour growth in various types of human cancer, including breast [123], ovarian [124], lung [125] and colon cancers [126]. However, its role in breast cancer treatment in clinical settings has not been revealed [118].

1.9 DNA repair mechanisms

Human DNA is constantly exposed to different types of DNA-damaging agents. Failure in the process of repairing these lesions leads to the formation of mutations, where defects in those genes involved in DNA repair can lead to the formation of cancer [127]. Different DNA repair pathways are involved in the process of repairing damaged DNA, depending on the type of damage, including single-strand breaks; base excision repair (BER), nucleotide excision repair (NER), mismatch repair (MMR), double-strand breaks; non-homologous end-joining (NHEJ) and homologous recombination (HR) [127].

1.9.1 Base excision repair

BER is a highly conserved DNA repair mechanism that deals with oxidative damage and exogenous insults to ensure the integrity of DNA [128]. Cancer cells rely on high BER activity to encounter increased oxidative stress levels. There are at least 30 proteins that are involved in either short-patch repair or long-patch BER. Short-patch repair involves the removal of a single damaged base and the incorporation of a single nucleotide via DNA polymerase (POL β) [129], polynucleotide kinase-phosphatase (PNKP), X-ray repair cross-complementing group 1 (XRCC1) and DNA Ligase III α (LigIII α) [128]. The alternative procedure is long-patch repair, where more than one nucleotide is synthesised (possibly up to 13) to displace the damaged area [129]. This pathway is carried out via the coordination of many replication-associated factors, for example, proliferating cell nuclear antigen (PCNA), replication factor C (RFC), DNA polymerase delta (POL δ), DNA polymerase epsilon (POL ϵ) and FEN1 [129]. The factors that determine which sub-pathway is activated are still being resolved; however, the cell cycle phase, the intracellular concentration of ATP and the initiating glycosylase can play important roles in determining the molecular steps of BER [129].

1.9.2 Mismatch repair

MMR plays a key role in repairing and recognising misincorporation, deletions and erroneous insertions of bases that arise during DNA recombination and replication [127]. The main proteins that are involved in the MMR system include PMS1 homologue 2 (PMS2), MutS homologue 6 (MSH6), mutL homolog 1 (MLH1) and MutS protein homologue 2 (MSH2) [130]. The deficiency of the MMR pathway may lead to genetic instability, hence the development of cancer. In breast cancer, MMR deficiency (dMMR) was associated with an increased risk of death, especially in tumours with positive HRs [131]. It was also reported that the OS rate of patients with dMMR luminal B tumours was worse in comparison to patients with the same intrinsic subtype, but with non-dMMR [131].

1.9.3 Nucleotide excision repair

NER plays an important role in protecting the cells against DNA lesions. NER removes bulky covalent adducts that are induced by UV light, electrophilic chemical mutagens, ionising irradiation and active endogenous metabolites [127]. There are two mechanisms that NER is used to detect DNA damage, including transcription-coupled NER (TC-NER) and global genomic NER (GG-NER). TC-NER is used to permit unperturbed gene expression by removing transcription-blocking lesions. The deficiency in the TC-NER sub-pathway may cause a severe premature ageing condition, for example, Cockayne syndrome [132]. GG NER sub-pathway examines the whole genome for helix distortion. The distribution in GG-NER may lead to cancer predisposition [132]. One of the important proteins in the NER pathway is Xeroderma pigmentosum group C proteins (XPC), as it identifies damaged DNA and plays a role in the activation of the NER pathway. Other important proteins in the NER pathway include RAD23B, XPA, LIG1 and excision repair cross-complementation group 1 (ERCC1) [132].

1.9.4 DNA double-strand breaks repair

Two main pathways are used to repair DNA double-strand breaks, including homologous recombination (HR) and non-homologous end-joining (NHEJ) [127]. The exposure to ionising radiation is one of the reasons that causes DNA double-strand breaks [133]. NHEJ repair mechanism uses microhomologies, which are short homologous DNA sequences to guide the repair process, while the HR repair mechanism needs homologous sequences [127]. The NERJ pathway is activated during all phases of the cell cycle, whereas the HR pathway is only activated in the late S and G2 phases [134]. Many important proteins are essential for the NERJ pathway, such as XRCC4-XLF, XRCC5 (Ku80), XRCC6 (Ku70) and ligase 4 [127]. For the HR pathway, several tumour suppressor genes are involved, including ataxia telangiectasia mutated (*ATM*), *BRCA1* and *BRCA2*. The deficiency in the HR pathway may cause the progression of high-grade serous ovarian carcinoma [135]. Moreover, poorly defined NHEJ may play a role in the progression of leukaemia [136].

1.10 Upregulation of DNA repair in cancer: driving therapy resistance and tumour progression

Anti-cancer treatments, including ionising radiation and chemotherapeutic agents, typically cause cell death by inducing lethal DNA lesions, however, tumours with heightened DNA repair capacity can counteract this damage [137]. The ability of cancer cells to repair therapy-induced DNA damage makes them resistant to genotoxic treatments [137]. Therefore, targeting DNA repair pathways in cancer cells is a potential therapeutic approach [137].

Many DNA repair pathways are active in cancer cells, including BER, HR and NHEJ, fortifying tumours against DNA damage [138]. For example, enhanced activity of the BER pathway has been implicated in tumour resistance to therapy, as it enables efficient repair of DNA lesions caused by anti-tumour agents, such as floxuridine, temozolomide and pemetrexed [138]. Furthermore, the upregulation of DSB repair proteins in the NHEJ pathway causes tumour

resistance to DNA damage induced by radiation or drug-induced DSB, which prevents apoptosis and enhances tumour progression [138].

The overexpression of DNA repair not only causes treatment resistance but also enhances tumour growth under stress [108]. Oncogenic-driven malignancies, such as RAS-driven and MYC tumours, experience high levels of DNA replication stress and damage, which is encountered in cancer cells via the hyperactivating of DNA damage response (DDR) networks, for example, activating ataxia telangiectasia mutated and *Rad3* related Checkpoint kinase 1 (*ATR/CHK1*) signalling for stalled forks and HR pathway for fork breakage, which allow continuous tumour proliferation [108]. Moreover, the upregulation of metabolic processes causes the upregulation of DNA repair pathways. For example, elevated glycolysis activity causes the production of excess lactate, which results in cisplatin-resistance through the increased activity of DNA repair pathways [138]. Similarly, leukaemia cells that harbour the oncogene *BCR-ABL* show elevated levels of the HR protein RAD51, which enhances the DSB repair capacity, hence increasing their resistance to mitomycin C and cisplatin [139].

Breast cancer cells, particularly aggressive subtypes, show upregulation of key DNA repair proteins, which increases their resistance to anti-cancer treatments [140]. The overexpression of RAD51 is reported in invasive breast carcinoma, as western blot analysis showed an increase of RAD51 protein levels by 2-7 fold in comparison to normal cells [139]. Also, the overexpression of RAD51 is associated with higher tumour grade in invasive ductal carcinoma [139]. The BER pathway is commonly upregulated in breast cancer. Upregulation of BER AP endonuclease 1 (APE1) protein was associated with the onset of chemoresistance in hepatic cancer, ovarian and neurologic tumours, while the downregulation of its expression sensitises tumour cells to DNA damage caused by ionising radiation and chemotherapeutic drugs [141]. The high nuclear expression of APE1 in TNBC is associated with poor patient outcome and shows resistance to platinum-based chemotherapy [142]. An in vitro study reported that the downregulation of APE1 expression in ZR-75-1 and MCF-7 cell lines increased their sensitivity to Olaparib. Also, the study further explored the effect of APE1 downregulation in vivo, and

similar results are found, as the reduction of APE1 expression caused a decrease in the volume and weight of MCF-7 xenografted tumours that were treated with Olaparib [143].

Poly (ADP-ribose) polymerase-1 (PARP-1), which is an important BER protein and DNA damage sensor, is upregulated in breast cancer. One study reports that in surgical samples of around 8000 primary malignant and normal human tissues, PARP1 expression was found to be upregulated in approximately 30% of primary breast carcinoma compared to 2.9% of normal tissue [144]. A previous study showed that overexpression of PARP1 in breast cancer conferred resistance to Cyclic-dependent kinase (CDK) 4/6 inhibitors, and the inhibition of PARP1 caused high sensitivity to CDK4/6 inhibitors and antitumour effects in vitro and in vivo experiments. The study further suggests that patients with HR+/HER2- and low expression of PARP1 could be sensitive to CDK4/6 inhibitors in breast cancer [145].

Furthermore, PARP inhibitors work well in breast tumour that exhibits BRCA1 or BRCA2 deficiency, however, their efficacy diminishes if HR is restored or intact [137]. It was suggested that combining PARP inhibitors with agents that disrupt HR, such as ATM/ATR inhibitors, which prevent tumour cells from repairing PARP-induced DNA breaks, leads breast cancer cells to become more sensitive to the treatment [137]. Also, targeting other BER proteins such as XRCC1 or APE1 is being explored to enhance the efficacy of chemotherapy agents in breast cancer [146]. In principle, the combination of BER inhibitors and alkylating agents would increase the lethal accumulation of single-strand breaks in cancer cells [146].

Another approach is to target the signalling pathways that cause the upregulation of DNA repair. The Wnt/ β -catenin pathway has been associated with the increased expression of DDR proteins and PARP inhibitor resistance [137]. Therefore, using Wnt pathway blockers in combination with conventional therapy would lead to the reduction of DNA repair upregulation and enhance drug sensitivity in tumour cells [137]. Furthermore, there is growing interest in how tumour metabolism intersects with DNA repair, for example, targeting the glucose transporter type 1 (GLUT1) by a synthetic inhibitor known as WZB117, which made breast cancer cells sensitive to radiotherapy, as it increases the damage caused by ROS, and limits

the nucleotide pool used for rapid DNA repair [138]. Glutamine metabolism plays an important role in nucleotide biosynthesis, which in turn supports DNA repair and replication [137]. Studies have shown that targeting glutaminase (GLS) in BRCA-proficient tumours by using inhibitors, such as CB-839, can impair homologous recombination by decreasing nucleotide availability, which causes synthetic lethality with PARP inhibitors [147].

Overall, targeting the DNA repair pathway is crucial for enhancing cancer treatment outcomes. However, cancer cells are adaptable and develop compensatory mechanisms that allow them to bypass DNA repair inhibition [148]. For example, tumours with *BRCA1/2* mutation can restore homologous recombination by the overexpression of another repair protein, such as RAD51, or restore *BRCA* function by acquiring a secondary mutation, which leads to resistance against PARP inhibitors [148]. Targeting the regulatory pathways that drive the upregulation of DNA repair is a promising therapeutic approach. For example, the downregulation of glutamine metabolism leads to a decrease in the nucleotide pool, hence cutting off the ability of the tumour to fuel and sustain DNA repair, making it more sensitive to other therapeutic agents.

1.11 The potential association between SLC7A5 and DNA repair in breast cancer

Breast cancer cells often exhibit both metabolic reprogramming and genomic instability—two key hallmarks of cancer. One such metabolic adaptation is the elevated expression of the glutamine transporter SLC7A5, which facilitates the uptake of large neutral amino acids like leucine in exchange for intracellular glutamine [70]. Alongside this, increased expression of DNA repair enzymes such as FEN1 and EXO1 has also been observed in breast cancer, with prior studies linking these enzymes to poor patient outcomes and aggressive tumour behaviour [23, 149].

FEN1, a critical enzyme in the BER pathway, has been shown to interact with oestrogen receptor alpha (ER α) complexes, suggesting a regulatory link between hormonal signalling and DNA repair capacity [150]. Additionally, Madhusudan *et al.* reported that FEN1 overexpression correlates with poor prognosis and may operate within a broader DNA repair network involving ATM and other BER proteins [151]. ER signalling has also been shown to regulate Lethal giant larvae, a polarity protein that facilitates the trafficking of SLC7A5 from the cytosol to the plasma membrane, further tying hormonal pathways to metabolic regulation [152].

Similarly, EXO1, a key enzyme in the MMR pathway [131], It has been implicated in breast cancer progression. Its overexpression has been associated with tumour development and poor prognosis [23].

Although no previous studies have directly investigated the link between glutamine metabolism and DNA repair in breast cancer, we hypothesise that this association is mediated through nucleotide availability. Specifically, we propose that leucine, imported via SLC7A5, sustains mTORC1 activity, which in turn regulates the pentose phosphate pathway (PPP)—a crucial source of ribose-5-phosphate (R5P) for nucleotide biosynthesis [153, 154]. This increased supply of nucleotide supports DNA repair processes, particularly those requiring BER and MMR enzymes, such as FEN1 and EXO1, respectively (Figure 1.5).

Collectively, these observations suggest a potential functional crosstalk between SLC7A5-mediated glutamine metabolism and DNA repair pathways involving FEN1 and EXO1, which influence tumour survival and growth. This thesis aims to explore these associations across different breast cancer subtypes.

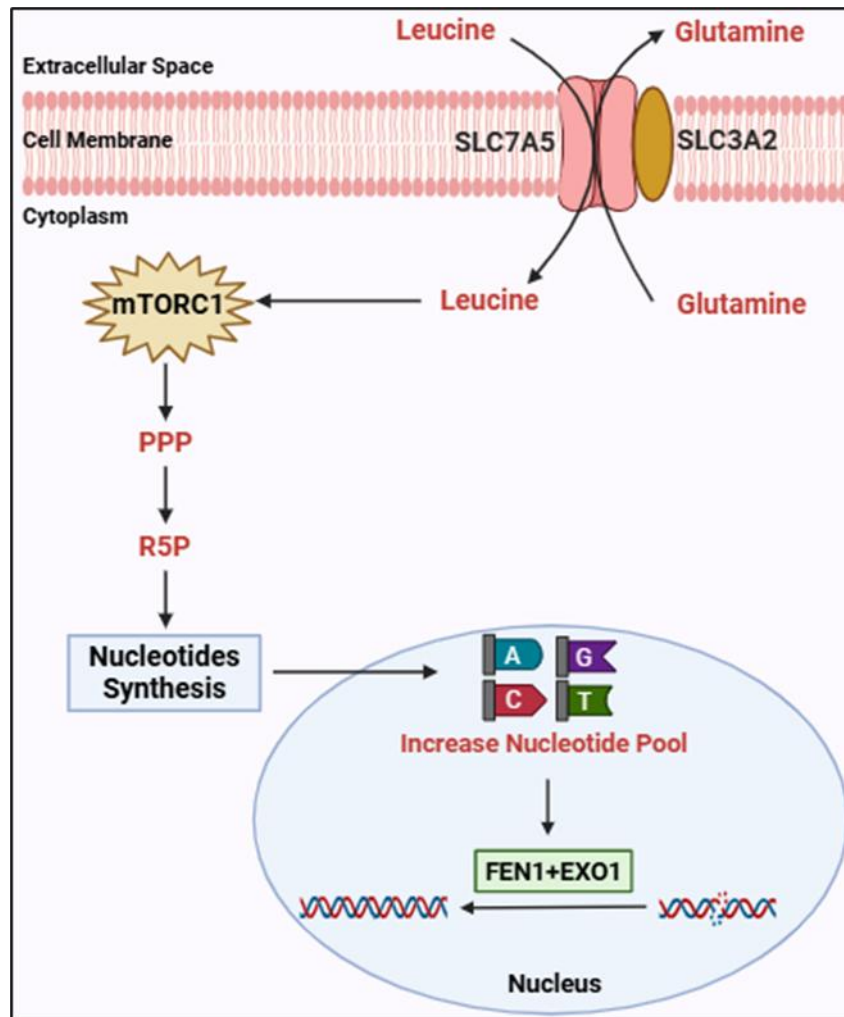


Figure 1.5. Proposed molecular pathway linking altered glutamine metabolism and DNA repair in tumour cells. Leucine is transported into the tumour cell in exchange for glutamine via solute carrier family 7 member 5 (SLC7A5) with the aid of SLC3A2. Leucine activates mammalian target of rapamycin complex 1 (mTORC1), which in turn activates the pentose phosphate pathway (PPP), which generates ribose-5-phosphate (R5P) for nucleotide biosynthesis. This increases the nucleotide pool, which is used by the DNA repair enzymes, such as base excision repair enzyme flap endonuclease 1 (FEN1) and mismatch repair enzyme exonuclease 1 (EXO1), to repair damaged DNA. Figure created using BioRender.

1.12 Hypothesis

Alterations in glutamine metabolism directly impact the efficiency of DNA repair pathways in breast cancer.

In this thesis, the interactions between the glutamine transporter SLC7A5 and the DNA repair proteins FEN1 and EXO1 in breast cancer were investigated.

The specific aims were:

1.13 Aims

1. To further investigate at the mRNA and protein levels the correlation between SLC7A5 and DNA repair proteins (FEN1 and EXO1) in breast cancer with clinicopathological variables, biological markers (Chapters 3 and 6).
2. To confirm the prognostic utility of SLC7A5 and DNA repair (FEN1 and EXO1) in breast cancer (Chapters 3 and 6).
3. To investigate the impact of targeting both SLC7A5 and FEN1 in vitro on breast cancer cell proliferation, migration, invasion, cell cycle and apoptosis (Chapter 4).
4. To investigate the potential reciprocal regulatory relationship between SLC7A5 and FEN1 in breast cancer cell lines, assessing how the knockdown of each gene affects the expression of the other, and whether these alterations are linked to metabolic changes, particularly in mitochondrial function (Chapter 5).
5. To identify shared protein networks and enriched biological pathways associated with SLC7A5 and FEN1 high expression (Chapter 5).

Chapter 2 General materials and methods

2.1 Patient cohort

2.1.1 Molecular Taxonomy of Breast Cancer International Consortium (METABRIC) cohort

The METABRIC study is a publicly available dataset comprising of 1,980 primary breast cancer fresh-frozen samples collected from tumour banks in the UK and Canada. DNA and RNA were extracted from each sample and used for genomic and transcriptomic profiling. The integrity and quality of DNA were evaluated using agarose gel electrophoresis, while RNA quality was assessed using the Agilent 2100 Bioanalyser Nanochip system (Agilent Technologies, Wokingham, UK). For genomic profiling, DNA was hybridised to Affymetrix SNP 6.0 arrays (Affymetrix, Santa Clara, CA, USA) at AROS Applied Biotechnology (Aarhus, Denmark). For gene expression analysis, total RNA was amplified using the Illumina TotalPrep RNA Amplification Kit (Ambion, Warrington, UK), and the resulting biotin-labelled cRNA was hybridised onto the Illumina Human HT-12 v3 Expression platform. The raw expression data were pre-processed, log₂-transformed, and quantile normalised prior to analysis [155].

Differential gene expression analysis was performed using the Linear Models for Microarray Data (LIMMA) package from Bioconductor. The prediction analysis of microarray 50 (PAM50) gene signature was used to classify breast tumours into intrinsic subtypes (luminal A, luminal B, HER2-enriched, basal-like, and normal-like), as originally described in the METABRIC publication [155].

Clinical and pathological data were also obtained for each sample, including tumour size, grade, nodal status, ER, PR, and HER2 status, as well as patient outcome. Notably, HER2-positive patients in the cohort did not receive trastuzumab, as the cohort was assembled prior to the routine implementation of HER2-targeted therapies. Patients with ER-positive and/or lymph node-negative tumours generally did not receive adjuvant chemotherapy, whereas ER-

negative and/or node-positive patients were more likely to receive systemic treatment. The characteristics of the METABRIC cohort are summarised in Table 2.1.

2.1.2 External cohort

The online dataset, Breast Cancer Gene-Expression Miner v5.1 (bc-GenExMiner v5.1) (<https://bcgenex.ico.unicancer.fr/BC-GEM/GEM-Accueil.php?js=1>), was used to further assess the *mRNA* expression of all the clinicopathological parameters and biomarkers that were included in this research. This dataset contains transcriptomic data from a pooled cohort of breast cancer patients (n=4,827), incorporating The Cancer Genome Atlas (TCGA), SCAN-B RNA sequencing data, and the Genotype-Tissue Expression (GTEx) project [156]. This tool allows the evaluation of candidate gene expression in relation to clinical outcomes through three main analytical modules: correlation, expression, and prognostic analysis. The correlation module enables the computation of Pearson correlation coefficients between the gene of interest and other genes across the dataset, identifying co-expressed genes that may suggest functional associations. The expression module supports comparisons of gene expression levels between different prognostic subgroups, such as nodal status, hormone receptor status, and molecular subtypes [156].

The prognostic module provides survival analyses using univariate Cox proportional hazards models and Kaplan–Meier curves to assess the impact of gene expression on various survival endpoints, including overall survival (OS). Subgroup analyses can be conducted by stratifying the cohort based on key clinicopathological features, such as, hormone receptor, nodal status and molecular subtypes [156].

The KM-plotter dataset (<http://kmplot.com/>) is another external dataset that was utilised as a validation cohort to evaluate the association between a selected gene and breast cancer patient outcomes at both the *mRNA* and protein levels [157]. This online tool integrates gene expression and clinical data from multiple publicly available datasets, including Gene Expression Omnibus (GEO), European Genome-phenome Archive (EGA), and TCGA,

covering more than 5,000 breast cancer cases [157]. It enables survival analysis across various clinical endpoints such as OS, recurrence free survival (RFS), and distant metastasis-free survival (DMFS) [157]. The platform allows stratification by key clinicopathological variables, including hormone receptor status (ER, PR, HER2) molecular subtype, and lymph node involvement. Expression levels are dichotomised (for example, high vs low) using automated best cut-off determination, and results are displayed via Kaplan–Meier survival plots, along with hazard ratios and log-rank p-values to determine statistical significance [157].

2.1.3 Patients' protein expression cohorts

The protein expression of selected genes was assessed in the Nottingham cohort, which consisted of n=2,239 breast cancer patients. These patients were treated at Nottingham City Hospital between 1989 and 2006. Previously prepared Tissue Microarrays (TMAs) from Formalin Fixed Paraffin-Embedded (FFPE) archival tissues were used, composed of wax blocks containing 150 cores (0.6 mm) of tissues. These TMAs were analysed to investigate a broad range of biological biomarkers [158]. The association between the selected genes and clinicopathological parameters and different BC molecular biomarkers was investigated. Patient management followed a standardised protocol based on tumour characteristics, including the Nottingham Prognostic Index (NPI) and hormone receptor status. Patients with a favourable prognosis (NPI score ≤ 3.4) did not receive adjuvant therapy. In contrast, those with an unfavourable prognosis (NPI score > 3.4) were administered endocrine therapy. Premenopausal patients in the moderate to poor prognostic categories were treated with chemotherapy, whereas postmenopausal patients in these same prognostic groups were managed with hormonal therapy. None of the patients received neoadjuvant treatment. The characteristics of the Nottingham cohort were summarised in Table 2.1.

Table 2.1 A summary of the breast cancer cohorts used.

Parameters	METABRIC Cohort	Nottingham Cohort
	mRNA	protein
	n (%)	n (%)
Grade		
1	170 (9)	438 (20)
2	770 (41)	774 (35)
3	952 (50)	1027 (46)
Tumour size (cm)		
≤ 2.0	858 (44)	1241 (55)
> 2.0	1094 (56)	992 (44)
Lymph node stage		
1	1035 (55)	1457 (65)
2	522 (28)	609 (27)
3	316 (17)	173 (8)
ER		
Negative	474 (24)	565 (25)
Positive	1506 (76)	1559 (70)
HER2		
Negative	1733 (88)	1641 (73)
Positive	247 (13)	232 (10)
PR		
Negative	940 (48)	777 (35)
Positive	1040 (53)	1096 (49)
Triple Negative		
No	1660 (84)	1676 (75)
Yes	320 (16)	334 (15)
NPI		
GPG	680 (34)	811 (36)
MPG	1101 (56)	1106 (50)
PPG	199 (10)	316 (14)
Ki67		
High	NA	846 (55)
Low		703 (45)
PAM50 subtype		
Luminal A	718 (41)	583 (37)
Luminal B	488 (28)	542 (34)
Basal	329 (19)	334 (21)
HER2	240 (14)	117 (7)

NPI: Nottingham Prognostic Index; **GPG:** Good prognostic group; **MPG:** Moderate prognostic group; **PPG:** Poor prognostic group.

2.1.4 Patient's clinical outcome and events definition

Outcome data included breast cancer-specific survival (BCSS), which was defined as the time from diagnosis to the time of death as a result of breast cancer in months. Distant metastasis-free survival (DMFS) was defined as the time from diagnosis to the time of developing distant metastasis in months. Recurrence-free survival (RFS) was defined as the time from diagnosis to the time of developing local or regional recurrence in months. Patient survival was censored if one of the following occurred: the patient was lost to follow-up, still alive, or died as a result of any other cause.

2.2 Immunohistochemistry (IHC) and antibody optimisation

The optimisation of all the primary antibodies was conducted on breast TMA sections, before the actual staining to achieve specific staining with minimal background interference. The optimisation process involved using different antibody dilutions and incubation times to ensure these variables did not affect the staining quality. Detailed Information on all the antibodies used in this study is provided in Table 2.2.

Positive control tissues were included and selected based on the antibody supplier's recommendation or by selecting specific tissues that showed high or low expression of the targeted proteins, from the Human Protein Atlas (<https://www.proteinatlas.org/>) (Table 2.2).

2.2.1 IHC staining

IHC staining was performed on 4 µm TMA sections using Novolink Polymer Detection System (RE7150-K, Leica Biosystems, UK). Labelled tissue slides were heated at 60°C for 10 minutes, then allowed to cool at room temperature for 5 minutes. Deparaffinisation was carried out

using xylene baths two times for 5 minutes each, followed by rehydration in alcohol three times for 2 minutes each, and a final three washes in water for 5 minutes each using a Leica Autostainer XL instrument (Leica Microsystems, UK). Antigen retrieval was performed using 1.0M sodium citrate buffer (PH 6), with heating for 20 minutes in a microwave (Whirlpool JT359 1000w). Afterwards, slides were cooled for 5 minutes under running tap water. They were placed in a flatbed tray, and a hydrophobic barrier pen was used around the tissue sections to create a defined hydrophobic barrier, ensuring reagents remained confined within the TMA cores.

Slides were washed with TBS-T buffer (Tris Buffered Saline containing 0.1% Tween 20, PH 7.6) before a peroxidase block was applied for 15 minutes to eliminate endogenous peroxidase activity. This was followed by three washes in TBS-T for 5 minutes each. A protein block was applied for 5 minutes to prevent non-specific binding, followed by another set of three TBS-T washes for 5 minutes each.

The primary antibody for each target was optimally diluted in Leica antibody diluent (AR9352, Leica, Biosystems, UK) and incubated for the required time (as detailed in Table 2.2). Slides were washed with TBS-T three times, 5 minutes each, before the post-primary solution was applied for 30 minutes, followed by another three washes in TBS-T for 5 minutes each. Novolink polymer was then applied for 30 minutes, followed by three additional washes in TBS-T for 5 minutes each. For visualisation, 3,3'-Diaminobenzidine (DAB) solution was applied for 5 minutes, followed by three washes in TBS-T for 5 minutes each. Counterstaining with haematoxylin was performed for 6 minutes, followed by dehydration in IMS alcohol three times for 2 minutes each. The slides were then cleared using xylene two times for 5 minutes each in a Leica Autostainer. Finally, the slides were mounted with a glass coverslip using DPX (BDH, Leica Microsystems, UK) and left to dry for 24 hours at room temperature.

2.2.2 Evaluation of Staining

High-resolution digital images, NanoZoomer slide scanner (Hamamatsu Photonics, Welwyn Garden City, UK), were used to scan stained TMA sections at 20x magnification. A semi-quantitative histochemical score (H-score) was used to assess the protein expression of the selected gene in invasive tumour cells. H-Score considers both the percentage and the intensity of stained tumour cells. The intensity of stained tumour cells was grouped as follows: negative = 0, weak = 1, moderate = 2 and strong = 3. The percentage of stained tumour cells ranged from 0% to 100%. The final H-Score was calculated by multiplication of the percentage of stained cells by the intensity, resulting in a total range between 0 and 300. Cores that were lost, folded or had less than 15% tumour were excluded. All cases were double-scored by another trained observer (Dr Ayat Lashen and Dr Ruth Parks), also the scores were given without knowing the clinicopathological data and patient outcome.

Table 2.2. Information about the antibodies used in the western blot.

Antibody	Supplier	Species	Product code	WB		IHC		Positive Control
				Dilution	Molecular weight	Dilution	Incubation Time	
SLC7A5	Abcam	Rabbit monoclonal	Ab208776	1:1000	40 kDa	1:50*	Overnight 4°C *	Testis*
FEN1	Novus Biologicals	Rabbit polyclonal	NB100-321	1:2000	50 kDa	1:100	1 hour	Ovary
EXO1	Thermo Fisher Scientific	Rabbit Polyclonal	PA5-86470	1:2000	115 kDa	1:100	Overnight 4°C	Stomach

NA: Not Available; * Staining and scoring were conducted by previous PhD student Dr Rokaya El Ansari

2.3 Cell lines

American Type Culture Collection (Rockville, MD, USA) was the source for all breast cancer cell lines that were used, including normal-like cell line MCF-10A, luminal breast cancer cell lines HCC-1500, MCF-7, ZR-751, and BT-474, and triple-negative breast cancer cell lines MCF-10DCIS, MDA-MB-436, MDA-MB-468 and MDA-MB-231 (Table. 2.3). HCC-1500, MCF-7, ZR-751, and MDA-MB-231 were cultured in Roswell Park Memorial Institute (RPMI-1640) medium (AE25719279, GE Healthcare Life Science, UT, USA), while BT-474 was cultured in Dulbecco's Modified Eagle medium (DMEM) (RNBH6547, Sigma-Aldrich, UK). MDA-MB-468 was cultured in DMEM/F12 (no HEPES) (11320033, Thermo Fisher Scientific, UK), while MDA-MB-436, MCF10A and MCF10DCIS were cultured in DMEM/F12 with L-Glutamine and HEPES (11330032, Thermo Fisher Scientific, UK). However, MCF10A and MCF10DCIS media were further supplemented with horse serum (16050-122, Invitrogen, UK), hydrocortisone (H-0888, Sigma, UK), cholera Toxin (C-8052, Sigma, UK), Insulin (I-1882, Sigma, UK), Penicillin-Streptomycin (15070-063, Invitrogen, UK) and Epidermal Growth Factor from murine submaxillary gland (E1257, Sigma, UK). All the mediums were supplemented with 10% foetal bovine serum (Sigma-Aldrich, UK), except for MCF10A and MCF10DCIS. All cell lines were checked regularly for mycoplasma contamination, The test was performed by using the MycoAlert Detection kit (CUL001B, R&D Systems, UK).

2.3.1 Thawing of cell lines

Stocks were thawed rapidly at room temperature, and were supplemented with complete cell culture media by using a 15 ml Falcon tube. After that, the tube was centrifuged (3-16KL, Sigma, Germany) for 5 minutes at 1,500 revolutions per minute (rpm). Fresh media was used to resuspend the pellet, which was transferred to an appropriate flask size, and it was incubated at 37°C in a humidified environment with 5% CO₂.

2.3.2 Passaging of cell lines

Once the cells were confluence (between 75% and 85%), all the spent media was discarded, and Dulbecco's Phosphate Buffered Saline (DPBS) (RNBH8631, Sigma Life Science, UK) was used to wash the cells twice; after 2-5 ml of trypsin (29259717, Sigma Life Science, USA) was added to encourage detachment, then cells were incubated with trypsin for 3-5 minutes at 37°C. Thereafter, cells were checked under the microscope to make sure that they were fully detached, then neutralised by adding fresh media, then the cells were centrifuged for 5 minutes at 1,500 rpm. Depending on the cell line, the pellet was resuspended in a fresh growth medium in an appropriate proportion; and transferred into a new flask, which was labelled with the date, the cell line name and the passage number. The flask was incubated in a humidified environment with 5% CO₂ at 37°C.

2.3.3 Cryopreservation of cell lines

Cells were trypsinised and the pellet was resuspended in a freezing solution, which is composed of 10% Dimethyl sulfoxide (DMSO) (SHBK2703, Sigma-Aldrich, UK) and 90% cell line growth media. Thereafter, the cell suspension was aliquoted into 0.5 ml cryovials, which then was stored in a -80°C freezer overnight and moved to a liquid nitrogen tank for long-term storage.

2.3.4 Cell lysate

After the cell suspension was obtained, the cells were counted by adding 20 μ l of trypan blue (T8154, Sigma-Aldrich, UK) and mixing it with 20 μ l of cell suspension, following that 15 μ l of the mixture was injected into the groove between the haemocytometer and the coverslip, then viable cells were counted under the microscope, where the average of counting the 4 outside squares was calculated, which was multiplied by 10,000 and then further multiplied by the dilution factor for trypan blue (x2), which will give an estimated number of cells per ml. After obtaining the number of cells per ml, the pellet was obtained again after the cell suspension was centrifuged for 5 minutes at 1500 rpm (3-16KL, Sigma, Germany). The pellet was placed on ice, and resuspended in an appropriate amount of RIPA lysis buffer (for each 1×10^7 cell per ml, 1ml of RIPA lysis buffer was used), the lysis buffer contains RIPA buffer (89901, Thermo Fisher Scientific, UK), phosphatase inhibitor (Sigma-Aldrich, UK) and mini protease inhibitor cocktail complete (04693124001, Roche, UK). The cell suspension was kept on ice for 15 minutes, and the tube was gently inverted every couple of minutes. Following that, the tube was centrifuged (1-15K, Sigma, Germany) at 13,000 rpm for 20 minutes at 4°C. Finally, the supernatant was collected and stored in a -20°C freezer until required.

Table 2.3. Investigation of different breast cancer cell lines that were used.

Cell-lines	Receptor status	Subtype	Reference
BT-474	ER+, PR+ and HER2+	Luminal-B	[159]
HCC-1500	ER+, PR+ and HER2-	Luminal-A	[159]
MCF-7	ER+, PR+ and HER2-	Luminal-A	[160]
MCF-10A	ER-, PR- and HER2-	Normal-Like	[159]
MCF-10DCIS	ER-, PR- and HER2-	Triple-Negative	[159]
MDA-MB-231	ER-, PR- and HER2-	Triple-Negative	[159]
MDA-MB-436	ER-, PR- and HER2-	Triple-Negative	[159]
MDA-MB-468	ER-, PR- and HER2-	Triple-Negative	[159]
ZR-751	ER+, PR- and HER2-	Luminal-B	[159]

2.3.5 Protein quantification

Pierce BCA Protein Assay Kit (23225, Thermo Fisher Scientific, UK) was used to perform the protein quantification for lysate of different breast cancer cell lines, by following the manufacturer's procedure. First, the cell lysate of each breast cancer cell line was diluted by adding 16 μ l of distilled water to 4 μ l of the cell lysate, then 8 μ l of the mix was added to 96 plates in duplicate. Next, the BCA working reagent was prepared by mixing BSA reagent A with BSA reagent B in the following proportion: 50A:1B. Finally, in dark conditions, 200 μ l of BSA working reagent was added in duplicate to each well, and the plate was then stored in a 37°C incubator for 30 minutes. Infinite F50 (Tecan, Switzerland) was used to measure the absorbance at 570nm.

2.4 Western blotting (WB)

WB was used to identify and validate the expression of specific targeted protein in different breast cancer cell lines. WB was applied on a mixture of cell lysates, including whole-cell lysates of different BC cell lines, HCC-1500, MCF-10A, MCF-10DCIS, MCF-7, ZR-751, BT-474, MDA-MB-436, MDA-MB-231 and MDA-MB-468.

2.4.1 Sample preparation and gel electrophoresis

Samples of approximately 20 μ l volume were prepared by mixing 5 μ l of NuPAGE LDS Sample Buffer (4x) (Novex Life Technologies), 2 μ l NuPAGE Reducing Agent (10x) (NP0009, Novex Life Technologies) and around 13 μ l of lysate protein (10-20 μ g). Vortex was used to mix the samples well, after that they were placed in the heat block for 5 minutes at 100°C, then they were kept on ice. Thereafter, Bolt 4-12% Bis-Tris Plus Gels (NW04120BOX, Novex Life

Technologies, UK) was placed on electrophoresis running tank, which was filled up with 1x MOPS running buffer, which was prepared by adding 50 ml 20x MOPS SDS running buffer (B000102, Novex Life Technologies, UK) into 950 ml deionised water. Following that, 5 µl of PageRuler™ Plus Prestained Protein Ladder (26616, Thermo Scientific, UK) and 20 µl of samples were loaded into the gel. The gel was run at 160v for 1 hour.

2.4.2 Transfer of proteins and staining

Proteins were transferred to Polyvinylidene difluoride (PVDF) membrane (R9DA13833, Merck Millipore, Ireland) in the presence of 1x Transfer Buffer, and electro-blotting was performed at 10v for 90 minutes. The 1x Transfer Buffer was prepared by mixing 50 ml 20x Transfer buffer (BT0006, Novex Life Technologies, UK) with 100 ml Methanol, 849 ml deionised water and 1 ml anti-oxidant (1771606, Novex Life Technologies, UK). After that, a blocking buffer was used to block for 1 hour at room temperature, which was prepared by adding 5% Marvel milk (Premier International Foods, UK) to Phosphate Buffer Saline (PBS) (B98849, Oxoid, UK) containing 0.1% Tween-20 (Sigma-Aldrich, UK). Then the membrane was removed from the blocking buffer, and it was incubated with the primary antibody on a roller mixer at 4°C overnight. The primary antibody was prepared at the optimal dilutions detailed in the table (Table. 2.2). The loading control anti-β-actin (A5441, Sigma-Aldrich, UK) was included in all experiments at the following dilution 1:5000. On the following day, the membrane was taken out of the cold room and washed by PBS-Tween20 3 times for 10 minutes each, then the membrane was incubated with IRDye 800 CW donkey anti-rabbit fluorescent secondary antibody (926-32213-LI-COR Biosciences) and IRDye 680 RD donkey anti-mouse fluorescent secondary antibody (926-68072-LI-COR Biosciences), at the following dilution 1:15000 for one hour at the room temperature.

2.4.3 Detection Method

After the incubation with secondary antibody, the membrane was washed with PBS-Tween 20 3 times for 10 minutes each. For fluorescent detection, protein bands were visualised by using Odyssey Fc with Image Studio 4.0 (LI-COR Biosciences), at the following wavelengths 600, 700 and 800nm.

2.4.4 Western blotting using Enhanced Chemiluminescence (ECL)

The membrane was incubated with secondary Ab anti-rabbit (7074S, Cell Signalling, UK) or anti-mouse (7076S, Cell Signalling, UK) monoclonal horseradish peroxidase (HRP) conjugate at a concentration of 1:5000 for 1 hour at room temperature with rocking, then the membrane was washed 3 times with wash buffer for 10 minutes each. ECL reagent (34580, Thermo Scientific, USA) was prepared by mixing 1 ml reagent A with 1 ml reagent B. The wash buffer was discarded, and the membrane was placed on plastic pouch, then 1 ml of the ECL mixture was gently pipetted on the membrane making sure that it covered it all and incubated for 1 minute in the dark at room temperature. Protein bands were visualised by chemiluminescence using an Odyssey Fc (Li-Cor Biosciences, U.S.A).

2.5 Transient knockdown

FEN1 (s5104, 4390824, Thermo Fisher Scientific, UK) (Antisense sequence: '5-UUCUCCAUCAUGCGAAUGGtg-3') and SLC7A5 (s15653, 4392420, Thermo Fisher Scientific, USA) (Antisense sequence: '5-UUGGGAUCUAGAUUGGACa-3') Small interfering RNA (siRNAs) oligonucleotides, and the validation construct of *FEN1* (s5103, 4390824, Thermo Fisher Scientific, UK) (Antisense sequence: '5-

AAAGUAGCUCUUGAUGUCAAtt-3'), SLC7A5 (s15655, 4392420, Thermo Fisher Scientific, UK) ('5-UCAAGCUCAGGCCUUUCUGUgg-3'), and scrambled negative siRNA control (4390843, Thermo Fisher Scientific, UK). Constructs were diluted in 50 µl nuclease water to make a stock solution of 100µM. Transfection of siRNA was performed by using Lipofectamine 3000 reagent (L3000015, Thermo Fisher; UK) and according to the manufacturer's protocol. Cells were seeded in T25 flasks at 60-70% confluency and incubated overnight. 1 µl of the stock siRNA solution was diluted in 0.75 ml Opti-MEM reduced serum medium (11058021, Thermo Fisher, UK), and 20 µl of Lipofectamine was diluted in 0.75 ml Opti-MEM for 5 minutes. The diluted siRNA and Lipofectamine were mixed to make the transfection master mix and incubated at room temperature for 15 minutes. Cells were washed with Opti-MEM, and 1.5 ml of master mix solution was added. Transfected cells were incubated overnight at 37°C in a 5% CO₂ incubator. The next day, Opti-MEM was discarded and replaced with cell-specific media. The efficiency of the transfection was checked at days 5 and 7 using WB.

2.6 CellTiter 96 Aqueous One Solution Cell Proliferation Assay (MTS assay)

The effect of FEN1 knockdown (KD) and SLC7A5 KD on cell proliferation were assessed via The CellTiter 96® aqueous One Solution Reagent which consists of [3-(4,5 dimethyl 2 yl) 5-(3 carboxymethoxyphenyl) 2-(4 sulfophenyl) 2H tetrazolium, inner salt;(MTS) assay was carried out (G3580, Promega, UK). One day after the cell transfection, control and transfected cells were seeded in triplicate, in a 96-well plate at a density of 2,000 cells per well, and the plate was incubated at 37°C in a 5% CO₂ incubator. Thereafter, 20 µl of MTS assay was added to each well, at 48hour (h), 72h, 96h and 120h post-transfection and incubated for two hours at 37°C in a 5% CO₂ incubator. A microplate reader (TECAN Infinite F50) was used to measure the absorbance at 490nm.

2.7 Cell count

Control and transfected cells were seeded in a 12-well plate in duplicate at a density of 10,000 cells per well. Cells were counted at 0h, 24h, 48h and 72h, 3 days post-transfection. On the indicated day, media was removed, and cells were washed with PBS and then trypsinised, and were counted using a cell counter (CDBF, DeNovix, USA). The experiment was performed in duplicate, three times independently.

2.8 Wound healing assay

To assess the migration ability of the control and transfected cells, a culture-Inserts 2 well (IB-81176, Thistle Scientific Ltd), which has a built-in gap was used according to the manufacturer protocol. Cells were seeded at density of 75,000 at each side of the plate in 70 µl of DMEM (10% FBS) and incubated for 24 hours at 37°C and 5% CO₂.

On the next day, the plastic septum that separates the two sides of the insert was removed by using a pair of tweezers, which creates a gap that looks like a wound. The plate was then washed twice with 1 ml of low serum medium (DMEM with 1% FBS), then 2 ml of the low serum medium was added to the inserts. The wounds were observed by taking images several times via light microscopy (Lecia DMI 3000B, Leica microsystems, Germany), at the following points, for MCF-7: Time (T) 0h, T24h, T48h and T72h, for MDA-MB-436: T0h, T6h, T12h and T15h, for MDA-MB-231: T0h, T12h, T24h and T48h. To calculate the percentage of wound closure, Image J software (version 1.52) was used. Using the freehand selection tool, the area of the wound (the cell-free gap) was manually outlined and measured in pixels. For each time point, the wound area was recorded, and then the percentage of wound closure was calculated using the following formula:

$$\text{Wound Closure (\%)} = \left(\frac{\text{Initial Wound Area (0h)} - \text{Wound Area at Time T}}{\text{Initial Wound Area (0h)}} \right) \times 100$$

This calculation was repeated for each biological replicate, and the results were averaged.

2.9 Transwell invasion assay

Cell invasion was assessed using Matrigel-coated Boyden chambers (662638, Greiner Bio-One, Germany); the inserts were placed in 12-well plates (150628, Thermo Fisher Scientific). The low growth factor extracellular matrix (A14133-01, Gibco, Fisher Scientific) was diluted in ice-cold serum-free media to 0.5mg/ml. Then, 50 μ l of diluted ECM was used to coat the inserts. The plate was then placed in the incubator at 37°C in 5% CO₂ for two hours to allow Matrigel solidification into the membrane. Control and transfected cells were trypsinised, then cells were centrifuged and suspended (cell density of 150000 per insert) in 200 μ l of low serum media (DMEM+1%FBS) and 1mM hydroxyurea (A10831.03 Hydroxyurea, 98%, Thermo Scientific Chemicals, UK), and 600 μ l of DMEM (10% FBS) was added to the bottom of the chamber to create chemotactic gradient. Cells were incubated for 24 hours at 37°C and 5% CO₂.

After 24 hours, cotton buds (from Lidl) were used to wipe the upper part of the membrane, and then the inserts were washed 3 times with PBS. The inserts were then placed in the wells containing 500 μ l of 4% paraformaldehyde and incubated at room temperature for 15 minutes. Thereafter, the inserts were washed 3 times with PBS, and placed in the wells containing 500ul of DAPI (62248, Thermo Fisher Scientific, UK) (1:1000) for 15 minutes at room temperature. The inserts were washed 3 times with PBS, and then the basal part of the membrane was removed by scalpel and placed on the microscope slide (J1800AMNZ, Eprexia, USA) facing up coverslips (12323138, Borosilicate Glass Circle Coverslips, Fisher Scientific, UK), and then 10 μ l of mount media (10622689, Immuno-Mount, Fisher Scientific, UK) was added, and coverslips were placed on the slide to cover it. After that, fluorescence microscope (Lecia DMI 3000B, Leica microsystems, Germany) was used to take images of

different view fields on the membrane, the total number of DAPI stained nuclei was counted using ImageJ software, then the average number of invaded cells was calculated by dividing the total number of invaded cells on the number of images taken.

2.10 Cell Cycle

Cells were seeded in a 6-well plate, 100,000 cells per well, then on the fifth day after transfection, they were harvested and spun down (3-16KL, Sigma, Germany) for 5 minutes at 1,500 rpm, the supernatant was removed, and the pellet was washed with PBS. Cells were fixed for two hours in 70% ethanol. After fixation, the cells were centrifuged to discard the 70% ethanol, and then washed twice with PBS, after each wash centrifuged at 1000 RPM for 5 minutes. The cells were incubated on ice for 15 minutes. Propidium iodide (PI) staining solution was prepared, which contains the following: 0.1% (v/v) Triton X-100, 10 µg/ml PI (P4864-10ml, Sigma), and 100 µg/ml DNase-free RNase A (2201416-10ml, Invitrogen) in PBS. The cell pellet was suspended in 200 µl of PI staining solution, and then kept in the dark at room temperature for 30 minutes. Samples were then transferred to a flow cytometer (CytoFlex S Flow Cytometer, Beckman Coulter, US). For analysis, Kaluza Analysis 2.1 software (Beckman Coulter) was used (Figure 2.1).

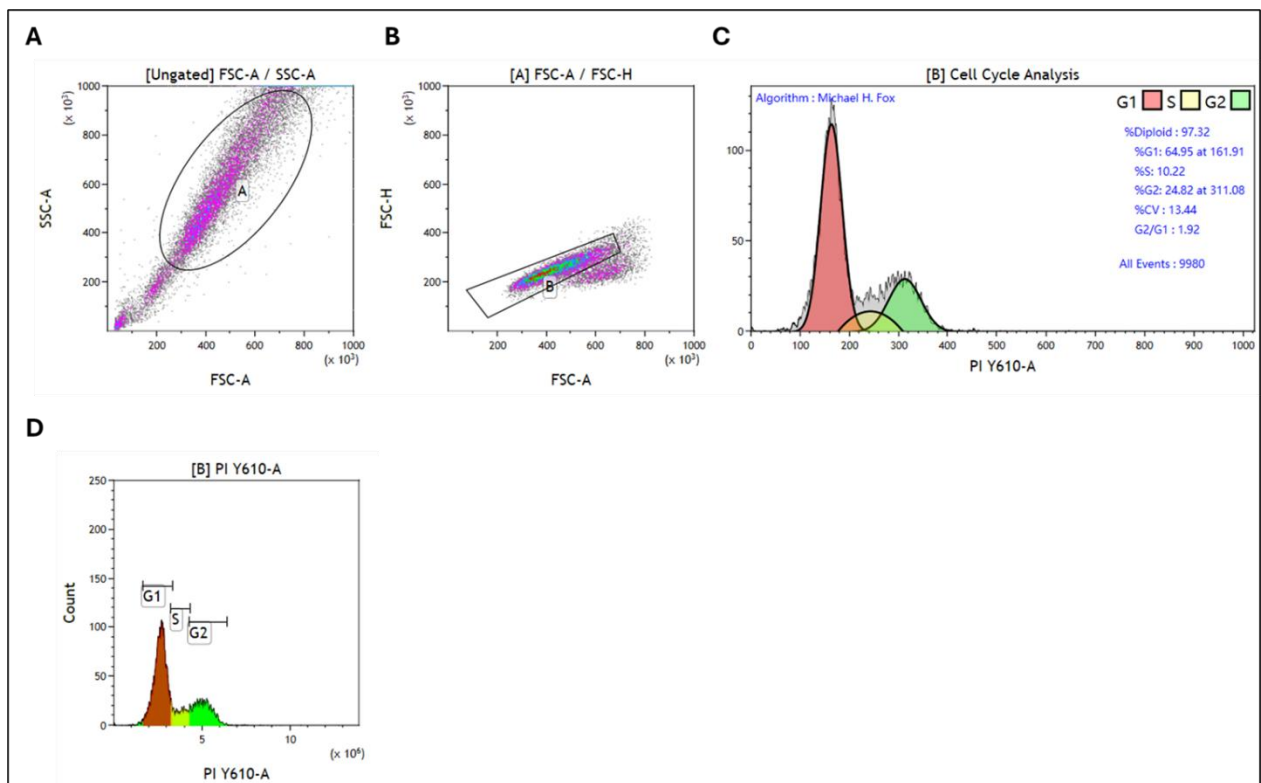


Figure 2.1 Flow Cytometry Analysis of Cell Cycle Distribution for MCF-7 cell line (control) Using Kaluza Software. (A) Forward and Side Scatter Plot (FSC-A/SSC-A): The first step in data processing involved selecting the main cell population while excluding debris. The forward scatter area (FSC-A) was plotted against the side scatter area (SSC-A), and a gating region “A” was drawn to include only intact, viable cells. (B) Doublet Discrimination (FSC-A/FSC-H): To ensure single-cell analysis, forward scatter height (FSC-H) was plotted against forward scatter area (FSC-A). A gating region “B” was applied to eliminate cell aggregates or doublets, retaining only single-cell events for further analysis. (C) Cell Cycle Distribution Analysis: DNA content was measured using PI fluorescence intensity (PI Y610-A) to determine the percentage of cells in each phase of the cell cycle. The Michael H. Fox algorithm was applied to fit the data and calculate cell cycle phases. The distribution showed 64.95% of cells in G1 phase, 10.22% in S phase, and 24.82% in G2 phase, with a G2/G1 ratio of 1.92 and a coefficient of variation (CV) of 13.44%, confirming high-quality data acquisition. (D) Histogram Representation of Cell Cycle Phases: The final histogram depicts the DNA content distribution with distinct peaks for G1 (brown), S (orange), and G2 (green) phases, with the x-axis representing PI fluorescence intensity (PI Y610-A) and the y-axis representing the cell count.

2.11 Apoptosis

Cells were seeded in a 6-well plate at a density of 100,000 cells per well to be assessed for apoptosis (BD Biosciences, 556547, UK). On the fifth day post-transfection, cells were harvested and centrifuged at 1500 rpm for 5 minutes (3-16KL, Sigma, Germany), the supernatant was removed, and cells were washed twice in ice-cold PBS. Pellet was resuspended in 100 μ l Annexin V binding buffer, which is prepared by mixing 1 ml of binding buffer with 9 ml of pure water. 1 μ l of each Annexin V and PI was added to the samples. After that, samples were incubated for 15 minutes in the dark at room temperature. Samples were then topped up with 300 μ l of the Annexin V binding buffer. Samples were run on a flow cytometer (CytoFlex S Flow Cytometer, Beckman Coulter, US). For analysis, Kaluza Analysis 2.1 software (Beckman Coulter) was used (Figure 2.2).

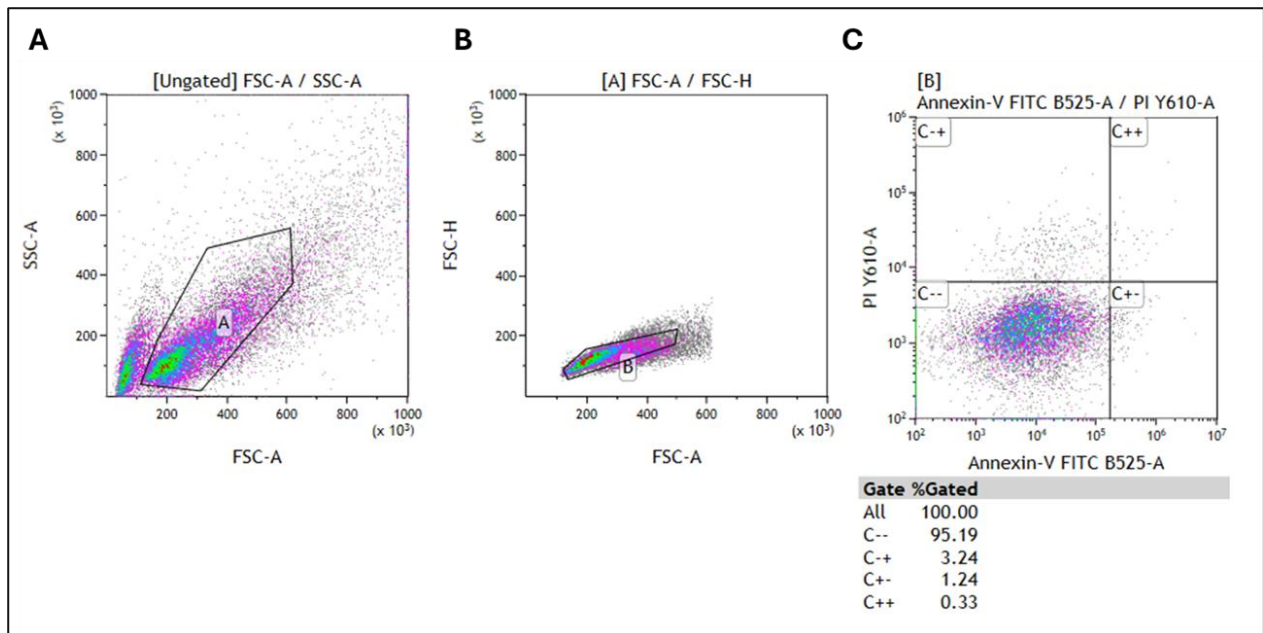


Figure 2.2. Gating strategy and apoptosis assessment of MCF-7 cells using Annexin V-FITC and Propidium Iodide (PI) dual staining, analysed by flow cytometry with Kaluza Analysis Software (Beckman Coulter). (A) Forward and Side Scatter Plot (FSC-A/SSC-A): The initial gating strategy involved selecting the main population of viable cells while excluding debris and dead cells. A region “A” was drawn to isolate intact cells based on their forward scatter area (FSC-A) and side scatter area (SSC-A). (B) Doublet Discrimination (FSC-A/FSC-H): To ensure single-cell analysis, forward scatter height (FSC-H) was plotted against forward scatter area (FSC-A). A gating region “B” was applied to eliminate doublets and aggregates, ensuring only single events were analysed for apoptosis quantification. (C) Apoptosis Assessment via Annexin V/PI Staining: Cells were stained with Annexin V-FITC (B525-A) and Propidium Iodide (PI Y610-A) to differentiate between viable, early apoptotic, and late apoptotic/necrotic populations. The quadrant gating strategy was applied: C-- (Bottom left quadrant): Viable cells, negative for both Annexin V and PI. C+ - (Bottom right quadrant): Early apoptotic cells, Annexin V-positive but PI-negative. C-+ (Top left quadrant): Necrotic cells, PI-positive but Annexin V-negative. C++ (Top right quadrant): Late apoptotic/necrotic cells, positive for both Annexin V and PI. The percentage of cells in each quadrant was calculated, showing 3.24% early apoptotic cells (C+ -), 1.24% necrotic cells (C- +), and 0.33% late apoptotic/necrotic cells (C+ +), indicating the apoptotic response of MCF-7 cells under experimental conditions.

2.12 Cell Mito Stress assay

Real-time oxygen consumption rates (OCR) and extracellular acidification rates (ECAR) measurements were determined using the Seahorse Extracellular Flux (XF96) analyser (Seahorse Bioscience, MA, USA), and the Seahorse XF Mito Stress test kit was used (103015-100, Agilent Technologies).

Cells were plated in XF96 cell culture microplate at a concentration of 80k cells/well (MCF-7 and MDA-MB-436), cells then incubated at 37°C in a 5% CO₂ incubator overnight to allow the cells to adhere and reach the desired confluency. In the next day, the growth medium was replaced with the seahorse DMEM medium that was brought to 7.4 Ph (103680-100, Agilent Technologies) and supplemented with 10 mM glucose (103577-100, Agilent Technologies), 1mM pyruvate (103578-100, Agilent Technologies) and 2 mM glutamine (103579-100, Agilent Technologies). Then the cells were incubated for one hour at 37°C in a non-CO₂ incubator. Before the assay day, the XF sensor cartridge was hydrated with Seahorse XF calibrant (102416-100, Agilent Technologies) and incubated for 24 hours at 37°C in a non-CO₂ incubator. The cartridge was then loaded with sequential injections of 1.5µM Oligomycin, 2.00µM FCCP and 0.5 µM Rotenone/antimycin A into the designated ports.

After that, the Pierce BCA Protein Assay Kit was used for protein quantification for normalisation. To analyse the OCAR and ECAR data, Agilent Seahorse Wave 2.6 software (Agilent Technologies, USA) was used. The first step is to upload the seahorse assay data file. Before proceeding with the data visualisation, normalisation was performed to account for variation in cell number or protein content. This was done via the selection of normalisation option and applying a correction factor, which was the BCA assay protein values, then the normalisation method was “per µg of protein content”. The next step was to generate the appropriate graphs, which was done by navigating to the “Graph” section, and selecting OCR,

ECAR, energy map plot, basal respiration, ATP production, maximal respiration, spare respiration capacity and proton leak. Once the analysis was completed, the raw data were exported to GraphPad Prism software for further statistical analysis.

2.13 Co-Immunoprecipitation and mass spectrometry

To investigate any interaction between FEN1 and SLC7A5, Co-Immunoprecipitation (CO-IP) was used. First, CO-IP lysis buffer mix was prepared, which contains Protease Inhibitor (PI) cocktails (P8340-1ML, Sigma, UK), phenylmethylsulfonyl fluoride (PMSF) (10837091001, Sigma, UK) and dithiothreitol (DTT) (D0632, Sigma, UK).

Samples, lysate, antibody (FEN1/SLC7A5) and immunoglobulin G (IgG) (2918772, EMD Millipore, USA) were all prepared at a weight of 0.5 mg for each condition. Samples were incubated with the captured antibody for 3 hours at 4°C on the Eppendorf roller. Thereafter, PureProteome Protein A Magnetic Bead System (LSKMAGA10, Sigma, UK) were vortexed, and 50 µl was added to an empty clean 1.5 ml microcentrifuge tube for each condition, then the tubes were engaged on the magnetic stand for 30 seconds. The supernatant was removed with a pipette and discarded. The beads were disengaged from the magnetic stand and washed with 1 ml wash buffer (PBS+0.1 % Tween 20) for 5 minutes, then the beads were engaged again on the magnetic stand, and the supernatant was removed. This step was repeated 3 times. The beads were then washed 3 times with lysis buffer, this time for 5 minutes each time. Samples were then transferred to bead tubes and incubated for 2 hours at 4°C on an Eppendorf roller. The beads were reengaged on the magnetic stand, then the sample was removed from the tube, as the protein complex is now attached to the beads. Then the beads were washed 3 times with 500 µl lysis buffer for 5 minutes each on the roller. Beads were washed again with 1 ml wash buffer 3 times for 5 minutes each on the roller. 100 µl wash buffer was added to the beads, and then transferred into a fresh Eppendorf tube. The beads-

buffer mix they were engaged on a magnetic stand, and the supernatant was removed. Elution buffer was prepared by mixing 0.2 g of glycine with 200 ml of water, then 15 μ l of elution buffer was added per sample to the beads. After that, the Eppendorf was incubated on a hot plate with the shaker for 15 minutes at 56°C. Thereafter, the Eppendorf was engaged on the magnetic stand, and the supernatant was separated from the beads and transferred to a fresh Eppendorf. The samples were then neutralised to reach pH 7 by adding 1.5 μ l per sample of neutralisation buffer, which contains 1g of Tris and 1000 ml of water. Lamella buffer was added to the sample, and then the samples were kept in a -80°C freezer.

Samples were then prepared to be sent to mass spectrometry (Cambridge Centre for Proteomics) for liquid chromatography-tandem mass spectrometry runs (LC-MS/MS), 15 μ l of sample was loaded into the gel, then the samples were run at 80V for 5-8 minutes, the bands were then excised and transferred into 1.5 ml tubes that contained 50 μ l pure water.

2.14 Statistical Analysis

The statistical analysis was performed by using SPSS 26.0 statistical software (SPSS Inc., Chicago, IL, USA). A Chi-square test was conducted to examine the associations between categorical variables, including correlations with clinicopathological parameters and other biological biomarkers. Pearson's correlation coefficient was used to assess relationships between two continuous normalised datasets. Kaplan-Meier survival analysis and log-rank tests were performed to assess the association between biomarkers and clinical outcomes. Additionally, multivariate Cox regression analysis was conducted to determine the independent prognostic significance of specific biomarkers.

GraphPad Prism software version 10.0 (GraphPad Prism Inc., San Diego, CA, USA) was used for statistical analysis. In vitro, data were represented in mean \pm standard errors of the mean (SEM); experiments were done in three independent experiments. One-way analysis of variance (ANOVA) with Dunnett's multiple comparisons test, and two-way ANOVA with Šídák's multiple comparisons test were used to determine the significant differences between control and the other conditions. A P-value of <0.05 was considered significant.

Chapter 3 The prognostic significant of SLC7A5/FEN1 high expression in breast cancer

3.1 Introduction

Metabolic reprogramming is considered a hallmark of cancer, which is influenced by diverse factors, such as nutrient availability, the origin of tissue and cell-matrix adhesion and cell-cell interactions within the tumour microenvironment [161]. To meet the high demands of proliferation, cancer cells must alter their metabolic pathways. These changes are controlled by many oncogenic alterations which influence the cellular signalling pathways [69]. This results in the rapid generation of adenosine triphosphate (ATP) to maintain energy status, macromolecule biosynthesis via the excessive production of intermediates, and maintaining the redox homeostasis to decrease the effect of cellular reactive oxygen species (ROS) [162]. Altered glutamine metabolism is an example of metabolic reprogramming in cancer cells [1]. Many cancer cell types can become addicted to glutamine and stop proliferating or grow without it [69]. Glutamine metabolism is important for the biosynthesis of lipids, proteins and nucleotides. Solute carrier family 7 member 5 (SLC7A5) is one of the key cellular glutamine transporters, where its overexpression is seen in breast cancer (BC) [69]. SLC7A5 functions as an amino acid exchanger where it transports the intracellular glutamine in exchange for large neutral amino acids, such as tryptophan, phenylalanine and leucine, hence, it works as an amino acid supplier for cancer cells. Also, it maintains the intracellular levels of leucine [69], which is a key regulator of the mammalian target of rapamycin complex 1 mTORC1 signalling pathway, which plays an important role in the biosynthesis of nucleotides and enhances cell proliferation [154].

Increasing the availability of nucleotides for DNA repair via altered glutamine metabolism is essential for cancer cells, as a result of the high oxidative stress [163]. Several DNA repair mechanisms can be activated to encounter the damaged DNA, including single-strand breaks; base excision repair (BER), mismatch repair (MMR), nucleotide excision repair (NER), double-strand breaks; homologous recombination (HR) and non-homologous end joining (NHEJ)

[127]. However, the most commonly used pathway to encounter high oxidative stress in cancer cells is BER [128]. There are at least 30 proteins that are involved in either short-patch repair or long-patch BER [128]. One of the important enzymes used in long-patch BER is flap structure-specific endonuclease (FEN1). In addition to this, FEN1 plays a key role in DNA replication by helping Okazaki fragment maturation, it also maintains telomere stability and apoptosis [151]. The overexpression of FEN1 *mRNAs* as well as its protein is associated with poor survival outcome and aggressive breast cancer [151]. The high expression of DNA repair protein leads to genomic instability, which is one of the cancer hallmarks [101].

There is no confirmed connection between cancer metabolism and DNA repair pathways, however, it was suggested that there are three main principal links that connect cancer metabolism to DNA damage and repair mechanisms [163]. 1. Reactive oxygen species levels regulated via different metabolic pathways, hence regulating the DNA repair machinery, which is activated because of the oxidative DNA damage. 2. Chromatin remodelling through the regulation of acetyl- and methyl-group donors, which happen via different metabolic pathways, hence influencing the accuracy of double-strand break repair. 3. The availability of a nucleotide pool is affected by metabolic pathways that provide glutamine, aspartate and other important nutrients, which impact the synthesis of de novo nucleotide, and thereby influence the DNA repair response [163].

Although previous studies by Elanasri *et al.* and Madhusudan *et al.* have independently examined the effect of SLC7A5 and FEN1 in breast cancer [70, 151], the impact of their high expression has not been explored. In this chapter, the aim is to address this gap by evaluating the combined expression of SLC7A5 and FEN1 in breast cancer and its association with clinical outcomes.

3.1.1 Hypothesis

The high expression of both SLC7A5/FEN1 is associated with specific clinicopathological features and molecular biomarkers, and it serves as a potential prognostic marker in breast cancer patients.

3.1.2 Aims

1. To investigate, at mRNA and protein levels, the correlation of high expression of both SLC7A5 and FEN1 with clinicopathological parameters and relevant molecular biomarkers in large breast cancer cohorts.
2. To determine the prognostic value of the high expression of SLC7A5/FEN1 in breast cancer.

3.2 Methods

3.2.1 SLC7A5 and FEN1 genomic and transcriptomic analysis in breast cancer

METABRIC dataset (n=1,980) was used to determine the correlation between SLC7A5 and FEN1, further described in Chapter 2, Section 2.1.1.

To validate the results, the Breast Cancer Gene-Expression Miner v5.1 (bc-GenExMiner v5.1) online database was used further described in Chapter 2, Section 2.1.2.

The expression levels of SLC7A5 and FEN1 were categorised into high and low groups based on their respective median values.

3.2.2 SLC7A5/FEN1 protein expression in breast cancer

The expression of SLC7A5 and FEN1 proteins was evaluated in a cohort of 1108 and 648 patients, respectively. The patients with early-stage, primary operable invasive breast cancer presented to Nottingham City Hospital, UK, between 1986 and 2006. The clinicopathological parameters and biological markers associated with the expression of SLC7A5/FEN1 within the cohort were investigated. Survival data included breast cancer-specific survival (BCSS), distant metastasis-free survival (DMFS) and recurrence-free survival (RFS). Patient survival was censored if any of the following occurred: the patient was lost to follow-up, remained alive, or died from causes unrelated to breast cancer. The clinicopathological characteristics of this cohort are detailed in Chapter 2, Section 2.2.

The IHC staining and evaluation processes are described in detail in Chapter 2. In summary, IHC staining was conducted on TMA sections from invasive breast cancer patients using the Novolink polymer detection system. The sections were incubated overnight at 4 °C with an SLC7A5 antibody at a dilution of 1:200 (EPR17573, Abcam) and for 1 hour at room temperature or with FEN1 antibody at a dilution of 1:100 (NB100-321, Novus Biologicals). The evaluation of membranous staining for SLC7A5 and nuclear staining of FEN1 was performed using the H-score method. The staining and scoring of the amino acid transporter *SLC7A5*

was performed by Dr Rokaya El Ansari, as the cut-off was derived from the prediction of patient survival using X-tile (<https://medicine.yale.edu/lab/rimm/research/software.aspx>; Yale University) (high SLC7A5 expression=195 and low SLC7A5 expression=913) . For the DNA repair protein, FEN1 expression was categorised into high expression (n=159) and low expression (n=489) based on the median H-score value, which was 0. Blind double scoring was performed by a pathologist to evaluate the reliability of scoring. Cohen's kappa test showed a good reliability between the observers (0.851, $P=6.6 \times 10^{-15}$).

The specificity of FEN1 antibody was tested by using Western blotting Chapter 2 section 2.4, which was performed using whole lysates from BT-474, HCC1500, ZR-751, MDA-MB-231, MCF-7, MCF-10A and MCF10DCIS.

3.2.3 Statistical analysis

Statistical analysis was performed using SPSS software Version 28.0.0.0 (SPSS Inc., Chicago, IL, USA). To examine the correlation between SLC7A5 and FEN1, Pearson's correlation coefficient was used. For the association of the SLC7A5/FEN1 expression with clinicopathological parameters and hormonal receptor expression profile, the Chi-squared test. Kaplan-Meier and log-rank tests were used to evaluate the clinical outcomes. A multivariate Cox regression analysis was performed to determine independent prognostic factors. The P-value of <0.05 was considered statistically significant.

3.3 Results

3.3.1 FEN1 expression in breast cancer

The correlation between SLC7A5 and FEN1 in the METABRIC dataset showed a moderate positive correlation ($r=0.51$, $P=1.6 \times 10^{-128}$) (Figure 3.1A). The dataset bc-GenExMiner v5.1 was used for validation which showed a similar correlation (Figure 3.1B).

Western blot was used to validate FEN1 protein expression in different breast cancer cell lines, FEN1 bands were observed in BT-474, HCC-1500, ZR-751, MDA-MB-231, MCF-7, MCF10-A and MCF10-DCIS cell lines at around 50 kDa (Figure 3.2).

The expression of FEN1 protein was observed in the nucleus and cytoplasm of invasive breast cancer (Figure 3.3A and B). Within TMA cores, the staining intensity of FEN1 ranged from high ($n=159$) to low ($n=489$).

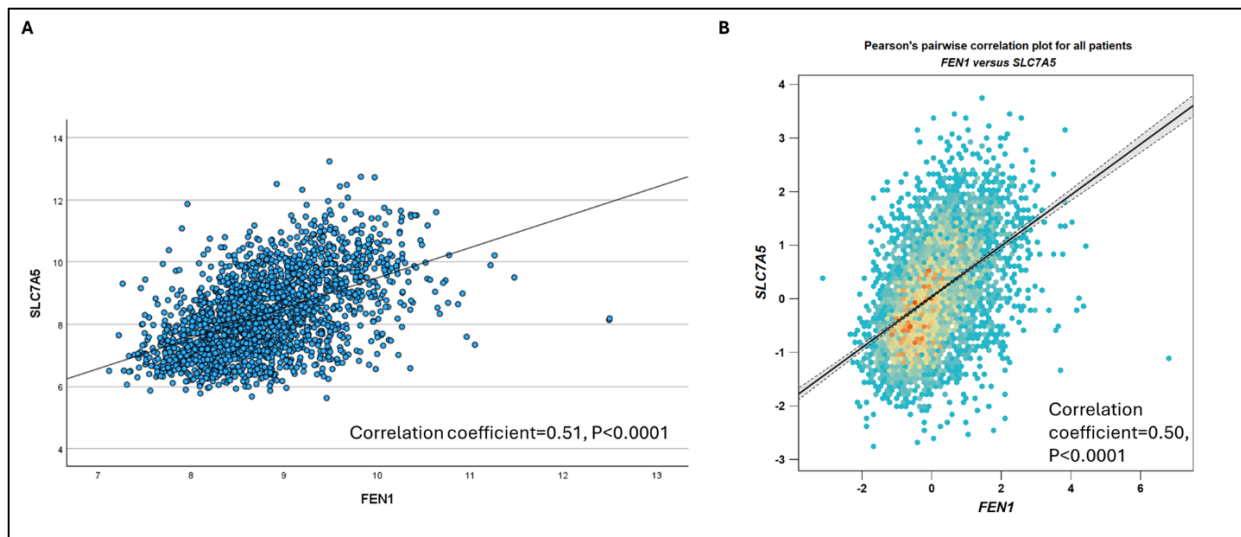


Figure 3.1. SLC7A5 mRNA correlation with FEN1 mRNA in METABRIC and GeneMiner datasets. (A) Scatter plot showing the positive correlation between SLC7A5 and FEN1 mRNA expression in the METABRIC dataset (correlation coefficient=0.51, $P < 0.0001$). (B) Similar correlation observed in the bc-GenExMiner v5.1 dataset (correlation coefficient=0.50, $P < 0.0001$).

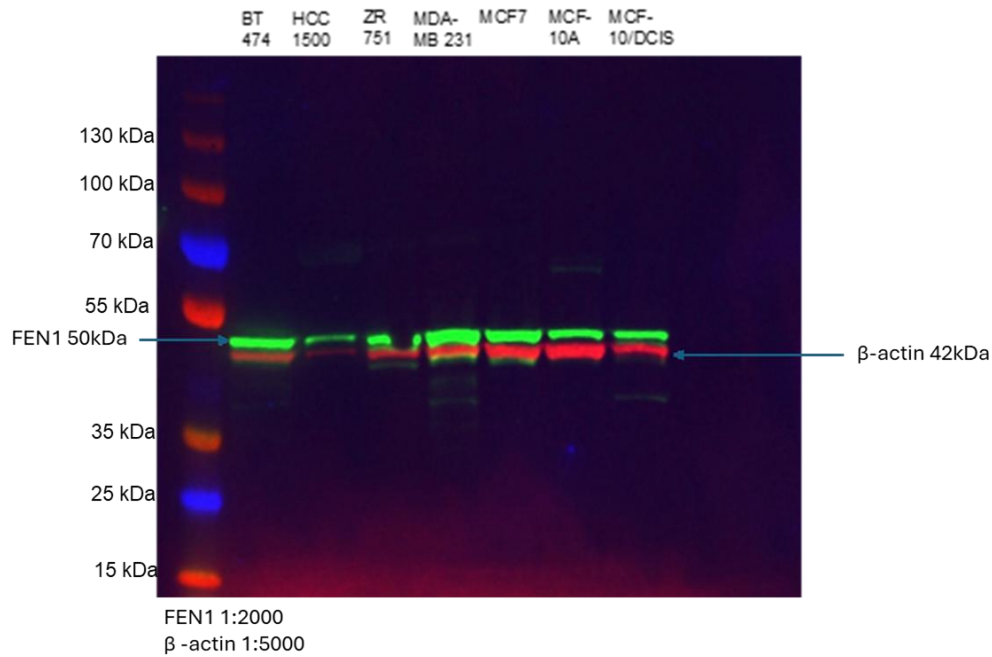


Figure 3.2. FEN1 protein expression in normal breast and breast cancer cell lines using Western Blot. Western blot was performed to assess FEN1 protein expression (50 kDa) across a panel of breast cancer cell lines including BT-474 (luminal B), HCC-1500 (Luminal A), ZR-751 (luminal B), MDA-MB-231 (triple-negative), MCF-10DCIS (triple-negative) and the normal-like mammary epithelial cell line MCF-10A. FEN1 was detected using an anti-FEN1 antibody (1:2000). β -actin (42 kDa) was used as a loading control and was detected using an anti- β -actin antibody (1:5000). Protein bands were visualised using IRDye conjugated secondary antibodies at the following concentration 1:15000 and imaged using the LI-COR Odyssey system. FEN1 is shown in green, and β -actin is shown in red.

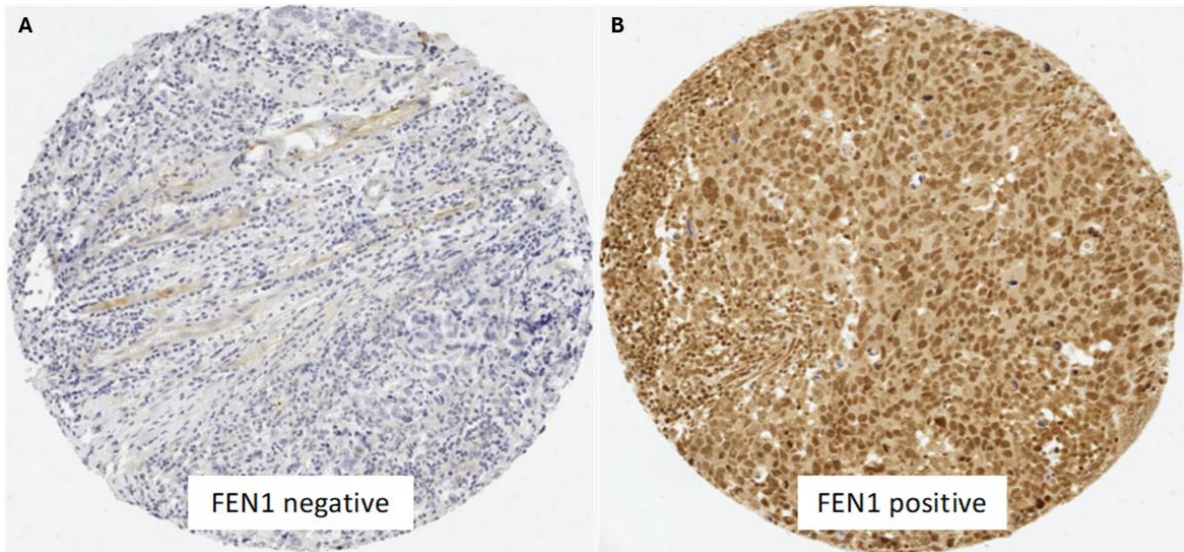


Figure 3.3. FEN1 protein expression in invasive breast cancer using immunohistochemistry (A) Representative image showing Low FEN1 protein expression, (B) High FEN1 protein expression. immunohistochemistry was performed using rabbit polyclonal primary antibody against FEN1, diluted at 1:100, with 1 hour incubation at 4 °C. Positive immunoreactivity is detected in the nucleus and cytoplasm of the invasive breast cancer cells. Magnification x20.

3.3.2 SLC7A5/FEN1 association with clinicopathological parameters in breast cancer

To explore the prognostic value of SLC7A5 and FEN1 high expression at both mRNA and protein levels in breast cancer, the cases were split into four subgroups: high SLC7A5/high FEN1 expression (SLC7A5+FEN1+), high SLC7A5/low FEN1 expression (SLC7A5+FEN1-), low SLC7A5/high FEN1 expression (SLC7A5-FEN1+) and low SLC7A5/low FEN1 expression (SLC7A5-FEN1-). In the METABRIC mRNA dataset, the group sizes were: SLC7A5+FEN1+ (n=692), SLC7A5+FEN1- (n=316), SLC7A5-FEN1+ (n=297) and SLC7A5-FEN1- (n=664). Similarly, in the Nottingham protein expression cohort, the group sizes were: SLC7A5+FEN1+ (n=20), SLC7A5+FEN1- (n=70), SLC7A5-FEN1+ (n=87) and SLC7A5-FEN1- (n=271).

The high expression of both SLC7A5 and FEN1 mRNA was significantly associated with larger tumour size, higher tumour grade, positive lymph node stage and poor Nottingham prognostic index (NPI) (Table 3.1; all $P < 0.01$). SLC7A5+FEN1+ subgroup protein expression was consistent with mRNA analysis for size, grade and NPI (Table 3.2; $P < 0.01$) but not lymph node stage (Table 3.2; $P = 0.5$).

3.3.3 SLC7A5/FEN1 high expression association with breast cancer biomarkers

The subgroup SLC7A5+FEN1+ mRNA was associated with negative ER and PR tumours and HER2-positive tumours (Table 3.1; all $P < 0.01$). Despite this, SLC7A5+FEN1+ mRNA was associated with TN tumours (Table 3.1; $P < 0.01$). Furthermore, investigation of SLC7A5+FEN1+ mRNA in intrinsic (PAM50) subtypes showed primarily in luminal B, HER-2 and basal subtypes (Table 3.1; $P < 0.01$).

The subgroup SLC7A5+FEN1+ protein expression showed similar results (Table 3.2; all $P < 0.01$), except for the HER2 status, where SLC7A5+/FEN1- was associated with HER2-positive breast cancer (Table 3.2; $P < 0.05$). Also, SLC7A5+FEN1+ protein expression showed high expression of the proliferation marker Ki67 (Table 3.2; $P < 0.01$).

Table 3.1. Clinicopathological and molecular biomarkers association of SLC7A5/FEN1 mRNA expression in breast cancer

Parameters	SLC7A5/FEN1 mRNA				P-value
	SLC7A5-FEN1- n (%)	SLC7A5-FEN1+ n (%)	SLC7A5+ FEN1- n (%)	SLC7A5+ FEN1+ n (%)	
Tumour size					0.00008
< 2.0cm	345 (40)	123 (14)	129 (15)	261 (30)	
≥ 2.0cm	333 (30)	180 (17)	171 (16)	410 (38)	
Grade					2.6×10⁻⁹⁸
1	129 (76)	14 (8)	15 (9)	12 (7)	
2	366 (48)	149 (19)	128 (17)	127 (17)	
3	148 (16)	131 (14)	146 (15)	527 (55)	
Lymph Node Stage					0.00005
1	407 (39)	165 (16)	147 (14)	316 (31)	
2	190 (31)	92 (15)	102 (16)	138 (38)	
3	83 (26)	49 (16)	58 (18)	126 (39)	
NPI					2.7×10⁻⁵¹
GPG	362 (54)	113 (17)	99 (15)	103 (15)	
MPG	275 (25)	157 (14)	178 (16)	483 (44)	
PPG	27 (14)	27 (14)	39 (20)	106 (53)	
ER					3.9×10⁻⁹⁶
Positive	642 (43)	295 (20)	228 (15)	341 (22)	
Negative	41 (9)	12 (3)	79 (17)	342 (72)	
PR					2.5×10⁻⁵⁸
Positive	493 (47)	200 (19)	143 (14)	204 (20)	
Negative	190 (20)	107 (11)	164 (17)	479 (51)	
HER2					2.1×10⁻²⁸
Positive	26 (11)	17 (7)	47 (19)	157 (64)	
Negative	657 (38)	290 (17)	260 (15)	526 (30)	
Triple Negative					1.8×10⁻⁶²
No	654 (39)	303 (18)	255 (15)	448 (27)	
Yes	29 (9)	4 (1)	52 (16)	235 (73)	
PAM50 Subtype					9.0×10⁻²⁰²
Luminal A	441 (62)	91 (13)	124 (17)	57 (8)	
Luminal B	82 (17)	156 (32)	57 (12)	190 (39)	
HER2	14 (9)	24 (10)	49 (20)	153 (64)	
Basal	15 (5)	9 (3)	35 (11)	270 (82)	
Normal-like	110 (56)	15 (8)	50 (26)	21 (11)	

NPI: Nottingham prognostic index; **GPG:** Good prognostic group; **MPG:** Moderate prognostic group; **PPG:** Poor prognostic group. **P values in bold mean statistically significant.**

Table 3.2. Clinicopathological and molecular biomarkers association of SLC7A5/FEN1 protein expression in breast cancer

Parameters	SLC7A5/FEN1 Protein				<i>P</i> -value
	SLC7A5-FEN1- n (%)	SLC7A5-FEN1+ n (%)	SLC7A5+ FEN1- n (%)	SLC7A5+ FEN1+ n (%)	
Tumour size					0.009
< 2.0cm	152 (66)	46 (20)	28 (12)	5 (2)	
≥ 2.0cm	119 (55)	41 (19)	42 (19)	15 (7)	
Grade					3.0x10⁻¹⁵
1	58 (82)	12 (17)	1 (1)	0 (0)	
2	110 (72)	36 (24)	7 (5)	0 (0)	
3	103 (46)	39 (17)	62 (28)	20 (20)	
Lymph Node Stage					0.5
1	171 (65)	48 (18)	35 (13)	11 (4)	
2	79 (54)	33 (22)	28 (19)	7 (5)	
3	21 (58)	6 (17)	7 (19)	2 (6)	
NPI					3.1x10⁻⁹
GPG	104 (78)	25 (19)	4 (3)	0 (0)	
MPG	137 (56)	51 (21)	45 (18)	14 (6)	
PPG	30 (44)	11 (16)	21 (31)	6 (9)	
Ki67					0.0002
Positive	112 (55)	34 (17)	45 (22)	14 (7)	
Negative	89 (67)	32 (24)	10 (8)	2 (2)	
ER					3.2x10⁻¹⁷
Positive	219 (72)	59 (19)	23 (8)	5 (2)	
Negative	50 (36)	27 (19)	47 (34)	15 (11)	
PR					1.3x10⁻⁹
Positive	175 (74)	39 (16)	20 (8)	4 (2)	
Negative	86 (44)	46 (24)	46 (24)	16 (8)	
HER2					0.04
Positive	34 (47)	18 (25)	18 (25)	3 (4)	
Negative	227 (63)	66 (18)	51 (51)	16 (4)	
Triple Negative					5.0x10⁻¹⁵
No	236 (69)	65 (19)	33 (10)	8 (2)	
Yes	25 (29)	19 (22)	31 (36)	12 (14)	
Molecular subtypes					1.8x10⁻¹²
Luminal A	77 (74)	24 (23)	3 (3)	0	
Luminal B	84 (67)	22 (18)	15 (12)	4 (3)	
HER2	17 (47)	6 (17)	10 (28)	3 (8)	
Basal	25 (29)	19 (22)	31 (36)	12 (14)	

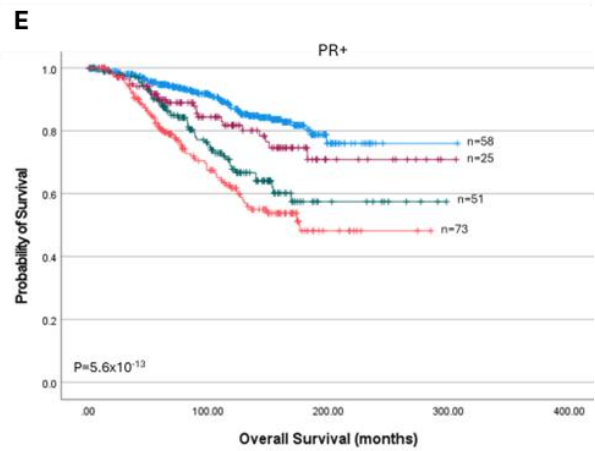
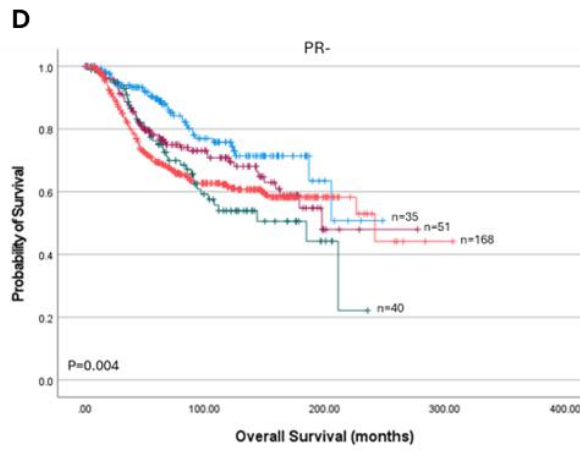
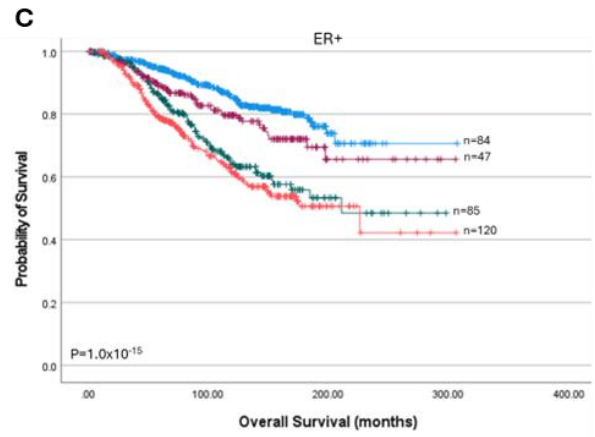
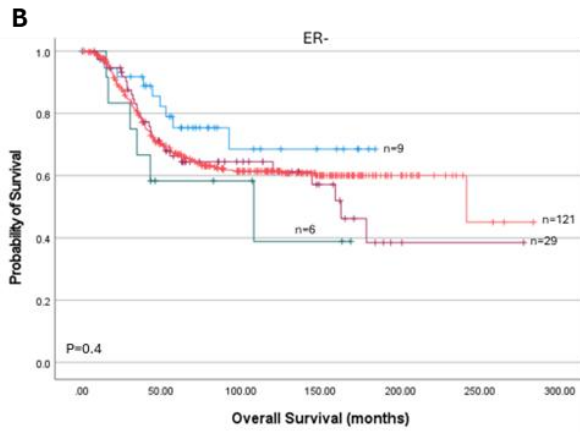
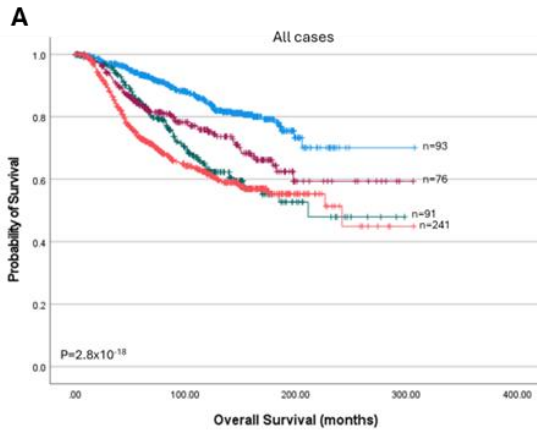
NPI: Nottingham prognostic index; **GPG:** Good prognostic group; **MPG:** Moderate prognostic group; **PPG:** Poor prognostic group. **TNBC:** Triple Negative Breast Cancer. **P values in bold mean statistically significant.**

3.3.4 Prognostic value of high SLC7A5/high FEN1 expression

SLC7A5+FEN1+ mRNA was associated with poor patient outcome in all cases (Figure 3.4A; $P=2.8 \times 10^{-18}$). Moreover, SLC7A5+FEN1+ was associated with worse patient outcomes in ER+ (Figure 3.4C; $P=1.0 \times 10^{-15}$), PR+ (Figure 3.4E; $P=5.6 \times 10^{-13}$), HER2- (Figure 3.4F; $P=1.1 \times 10^{-15}$) and non-triple negative tumours (Figure 3.4H; $P=1.5 \times 10^{-18}$). Multivariate Cox-regression showed that SLC7A5+FEN1 mRNA expression was a predictor of shorter overall survival independent of tumour size and lymph node stage in all cases and ER+ breast cancer (Table 3.3; $P=4.4 \times 10^{-7}$), but not ER- breast cancer (Table 3.3; $P>0.05$).

At the protein level, SLC7A5+FEN1+ tumours were similarly associated with worse patient outcome in terms of BCSS: all cases (Figure 3.5A; $P=0.001$), ER+ (Figure 3.5C; $P=0.00003$), PR+ (Figure 3.5E; $P=0.0007$), HER2- (Figure 3.5F; $P=0.001$) and non-triple negative tumours (Figure 3.5H; $P=0.001$). Moreover, SLC7A5+FEN1+ was significantly associated with shorter DMFS: in all cases (Figure 3.6A; $P=0.012$), ER+ (Figure 3.6C; $P=0.001$), PR+ (Figure 3.6E; $P=0.02$) and triple negative tumours (Figure 3.6I; $P=0.01$). SLC7A5+FEN1+ was also associated with poor RFS in all cases (Figure 3.7A; $P=0.03$), ER+ (Figure 3.7C; $P=0.002$), PR+ (Figure 3.7E; $P=0.003$), HER2- (Figure 3.7F; $P=0.03$) and non-triple negative tumours (Figure 3.7H; $P=0.01$).

Multivariate Cox-regression analysis was used to investigate the independent prognostic value of SLC7A5+FEN1+ protein in all cases, as well as in tumours characterised as ER+ and ER- separately. The results showed that the SLC7A5+FEN1+ subgroup was a predictor of reduced survival and distant metastasis in all cases and tumours characterised with ER+ (Table 3.4; all $P<0.05$), but not in tumours characterised as ER- (Table 3.4).



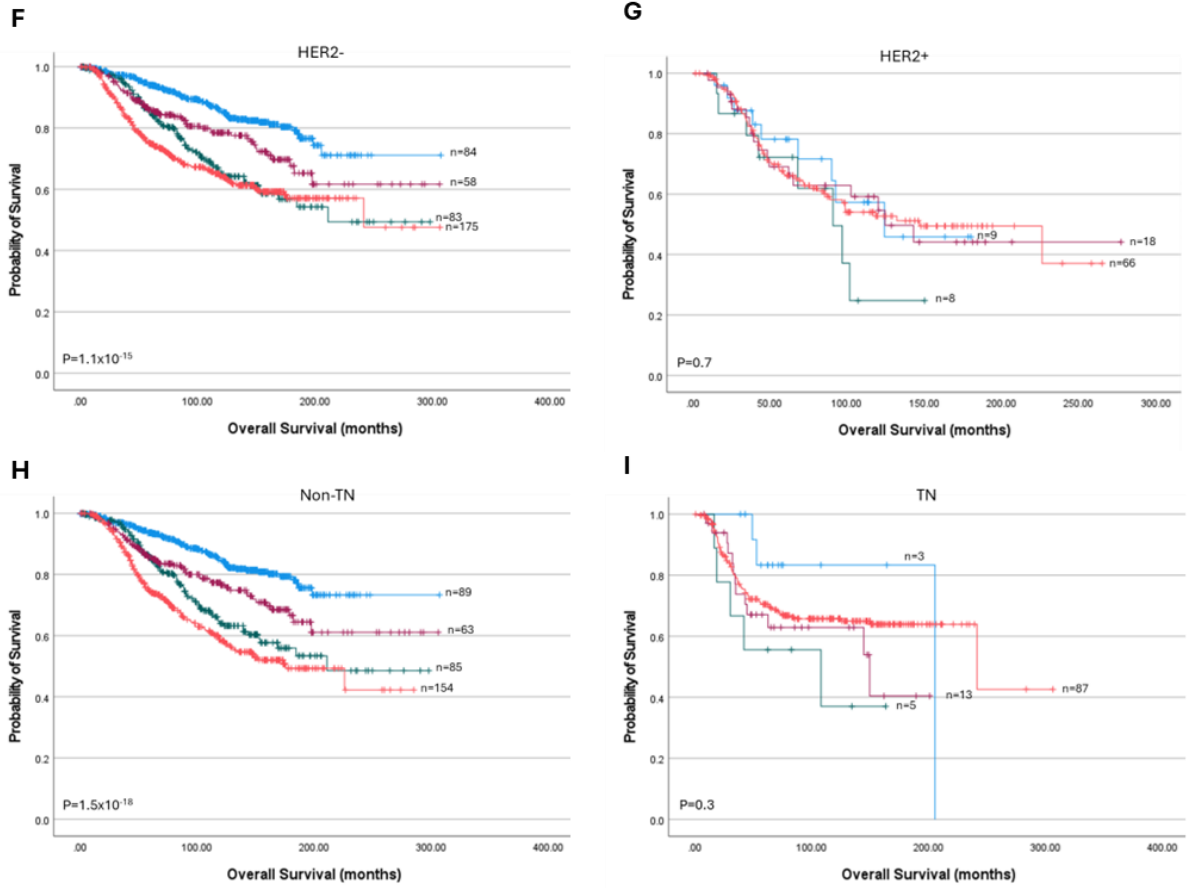
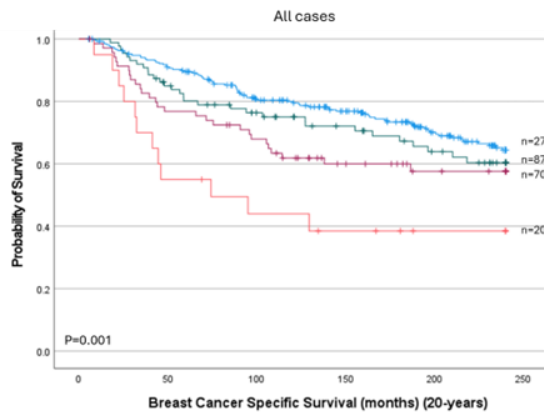
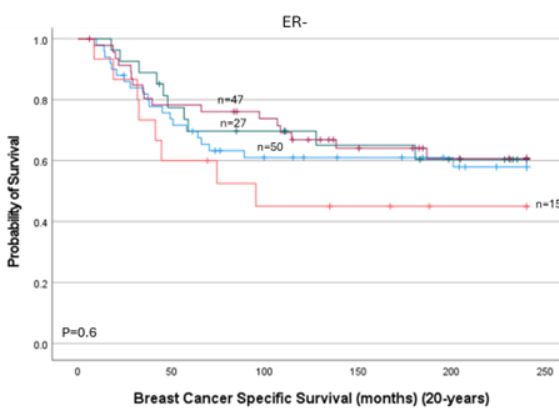
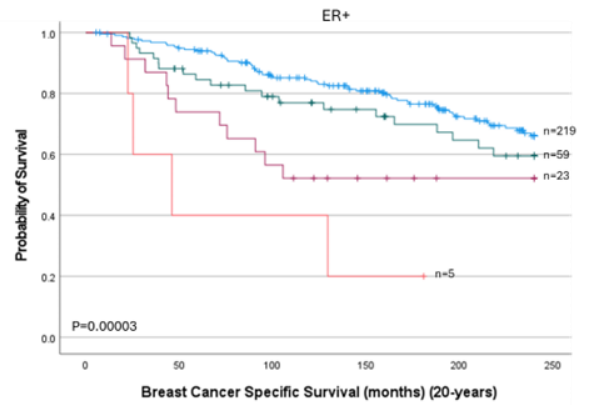
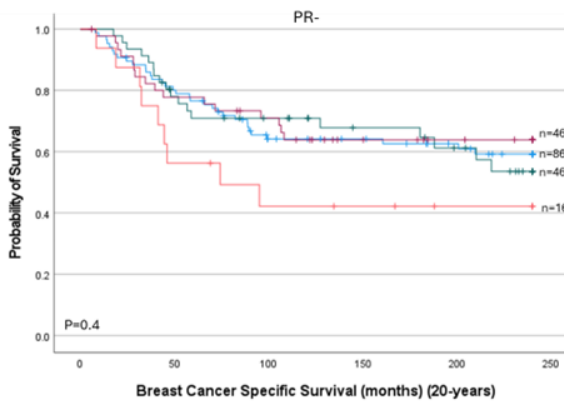
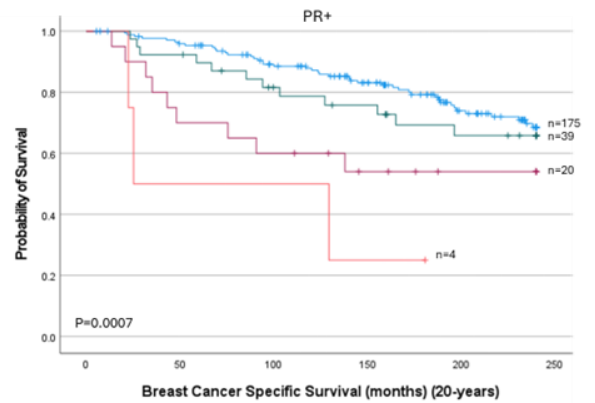


Figure 3.4. SLC7A5/FEN1 mRNA expression in breast cancer patient outcome using the METABRIC cohort. (A) all cases, (B) ER-, (C) ER+, (D) PR-, (E) PR+, (F) HER2-, (G) HER2+, (H) Non-Triple Negative (Non-TN) and (I) Triple Negative (TN) breast cancer. Blue=SLC7A5-FEN1-, green=SLC7A5-FEN1+, purple=SLC7A5+FEN1- orange line= SLC7A5+FEN1+.

Table 3.3. Multivariate Cox analysis of associations between SLC7A5/FEN1 mRNA expression and clinicopathological parameters in all cases and ER+/- breast cancer patients.

Parameters	SLC7A5/FEN1 mRNA					
	All Cases		ER+		ER-	
	HR (95% CI)	<i>p</i> -value	HR (95% CI)	<i>p</i> -value	HR (95% CI)	<i>p</i> -value
SLC7A5-FEN1-	Reference		Reference		Reference	
SLC7A5-FEN1+	2.1 (1.5-2.8)	0.000002	2.2 (1.6-3.1)	4.6×10⁻⁷	1.8 (0.6-5.1)	0.3
SLC7A5+FEN1-	1.6 (1.2-2.2)	0.003	1.4 (0.9-2.0)	0.1	1.4 (0.6-3.0)	0.4
SLC7A5+FEN1+	2.2 (1.7-2.9)	4.3×10⁻⁹	2.6 (1.9-3.5)	1.1×10⁻⁹	1.2 (0.6-2.5)	0.6
Grade	1.2 (1.0-1.4)	0.08	1.1 (1.0-1.3)	0.4	0.9 (0.6-1.5)	0.8
Size	1.7 (1.4-2.1)	1.1×10⁻⁷	1.6 (1.2-2.0)	0.0002	1.7 (1.2-2.4)	0.002
Lymph Node Stage	1.9 (1.7-2.1)	2.6×10⁻²⁵	1.9 (1.6-2.2)	8.0×10⁻¹⁷	1.9 (1.6-2.4)	9.5×10⁻¹⁰

P values in bold mean statistically significant.

A**B****C****D****E**

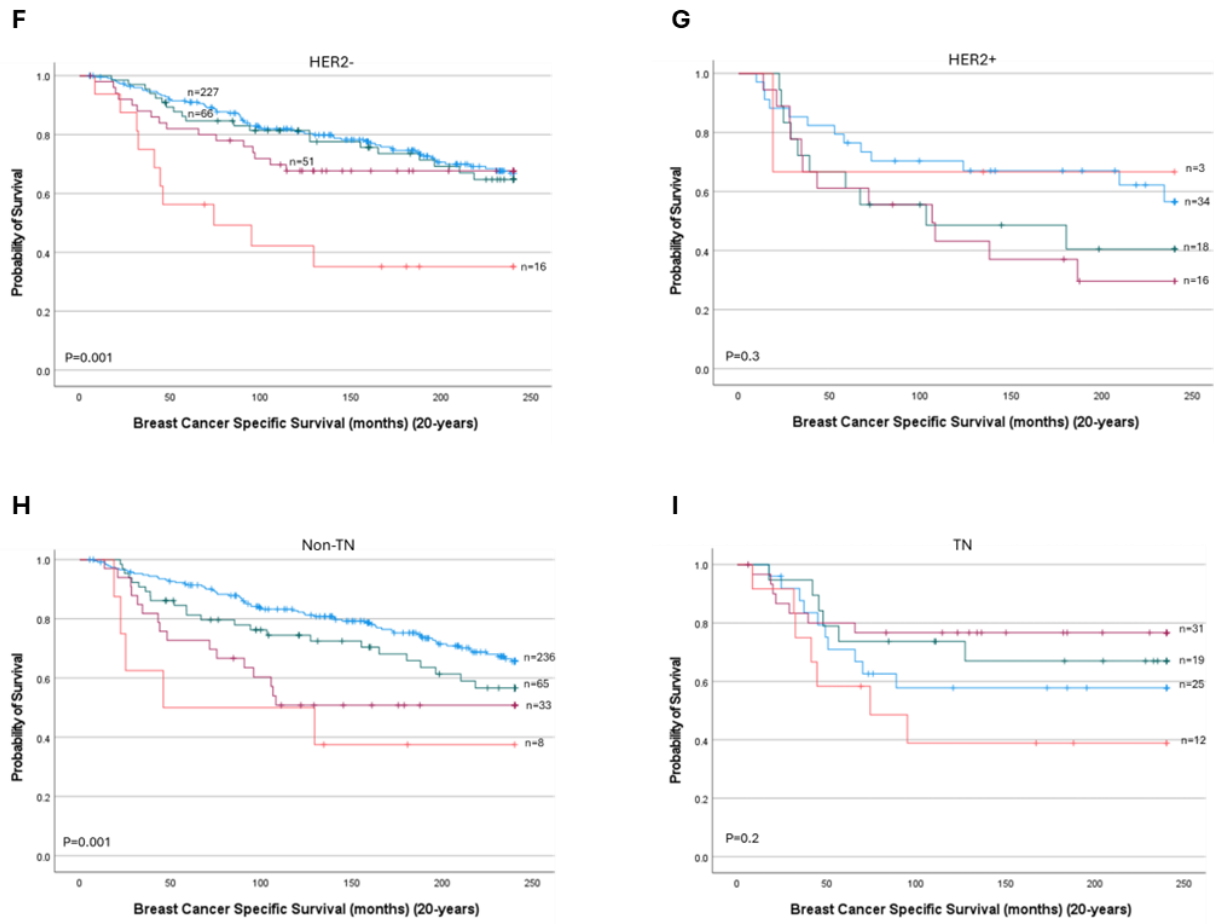
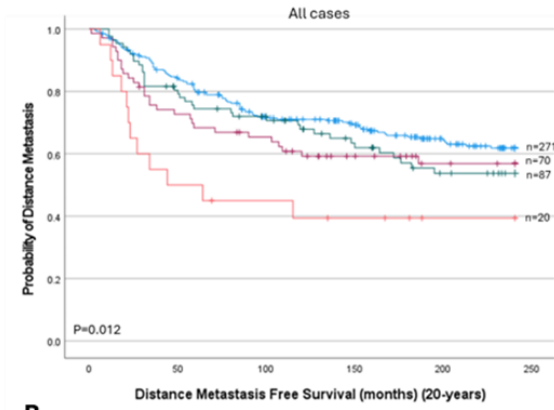
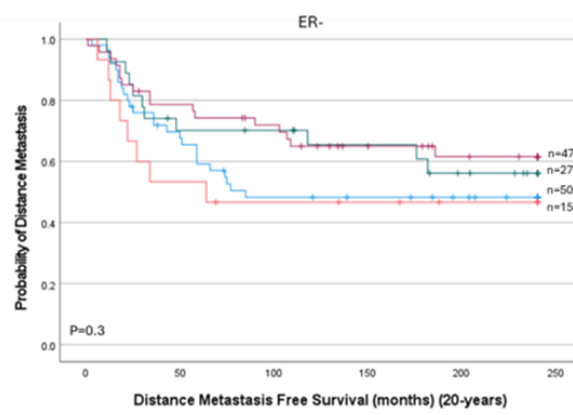
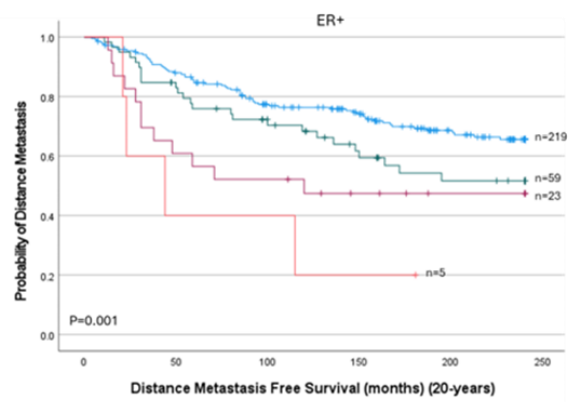
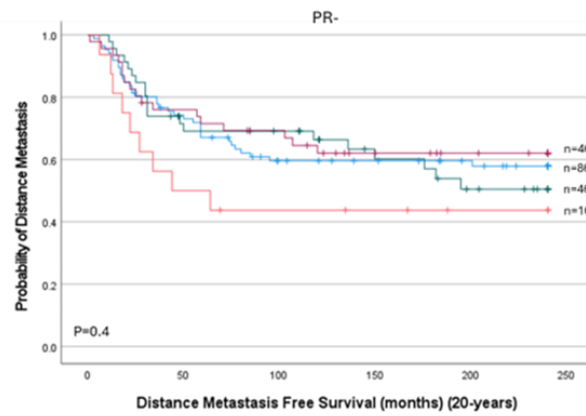
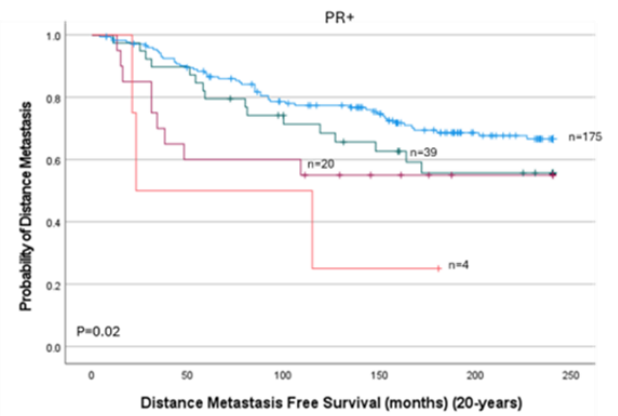


Figure 3.5. SLC7A5/FEN1 protein expression and its association with Breast Cancer Specific Survival (BCSS) in invasive breast cancer: A) FEN1/SLC7A5 in all cases, B) FEN1/SLC7A5 in ER-, C) FEN1/SLC7A5 in ER+, D) FEN1/SLC7A5 in PR-, E) FEN1/SLC7A5 in PR+, F) FEN1/SLC7A5 in HER2-, G) FEN1/SLC7A5 in HER2+, H) FEN1/SLC7A5 in Non-Triple Negative (Non-TN) and I) FEN1/SLC7A5 in Triple Negative (TN) in breast cancer. Blue line represents low FEN1 and low SLC7A5, Green line represents high FEN1 and low SLC7A5, purple line represents low FEN1 and high SLC7A5, and orange line represents high FEN1 and high SLC7A5.

A**B****C****D****E**

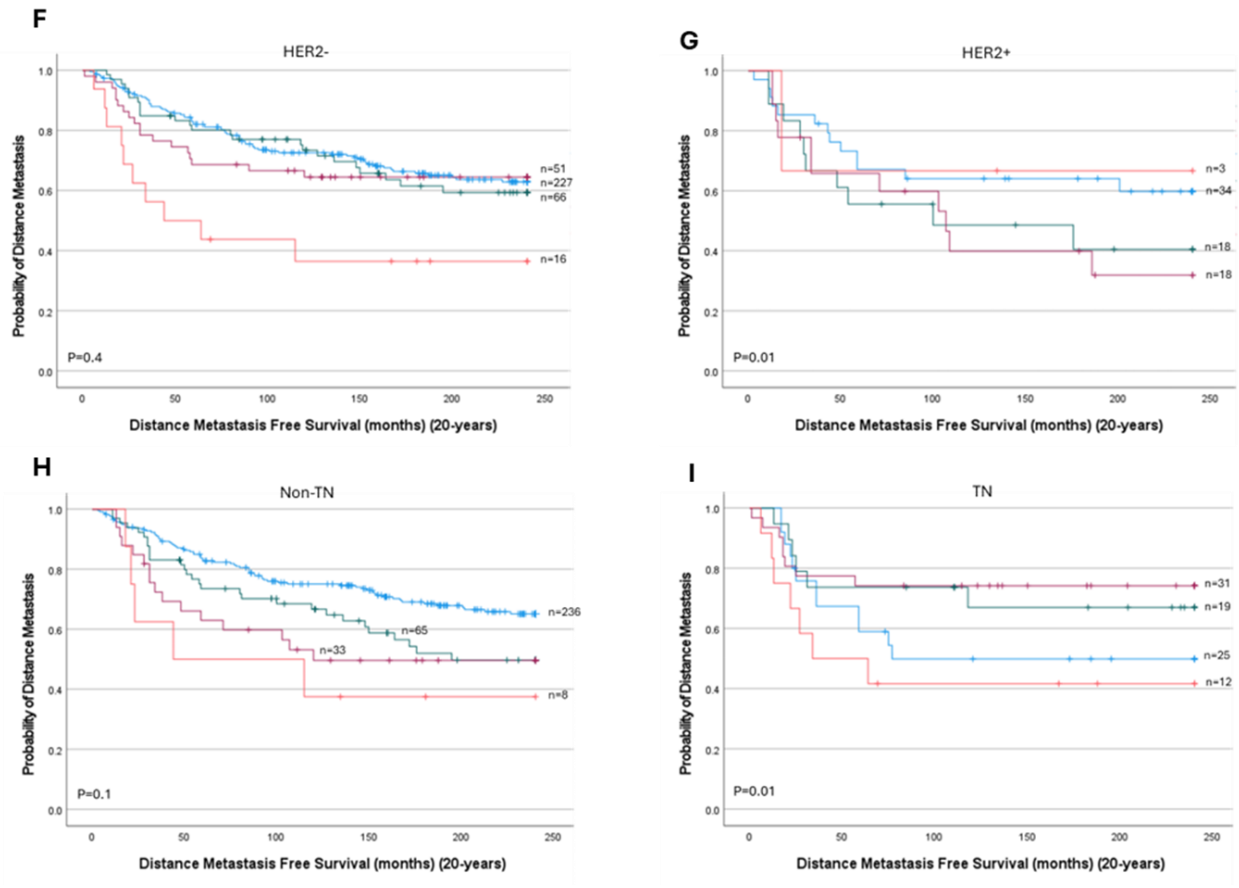
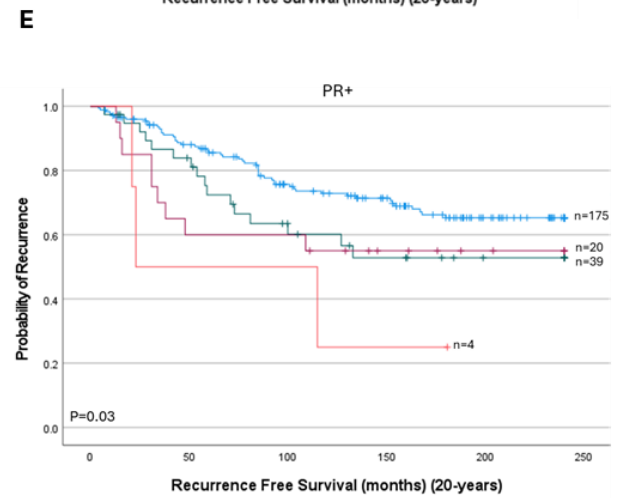
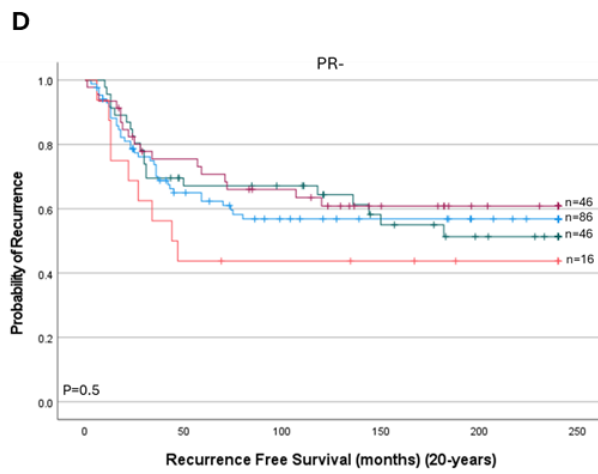
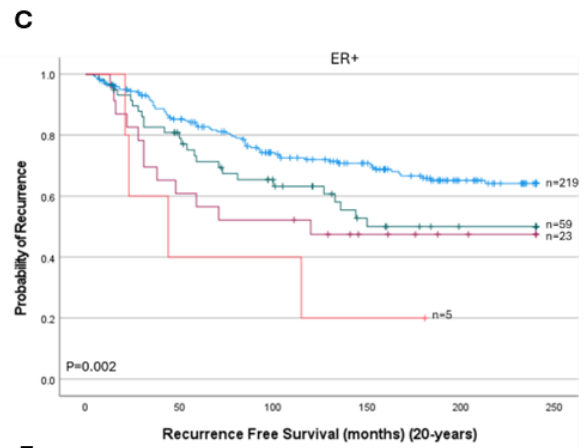
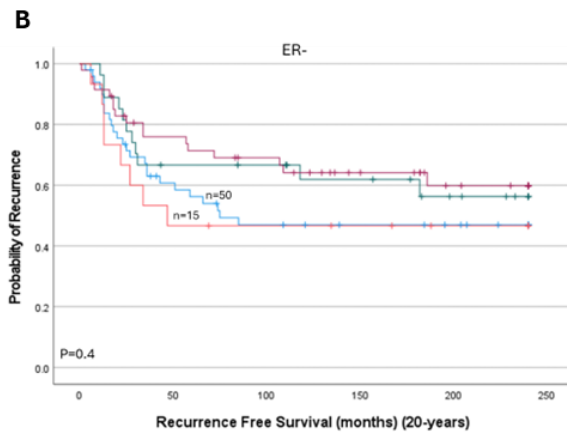
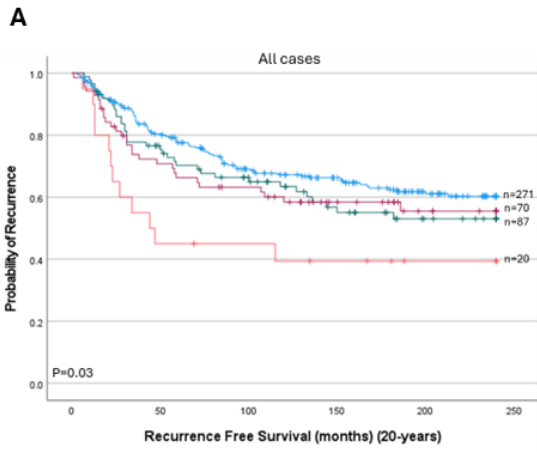


Figure 3.6. SLC7A5/FEN1 protein expression and its association with distance metastasis free survival (DMFS) in invasive breast cancer: A) FEN1/SLC7A5 in all cases, B) FEN1/SLC7A5 in ER-, C) FEN1/SLC7A5 in ER+, D) FEN1/SLC7A5 in PR-, E) FEN1/SLC7A5 in PR+, F) FEN1/SLC7A5 in HER2-, G) FEN1/SLC7A5 in HER2+, H) FEN1/SLC7A5 in Non-Triple Negative (Non-TN) and I) FEN1/SLC7A5 in Triple Negative (TN) in breast cancer. Blue line represents low FEN1 and low SLC7A5, Green line represents high FEN1 and low SLC7A5, purple line represents low FEN1 and high SLC7A5, and orange line represents high FEN1 and high SLC7A5.



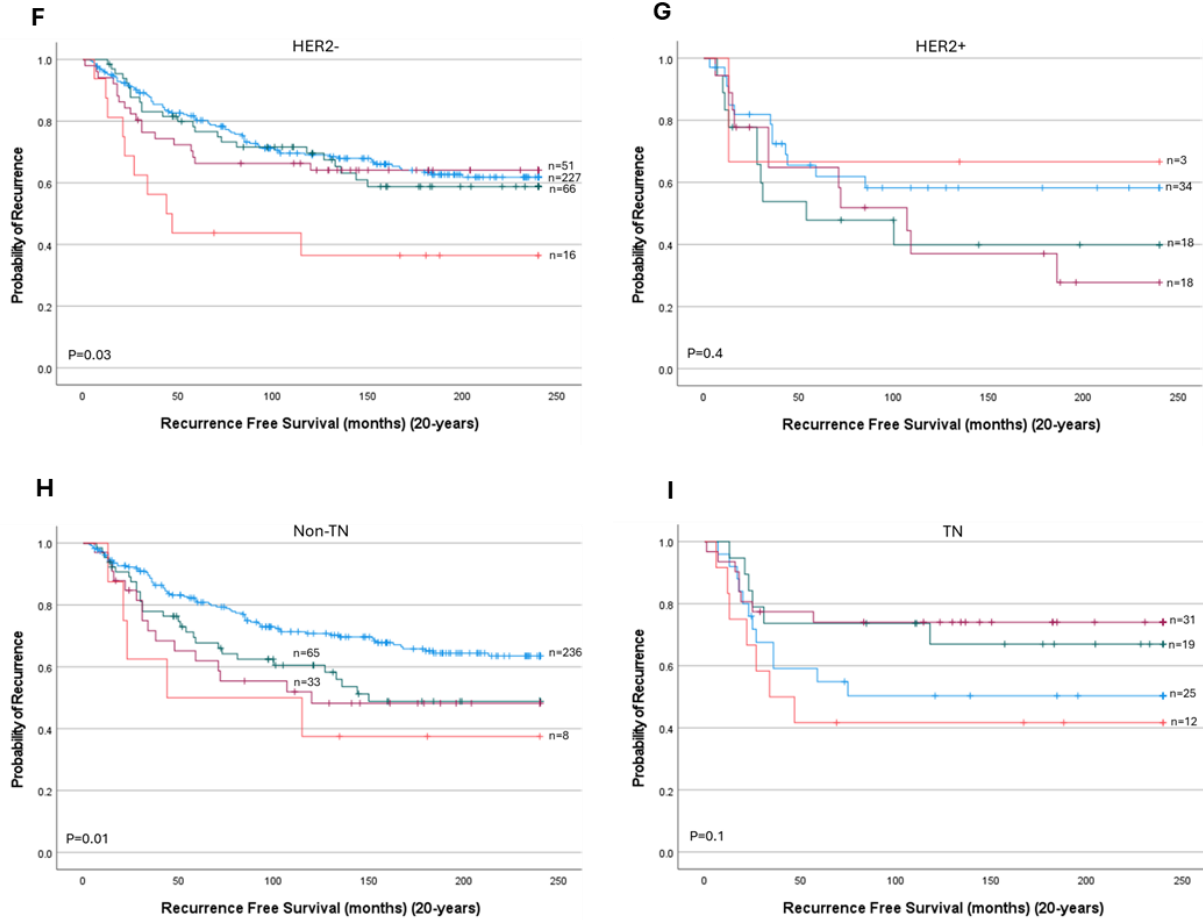


Figure 3.7. SLC7A5/FEN1 protein expression and its association with recurrence free survival (RFS) in invasive breast cancer: A) FEN1/SLC7A5 in all cases, B) FEN1/SLC7A5 in ER-, C) FEN1/SLC7A5 in ER+, D) FEN1/SLC7A5 in PR-, E) FEN1/SLC7A5 in PR+, F) FEN1/SLC7A5 in HER2-, G) FEN1/SLC7A5 in HER2+, H) FEN1/SLC7A5 in Non-Triple Negative (Non-TN) and I) FEN1/SLC7A5 in Triple Negative (TN) in breast cancer. Blue line represents low FEN1 and low SLC7A5, Green line represents high FEN1 and low SLC7A5, purple line represents low FEN1 and high SLC7A5, and orange line represents high FEN1 and high SLC7A5.

Table 3.4. Multivariate Cox analysis of associations between SLC7A5/FEN1 protein expression and clinicopathological parameters in all cases and ER+/- breast cancer patients.

<i>Breast Cancer Specific Survival</i>						
Parameters	All Cases		ER+		ER-	
	HR (95% CI)	p-value	HR (95% CI)	p-value	HR (95% CI)	p-value
SLC7A5-FEN1-	Reference		Reference		Reference	
SLC7A5-FEN1+	1.1 (0.7-1.7)	0.7	1.3 (0.8-2.2)	0.3	0.7 (0.3-1.6)	0.4
SLC7A5+FEN1-	1.3 (0.8-2.1)	0.2	2.1 (1.1-4.2)	0.03	0.8 (0.4-1.5)	0.4
SLC7A5+FEN1+	2.5 (1.3-4.7)	0.005	6.5 (2.2-9.1)	0.0001	1.3 (0.6-3.0)	0.6
Grade	1.2 (0.9-1.6)	0.2	1.2 (0.9-1.6)	0.3	1.3 (0.7-2.6)	0.4
Size	1.8 (1.3-2.5)	0.0009	2.1 (1.3-3.2)	0.001	1.4 (0.8-2.4)	0.3
Lymph Node Stage	2.3 (1.8-2.9)	1.1x10⁻¹¹	2.3 (1.7-3.1)	2.5x10⁻⁷	2.3 (1.5-3.3)	0.00002
<i>Distance Metastasis Free Survival</i>						
Parameters	HR (95% CI)	p-value	HR (95% CI)	p-value	HR (95% CI)	p-value
SLC7A5-FEN1-	Reference		Reference		Reference	
SLC7A5-FEN1+	1.2 (0.8-1.7)	0.5	1.5 (1.0-2.4)	0.08	0.6 (0.3-1.3)	0.2
SLC7A5+FEN1-	1.2 (0.8-1.9)	0.4	2.2 (1.2-4.2)	0.02	0.6 (0.3-1.1)	0.08
SLC7A5+FEN1+	2.3 (1.2-4.4)	0.01	4.5 (1.6-13.0)	0.005	1.2 (0.5-2.8)	0.6
Grade	1.0 (0.8-1.3)	0.7	1.0 (0.7-1.3)	0.9	1.1 (0.6-1.9)	0.7
Size	1.7 (1.2-2.3)	0.002	2.1 (1.4-3.2)	0.0003	1.0 (0.6-1.7)	0.9
Lymph Node Stage	2.2 (1.7-2.7)	1.4x10⁻¹¹	2.1 (1.6-2.8)	7.6x10⁻⁷	2.3 (1.6-3.3)	0.00001
<i>Recurrence Free Survival</i>						
Parameters	HR (95% CI)	p-value	HR (95% CI)	p-value	HR (95% CI)	p-value
SLC7A5-FEN1-	Reference		Reference		Reference	
SLC7A5-FEN1+	1.1 (0.8-1.5)	0.7	1.4 (0.9-2.1)	0.1	0.6 (0.3-1.3)	0.2
SLC7A5+FEN1-	1.1 (0.7-1.6)	0.6	1.5 (0.8-2.8)	0.2	0.7 (0.4-1.2)	0.2
SLC7A5+FEN1+	1.7 (0.9-3.2)	0.1	2.9 (1.0-8.0)	0.05	1.1 (0.5-2.4)	0.9
Grade	1.0 (0.8-1.2)	0.8	1.0 (0.7-1.2)	0.6	1.0 (0.6-1.7)	0.9
Size	1.3 (1.0-1.8)	0.03	1.6 (1.1-2.2)	0.01	1.0 (0.6-1.6)	1.0
Lymph Node Stage	1.9 (1.5-2.3)	7.0 x10⁻¹⁰	1.9 (1.5-2.5)	0.2x10⁻⁵	1.9 (1.3-2.6)	0.0004

P values in bold mean statistically significant.

3.4 Discussion

Alterations in the metabolic profile and genomic instability are two cancer hallmarks [1]. One of the examples of metabolic modulation in cancer cells is the changes in glutamine metabolism [69]. SLC7A5 is one of the most important transporters in glutamine metabolism, and it is highly expressed in breast cancer [70]. The main function of SLC7A5 is to supply cancer cells with amino acids and to maintain leucine intracellular levels in exchange for glutamine [70], in turn activating mTORC1, which plays a key role in the regulation of nucleotide biosynthesis, protein translation and cell growth [70]. Breast cancer cells exhibit high levels of oxidative stress, and as an adaptive response to this type of DNA damage, there is a high expression of the long-patch DNA base excision repair protein FEN1, which is involved in the repair of DNA base damage caused by oxygen reactive species [151]. This altered expression of DNA repair proteins leads to genomic instability [151]. In this Chapter, the prognostic significance of the combined high expression of SLC7A5 and FEN1 and their association with clinicopathological features and biomarkers in large cohort of breast cancer were explored.

In this Chapter, the results indicated that the high expression of SLC7A5 and FEN1 at both the mRNA and protein levels was associated with worse prognostic clinicopathological parameters, including larger tumour size and higher tumour grade. This was supported by other studies that addressed the prognostic value of SLC7A5 and FEN1 individually. In concordance with Elanasri *et al.* and Madhusudan *et al.*, high expression of SLC7A5 and FEN1 was correlated with poor clinicopathological parameters [70, 151].

With respect to breast cancer biomarkers, SLC7A5 and FEN1 high expression was associated with ER-, PR-, HER2+ and triple-negative tumours at both the mRNA and protein levels. Similar to a previous study, where SLC7A5 expression at both the mRNA and protein levels

in breast cancer patients were correlated with ER receptor negativity, PR receptor negativity and HER2 positivity [164]. Another recent study demonstrated that triple-negative breast cancer exhibited high expression of SLC7A5 in comparison to non-triple-negative tumours [165]. This was anticipated, as these tumours have higher demands for nutrients and energy to fuel their aberrant cell proliferation and continue surviving [69]. For FEN1 expression, it was reported that FEN1 expression was associated with breast cancer tumours characterised by HER2-positive tumours [166], triple negative, ER and PR negative tumours [167]. This reflects the importance of FEN1 in breast tumours that are characterised with different biomarkers, as FEN1 plays a critical role in the BER pathway which is responsible for the repair of oxidative base damage, this pathway is essential for breast cancer cells to overcome the DNA damage caused by the high oxidative stress [151]. Furthermore, analysis of the PAM50 breast cancer intrinsic subtypes revealed that high expression of SLC7A5 and FEN1 was particularly elevated in luminal B, HER2-enriched, and basal-like subtypes. These subtypes are characterised by higher proliferation rates and aggressive behaviour, consistent with the roles of SLC7A5 in supporting glutamine metabolism and FEN1 in maintaining DNA repair and genomic stability under oxidative stress [70, 151]. Elevated SLC7A5 expression has been previously associated with aggressive subtypes such as luminal B, HER2-positive and basal-like breast cancers [70, 164]. Similarly, FEN1 expression was shown to be elevated in luminal B, HER2+ and triple-negative tumours [151, 167]. Together, the high expression of SLC7A5 and FEN1 in these subtypes supports their potential role in promoting tumour cell survival and proliferation through metabolic adaptation and DNA repair.

In this study, the high expression of both SLC7A5 and FEN1 mRNA was correlated with worse OS in patients with tumours characterised with ER+, PR+, HER2- and non-triple negative, similarly at the protein level it was associated with worse patient outcome in terms of BCSS, DMFS and RFS. Moreover, the high expression of both SLC7A5 and FEN1 at both the mRNA and protein levels was associated with poor survival in multivariable analysis in the ER+ cohort. Previous studies demonstrated that high expression of SLC7A5 in breast tumours that

were characterised as ER+ had a poor survival outcome [167, 168]. Similarly, Madhusudan *et al* research group showed that the high expression of FEN1 protein (nuclear) was associated with worse survival outcome in ER+ breast cancer patients [151]. These findings indicate that the high expression of both SLC7A5 and FEN1 has prognostic significance in breast cancer.

There are currently no studies that have previously investigated the association between glutamine metabolism and DNA repair in breast cancer. It is reasonable to suggest that one of the ways that glutamine metabolism is associated with DNA repair mechanisms in breast cancer cells is the *de novo* nucleotide synthesis, which controls the availability of the nucleotide pool, hence increasing DNA repair pathway activities [162]. This happens through increasing the intracellular levels of leucine, in exchange for glutamine, in breast cancer cells, which is controlled by SLC7A5. Leucine activates the mTORC1, which controls the pentose phosphate pathway (PPP), hence generating ribose-5-phosphoribosyl-1-pyrophosphate (PRPP), which is required for the formation of purine and pyrimidine rings in nucleotides [154]. This increases the availability of the nucleotide pool, hence the activity of the FEN1 base excision DNA repair protein increases, as sufficient nucleotide supply is essential for gap-filling DNA synthesis during long-patch BER [162].

Here, it was shown that there is an association between SLC7A5 and FEN1. The study showed that the high expression of both SLC7A5 and FEN1 appeared to play a role as a prognostic biomarker in breast cancer patients. Exploring the pathways that link altered glutamine metabolism and DNA repair in different breast cancer subtypes will lead to the discovery of possible prognostic and predictive biomarkers that will guide to personalised treatment for breast cancer patients.

Chapter 4 Assessing the functional impact of SLC7A5 and FEN1 knockdown on breast cancer cell behaviour

4.1 Introduction

Breast cancer is a highly heterogeneous disease characterised by distinct molecular subtypes that influence prognosis and therapeutic response [69]. Among the key factors contributing to breast cancer progression are defects in metabolic reprogramming and DNA repair, which enable tumour cells to sustain proliferation, enhance metastatic potential and resist apoptosis [163]. SLC7A5 and FEN1 are two critical proteins implicated in these processes, making them potential therapeutic targets in breast cancer [70, 151].

Given their roles in metabolic regulation and DNA repair, SLC7A5 and FEN1 are likely to influence fundamental cancer cell behaviours, including proliferation, migration, invasion, cell cycle progression and apoptosis. The overexpression of SLC7A5 is linked to many types of cancers, including lung [168], gastric [169], pancreatic [170] and breast [171], where it promotes tumour growth by increasing the nutrient supply and enhancing metabolic signalling [70]. In breast cancer cell lines, such as MCF-7, overexpression of SLC7A5 is associated with a high proliferation rate [172]. Conversely, knockdown of SLC7A5 induces cell cycle arrest at the G1 phase in oesophageal cancer [173] and gastric cancer [174]. Additionally, inhibition of SLC7A5 expression in bladder cancer cells limits the ability of those cells to migrate [175].

Similarly, the upregulation of FEN1 contributes to the high proliferation rate in many tumours, such as lung [176], prostate [177], and breast [178]. In addition, the knockdown of FEN1 in cal-27, an oral squamous cell carcinoma cell line, decreases the cell proliferation rate, enhances the apoptosis rate and attenuates the migration ability of the cells [179]. Moreover, the downregulation of FEN1 in lung cancer cells causes cell cycle arrest at G1/S phase and G2/M phase [180]. These findings highlight the role of FEN1 in promoting cancer cell survival and proliferation.

There is growing interest in how metabolic pathways and DNA repair mechanisms are co-regulated in cancer [163]. Metabolic reprogramming has been shown to influence DNA repair capacity, suggesting a potential interplay between these two pathways [163]. However, despite this emerging evidence, direct studies linking SLC7A5 and FEN1 in breast cancer remain limited. Exploring their functional relationship would provide valuable insights into how metabolic adaptation and DNA repair coordination contribute to tumour progression.

Chapter 3 explored the clinical association between SLC7A5 and FEN1 expression in breast cancer cohorts. Building on those findings, the current chapter investigates their functional interplay using cell-based assays.

4.1.1 Hypothesis

SLC7A5 and FEN1 contribute to breast cancer cell survival, proliferation, and metastatic potential by regulating metabolic and DNA repair pathways. Their singular knockdown will reduce cell proliferation, impair migration and invasion, induce cell cycle arrest, and promote apoptosis, with a more profound effect in double knockdown conditions due to the combined distribution of metabolic homeostasis and DNA repair.

4.1.2 Aims

1. To assess the effect of single and double knockdown of SLC7A5 and FEN1 on cell proliferation in breast cancer cell lines.
2. To determine the impact of SLC7A5 and FEN1 single and double knockdown on cell migration and invasion.
3. To examine alterations in cell cycle progression following SLC7A5 and FEN1 single and double knockdown.
4. To determine whether the singular and double knockdown of SLC7A5 and FEN1 enhances apoptosis.

4.2 Methods

4.2.1 FEN1 and SLC7A5 cell transfection with small interfering RNA (siRNA)

MCF-7, MDA-MB-436, and MDA-MB-231 were transfected with two different siRNA constructs, primary construct and validation construct of FEN1 and SLC7A5, singular or combined, along with scrambled siRNA negative control as described in chapter 2 (section 2.5), FEN1 and SLC7A5 siRNA knockdown efficiency were validated by using western blotting as described in chapter 2 (section 2.4).

4.2.2 Cell proliferation and count

To investigate the effect of FEN1 and SLC7A5 on breast cancer cell proliferation. MTS assay and live-cell counting (described in Chapter 2, sections 2.6 and 2.7, respectively) were performed in three different breast cancer cell lines, including MCF-7, MDA-MB-436 and MDA-MB-231. Both singular and double knockdowns were assessed.

4.2.3 Wound healing assay and invasion assay

To assess the migration ability of breast cancer cell lines, a wound healing assay was conducted as described in chapter 2 (section 2.8). The wounds were observed by taking images several times via light microscopy (Leica DMI 3000B, Leica microsystems, Germany), at the following points, for MCF-7: Time (T) 0, T24, T48 and T72 hour (h), for MDA-MB-436: T0, T6, T12 and T15h, for MDA-MB-231: T0, T12, T24 and T48h. The time points were chosen based on the intrinsic migration rates of different breast cancer cell lines, allowing for the detection of significant differences in wound closure. Highly migratory cell lines, such as MDA-MB-436 and MDA-MB-231, were assessed at shorter intervals (T6-T15 and T12-T48, respectively) to capture their faster wound closure dynamics. In contrast, MCF-7 cells, which

exhibit slower migration, were monitored over a longer duration (up to 72 hours) to observe progressive changes [181].

Additionally, the time points were strategically selected to differentiate between the rapid migration observed in the control group and the potentially reduced migration in the experimental groups (singular knockdowns of FEN1 and SLC7A5, as well as double knockdown conditions).

The invasion assay was conducted as described in Chapter 2 (section 2.9).

4.2.4 Cell Cycle and Apoptosis

Cell cycle assay and apoptosis assay were conducted as described in Chapter 2 (sections 2.10 and 2.11, respectively). In the apoptosis experiment, the analysis focused exclusively on early apoptosis to determine the impact of SLC7A5 and FEN1 knockdown in breast cancer cell lines. Late apoptosis was excluded from the final interpretation to avoid potential confounding effects from secondary necrosis, which can arise due to prolonged cellular damage and compromise the accuracy of apoptotic measurements. Early apoptotic cells, identified by Annexin V positivity without propidium iodide staining, provide a more reliable indication of programmed cell death rather than necrotic cell death, which may result from unrelated stress or experimental conditions [182, 183].

4.2.5 Statistics

GraphPad Prism software version 10.0 (GraphPad Prism Inc., San Diego, CA, USA) was used for statistical analysis. In vitro, data were represented in mean \pm standard errors of the mean (SEM); all experiments were done in three independent experiments. One-way analysis of variance (ANOVA) with Dunnett's multiple comparisons test, and two-way ANOVA with Šídák's multiple comparisons test were used to determine the significant differences between the control and the other conditions. A P-value of <0.05 was considered significant.

4.3 Results

4.3.1 The effect of FEN1 and SLC7A5 knockdown on breast cancer cell proliferation

Western blot was used to determine the efficacy of FEN1 and SLC7A5 knockdown in MCF7, MDA-MB-436 and MDA-MB-231 (Figure 4.1,4.2,4.3 and 4.4).

In MCF-7 cells, FEN1 knockdown significantly reduced proliferation at 120h in comparison to control (Figure 4.5 A; $P < 0.01$), while the knockdown of SLC7A5 did not show a significant effect (Figure 4.5 B; $P > 0.05$). However, the double knockdown (DKD) condition showed a profound decrease in proliferation at 96h and 120h (Figure 4.5 C; $P < 0.01$ and $P < 0.001$, respectively). For the MDA-MB-436 cells, the singular knockdown of FEN1 and SLC7A5 showed a decrease in cell proliferation at 120h (Figure 4.5 D and E; $P < 0.05$). The DKD condition led to a further decline in proliferation across all time points (Figure 4.5 F; $P < 0.01$). A similar trend was observed in MDA-MB-231, as DKD led to the most significant suppression of proliferation (Figure 4.5 G, H and I; all $P < 0.05$).

In addition to the MTS assay, live-cell counting was performed to independently evaluate cell proliferation dynamics (Figure 4.6). In MCF-7 cells, singular knockdown of FEN1 and SLC7A5 showed a moderately significant reduction in cell numbers by 72h in comparison to the control (Figure 4.6 A; $P < 0.05$). The DKD significantly reduced cell numbers (Figure 4.6 A; $P < 0.05$).

In MDA-MB-436 and MDA-MB-231, live-cell counts followed a similar pattern, with DKD exhibiting the most substantial decrease in cell population at 72h in comparison to control (Figure 4.6 B and C; all $P < 0.001$). Notably, MDA-MB-231 was more sensitive to DKD at 72h, showing a significant decrease in comparison to the singular knockdown of FEN1 and SLC7A5 (Figure 4.6 C; all $P < 0.01$).

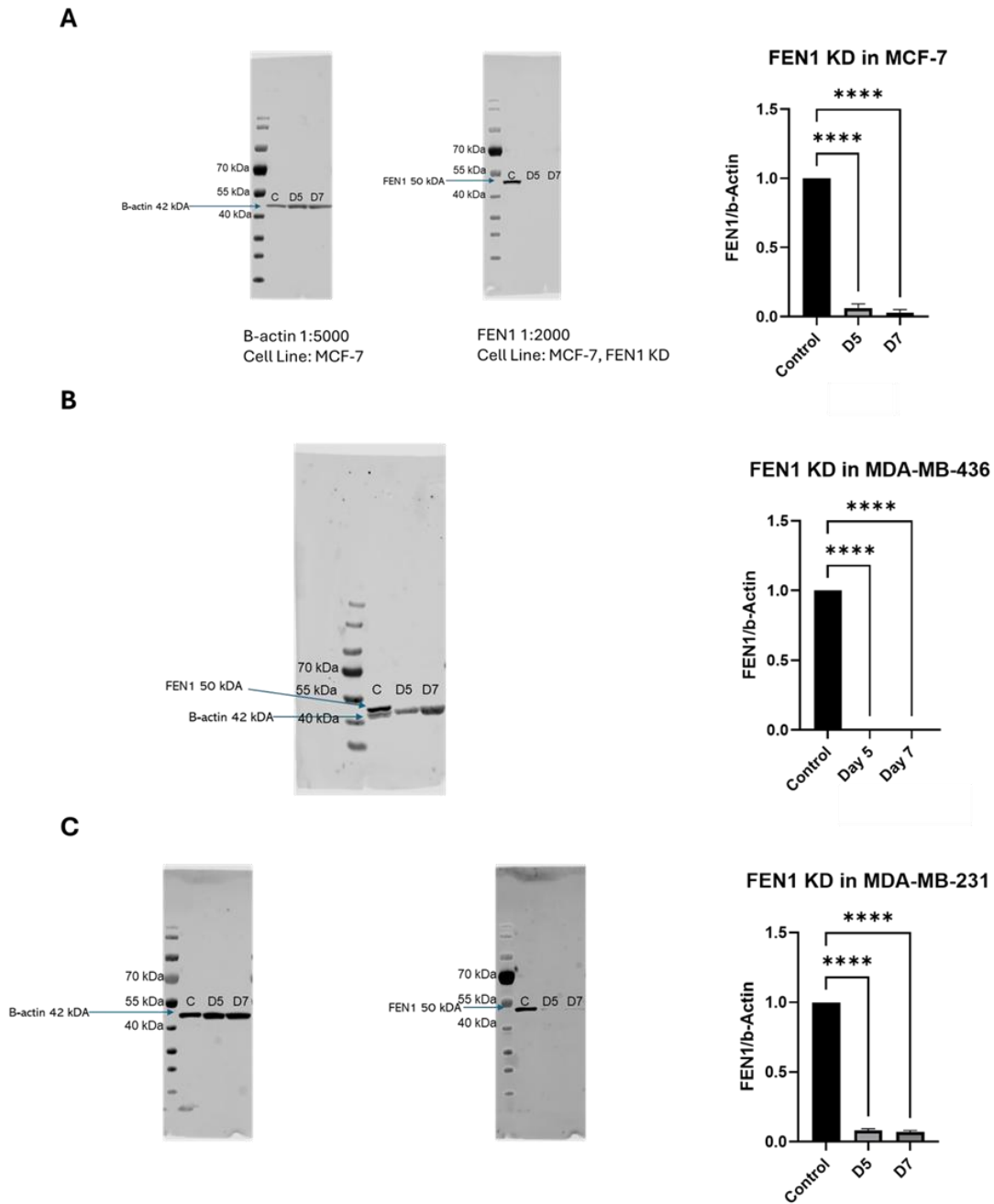


Figure 4.1. Validation of FEN1 knockdown efficiency using the primary siRNA construct in different breast cancer cell lines. (A-C) Western blot analysis was performed to assess FEN1 protein expression following siRNA mediated knockdown in (A) MCF-7, (B) MDA-MB-436, and (C) MDA-MB-231 breast cancer cell lines. β -actin was used as a loading control. Quantification of FEN1 expression levels, normalised to β -actin, is shown in the adjacent bar graphs. Data are presented as mean \pm standard errors from three independent experiments. Statistical significance was determined using one-way ANOVA, P-values ****<0.001, C, negative control; D5, day 5 post-knockdown; D7, day 7 post-knockdown.

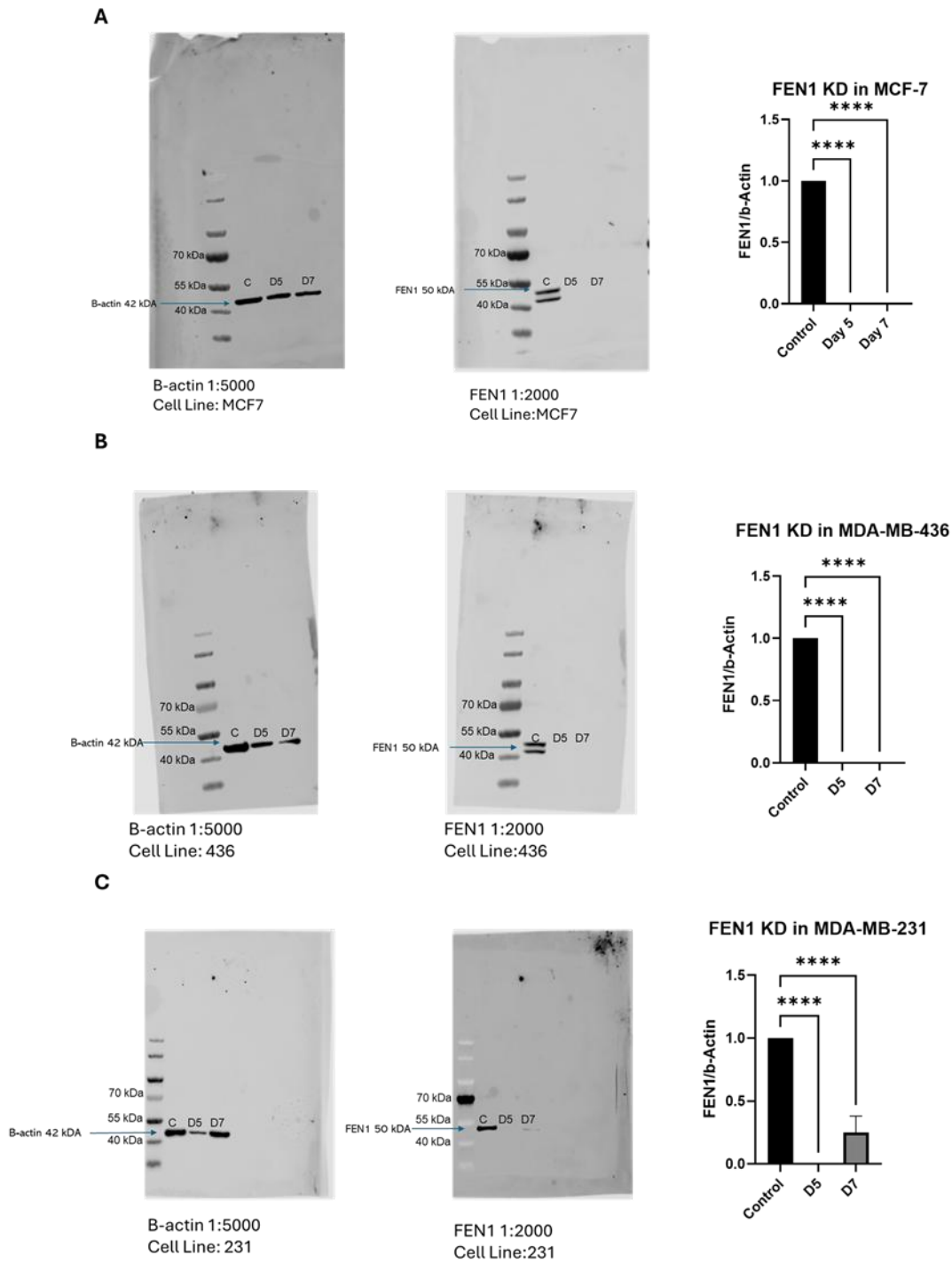


Figure 4.2. Validation of FEN1 knockdown efficiency using a second siRNA construct in different breast cancer cell lines. (A-C) Western blot analysis was performed to assess FEN1 protein expression following siRNA mediated knockdown in (A) MCF-7, (B) MDA-MB-436, and (C) MDA-MB-231 breast cancer cell lines. β -actin was used as a loading control. Quantification of FEN1 expression levels, normalised to β -actin, is shown in the adjacent bar graphs. Data are presented as mean \pm standard errors from three independent experiments. Statistical significance was determined using one-way ANOVA, P-values **** <0.001 , C, negative control; D5, day 5 post-knockdown; D7, day 7 post-knockdown.

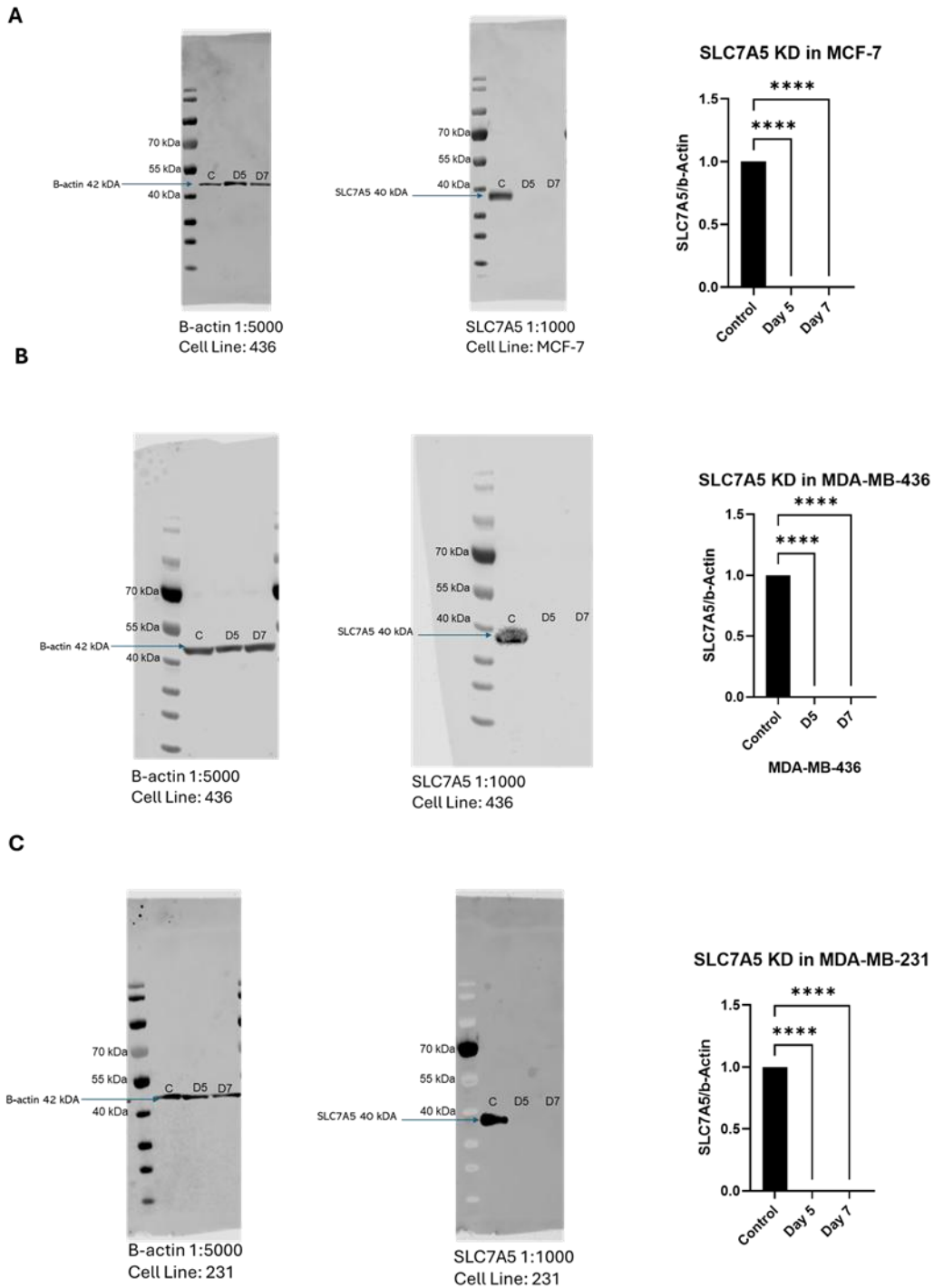


Figure 4.3. Validation of SLC7A5 knockdown efficiency using the primary siRNA construct in different breast cancer cell lines. (A-C) Western blot analysis was performed to assess SLC7A5 protein expression following siRNA mediated knockdown in (A) MCF-7, (B) MDA-MB-436, and (C) MDA-MB-231 breast cancer cell lines. β -actin was used as a loading control. Quantification of SLC7A5 expression levels, normalised to β -actin, is shown in the adjacent bar graphs. Data are presented as mean \pm standard errors from three independent experiments. Statistical significance was determined using one-way ANOVA, P-values ****<0.001, C, negative control; D5, day 5 post-knockdown; D7, day 7 post-knockdown.

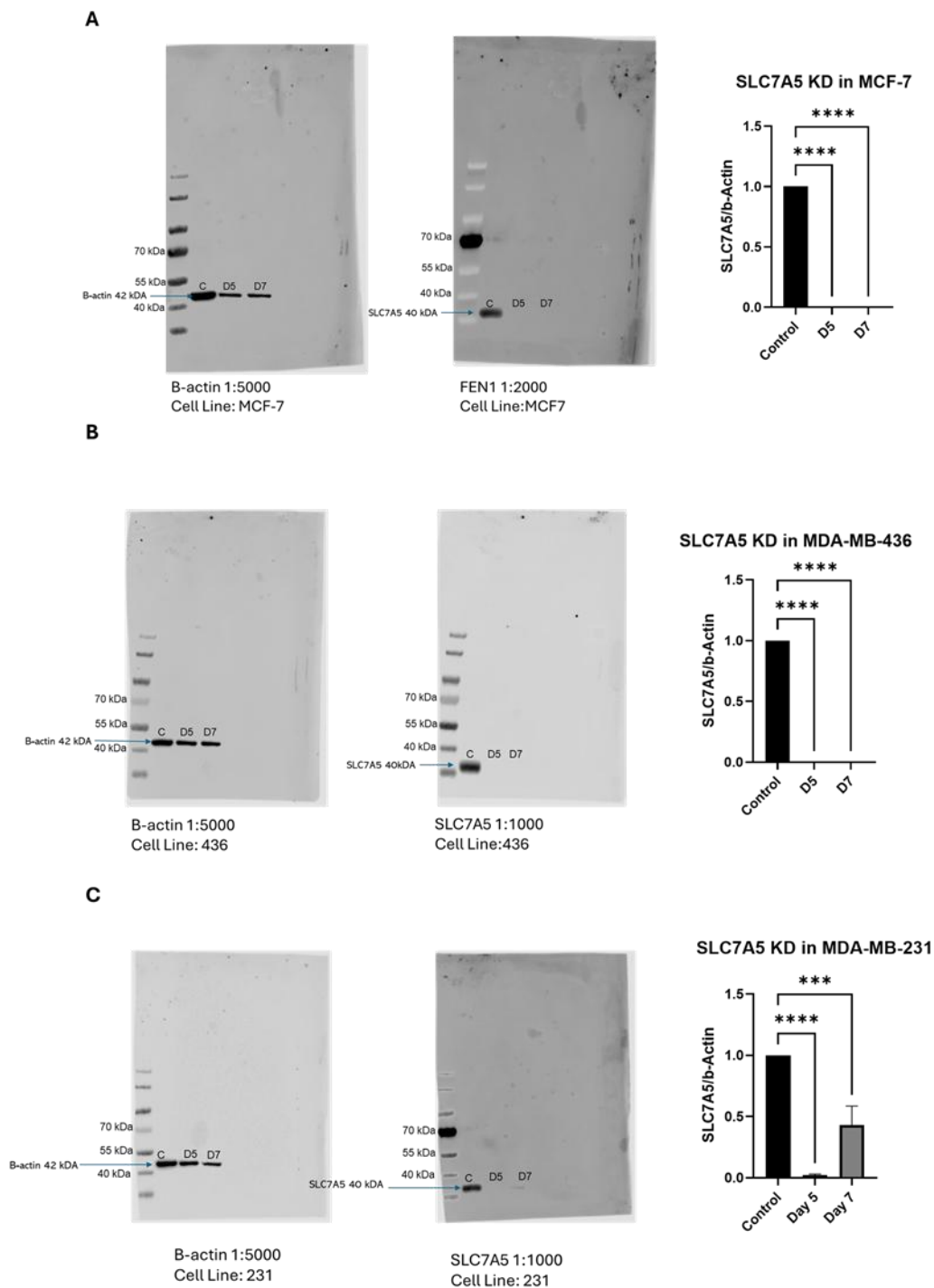


Figure 4.4. Validation of SLC7A5 knockdown efficiency using a second siRNA construct in different breast cancer cell lines. (A-C) Western blot analysis was performed to assess SLC7A5 protein expression following siRNA mediated knockdown in (A) MCF-7, (B) MDA-MB-436, and (C) MDA-MB-231 breast cancer cell lines. β -actin was used as a loading control. Quantification of SLC7A5 expression levels, normalised to β -actin, is shown in the adjacent bar graphs. Data are presented as mean \pm standard errors from three independent experiments. Statistical significance was determined using one-way ANOVA, P-values *** <0.001 and **** <0.0001 , C, negative control; D5, day 5 post-knockdown; D7, day 7 post-knockdown.

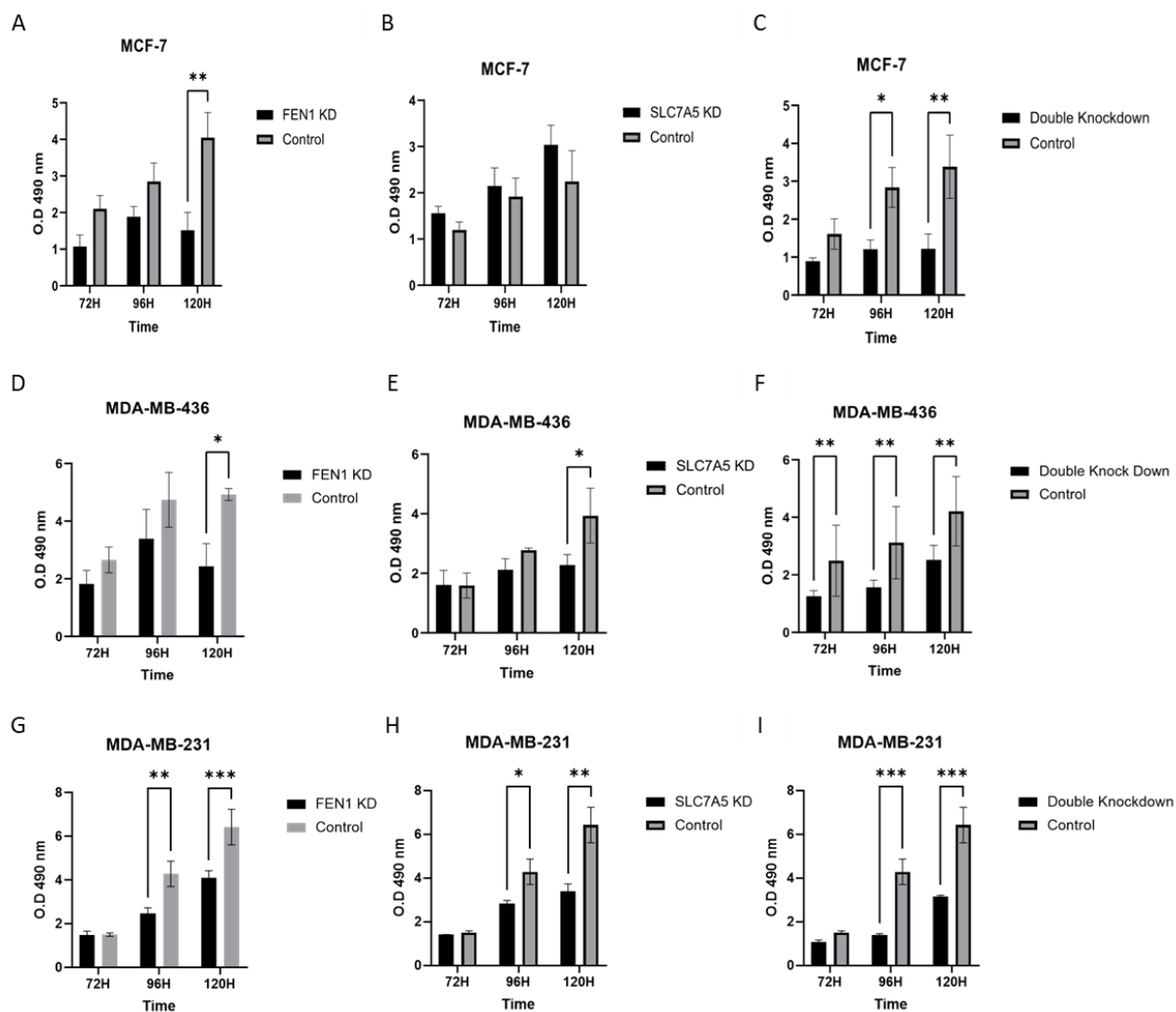


Figure 4.5. The effect of singular and double knockdown of FEN1 and SLC7A5 by siRNA on cell proliferation in breast cancer cell lines. (a) FEN1 knockdown (KD), (b) SLC7A5 KD and (c) FEN1 and SLC7A5 Double KD (DKD) in MCF-7. (D) FEN1 KD, (E) SLC7A5 KD and (F) FEN1 and SLC7A5 DKD in MDA-MB-436. (G) FEN1 KD, (H) SLC7A5 KD and (I) FEN1 and SLC7A5 DKD in MDA-MB-231. P-values * <0.05 , ** <0.01 and *** <0.001 .

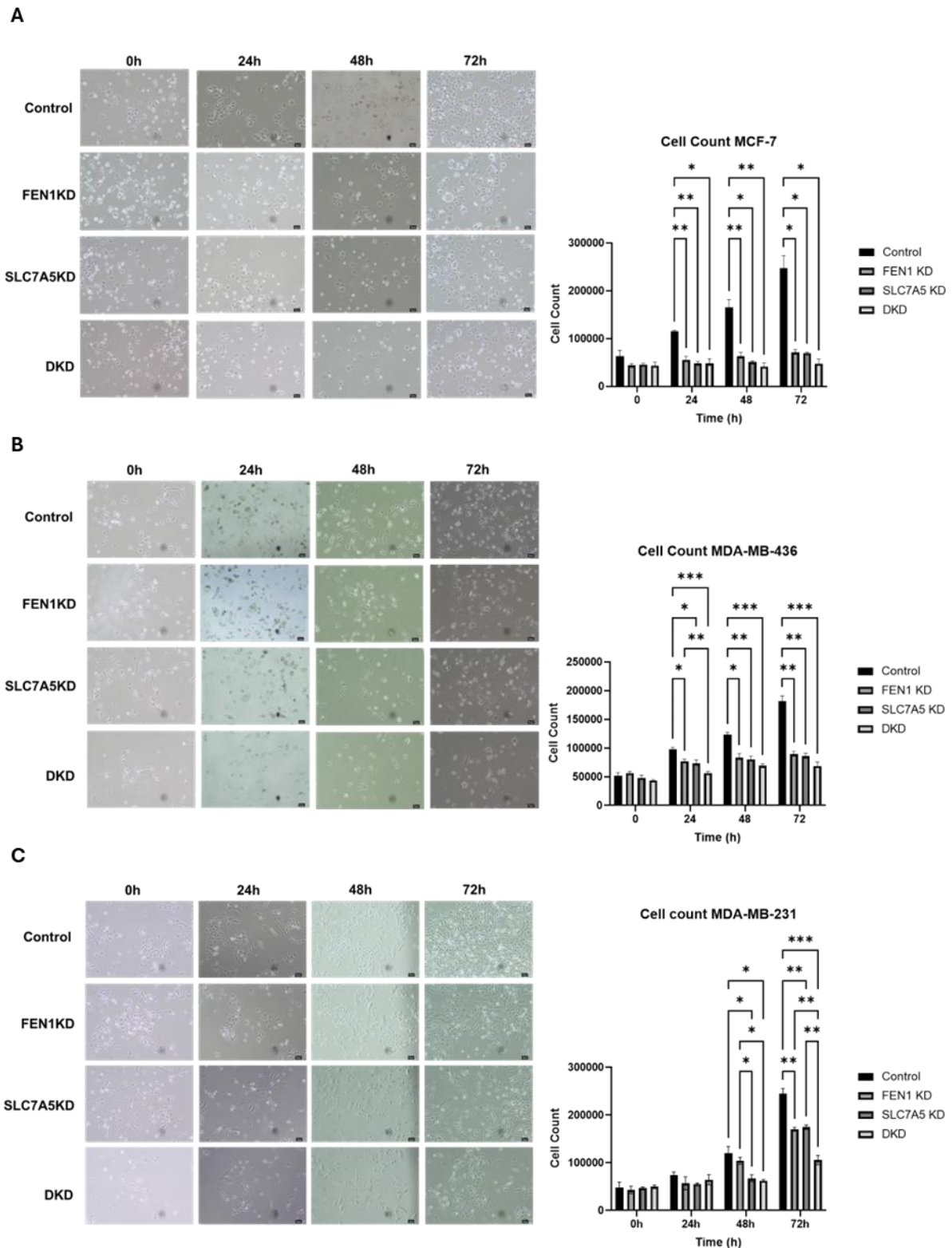


Figure 4.6. Singular and double knockdown of FEN1 and SLC7A5 and effect on cell count of BC cell lines. Total cell counts were determined every 24 hours in (A) MCF-7, (B) MDA-MB-436 and (C) MDA-MB-231. Values are shown as means \pm SD. Two-way analysis of variance (ANOVA) was used to assess variation between conditions. The P-values $* < 0.05$, $** < 0.01$ (N=3), KD, knockdown; and DKD, double knockdown.

4.3.2 Effect of FEN1 and SLC7A5 knockdown on cell migration and invasion in breast cancer cells

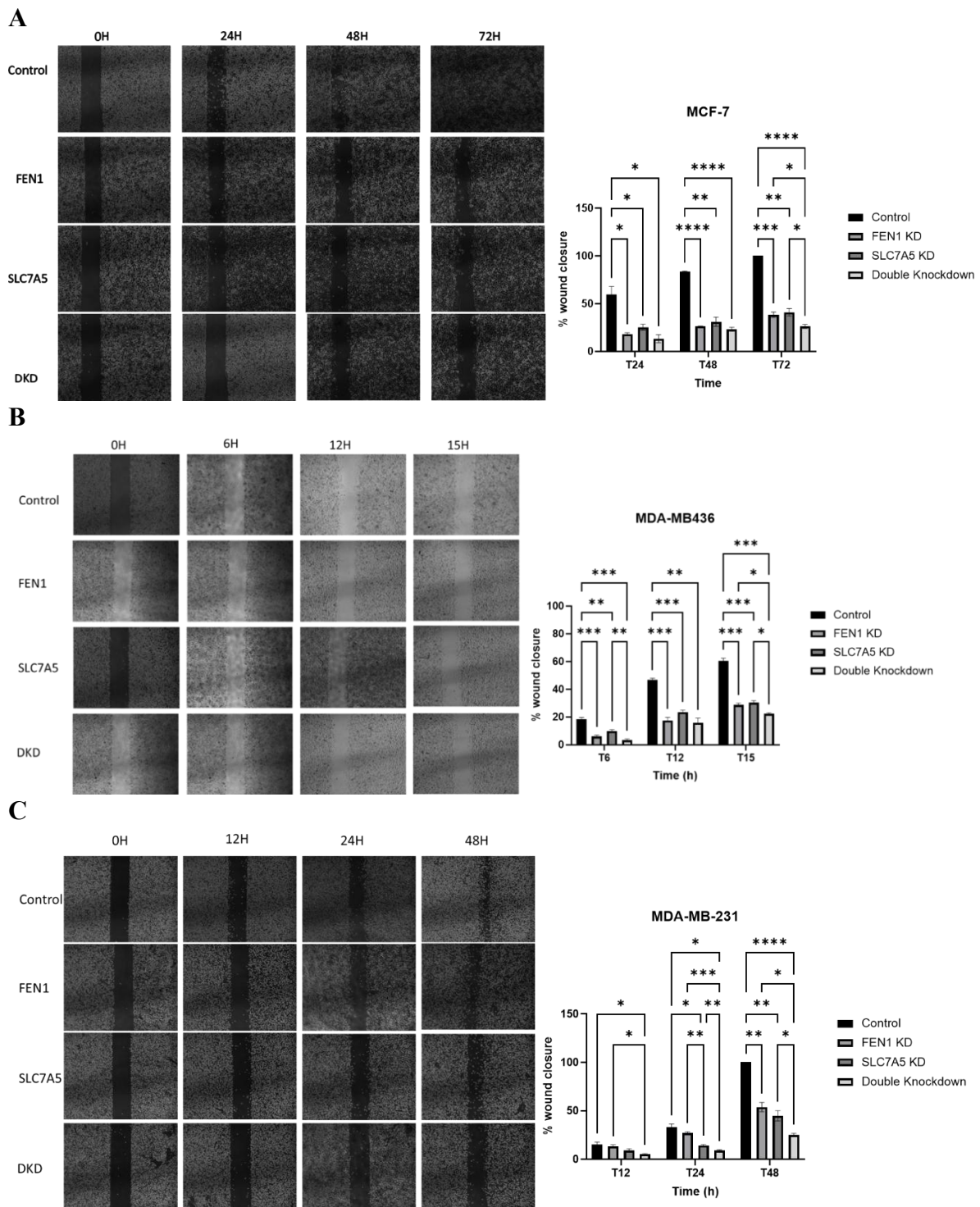
In the MCF-7 cell line (Figure 4.7 A), knockdown of either FEN1 or SLC7A5 significantly impaired cell migration compared to the control, with the DKD exhibiting the most profound decrease in wound closure, particularly at 72h, where wound closure was markedly reduced compared to both control and individual knockdowns of FEN1 and SLC7A5 (Figure 4.7 A; all $P < 0.05$). Notably, control cells exhibited robust migration, achieving complete wound closure by 72h, whereas DKD cells exhibited minimal closure, achieving only 26% wound closure by 72h.

Similarly, in MDA-MB-436 cells (Figure 4.7 B), Knockdown of either FEN1 or SLC7A5 reduced cell migration, but the DKD cells had a significantly greater impact at 72h in comparison to all other conditions (Figure 4.7 B; all $P < 0.05$). In addition to this, control cells showed rapid migration and wound closure across all time points, as at 15h it achieved 61% wound closure, whereas DKD cells exhibited reduced motility, achieving just 22% wound closure at 15h (Figure 4.7 B; $P < 0.001$).

A similar trend was observed in MDA-MB-231 cells, both FEN1 and SLC7A5 knockdown significantly impaired migration at 24h and 48h in comparison to the control, with DKD showing the most substantial reduction at 24h and 48h compared to all other conditions (Figure 4.7 C; all $P < 0.05$). Control cells closed the wound at 48h, while DKD only closed 25% of the wound gap (Figure 4.7 C; $P < 0.0001$).

To further assess the impact of FEN1 KD, SLC7A5 KD and DKD on metastatic potential, a Matrigel invasion assay was performed (Figure 4.8). In MCF-7 cells, both single knockdowns reduced the number of invading cells (Figure 4.8 A; $P < 0.001$), while DKD showed an even greater reduction (Figure 4.8 A; all $P < 0.05$). A similar trend was exhibited in the MDA-MB-436 cell line (Figure 4.8 B), with DKD showing the greatest suppression of invasion in comparison to all other conditions (Figure 4.8 B; all $P < 0.01$). In MDA-MB-231 cells (Figure 4.8 C),

knockdown of SLC7A5 significantly reduced invasion compared to control (Figure 4.8 C; $P < 0.01$), whereas FEN1 KD did not show a significant difference compared to control (Figure 4.8 C; $P > 0.05$). However, DKD led to profound loss of the invasion capability MDA-MB-231 cell line (Figure 4.8 C; all $P < 0.01$), suggesting that FEN1 KD alone may not be sufficient to impair invasion in the triple-negative breast cancer model, but the combined knockdown with SLC7A5 leads to a stronger inhibitory effect.



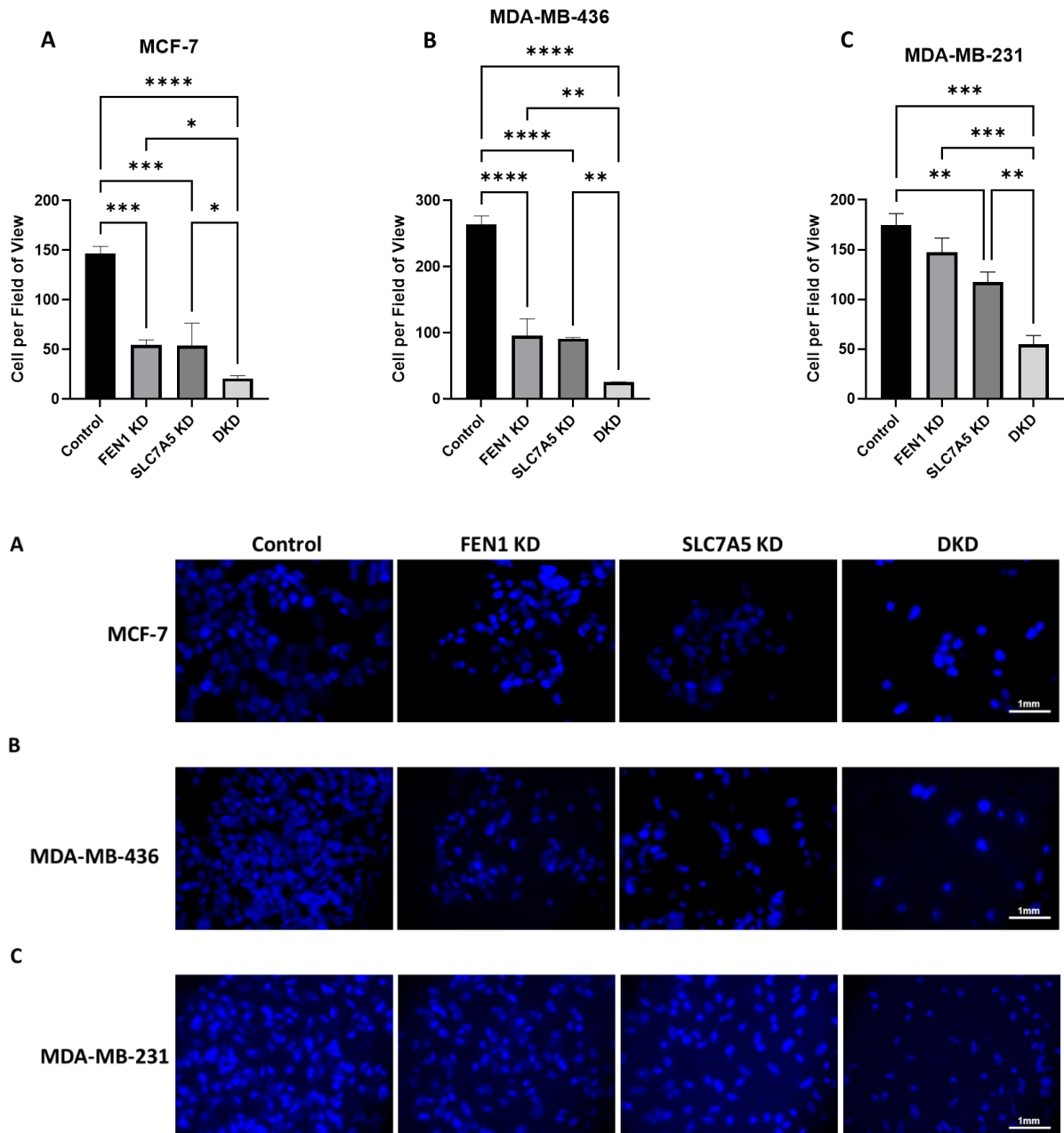


Figure 4.8. The effect of singular and double knockdown (DKD) of FEN1 and SLC7A5 by siRNA on cell invasion in (A) MCF-7, (B) MDA-MB-436 and (C) MDA-MB-231 cells. A Matrigel-coated Boyden chamber was used to test the ability of breast cancer cells to invade, and then ImageJ software was used to count the invaded cells. DKD significantly reduced the invasion ability of breast cancer cells in comparison to the control, FEN1 KD and SLC7A5 KD. Two-way analysis of variance (ANOVA) was used to assess variation between each condition. The P-values $* < 0.05$, $** < 0.01$, $*** < 0.001$ and $**** < 0.0001$ (N=3).

4.3.3 Impact of FEN1 and SLC7A5 knockdown on cell cycle progression and apoptosis in BC cell lines

For cell cycle progression, in MCF-7 cells, knockdown of FEN1 led to significant increase in the S phase population 15%, compared to control 11% (Figure 4.9 A and B; $P < 0.01$), while SLC7A5 KD led to cell cycle arrest at G1 phase 79% and decrease in S phase population 7% compared to the other conditions (Figure 4.9 A and B; all $P < 0.01$). The DKD exhibited a stronger S phase arrest, 19%, which inhibits the transition to G2/M phase (Figure 4.9 A and B; all $P < 0.01$). Similarly, in MDA-MB-436 cells (Figure 4.10), FEN1 KD showed an increase in S phase population of 20% compared to SLC7A5 KD 17% and control 13% (Figure 4.10 B; $P < 0.05$ and $P < 0.0001$, respectively). DKD exhibited an increase in S phase population of 20%, additionally, it caused an accumulation in G1 phase population 66%, which led to the decrease of cells transition to G2/M phase 14% compared to control and FEN1 KD (Figure 4.10 B; $P < 0.0001$ and $P < 0.001$, respectively). A similar trend was exhibited in MDA-MB-231 (Figure 4.11), the singular knockdown of FEN1 and SLC7A5 caused S phase arrest 18% and 16%, respectively, in comparison to control 14% (Figure 4.11 B; all $P < 0.01$). The DKD exhibited an even stronger S phase, 23%, compared to the other conditions (Figure 4.11 B; all $P < 0.05$).

For apoptosis, in the MCF-cell line, knockdown of FEN1 did not show significant results in comparison to control, while knockdown of SLC7A5 resulted in a moderate increase in apoptotic cells compared to control (Figure 4.12 A and B; $P < 0.01$), DKD further enhanced apoptosis compared to single knockdowns and the control (Figure 4.12 A and B; all $P < 0.01$). Similarly, in MDA-MB-436 cells, single knockdown of FEN1 and SLC7A5 led to an increase in apoptotic populations (Figure 4.13 A and B; all $P < 0.05$), with DKD showing a further increase in apoptosis compared to single knockdowns (Figure 4.13 A and B; all $P < 0.05$). In MDA-MB-231 cells (Figure 4.14), FEN1 KD caused a moderate increase in apoptotic cell population compared to control (Figure 4.14 A and B; $P < 0.01$), while SLC7A5 KD did not result in a

significant increase. DKD induced the highest level of apoptosis compared to other conditions (Figure 4.14 A and B; all $P < 0.01$).

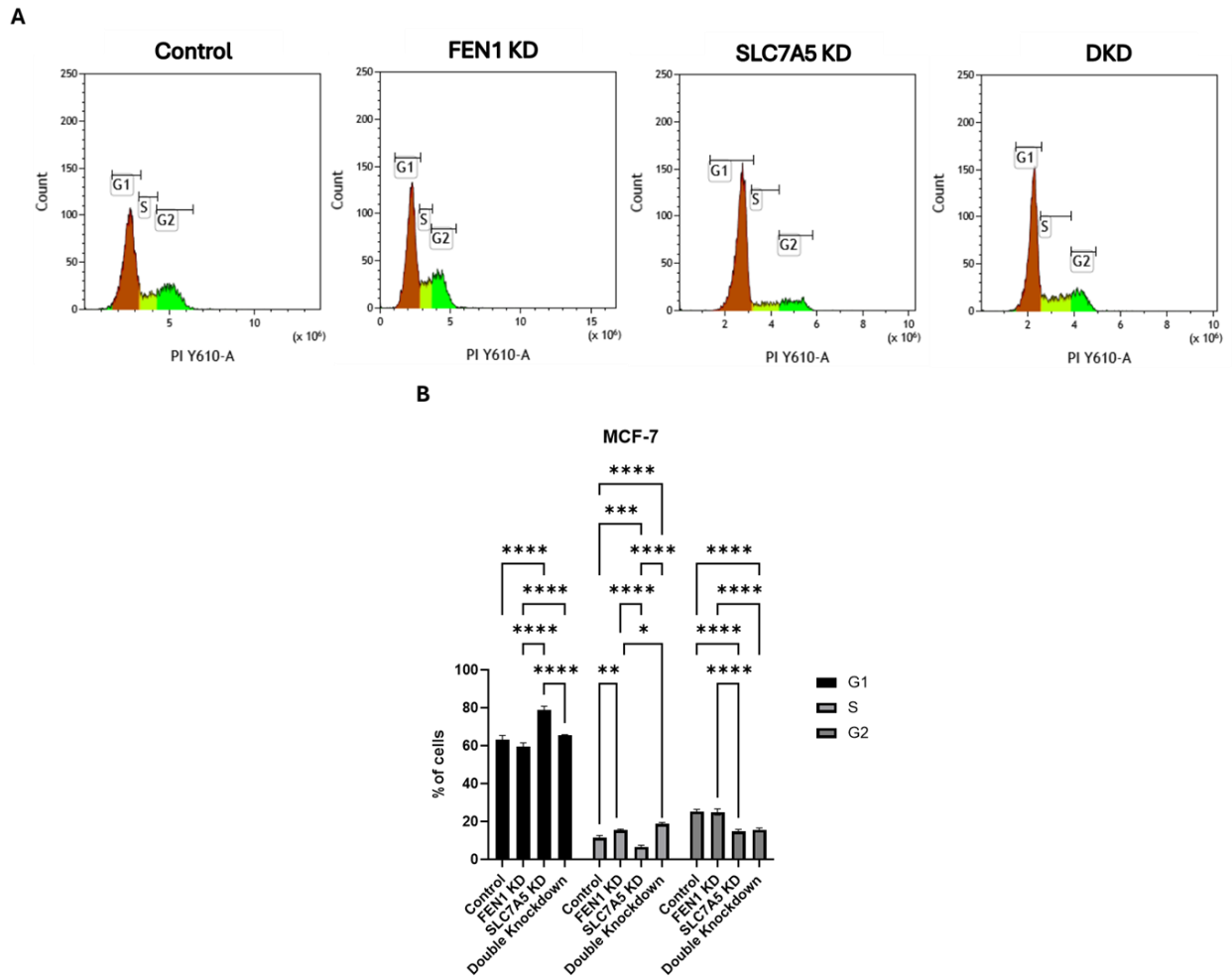
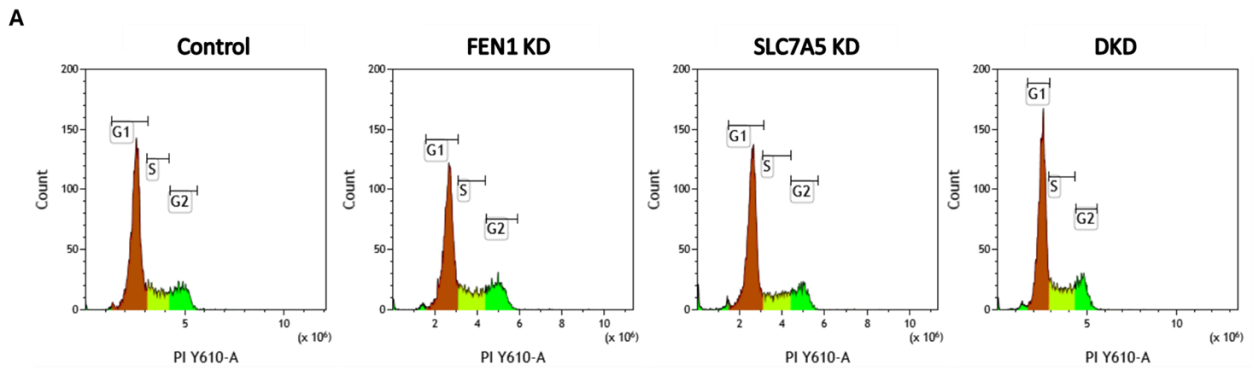


Figure 4.9. The effect of knockdown (KD) FEN1, SLC7A5 and Double knockdown (DKD) by siRNA on the cell cycle in the MCF-7 cell line. (A) Representative histogram from flow cytometry analysis showing cell cycle phase distribution in control, FEN1 KD, SLC7A5 KD and DKD conditions. The G1 phase is shown in brown, the S phase in red, and G2/M phase in green. (B) Quantification of cell cycle distribution, presented as the percentage of cells in G1, S, and G2/M phases for each condition. Two-way analysis of variance (ANOVA) was used to assess variation between each condition. The P-values $* < 0.05$, $** < 0.01$, $*** < 0.001$ and $**** < 0.0001$ (N=3).



B

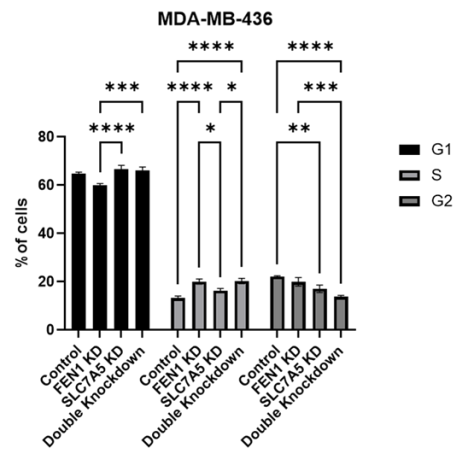


Figure 4.10. The effect of knockdown (KD) FEN1, SLC7A5 and Double knockdown (DKD) by siRNA on the cell cycle in the MDA-MB-436 cell line. (A) Representative histogram from flow cytometry analysis showing cell cycle phase distribution in control, FEN1 KD, SLC7A5 KD and DKD conditions. The G1 phase is shown in brown, the S phase in red, and G2/M phase in green. (B) Quantification of cell cycle distribution, presented as the percentage of cells in G1, S, and G2/M phases for each condition. Two-way analysis of variance (ANOVA) was used to assess variation between each condition. The P-values * <0.05 , ** <0.01 , * <0.001 and **** <0.0001 (N=3).**

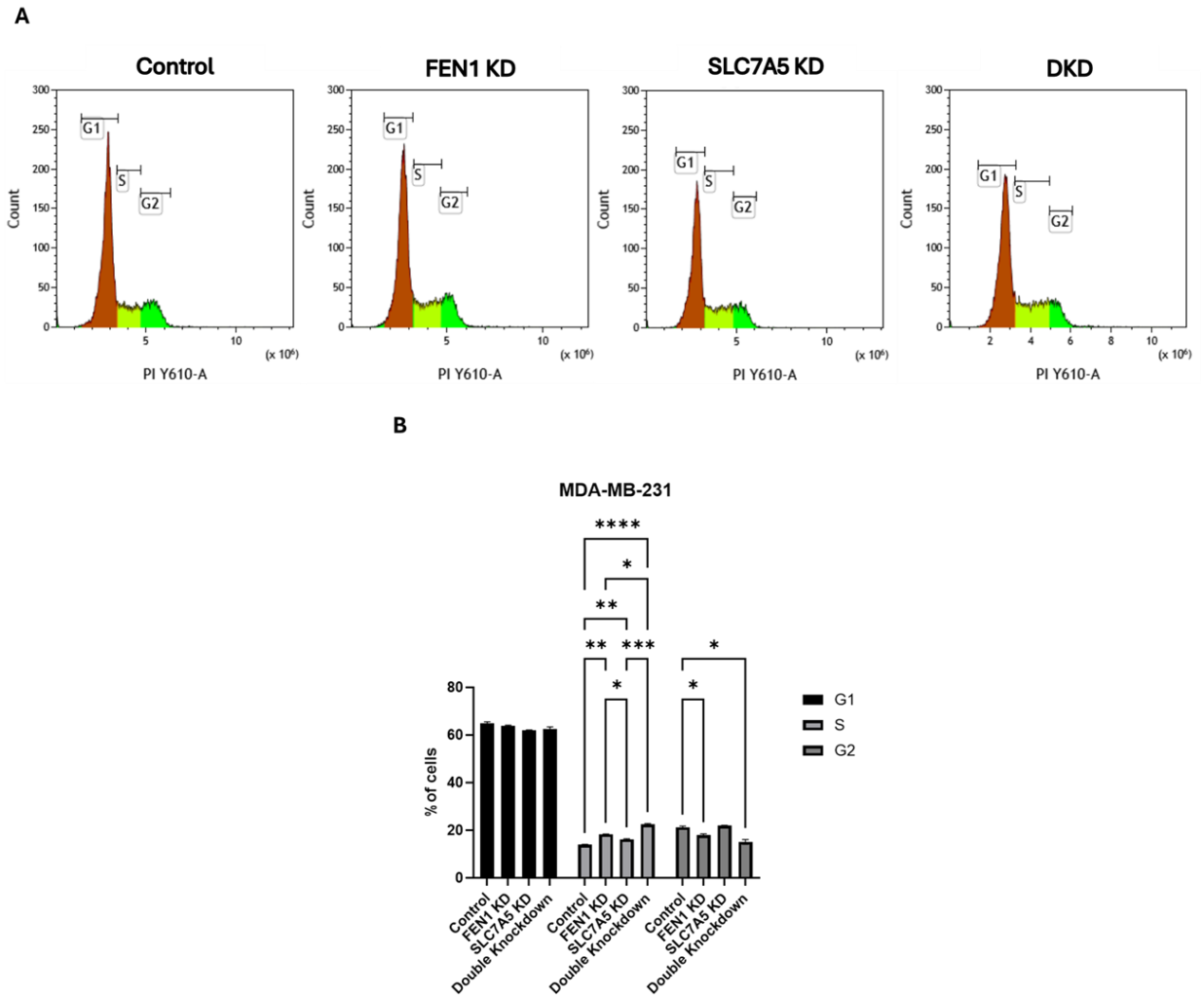
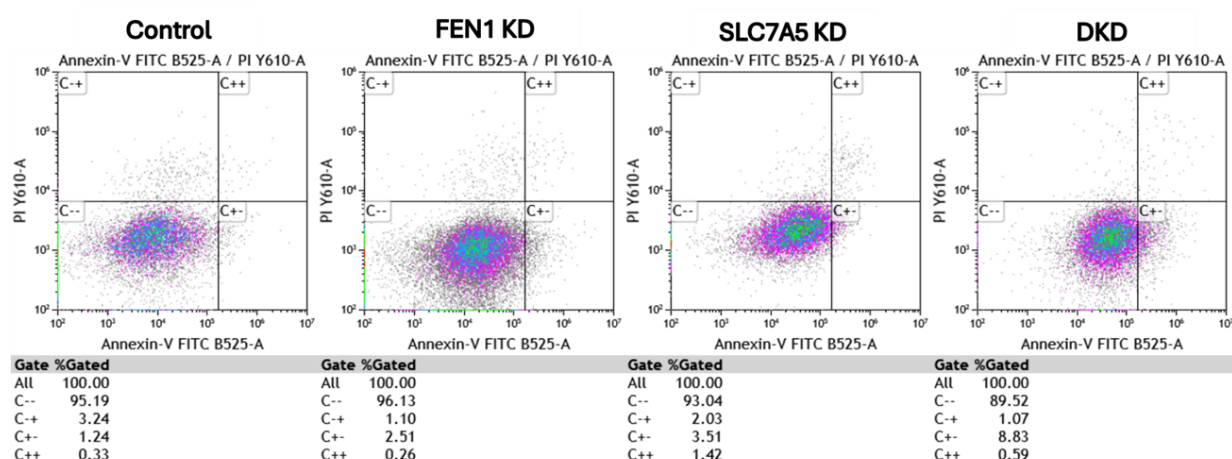


Figure 4.11. The effect of knockdown (KD) FEN1, SLC7A5 and Double knockdown (DKD) by siRNA on the cell cycle in the MDA-MB-436 cell line. (A) Representative histogram from flow cytometry analysis showing cell cycle phase distribution in control, FEN1 KD, SLC7A5 KD and DKD conditions. The G1 phase is shown in brown, the S phase in red, and G2/M phase in green. (B) Quantification of cell cycle distribution, presented as the percentage of cells in G1, S, and G2/M phases for each condition. Two-way analysis of variance (ANOVA) was used to assess variation between each condition. The P-values $* < 0.05$, $ < 0.01$, $*** < 0.001$ and $**** < 0.0001$ (N=3).**

A



B

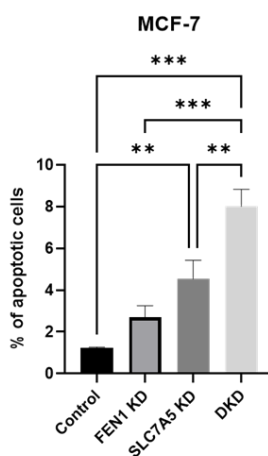
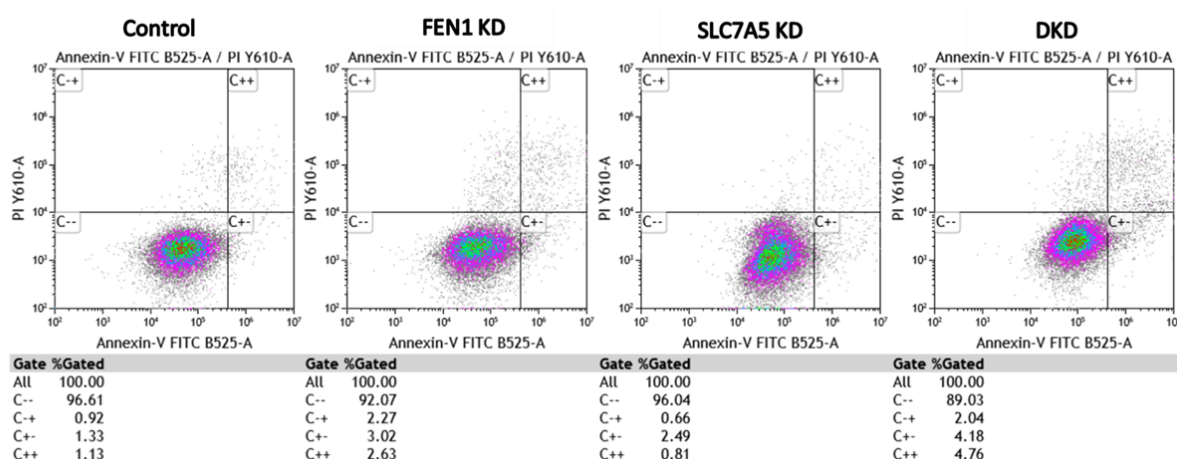


Figure 4.12. The effect of knockdown (KD) FEN1, SLC7A5 and Double knockdown (DKD) by siRNA on apoptosis in the MCF-7 cell line. (A) Representative flow cytometry dot plots showing Annexin V-FITC and Propidium Iodide (PI) staining in control, FEN1 KD, SLC7A5 KD and double knockdown (DKD) conditions. Cells were stained with Annexin V-FITC (x-axis) and PI (y-axis) to differentiate between live (C--, Annexin V-/PI-, lower-left quadrant), early apoptotic (C+-, Annexin V+/PI-, lower-right quadrant), late apoptotic (C++, Annexin V+/PI+, upper-right quadrant) and necrotic cells (C+, Annexin V-/PI+, upper-left quadrant). The percentage of cells in each quadrante is indicated in the tables below. (B) Quantification of apoptotic cells (% of Annexin V-positive/PI-negative cells) across conditions. Two-way analysis of variance (ANOVA) was used to assess variation between each condition. The P-values * <0.05 , ** <0.01 , *** <0.001 and **** <0.0001 (N=3).

A



B

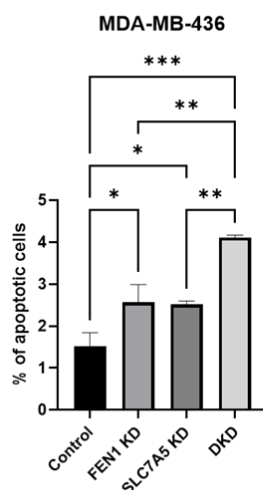


Figure 4.13. The effect of knockdown (KD) FEN1, SLC7A5 and Double knockdown (DKD) by siRNA on apoptosis in the MDA-MB-436 cell line. (A) Representative flow cytometry dot plots showing Annexin V-FITC and Propidium Iodide (PI) staining in control, FEN1 KD, SLC7A5 KD and double knockdown (DKD) conditions. Cells were stained with Annexin V-FITC (x-axis) and PI (y-axis) to differentiate between live (C--, Annexin V-/PI-, lower-left quadrant), early apoptotic (C+-, Annexin V+/PI-, lower-right quadrant), late apoptotic (C+++, Annexin V+/PI+, upper-right quadrant) and necrotic cells (C-+, Annexin V-/PI+, upper-left quadrant). The percentage of cells in each quadrante is indicated in the tables below. (B) Quantification of apoptotic cells (% of Annexin V-positive/PI-negative cells) across conditions. Two-way analysis of variance (ANOVA) was used to assess variation between each condition. The P-values * <0.05 , ** <0.01 , *** <0.001 and **** <0.0001 (N=3).

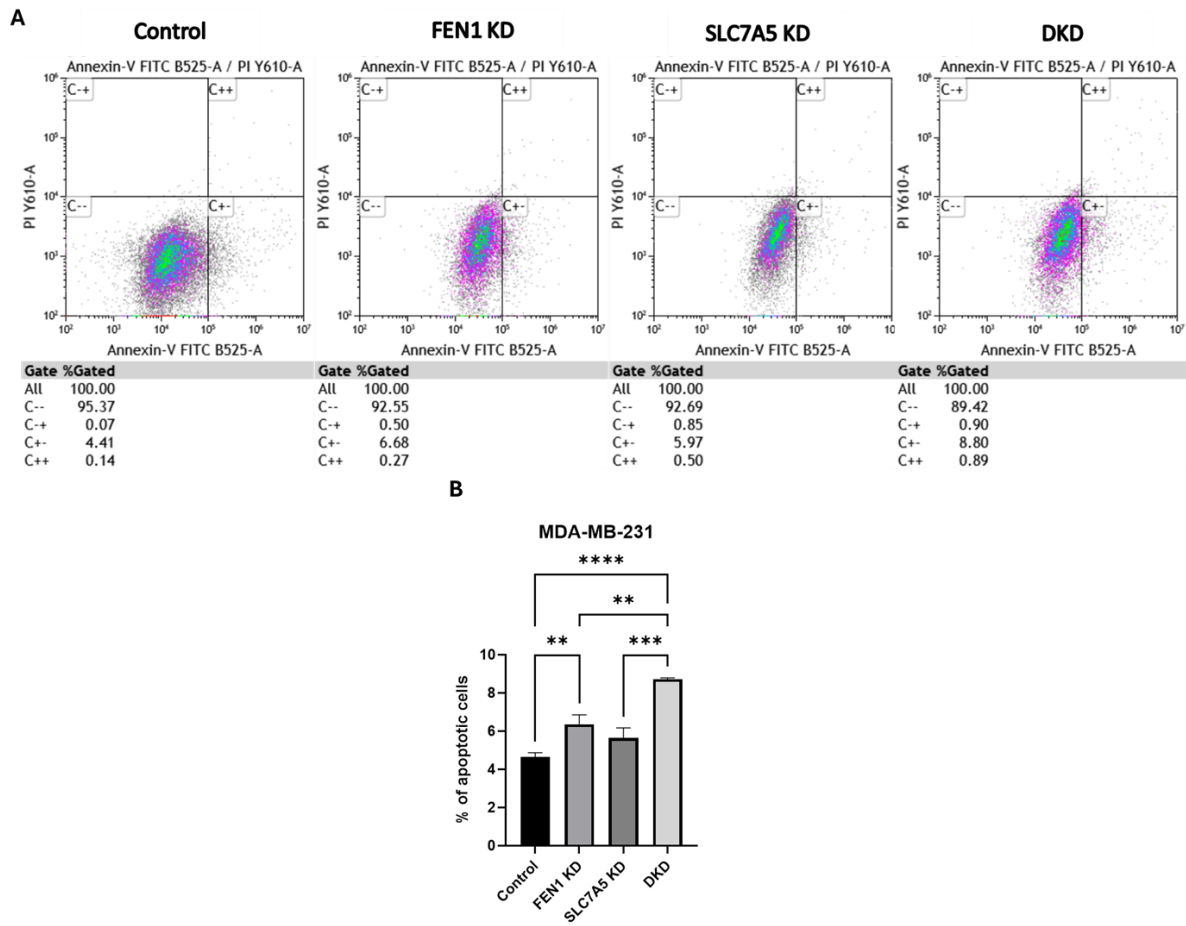


Figure 4.14. The effect of knockdown (KD) FEN1, SLC7A5 and Double knockdown (DKD) by siRNA on apoptosis in cell lines. (A) Representative flow cytometry dot plots showing Annexin V-FITC and Propidium Iodide (PI) staining in control, FEN1 KD, SLC7A5 KD and double knockdown (DKD) conditions. Cells were stained with Annexin V-FITC (x-axis) and PI (y-axis) to differentiate between live (C--, Annexin V-/PI-, lower-left quadrant), early apoptotic (C+-, Annexin V+/PI-, lower-right quadrant), late apoptotic (C++, Annexin V+/PI+, upper-right quadrant) and necrotic cells (C-+, Annexin V-/PI+, upper-left quadrant). The percentage of cells in each quadrante is indicated in the tables below. (B) Quantification of apoptotic cells (% of Annexin V-positive/PI-negative cells) across conditions. Two-way analysis of variance (ANOVA) was used to assess variation between each condition. The P-values * <0.05 , ** <0.01 , *** <0.001 and **** <0.0001 (N=3).

4.4 Discussion

Breast cancer progression is driven by complex molecular mechanisms that regulate key cellular processes, including proliferation, migration, invasion, cell cycle progression, and apoptosis. In the previous chapter, the prognostic value of SLC7A5 and FEN1 high expression in breast cancer was investigated. In this chapter, the impact of singular and double knockdown of SLC7A5 and FEN1 was explored through a series of assay experiments breast cancer cell proliferation, migration, invasion, cell cycle regulation, and apoptosis. While previous studies have highlighted the individual contributions of SLC7A5 and FEN1 to tumourigenesis, their potential interaction and combined effects in breast cancer remain unexplored.

In this chapter, the knockdown of SLC7A5 and FEN1 individually led to a significant reduction in breast cancer cell proliferation, while the DKD exhibited an even stronger effect in all used cell lines. A previous study showed that SLC7A5 plays a crucial role in maintaining amino acid homeostasis and activating the mammalian target of rapamycin complex 1 (mTORC1) pathway, essential for sustaining the robust growth of APC KRAS-mutant colorectal tumour cells in vivo [184]. SLC7A5 also attenuated the effect of suppressing the long intergenic non-protein coding RNA 857 (LIN00857) in colorectal tumours [185]. Consistent with these findings, the results suggest that SLC7A5 knockdown affects breast cancer proliferation by limiting essential nutrient transport and metabolic signalling [70].

Similarly, using cell counting kit-8 (CCK-8) proliferation assay knockdown of FEN1 in cholangiocarcinoma (CHOL) cell lines restrained their proliferation ability, while the overexpression of FEN1 was responsible for the increased formation of clones [186], the study further demonstrated that FEN1 regulates the tumour progression in CHOL via Wnt/b-catenin signalling pathway [186]. FEN1 has been shown to regulate tumour progression in hepatocellular carcinoma (HCC) [187], as the knockdown of FEN1 led to a decrease in colony formation and inhibited the G2 to M phase transition, ultimately impairing proliferation in HCC

cells [187]. These findings align with the results in this chapter, where FEN1 knockdown resulted in significant suppression in breast cancer cell proliferation. While the effects of singular knockdowns of SLC7A5 and FEN1 have been extensively studied, there has been limited investigation into the combined effect of knockdown of both genes. The double knockdown in this study provided new insights, demonstrating a more pronounced suppression of proliferation, highlighting a potential functional interplay between SLC7A5 and FEN1 in breast cancer cells.

The knockdown of SLC7A5 and FEN1 individually led to a reduction in the migratory and invasive abilities of breast cancer cell lines, while the DKD had the most significant effect. These findings indicate that both SLC7A5 and FEN1 contribute to the regulation of cancer cell motility and invasion, and their combined suppression may serve as a potential therapeutic approach. A previous study demonstrated that the knockdown of SLC7A5 in a KRAS mutant lung adenocarcinoma decreased their migration and invasion abilities [188]. Similarly, the knockdown of SLC7A5 in B16-F10 melanoma cell line caused the decrease of their ability for migration and invasion, the study suggested that SLC7A5 modulate the mitogen-activated protein kinase (MAPK) signalling pathway, which plays a crucial role in inducing proteolytic enzymes that degrade the basement membrane and promote cell invasion [189]. Moreover, SLC7A5 interferes with VEGF-A/VEGFR2 and mTOR signalling, hence playing a role in the regulation of angiogenesis, thereby contributing to the increase of metastasis [190]. These findings support the results in this chapter, where SLC7A5 knockdown led to a significant impairment in breast cancer cell migration and invasion.

Similarly, knockdown of FEN1 reduced the ability of HCC cell line for migration and invasion [187]. Furthermore, overexpression of FEN1 in CHOL cells, resulted in the downregulation of E-cadherin expression with N-cadherin and vimentin being, which suggests that FEN1 plays an important role in epithelial-mesenchymal transition (EMT) in cancer [186]. This aligns with the findings here, where FEN1 knockdown significantly reduced breast cancer cell migration and invasion, potentially due to EMT suppression.

The knockdown of SLC7A5 and FEN1 in breast cancer cells significantly disrupted cell cycle progression and increased apoptosis, with the most pronounced effects observed in the DKD condition. Flow cytometry analysis revealed that SLC7A5 depletion caused cell cycle arrest in G1 phase in MCF-7 cells and S-phase arrest in MDA-MB-436 and MDA-MB-231 cells, while the downregulation of FEN1 resulted in S-phase accumulation in all cell lines, indicative of impaired cell cycle progression. The DKD condition further amplified this effect, suggesting a potential cooperative role of these two genes in regulating cell cycle checkpoints. Additionally, increased apoptotic rates were observed in all knockdown conditions, with DKD exhibiting the highest level of apoptosis, further reinforcing the essential role of these genes in breast cancer cell survival.

SLC7A5 has been widely implicated in cell cycle regulation due to its role in amino acid transport and metabolic signalling. Previous studies have shown that SLC7A5 knockdown leads to G1/S arrest in various cancers, including pancreatic and oesophageal cancer, ultimately suppressing proliferation [191, 192]. This is a result of the downregulation of both cyclin D1 (CCND1) and cyclin-dependent kinase 2 (CDK2), which play an important role in cell cycle regulation and the G1/S transition and help to regulate the exit of S phase [193]. Furthermore, SLC7A5 downregulation via the knockdown of Mitochondrial ribosomal protein L35 (MRPL35) was found to enhance apoptosis in non-small cell lung cancer [194]. SLC7A5 functions as an exchange glutamine transporter, as it transports intracellular glutamine in exchange with leucine, which in turn activates mTORC1 signalling pathway, which is known for its crucial role in cell cycle progression and promoting cell survival, thus avoiding apoptosis [70]. Consistently, the findings demonstrated that SLC7A5 knockdown led to disrupted cell cycle progression and an increase in apoptotic cell populations, suggesting that metabolic stress may contribute to cell death.

Similarly, overexpression of FEN1 inhibits cell apoptosis and causes the cell transition from S phase to G2/M phase in prostate cancer [177]. Furthermore, knockdown of FEN1 in ovarian cell lines causes S-phase cell cycle arrest and increased apoptosis [195]. FEN1 plays an important role in DNA repair, hence maintaining genomic stability and preventing the

accumulation of DNA damage that leads to apoptosis [195]. It is also involved in DNA replication through the process of Okazaki fragment maturation, and it is involved in re-initiating stalled replication forks [195]. These activities affect the cell cycle regulation, especially at the S-phase where the DNA replication takes place [195]. This aligns with the chapter's findings, as FEN1 knockdown significantly increased S-phase accumulation and induced apoptosis in breast cancer cells, likely due to defects in DNA replication and repair mechanisms.

While the individual effects of SLC7A5 and FEN1 knockdowns on cancer cell motility, cell cycle and apoptosis have been previously reported, there is a lack of studies examining their combined role. The results in this chapter highlight that DKD of SLC7A5 and FEN1 leads to a more pronounced reduction in migration and invasion compared to singular knockdowns, moreover, DKD has a greater impact on both cell cycle arrest and apoptosis compared to singular knockdowns, suggesting a functional interplay between SLC7A5 and FEN1 in regulating breast cancer metastasis, cell cycle and apoptosis. These findings raise important questions regarding the feasibility of targeting both genes simultaneously.

These findings suggest that SLC7A5 and FEN1 co-operate to regulate breast cancer cell survival, proliferation, and metastasis by integrating metabolic and DNA repair pathways.

Chapter 5 Functional interdependence of SLC7A5 and FEN1: Impact on mitochondrial function in breast cancer cells

5.1 Introduction

In previous chapters, the high expression of SLC7A5 and FEN1 was identified as a potential prognostic marker in breast cancer, where their upregulation was associated with poor survival outcomes (Chapter 3). Functional experiments further demonstrated that double knockdown of SLC7A5 and FEN1 significantly impaired breast cancer cell behaviours, including proliferation, migration, invasion, apoptosis, and cell cycle progression (Chapter 4). These findings suggested a possible functional relationship between the two genes, warranting further investigation into whether they influence each other's expression and share common molecular pathways.

mTORC1 plays a key role in the regulation of multiple aspects of cell metabolism, including mitochondrial oxidative phosphorylation (OXPHOS), mitochondrial fission, and ATP synthesis [196]. Disruption of this pathway is frequently observed in cancer and has been implicated in altered metabolic states that support tumour growth, such as breast cancer, prostate cancer, ovarian cancer, renal cell carcinoma and lung cancer [197]. In this context, SLC7A5 modulates amino acid availability, particularly leucine, thereby activating mTORC1 [198], while FEN1 contributes to DNA replication and repair, processes critical for mitochondrial genomic stability and oxidative stress response [199].

Mitochondria in cancer cells experience stress in many ways, including the increase in mitochondrial reactive oxygen species (mtROS) levels, because of nutrient depletion, metabolic stress, the disruption in the electron transport chain and electron leakage [200], which occur because of the OXPHOS. Researchers indicated the localisation of BER enzymes into mitochondria, including FEN1, to encounter oxidative stress and to repair mitochondrial DNA by cleaving the damaged DNA fragment, which allows the other DNA repair mechanisms to take place [201]. This means that the mitochondria are most likely playing a key role in establishing the association between glutamine metabolism and DNA repair.

Chapter 5 builds upon the previous chapters by exploring the regulatory interplay between SLC7A5 and FEN1 and assessing their combined impact on mitochondrial function. Also, to identify possible shared molecular interactions, a proteomic approach was used to identify mutual proteins pulled down with SLC7A5 and FEN1, followed by pathway enrichment analysis to uncover potential biological processes bridging glutamine metabolism and DNA repair.

5.1.1 Hypothesis

SLC7A5 and FEN1 are associated and affect the expression levels of each other, and their expression affects the mitochondrial function in breast cancer cell lines.

5.1.2 Aims

1. To investigate the effect of SLC7A5 knockdown on FEN1 expression in breast cancer cell lines.
2. To investigate the effect of FEN1 knockdown on SLC7A5 expression in breast cancer cell lines.
3. To assess whether metabolic alterations in the mitochondria accompany changes in SLC7A5 and FEN1 expression.
4. To identify shared proteins between SLC7A5 and FEN1 proteins in breast cancer cell lines.
5. To identify enriched biological pathways, with a focus on metabolism and DNA repair, associated with SLC7A5 and FEN1 expression.

5.2 Methods

5.2.1 Transient siRNA knockdown of SLC7A5 and FEN1

MCF-7 and MDA-MB-436 cell lines were transfected with SLC7A5 siRNA and FEN1 siRNA using Lipofectamine RNAiMAX as described in Chapter 2, Section 2.5. The efficiency of SLC7A5 and FEN1 siRNA knockdown was tested using Western blotting (Chapter 2 Section 2.4).

5.2.2 Western blotting

The expression of SLC7A5 and FEN1 were examined at the protein level, by Western blotting as described in Chapter 2 section 2.4, to determine the relative expression of SLC7A5 in FEN1 knockdown cells and vice versa.

5.2.3 Metabolic Flux Analysis

The Seahorse XF96 analyser and Seahorse XF Mito Stress test kit were used to measure Real-time oxygen consumption rates (OCR) and Extracellular acidification rate (ECAR) in MCF-7 and MDA-MB-436 cell lines as described in Chapter 2, section 2.12.

5.2.4 Co-immunoprecipitation and mass spectrometry

To investigate the potential association between SLC7A5 and FEN1 in both MCF-7 and MDA-MB-436 cell lines, co-immunoprecipitation experiments were performed, followed by Liquid Chromatography-Mass spectrometry in both cell lines (Chapter 2 Section 2.13). The pulldown experiment was conducted separately for SLC7A5 and FEN1 in each cell line. Across all the pulldown conditions in both MCF-7 and MDA-MB-436 cell lines, mass spectrometry identified a total of 2908 proteins.

Western blot was used to validate the pulldown of SLC7A5 and FEN1 in both cell lines.

5.2.5 Data analysis

For protein quantification and identification, raw mass spectrometry data were analysed using AMICA version 3.0.1 (<https://bioapps.maxperutzlabs.ac.at/app/amica>) [202], and data files were uploaded under the custom format option with the specification file. The data were extracted, normalised and used for comparative analysis. In both MCF-7 and MDA-MB-436 cell lines, SLC7A5 and FEN1 pulldown datasets were individually compared to the immunoglobulin G (IgG) control pulldown dataset, by using AMICAs built in the differential abundance analysis pipeline. A moderate t-test was used to assess the statistical significance of the data; the value 0.6 was chosen as a log₂ fold change threshold, and p-values <0.05 were applied to determine the significantly enriched proteins.

In MCF-7 cells, the Fold Change (FC) value for SLC7A5 was positive 2.3 (P<0.01), while the FC value for FEN1 was positive 17.3 (P<0.01), which indicated a higher abundance of the protein in the experimental pulldown compared to the IgG control. Also, 76 proteins were identified after the pulldown of SLC7A5, while 39 proteins were identified after the pulldown of FEN1. In MDA-MB-436 cells, the FC value for SLC7A5 was positive 4.4 (P<0.01), while the FC value for FEN1 was positive 17.3 (P<0.01). The number of proteins that were identified with the pulldown of SLC7A5 was 41, while 44 proteins were identified with the pulldown of FEN1.

A Venn diagram of the common proteins was generated by using InteractiVenn (<https://www.interactivenn.net/index.html#>) [203]. Protein-protein interaction (PPI) networks of the common proteins were constructed using STRING version 12.0 (<https://string-db.org/>) [204]. Gene ontology enrichment analysis of the common proteins was conducted using the GO biological process 2023 database within Enrichr (<https://maayanlab.cloud/Enrichr/#>) [205]. The results of the biological processes were ranked based on their combined score and P-values (P<0.05). Then the top 10 enriched pathways were selected and visualised as a bar plot displaying -log₁₀ transformed P-values by using GraphPad Prism software version 10.0

(GraphPad Prism Inc., San Diego, CA, USA). Enrichr does not specify a minimum number of input proteins or genes required for functional enrichment analysis. The platform accepts input lists of various sizes and applies Fisher's exact test, which is statistically valid even for small sample sizes.

5.2.6 Transcriptomic analysis of co-immunoprecipitant candidates in breast cancer cohorts

The METABRIC dataset (n=1,980) was used to determine the correlation between selected genes, further described in Chapter 2, Section 2.1.1.

Additionally, the Breast Cancer Gene-Expression Miner v5.1 (bc-GenExMiner v5.1) online database was used, to validate the findings, further described in Chapter 2, Section 2.1.2.

5.2.7 Statistical analysis

GraphPad Prism software version 10.0 (GraphPad Prism Inc., San Diego, CA, USA) was used for statistical analysis. In vitro, data were represented in mean \pm standard errors of the mean (SEM); experiments were done in three independent experiments. One-way analysis of variance (ANOVA) with Dunnett's multiple comparisons test, and two-way ANOVA with Šídák's multiple comparisons test were used to determine the significant differences between control and the other conditions. A P-value of <0.05 was considered significant.

5.3 Results

5.3.1 Impact of FEN1 knockdown on SLC7A5 expression and reciprocal effects in breast cancer cell lines

FEN1 protein levels were reduced in MCF-7 cells following the knockdown of SLC7A5, where it was decreased by 35% on day 5 after the knockdown and 90% on day 7 in comparison to the control (Figure 5.1A, B and C: $P < 0.0001$). However, in MDA-MB-436 cells, SLC7A5 knockdown led to a less substantial reduction in the level of FEN1 protein compared to the MCF-7 cell line, as it was reduced by 29% on day 5 after the knockdown and only by 23% on day 7 compared to the control (Figure 5.1D, E and F: $P < 0.01$). Additionally, the knockdown of FEN1 in MCF-7 cells caused a substantial reduction in the levels of SLC7A5 protein, with a 61% decrease on day 5 after the knockdown and a 53% decrease on day 7 (Figure 5.2A, B and C: $P < 0.01$). In contrast, the knockdown of FEN1 in the MDA-MB-436 cells had a less profound effect, as the level of SLC7A5 protein was only decreased by 28% on day 5 and 30% on day 7 after knockdown (Figure 5.2D, E and F: $P < 0.05$).

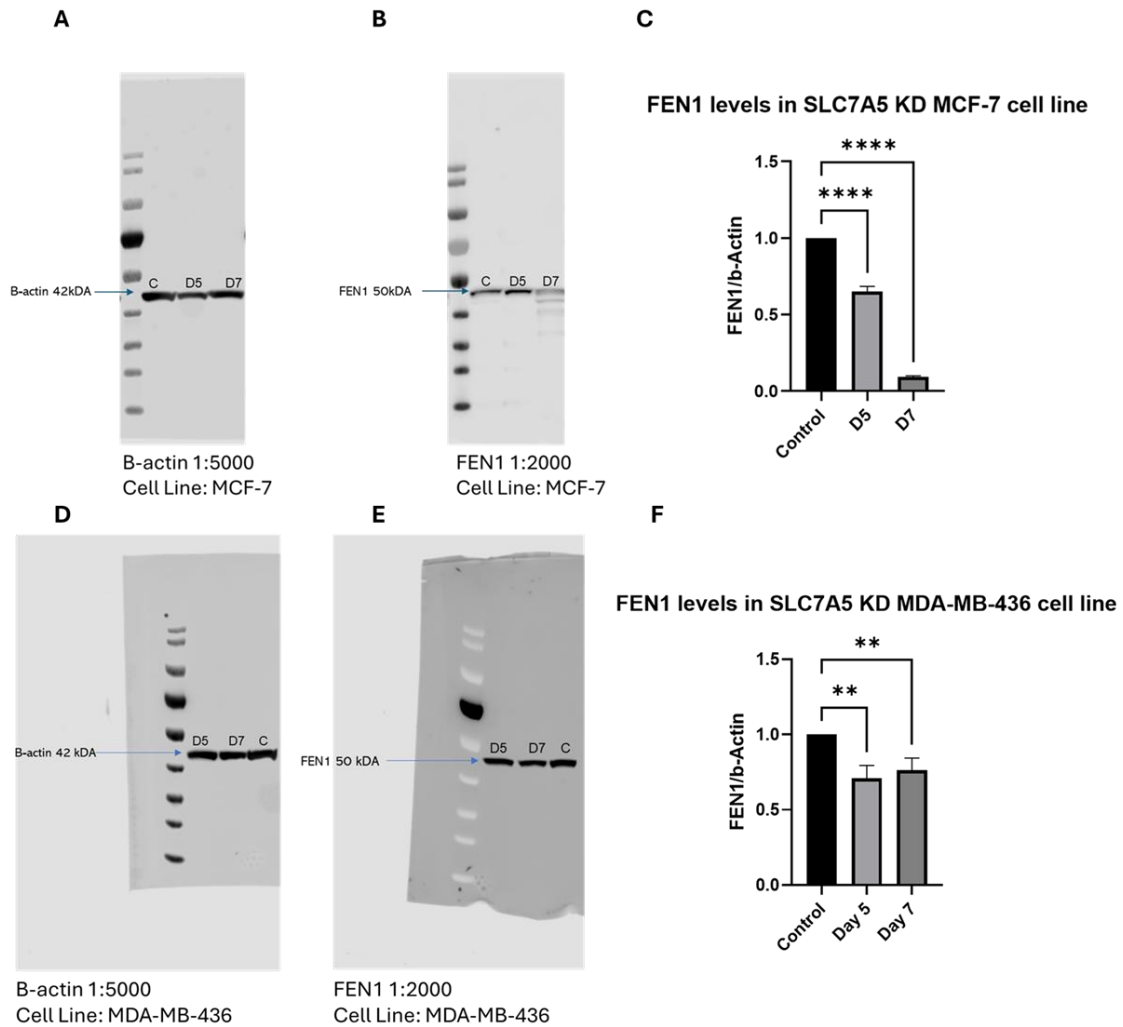


Figure 5.1. Effect of SLC7A5 knockdown on FEN1 protein levels in MCF-7 and MDA-MB-436 breast cancer cell lines. (A-B) Western blot analysis of FEN1 protein expression in the MCF-7 cell line following the knockdown of SLC7A5 on day 5 and day 7, compared to the control. β -actin was used as a loading control. (C) Quantification analysis of FEN1 protein levels normalised to β -actin in the MCF-7 cell line. (D-E) Western blot analysis of FEN1 protein expression in the MDA-MB-436 cell line following the knockdown of SLC7A5 on day 5 and day 7, compared to the control. β -actin was used as a loading control. (F) Quantification analysis of FEN1 protein levels normalised to β -actin in MDA-MB-436 cell line. Data presented as mean \pm SEM. N=3. **** $p < 0.0001$; ** $p < 0.01$.

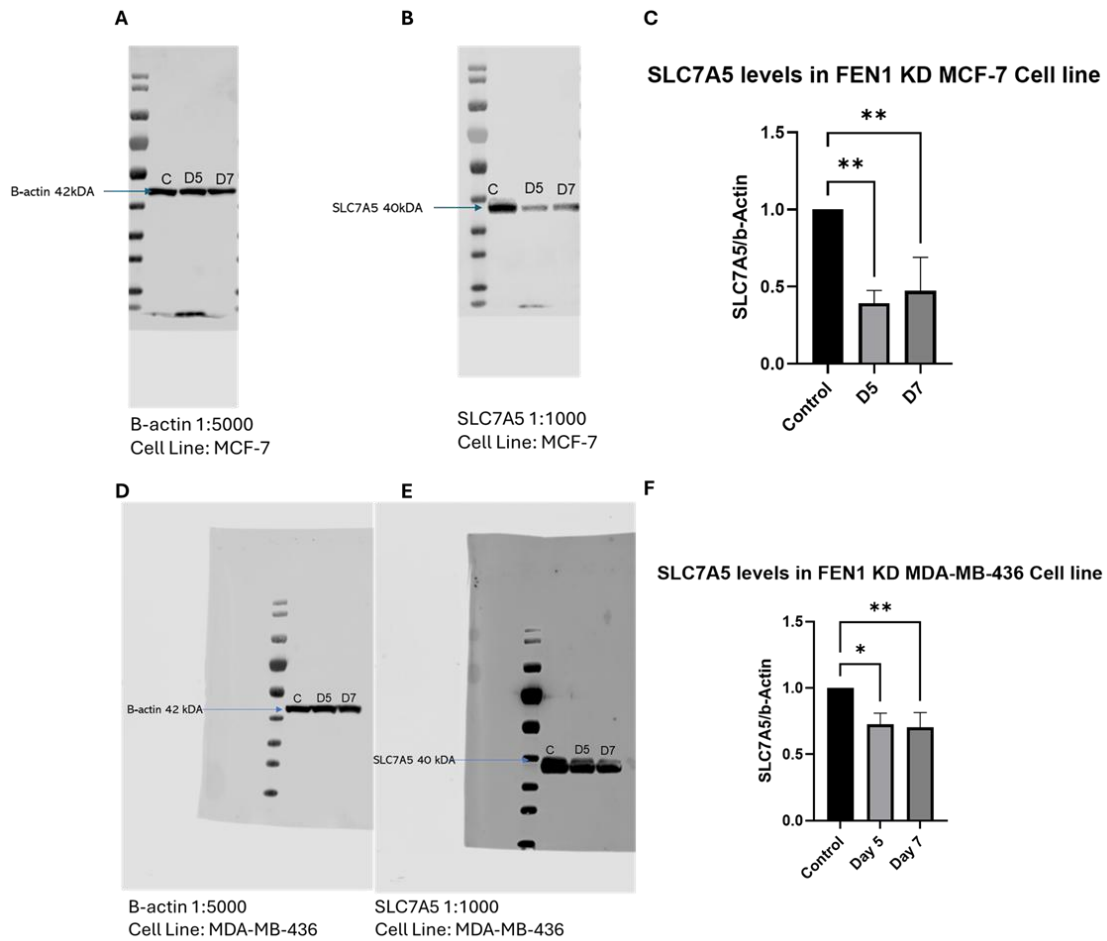


Figure 5.2. Impact of FEN1 knockdown on SLC7A5 protein levels in MCF-7 and MDA-MB-436 breast cancer cell lines. (A-B) Western blot analysis of SLC7A5 protein expression in the MCF-7 cell line following the knockdown of FEN1 on day 5 and day 7, compared to the control. β -actin was used as a loading control. (C) Quantification analysis of SLC7A5 protein levels normalised to β -actin in the MCF-7 cell line. (D-E) Western blot analysis of SLC7A5 protein expression in the MDA-MB-436 cell line following the knockdown of FEN1 on day 5 and day 7, compared to the control. B-actin was used as a loading control. (F) Quantification analysis of SLC7A5 protein levels normalised to β -actin in the MDA-MB-436 cell line. Data presented as mean \pm SEM. N=3. ** $p < 0.01$; * $p < 0.05$.

5.3.2 Effect of FEN1 and SLC7A5 knockdown on mitochondrial function in breast cancer cell line

In the MCF-7 cell line, single knockdown of FEN1 and SLC7A5 exhibited a significant reduction in basal respiration compared to the control cells (Figure 5.3B; $P < 0.0001$). The proton leak level was also significantly diminished in FEN1 KD cells, suggesting a reduction in mitochondrial membrane integrity. However, in SLC7A5 KD cells, the proton leak was less affected, with only a slight decrease compared to the control (Figure 5.3B; $P < 0.0001$). Similarly, ATP production-coupled respiration was markedly reduced in FEN1 KD cells, while SLC7A5 KD cells showed a moderate decrease (Figure 5.3B; all $P < 0.001$). Maximal respiration was significantly decreased in both FEN1 KD and SLC7A5 KD cells, in comparison to the control (Figure 5.3B; all $P < 0.001$). Spare respiratory capacity, which indicates the ability of cells to respond to increased energy demand, was significantly reduced in SLC7A5 KD cells (Figure 5.3B; $P < 0.01$), whereas FEN1 KD cells exhibited a slight reduction, but it was not statistically significant.

In contrast, the double knockdown of FEN1 and SLC7A5 resulted in a comparable reduction in basal respiration, proton leak and ATP production-coupled respiration to FEN1 KD (Figure 5.3B; all $P < 0.001$). Both DKD and FEN1 KD cells showed a significant decrease in basal respiration, proton leak and ATP production-coupled respiration compared to control and SLC7A5 KD (Figure 5.3B; all $P < 0.001$), indicating a loss of mitochondrial membrane integrity. However, Maximal respiration was markedly decreased in DKD cells, showing a significantly lower value compared to both FEN1 KD and SLC7A5 KD (Figure 5.3B; all $P < 0.05$). Similarly, spare respiratory capacity was significantly reduced in DKD and SLC7A5 KD cells ($P < 0.01$), while FEN1 KD exhibited a smaller but not statistically significant reduction in this parameter (Figure 5.3B). The OCR line graph (Figure 5.3A) illustrates a clear reduction in mitochondrial respiration in DKD cells compared to singular knockdowns and control, particularly after the sequential injection of oligomycin, FCCP, and rotenone/antimycin A.

In the MDA-MB-436 cell line, the line graph of OCR showed a decrease in the singular knockdown of FEN1 and SLC7A5 in comparison to control, while showing a more profound reduction in comparison to all conditions (Figure 5.4A).

Moreover, FEN1 KD and SLC7A5 KD led to a reduction in basal respiration, ATP production-coupled respiration, maximal respiration, and spare respiratory capacity compared to the control (Figure 5.4B: $P < 0.01$). FEN1 KD and SLC7A5 KD did not significantly affect proton leak in comparison to the control.

DKD cells showed a further reduction in basal respiration, ATP production-coupled respiration and maximal respiration, in comparison to the singular knockdowns and control (Figure 5.4B: all $P < 0.05$). Additionally, DKD cells exhibited a reduced proton leak and spare respiratory capacity, comparable to SLC7A5 KD levels and control (Figure 5.4B: all $P < 0.05$).

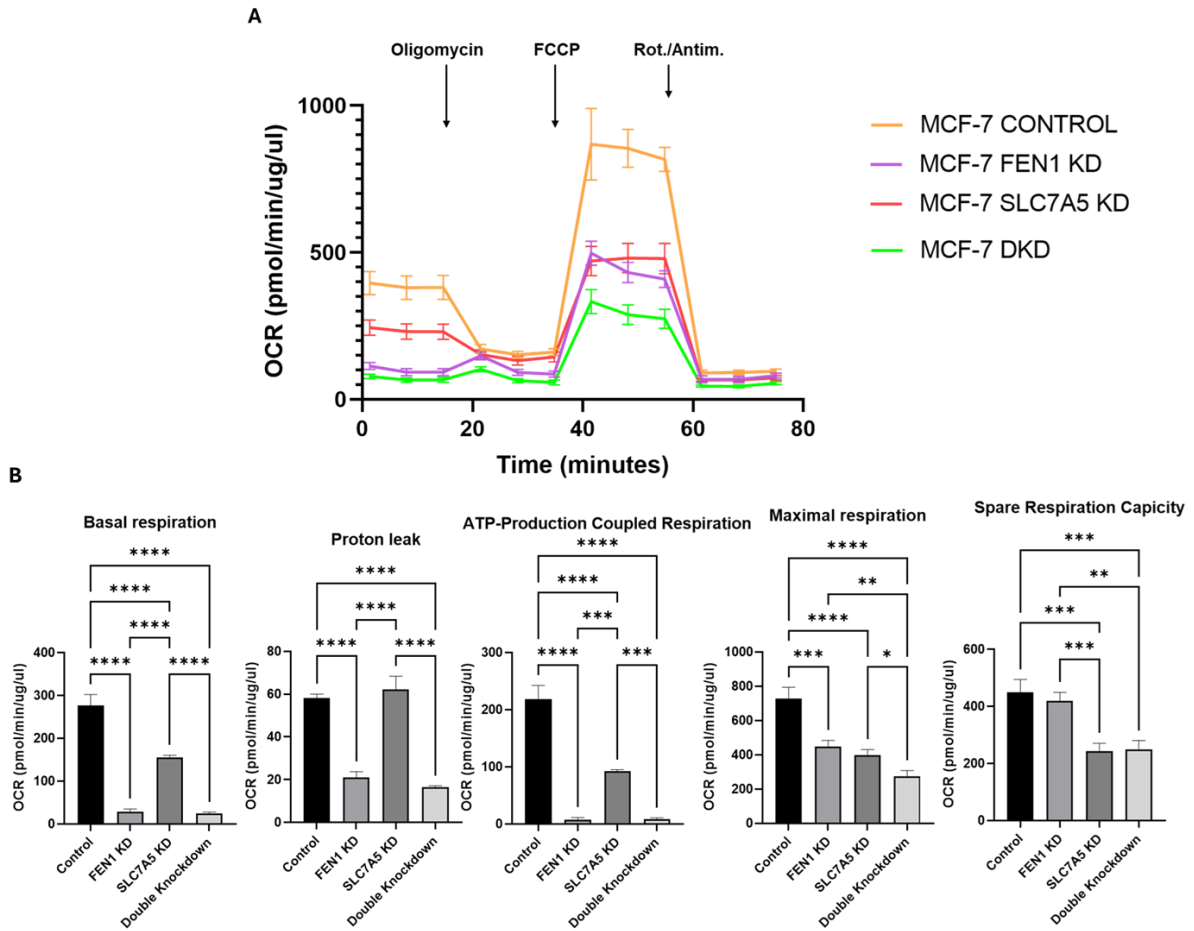


Figure 5.3. Effect of FEN1 and SLC1A5 knockdown on energy metabolism in MCF-7 BC cell line. MCF-7 harbouring DKD shows a significant decrease in mitochondrial oxygen consumption and mitochondrial ATP production. The Seahorse XF96 analyser was used to test the mitochondrial function of MCF-7 control, FEN1 KD, SLC7A5 KD, and FEN1/SLC7A5 DKD cells. (A) Representative real-time oxygen consumption rates (OCR) line graph of 3 repeats, bars represent means \pm SD. (B) Maximal respiration was significantly decreased in DKD cells in comparison to the control and the other two conditions. Data was normalised to mg protein content. The P-values * <0.05 , ** <0.01 , *** <0.001 and **** <0.0001 .

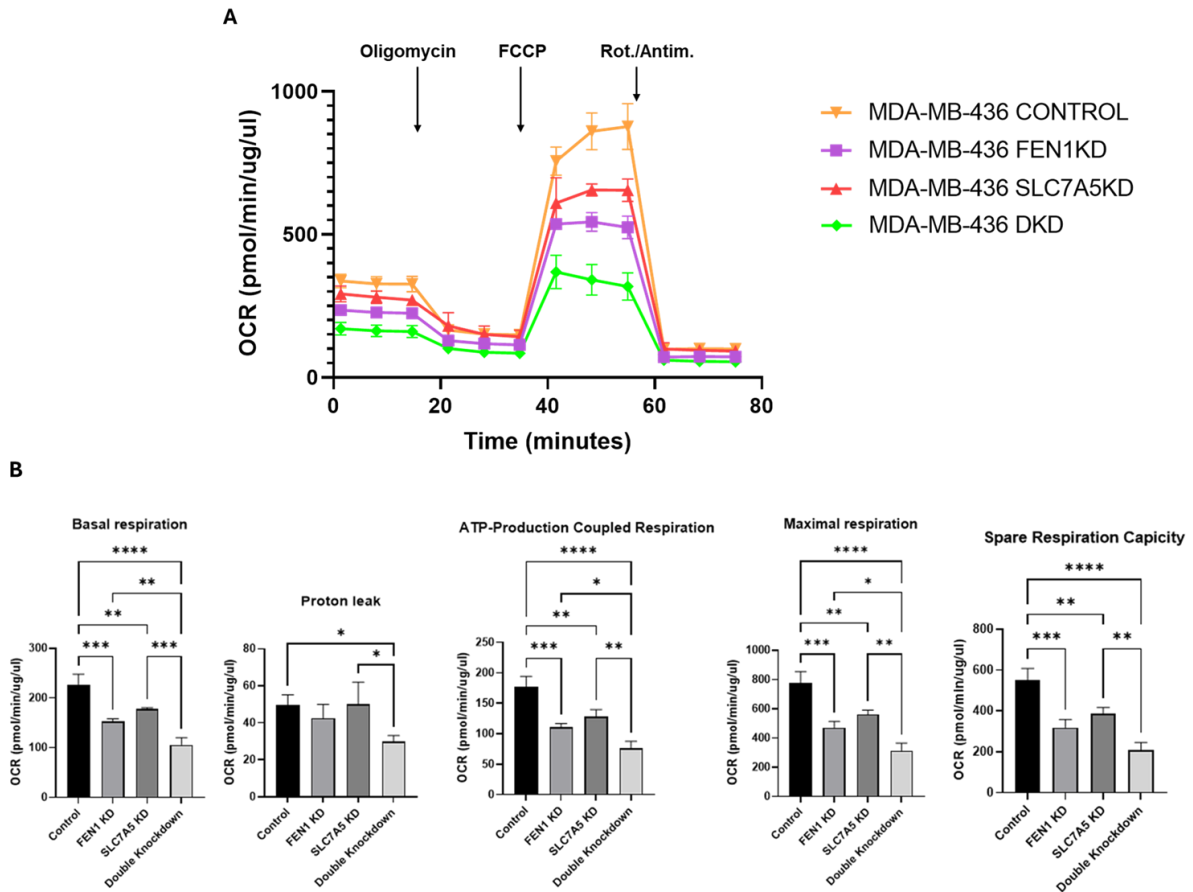


Figure 5.4. Effect of DKD on energy metabolism of MDA-MB-436 BC cell line. MDA-MB-436 harbouring DKD show a significant decrease in mitochondrial oxygen consumption and mitochondrial ATP production. The Seahorse XF96 analyser was used to test the mitochondrial function of MDA-MB-436 control, FEN1 KD, SLC7A5 KD and DKD cells. (A) Representative line graph of 3 repeats, bars represent means \pm SD. (B) Respiration (basal and maximum) and ATP production were significantly decreased in DKD cells in comparison to the control and the other two conditions. Data was normalised to mg protein content. The P-values * <0.05 , ** <0.01 , *** <0.001 and **** <0.0001 .

5.3.3 Impact of FEN1 and SLC7A5 knockdown on the metabolic phenotype of breast cancer cell line

In MCF-7 cells, single knockdown of FEN1 and SLC7A5 resulted in a significant increase in glycolytic activity, as indicated by elevated ECAR levels compared to both DKD and the control group (Figure 5.5A; all $P < 0.05$). The energy phenotype map further supports these findings, showing that both FEN1 KD and SLC7A5 KD conditions shifted toward a more glycolytic metabolic profile (Figure 5.5B). Conversely, DKD cells exhibited a distinct quiescent metabolic phenotype, characterised by a reduction in both oxidative and glycolytic capacities compared to the control and singular knockdown conditions (Figure 5.5B). This suggests that simultaneous depletion of FEN1 and SLC7A5 leads to a metabolic crisis, impairing the ability of the cells to engage in either energy production pathway.

For MDA-MB-436 cells, FEN1 KD showed a reduction in ECAR levels compared to control (Figure 5.6A; $P < 0.05$), while SLC7A5 KD exhibited a smaller but not statistically significant reduction in ECAR levels compared to control. However, DKD cells exhibited a significant reduction in ECAR compared to control and SLC7A5 KD cells (Figure 5.6A; $P < 0.01$).

The energy phenotype map (Figure 5.6B) revealed distinct metabolic states among the conditions. DKD cells demonstrated the most quiescent phenotype, characterised by decreased levels of both ECAR and OCR, indicating reduced glycolytic and oxidative activities. This suggests that DKD resulted in a metabolic shift towards a less active energy state compared to control and singular knockdown conditions.

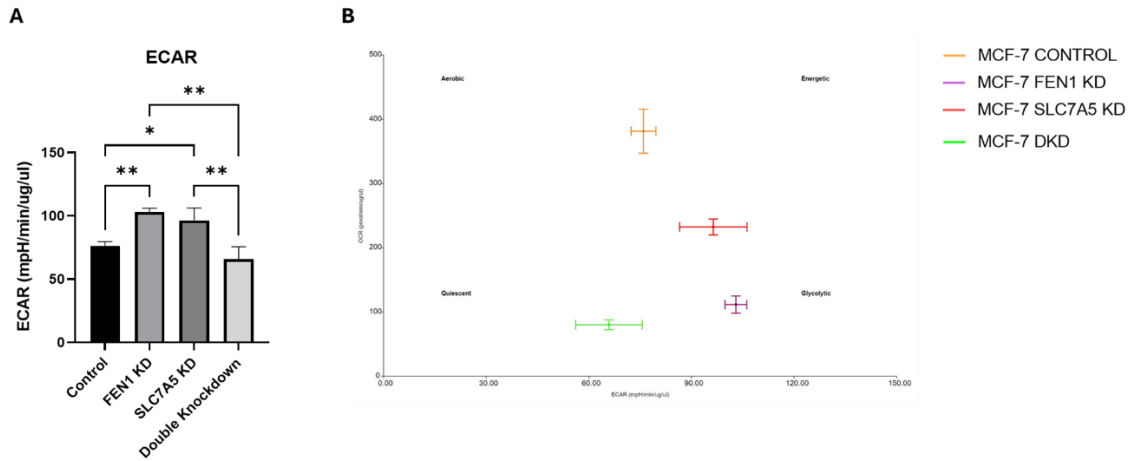


Figure 5.5. DKD shows quiescent energy phenotype compared to MCF-7 control and singular knockdown conditions. A. Extracellular acidification rate (ECAR) was determined by using Seahorse XF96 in MCF-7 control, FEN1 KD, SLC7A5 KD and DKD cell line. B. The energy map plot is representative of the metabolic phenotype of the cells. Data shown are means \pm SD. One-way analysis of variance (ANOVA) was used to assess variation between conditions. P-values $* < 0.05$, $** < 0.01$ (N=3).

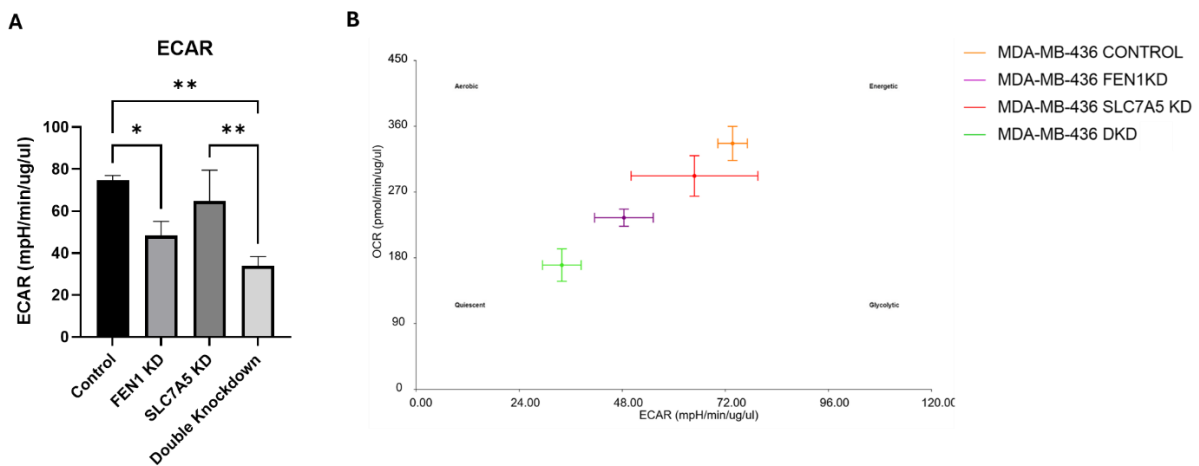


Figure 5.6. DKD shows quiescent energy phenotype in comparison to MDA-MB-436 control, FEN1 KD and SLC7A5 KD. A. Extracellular acidification rate (ECAR) was determined by using Seahorse XF96 in MDA-MB-436 control, FEN1 KD, SLC7A5 KD and DKD cell line. B. The energy map plot is representative of the metabolic phenotype of the cells. Data shown are means \pm SD. One-way analysis of variance (ANOVA) was used to assess variation between conditions. The P-values $* < 0.05$, $** < 0.01$ (N=3).

5.3.4 Identification of common protein partners between SLC7A5 and FEN1 in MCF-7 and MDA-MB-436 breast cancer cell line

To confirm the successful immunoprecipitation of FEN1 and SLC7A5 in both breast cancer cell lines, western blotting was performed following co-immunoprecipitation.

A Venn diagram was used to identify the common proteins between SLC7A5 and FEN1, which were 13 proteins in MCF-7 cells (Figure 5.8A). The common proteins showed high fold change (FC), which suggests that they were highly associated with both SLC7A5 and FEN1 pulldown (Table 5.1).

The Protein-Protein Interaction network (PPI) analysis for the mutual proteins showed multiple functionally enriched clusters and potential interactions between clusters representing DNA repair, nuclear transport, membrane repair, vesicle trafficking, and metabolic regulation (Figure 5.8B; PPI enrichment P-value $<1 \times 10^{-16}$).

Functional enrichment analysis was performed to investigate the biological significance of the identified common proteins and to determine the pathways associated with the shared proteins. The top 10 biological pathways are presented in Figure 5.9 ($P < 0.05$). The most significant pathways were import into nucleus, double-strand break repair via classical nonhomologous end joining (NHEJ), regulation of plasma membrane repair and pyrimidine ribonucleotide biosynthetic process (Figure 5.9).

In MDA-MB-436 cells, six common proteins were identified between SLC7A5 and FEN1 pulldown (Figure 5.10A). Three of these proteins showed positive FC, while the others showed negative FC, which indicated their downregulation in the pulldown in comparison to the IgG control (Table 5.2; $P < 0.05$). PPI was constructed to gain insight into the functional interaction between the upregulated proteins. The network formed distinct groups of interacting proteins, including glycerophospholipid metabolism, transport of ribonucleoproteins into the host nucleus, and glycerolipid metabolism (Figure 5.10B; PPI enrichment P-value $<1 \times 10^{-16}$).

Functional enrichment analysis was performed to determine the pathways associated with the upregulated shared proteins. The top 10 biological pathways are presented in Figure 5.11

($P < 0.05$). The results showed an association between the common proteins and mitochondrial function, nuclear transport and RNA metabolism.

A Venn diagram was used to identify overlapping proteins between the shared interactors of SLC7A5 and FEN1 in MCF-7 and MDA-MB-436 cell lines (Figure 5.11). However, no common proteins were found between the two datasets (Figure 5.11).

5.3.5 Cytidine triphosphate synthase 1 (CTPS1) and nucleoporin 205 (NUP205) correlate with SLC7A5 and FEN1 in MCF-7 and MDA-MB-436 cells.

In MCF-7 cells, CTPS1, a shared co-immunoprecipitant protein, showed a moderate positive correlation with both SLC7A5 ($r = 0.51$) and FEN1 ($r = 0.50$) (Table 5.3; all $P < 0.0001$). Similarly, in MDA-MB-436 cells, NUP205 demonstrated a moderate positive correlation with SLC7A5 ($r = 0.56$) and FEN1 ($r = 0.55$) (Table 5.3; all $P < 0.0001$). These findings were further supported by consistent results in the bc-GenExMiner dataset, reinforcing the association between the candidate proteins and the target genes (Table 5.3).

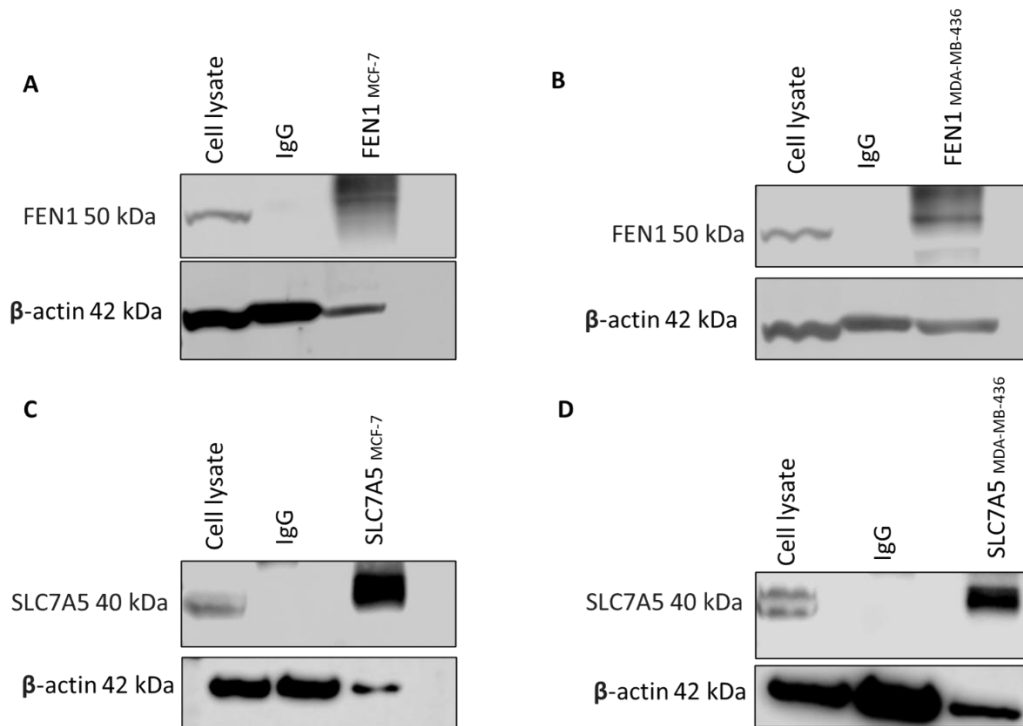


Figure 5.7. Validation of FEN1 and SLC7A5 immunoprecipitation in MCF-7 and MDA-MB-43 breast cancer cells. (A) FEN1 pulldown in MCF-7 cell line (B) FEN1 pulldown in MDA-MB-436 (C) SLC7A5 pulldown in MCF-7 (D) SLC7A5 pulldown in MDA-MB-436. In all WB, β -actin was used as a loading control and immunoglobulin (IgG) was used as a negative control.

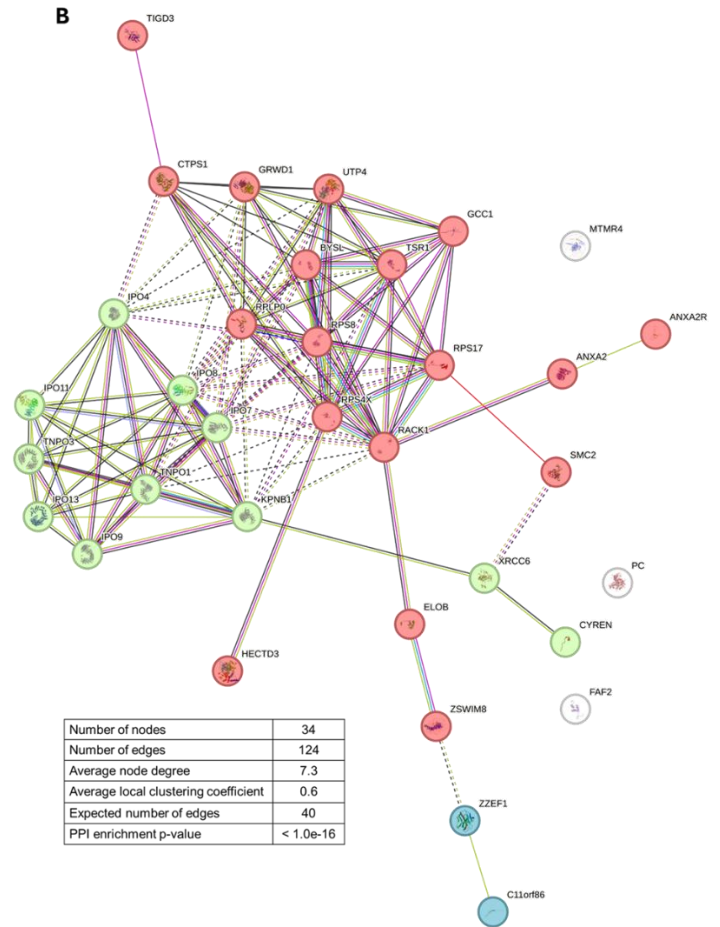
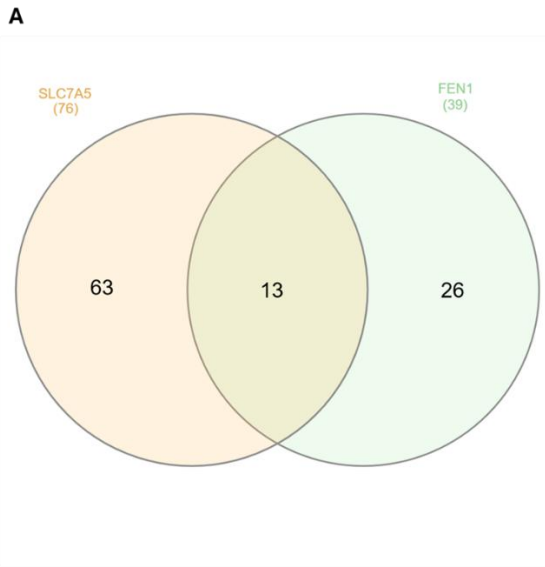


Figure 5.8. Venn Diagram of SLC7A5 and FEN1 pulldown and Protein-Protein Interaction (PPI) network of mutual proteins found between SLC7A5 and FEN1 in MCF-7 breast cancer cells. (A) The Venn diagram shows the overlap of proteins (n=13) found between SLC7A5 (red) and FEN1 (blue). **(B)** A Protein-Protein Interaction (PPI) network that was generated by using the STRING database displays the interactions between the shared proteins from the SLC7A5 and FEN1 pulldown experiment in MCF-7 cells. Nodes represent proteins, edges represent known interactions, and the colour-coded nodes show functionally distinct clusters. The green cluster, which represents DNA repair and genomic stability, the red cluster, which represents nuclear transport and mRNA processing, the blue cluster, which represents membrane repair and vesicle trafficking and the yellow cluster, which represents the metabolic regulation proteins. PPI enrichment p-value ($P < 1 \times 10^{-16}$).

Table 5.1. List of the shared proteins found from FEN1 and SLC7A5 pulldown in the MCF-7 cell line, with their respective fold change (FC) and P-values.

Gene Name	FEN1		SLC7A5	
	Log FC	P-value	Log FC	P-value
<i>MTMR4</i>	14.3	0.000009	13.3	0.00004
<i>HECTD3</i>	14.3	0.002	13.3	0.00004
<i>ZZEF1</i>	14.3	0.000009	13.3	0.00004
<i>GCC1</i>	14.1	0.001	13.8	0.0004
<i>PC</i>	13.3	0.00001	13.8	0.0004
<i>XRCC6</i>	13.8	0.0004	13.8	0.0004
<i>CTPS1</i>	13.3	0.00001	14.1	0.001
<i>FAF2</i>	14.3	0.000009	14.1	0.001
<i>IPO7</i>	14.1	0.001	15.2	0.0002
<i>RPLP0</i>	13.8	0.0004	15.1	0.0008
<i>SMC2L1</i>	14.9	0.0006	15.4	0.0003
<i>TNPO3</i>	14.3	0.002	15.9	0.00007
<i>ANXA2</i>	14.1	0.001	15.5	0.002

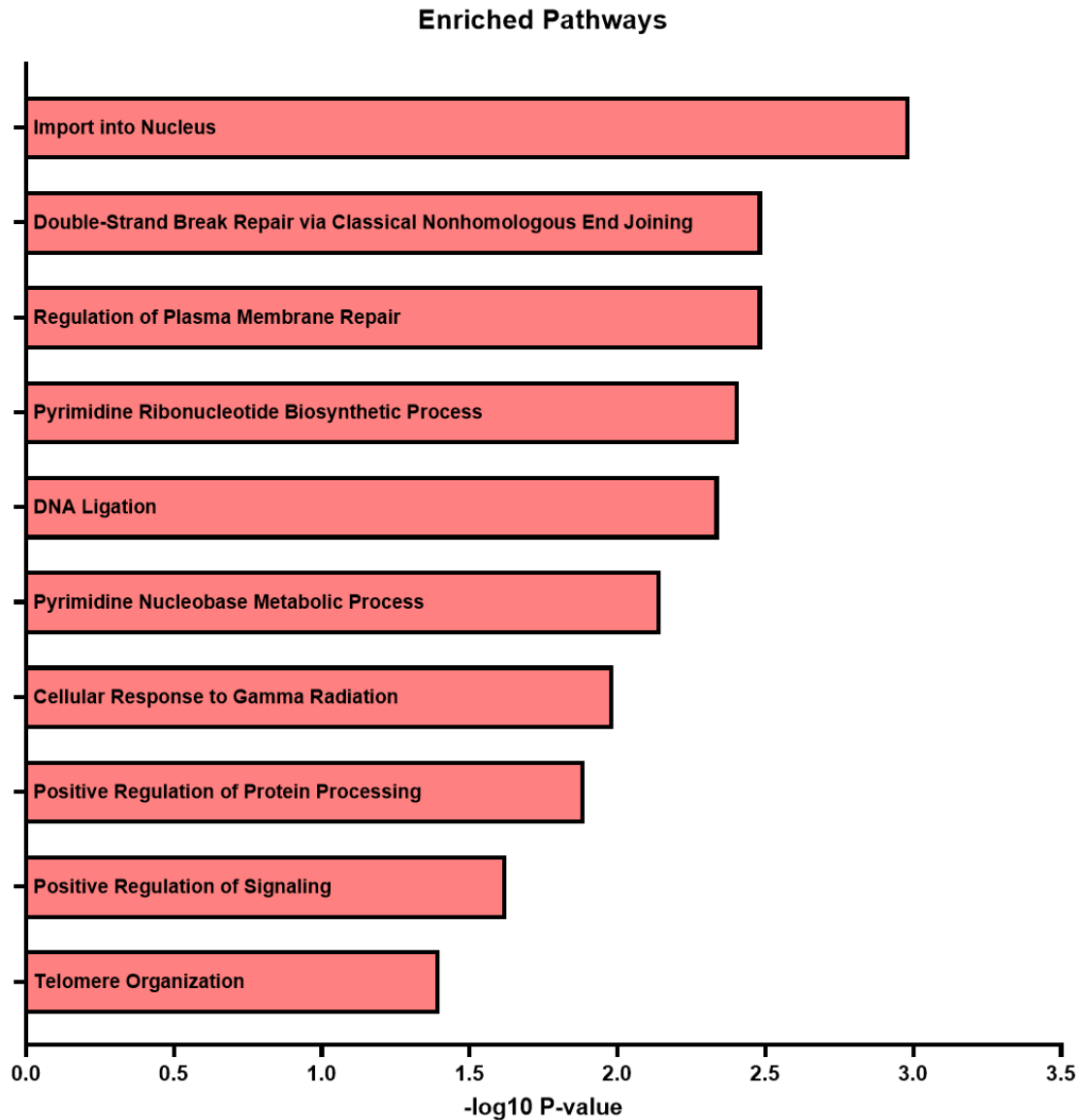


Figure 5.9. Functional enrichment analysis for the top 10 biological pathways derived from the shared proteins between SLC7A5 and FEN1 in the MCF-7 cell line. This bar graph represents the biological pathways enriched from the 13 shared proteins identified between SLC7A5 and FEN1 pulldown experiments in MCF-7 cells. The x-axis displays the \log_{10} -transformed P-values. The most significantly enriched pathways include import into the nucleus, double-strand break repair via classical nonhomologous end-joining (NHEJ), plasma membrane repair, pyrimidine biosynthesis/metabolic processes, and DNA ligation. The P-value obtained from the pathway enrichment analysis in Enrichr was computed using Fisher's exact test.

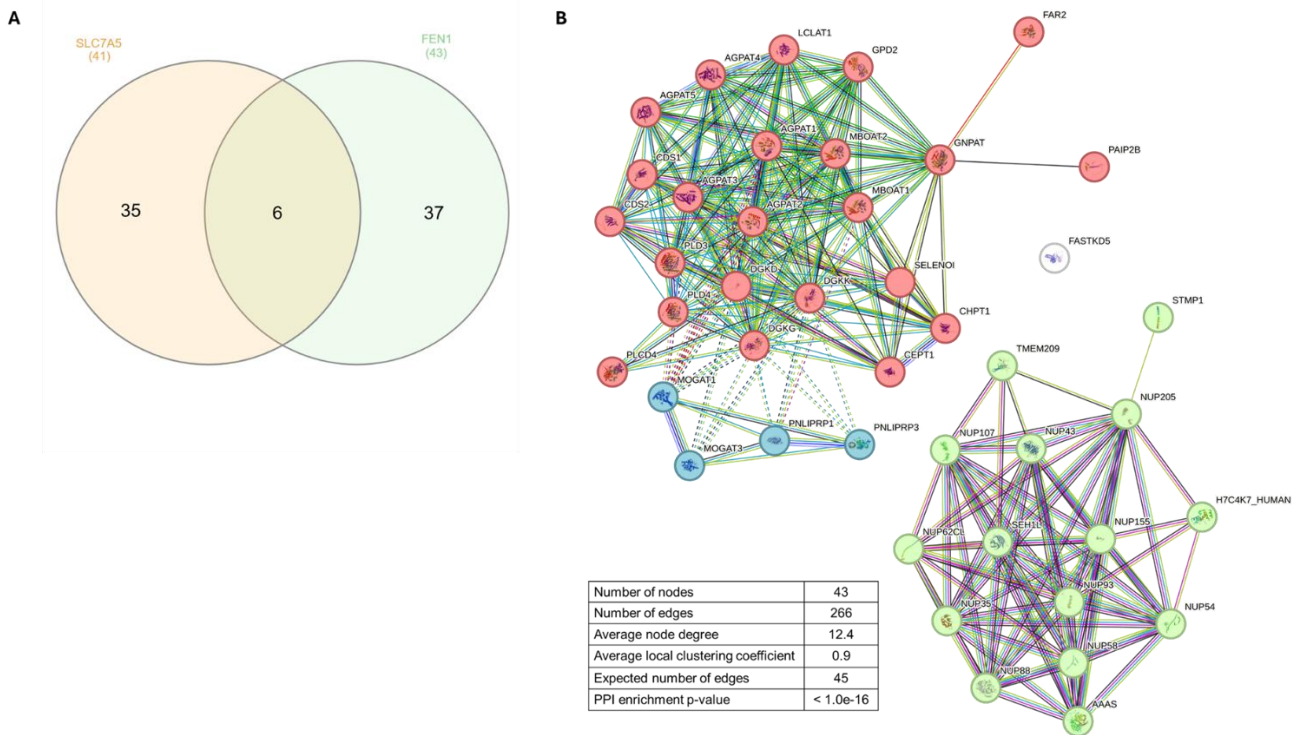


Figure 5.10. Venn Diagram of SLC7A5 and FEN1 pulldown and Protein-Protein Interaction (PPI) network of mutual proteins found between SLC7A5 and FEN1 in the MDA-MB-436 cell line. (A) The Venn diagram shows the overlap of proteins (n=6) found between SLC7A5 (red) and FEN1 (blue). (B) A PPI network that was generated by using the STRING database displays the interactions between the shared proteins from the SLC7A5 and FEN1 pulldown experiment in the MDA-MB-436 cell line. Nodes represent proteins, edges represent known interactions, and the colour-coded nodes show functionally distinct clusters. The network formed distinct groups of interacting proteins, including a red cluster which represents glycerophospholipid metabolism, a green cluster which represents transport of ribonucleoproteins into the host nucleus, and a blue cluster which represents glycerolipid metabolism. PPI enrichment p-value (1×10^{-16}).

Table 5.2. List of the proteins that were found common to SLC7A5 and FEN1 pulldown in the MDA-MB-436 cell line.

Gene Name	<i>FEN1</i>		<i>SLC7A5</i>	
	Log FC	P-value	Log FC	P-value
<i>NUP205</i>	13.3	0.001	15.3	0.001
<i>FASTKD5</i>	14.3	0.001	14.1	0.001
<i>DHAP-AT</i>	14.6	0.0004	13.8	0.0004
<i>PAN3</i>	-13.3	0.000007	-13.3	0.000007
<i>VPS51</i>	-13.3	0.000007	-13.3	0.000007
<i>TRIM47</i>	-13.3	0.000007	-13.3	0.000007

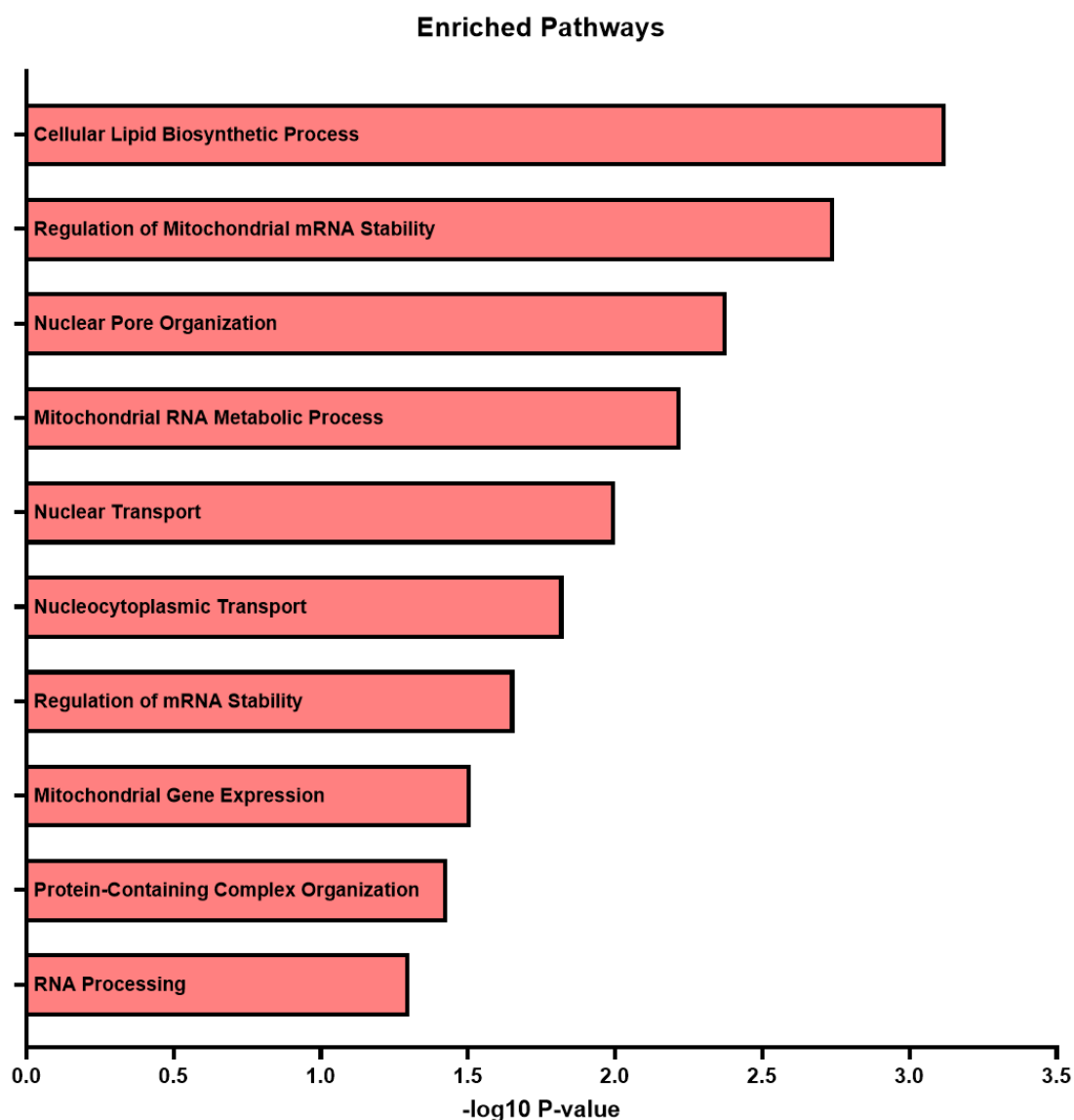


Figure 5.11. List of the top 10 biological pathways found in the enrichment analysis, derived from shared proteins between SLC7A5 and FEN1 in MDA-MB-436. This bar graph represents the biological pathways enriched from the 6 shared proteins identified between SLC7A5 and FEN1 pulldown experiments in MDA-MB-436 cells. The x-axis displays the log₁₀-transformed P-values. The most significantly enriched pathways include cellular lipid biosynthetic process, regulation of mitochondrial mRNA stability, nuclear pore organisation, mitochondrial RNA metabolic process and nuclear transport. The P-value obtained from the pathway enrichment analysis in Enrichr was computed using the Fisher's exact test.

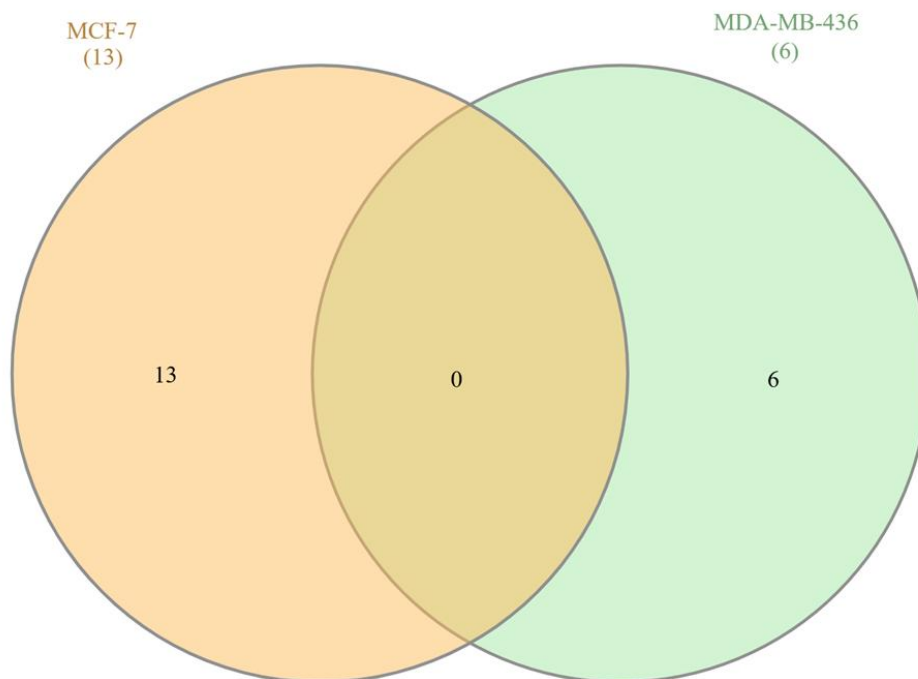


Figure 5.12. Venn diagram showing the overlap of significantly enriched shared proteins identified in FEN1 and SLC7A5 pulldown experiments between MCF-7 and MDA-MB-436 breast cancer cell lines. A total of 13 shared proteins were detected in the MCF-7 (orange circle), while 6 shared proteins were found in the MDA-MB-436 cell line (green circle). No shared proteins were common to both cell lines. The analysis was based on significantly enriched proteins identified by co-immunoprecipitation followed by mass spectrometry (fold change ≥ 0.6 ; $P < 0.05$), and proteins were considered shared if they were significantly enriched in both FEN1 and SLC7A5 pulldown conditions relative to IgG control.

Table 5.3. Correlation analysis of shared co-immunoprecipitant proteins identified between SLC7A5 and FEN1 mRNA in MCF-7 and MDA-MB-436 cell lines using METABRIC and bc-GeneMiner breast cancer datasets.

Cell line	Common protein	METABRIC r (p-value) n=1980	GeneMiner r (p-value) n=4421
MCF-7	CTPS1 mRNA vs SLC7A5	0.51 (< 0.0001)	0.55 (< 0.0001)
	CTPS1 mRNA vs FEN1	0.50 (< 0.0001)	0.58 (< 0.0001)
MDA-MB-436	NUP205 mRNA vs SLC7A5	0.56 (< 0.0001)	0.41 (< 0.0001)
	NUP205 mRNA vs FEN1	0.55 (< 0.0001)	0.47 (< 0.0001)

r: Pearson correlation coefficient. P values in bold mean statistically significant.

5.4 Discussion

Breast cancer cells exhibit the ability to modulate their metabolic and DNA pathways to support their proliferation and survival under stress conditions [200]. SLC7A5 and FEN1 are two critical regulators of glutamine metabolism and DNA repair, respectively. In the previous chapters, the high expression of both SLC7A5 and FEN1 was associated with poor survival outcome in breast cancer patient, suggesting their potential role in tumour progression (Chapter 3). Building on this, the functional impact of SLC7A5 and FEN1 double knockdown revealed significant effects on cancer cell behaviours, including proliferation, migration, invasion, cell cycle progression, and apoptosis (Chapter 4). This chapter explored the association between SLC7A5 and FEN1 by investigating their role in mitochondria and identifying shared interacting proteins.

The results in this chapter revealed that the levels of FEN1 protein were affected by the knockdown of SLC7A5 in MCF-7 and MDA-MB-436 cell lines. SLC7A5 plays a central role in activating mTORC1, which in turn is critical for the regulation of DNA repair, nucleotide biosynthesis, and metabolic adaptation [206]. The observed changes in FEN1 expression upon the depletion of SLC7A5 suggest that SLC7A5-mediated amino acid transport has an impact on the DNA repair mechanisms via metabolic pathways, more specifically, mTORC1. However, the effect was more profound in MCF-7 cells, which suggests that MCF-7 is more reliant on SLC7A5 expression than the MDA-MB-436 cell line, and knocking it down triggered stronger metabolic and regulatory effects, leading to the downregulation of FEN1 expression. The expression of SLC7A5 is associated with increased proliferation and poor prognosis in oestrogen receptor-positive breast cancer cell lines [70]. Also, the metabolic landscape of the triple-negative breast cancer cell line is more flexible, meaning that these cells are more likely to compensate for the loss of SLC7A5 through alternative pathways [207].

Similarly, the results showed that the downregulation of SLC7A5 protein levels was substantial in MCF-7 cells in comparison to the MDA-MB-436 cell line when FEN1 was knocked down. It was demonstrated that FEN1 levels were associated with an increase in ER activity [208]. Also, FEN1 interacts directly with $E\alpha$ protein, which leads to an increase in its transcriptional activity [209]. Moreover, oestrogen plays an important role in the upregulation of SLC7A5 expression, particularly in ER-positive breast cancer [210], as SLC7A5 is considered to be a direct transcriptional target for ER [153].

The Seahorse analysis revealed that after double-knockdown of SLC7A5 and FEN1, the production of ATP through OXPHOS was reduced in both cell lines, albeit at different levels, which suggests that both of these proteins contribute to mitochondrial bioenergetics. The knockdown of SLC7A5 also affects leucine-dependent mitochondrial activity, hence the activation of mTORC1, which led to metabolic stress [211]. A previous study demonstrated that upon the inhibition of mTORC1 activity in MCF-7 cells, there was a striking reduction in the intermediates of the tricarboxylic acid (TCA) cycle, which was accompanied by diminished respiration, indicating the impaired function of mitochondria, hence the reduction of ATP synthesis [212]. Furthermore, the study demonstrated that mTORC1 plays an important role in controlling mitochondrial activity, via the inhibition of the eukaryotic translation initiation factor 4E (eIF4E)-binding proteins (4EBPs), which in turn promote the translation of nucleus-encoded mitochondria-related mRNAs. In addition, the study found that mTORC1 signalling inhibits the degradation of mitochondria by suppressing autophagy [212].

FEN1 plays an important role in repairing the mitochondrial oxidative DNA damage through the long patch BER (LP-BER). Subcellular fractionation and immunofluorescence studies demonstrated the localisation of FEN1 in the mitochondria [201]. The previous study showed that after the removal of FEN1 expression in epithelial cells (HeLa) cell line, the activity of LP-BER was diminished in mitochondria. The study also demonstrated that the oxidative DNA damage in mitochondria was greater, and the recovery was slower in FEN1-depleted cells in comparison to control cells [201]. This supports the results of this Chapter, as it was

demonstrated that the double knockdown of SLC7A5 and FEN1 altered the mitochondrial function, which causes the reduction of ATP synthesis.

However, the effect of double knockdown was substantial in MCF-7 cells in comparison to MDA-MB-436 cells, the proton leak in MCF-7 was diminished, while in MDA-MB-436 cells, it was only slightly affected, which indicated to mitochondrial membrane damage that is likely as result of the high oxidative stress, which led to the severe reduction of ATP-linked respiration in MCF-7 cells compared to MDA-MB-436 cells. In general, TNBC cells tolerate high oxidative stress better than luminal cell lines [213], as they have a high expression of antioxidant enzymes, such as superoxide dismutase (SOD), catalase and glutathione peroxidase [214], they also maintain high levels of glutathione, which buffers oxidative stress [215], the nuclear factor erythroid 2-related factor 2 (NRF2) signalling is upregulated in TNBC, which promotes redox homeostasis and antioxidant responses [216].

Furthermore, TNBC cells have special metabolic characteristics in comparison to luminal cell lines, such as high glucose uptake for glycolysis, fatty acid oxidation, and increased lactate production [196], which enables TNBC cells to generate more ATP and decrease their oxidative stress. The results also showed that double knockdown of SLC7A5 and FEN1 caused both cell lines to switch to a quiescent state. Moreover, there was no noticeable change in the glycolytic activities of MCF-7 cells, that harbour the double knockdown mutation, which indicated that MCF-7 cell line managed to keep its glycolytic activity to compensate for the impaired OXPHOS metabolic process, while MDA-MB-436 cell line had a moderate decrease in their glycolytic activity, as it managed to keep some of its mitochondrial activity for the ATP production through OXPHOS. The primary signalling pathway for activating glycolysis is the PI3K/Akt pathway, as it increases the glucose uptake in cancer via inducing the expression of glucose transporter 1 (GLUT1) and GLUT4 [217], it is known that MCF-7 cell line harbours a PIK3CA mutation [218], furthermore, this mutation was found substantially higher in luminal cell line compared to the triple negative cell line [219]. Also, another way to increase the glycolytic activity in cancer cells is via mTORC1 signalling, as it affects the transcription and activity of enzymes that influence glycolysis [220]. The activity of mTORC1

is higher in triple-negative cell lines compared to luminal cell lines [221]. Moreover, FEN1 depletion, which causes the impaired function of mitochondria, activates AMP-activated protein kinase (AMPK), which in turn inhibits mTORC1 activity, hence lowering the glycolysis process [222]. This aligns with the results in the Chapter and further explains the higher glycolytic activity in MCF-7 cells compared to MDA-MB-436 cells after the double knockdown of SLC7A5 and FEN1. Notably, MDA-MB-436 cells are more reliant on mTORC1 signalling, whereas MCF-7 cells are more dependent on the PI3K/Akt pathway. However, the glycolysis effect on breast cancer cell lines needs further investigation, as more accurate reading of the glycolysis process could be achieved by using the Agilent Seahorse glycolysis stress kit, which provides the chance to measure key parameters for glycolysis, such as basal glycolysis, glycolytic capacity and glycolytic reserve.

This Chapter further explored the association between SLC7A5 and FEN1 in breast cancer cell lines. The proteomics analysis in the MCF-7 cell line showed a functional association between glutamine metabolism and DNA repair, which was through finding the common proteins between SLC7A5 and FEN1. Annexin A2 (ANXA2) is one of the common proteins, and it functions in repairing the plasma membrane damage. A previous study demonstrated its importance, showing that ANXA2 expression and function were required for invasive breast and prostate cancer [223]. Furthermore, it plays an important role in maintaining mitochondrial function, as it was demonstrated in a previous study that the downregulation of ANXA2 in lung cancer cells reduces the expression of Long Optic Atrophy 1 (L-OPA1) [224], which functions to mediate mitochondrial fusion and maintain its structural integrity [225]. Moreover, another common protein was CTPS1, which plays a key role in DNA synthesis, and it is particularly involved in the pyrimidine nucleobase metabolic process [226]. The upstream of *de novo* pyrimidine synthesis is controlled by mTORC1, while CTPS1 is the downstream of this process. Downregulation of mTORC1 signalling also affects the activity of CTPS1 in Mantle cell lymphoma (MCL) cell line [227], hence reducing the availability of the nucleotide pool, which is required for DNA repair via FEN1. This mechanistic link supports the correlation

results presented in this chapter, where CTPS1 expression in MCF-7 cells showed a moderate and positive association with both FEN1 and SLC7A5.

Another common protein was the DNA repair protein X-ray repair cross complementing 6 (XRCC6), which is specifically involved in the non-homologous end joining (NHEJ) pathway [228]. Even though there is no evidence of the involvement of XRCC6 in the repair of mtDNA, however, one study demonstrated the important role of XRCC6 in DNA repair under oxidative stress in cancer cells [229]. Furthermore, the PPI network further supports this evidence, as it showed the interaction between the DNA repair pathways, nucleotide synthesis and membrane dynamics. This suggests functional interactions between common proteins identified in SLC7A5 and FEN1 pulldowns in MCF-7 cells.

Few common proteins were found in MDA-MB-436 cells, including NUP205, Dihydroxyacetone Phosphate Acyl Transferase (DHAP-AT) and FAST Kinase Domains 5 (FASTKD5). The protein NUP205 is the main component of the nuclear pore complex (NPC), which plays an important role in nucleocytoplasmic molecule exchange. NUP205 was found to contribute to tumour progression, for example, its expression was found upregulated in lung cancer, bladder cancer and colorectal cancer [230]. Furthermore, there was study that investigated the effect of inhibiting the NPC assembly on the mTORC1 signalling in human melanoma cell line, the study demonstrated that inhibiting NPC assembly led to impair mTORC1 signalling, which reduced the phosphorylation of S6 kinase [231], which plays a crucial role in pyrimidine biosynthesis [232]. Moreover, the second common protein was DHAP-AT, also known as glyceronephosphate O-acyltransferase (GNPAT) is an enzyme that catalyses the initial step in the biosynthesis of plasmalogens, a subset of phospholipids [233]. It also participates in lipid metabolism [234]. The substrate of DHAP-AT is dihydroxyacetone phosphate (DHAP). It was previously shown that the fluctuation of DHAP levels influences the activity of mTORC1 activity, DHAP-AT role in managing the concentration of DHAP positions it as a potential modulator of mTORC1 signalling, thereby influencing the nucleotide biosynthesis [234]. This indicates the importance of NUP205 and DHAP-AT in the regulation of mTORC1, hence its contribution to nucleotide biosynthesis, which aligns with the results

from the MDA-MB-436 cell line, particularly NUP205, as it demonstrated a moderate positive correlation with both SLC7A5 and FEN1 mRNA expression. Furthermore, the PPI network analysis highlighted the interactions between nuclear transport and lipid biosynthesis.

Another common protein in the MDA-MB-436 cell line was FASTKD5, which helps to regulate the energy balance in mitochondria under stress conditions and process mitochondrial RNA [235]. In addition, FASTKD5 expression is upregulated in several cancer types, such as liver, lung, oesophageal and stomach cancers [236]. The dysfunction of FASTKD5 impairs the OXPHOS process in mitochondria [237], which supports the results from the sea-horse experiment, as after the double knockdown of SLC7A5 and FEN1 in MDA-MB-436, the function of mitochondria was partially impaired.

No overlapping shared proteins were found between the SLC7A5-FEN1 interactomes in MCF-7 and MDA-MB-436 cells, which suggests that the interaction landscape of these proteins is influenced by the molecular subtype of breast cancer. MCF-7 cells, which are ER+, and MDA-MB-436 cells, which are triple-negative, differ significantly in their transcriptional and metabolic profiles [238]. These differences may change the cellular environment and post-translational modifications of SLC7A5 and FEN1, resulting in distinct protein-protein interaction networks.

This chapter demonstrated that the expression of SLC7A5 and FEN1 is functionally interconnected in breast cancer cell lines, supporting the hypothesis that their expression levels influence each other and impact mitochondrial function. The double knockdown of SLC7A5 and FEN1 impaired mitochondrial activity, reduced ATP production, and altered protein interactions crucial in genomic stability and cancer survival. Furthermore, the findings highlighted how the association between SLC7A5 and FEN1 bridged the connection between glutamine metabolism and the DNA repair pathway, particularly through mTORC1 signalling and its effect on the availability of nucleotide pool, as well as the mitochondrial metabolism in breast cancer cell lines.

Chapter 6 Exploring EXO1 as a prognostic marker and its significant association with SLC7A5 in breast cancer

6.1 Introduction

In previous chapters, the interplay between glutamine metabolism and DNA repair pathways was explored through the assessment in breast cancer clinical cohorts and at the functional and proteomic levels in breast cancer cell lines. These findings highlighted the prognostic utility and the biological relevance of their high expression in relation to cancer cell behaviour. Building on this, the current chapters shift focus to further dissect the potential molecular links between metabolic regulation and DNA repair, specifically through the lens of the DNA mismatch repair (MMR) pathway.

DNA MMR is a critical mechanism that corrects errors in DNA replication, which helps in maintaining genomic stability. Key MMR proteins including postmeiotic segregation increased 1 (PMS1), postmeiotic segregation increased 2 (PMS2), MutL Homolog 1 (MLH1), MutL Homolog 3 (MLH3), MutS protein homologue 2 (MSH2), MutS homologue 3 (MSH3), MutS homologue 6 (MSH6) and Exonuclease 1 (EXO1) [239], these proteins work together to recognize and process mismatched DNA, preventing mutations from being permanently incorporated into the genome [239]. Defects in the MMR pathway lead to the accumulation of mutations, contributing to the cancer progression and development [239], such as colorectal cancer [240], endometrial cancer [241] and brain tumours [242]. The deficiency of DNA MMR proteins, including MSH2, MSH6, MLH1 and PMS2 in breast cancer, leads to the accumulation of mutations, promoting more aggressive tumour progression [131]. Notably, EXO1 upregulation has been linked to cancer development and progression, with studies showing its overexpression in ovarian cancer, where it contributes to chemoresistance [243]. Functionally, EXO1 is an enzyme that possesses 5' to 3' exonuclease and RNase H-like activity. It is known to interact with MSH2 in MMR and plays a role in homologous recombination [243].

There are growing evidence suggests a tight link between glutamine metabolism and DNA repair, with amino acids such as glutamine serving not only as metabolic fuel, but also as precursor for nucleotide biosynthesis, thereby influencing DNA replication and repair processes [244].

Although EXO1 was not the primary focus of earlier experimental chapters, it was identified as moderately correlated with SLC7A5 using the Breast Cancer Gene-Expression Miner v5.1 (bc-GenExMiner v5.1), also, it is known to work together with FEN1, particularly in DNA repair and replication [243], prompting further investigation into its clinical relevance in breast cancer.

This study aims to assess the relationship between SLC7A5 with mismatch DNA repair genes specifically EXO1 and their prognostic utility in breast cancer.

6.1.1 Hypothesis

The high expression of SLC7A5/EXO1 is associated with specific clinicopathological features and molecular biomarkers, and it serves as a potential prognostic marker in breast cancer patients.

6.1.2 Aims

1. Evaluate the clinicopathological significance of EXO1 at the mRNA and protein levels in breast cancer.
2. Assess the prognostic utility of EXO1 in breast cancer.
3. Investigate, at mRNA and protein levels, the correlation of SLC7A5 and EXO1 with clinicopathological parameters and relevant molecular biomarkers.
4. To find the prognostic value of the high expression of SLC7A5/EXO1 in breast cancer.

6.2 Methods

6.2.1 SLC7A5 and mismatch DNA repair genomic and transcriptomic analysis in breast cancer

The Molecular Taxonomy of Breast Cancer International Consortium (METABRIC) cohort (n=1980) was used to determine the correlation between SLC7A5 and mismatch DNA repair genes, including PMS1, PMS2, MLH1, MLH3, MSH2, MSH3, MSH6 and EXO1 [155]. This list of genes was preselected based on previous studies that identified them as core components of the MMR pathway [245, 246]. Breast Cancer Gene-Expression Miner v5.1 (bc-GenExMiner v5.1) online database was used for validation (previously described in Chapter 2, section 2.1.2) [156].

The METABRIC dataset was used to further assess the prognostic value of EXO1 and SLC7A5/EXO1 expression. EXO1 and SLC7A5 mRNA expression were dichotomised into low and high based on the median expression, the cases were then divided into 4 categories (SLC7A5+EXO1+, SLC7A5+EXO1-, SLC7A5-EXO1+ and SLC7A5-EXO1-). Then the association between the groups and clinicopathological parameters, molecular biomarkers and patient outcome were investigated. The MethSurv tool (<https://biit.cs.ut.ee/methsurv/>) was used to investigate the DNA methylation of EXO1 and its relation to patient outcome in TCGA data [247]. The level of EXO1 expression was dichotomised into low and high based on the median provided by the tool. UALCAN (<http://ualcan.path.uab.edu>) online resource was used to assess the expression of EXO1 and its promoter level of methylation in normal tissue and breast cancer tissue in the TCGA data [248]. TIMER dataset (<http://timer.cistrome.org/>) was used to assess the EXO1 mRNA expression in the following subsets: CD8+, CD4+, B cells, neutrophils and macrophages [249]. KM plotter (<http://kmplot.com/>) was also used as an external validation dataset [157].

6.2.2 EXO1 protein expression in breast cancer

The expression of EXO1 protein was evaluated in a cohort of 715 patients with early-stage primary operable invasive breast cancer who presented to Nottingham City Hospital, UK between 1986 and 2006, further description in Chapter 2 section 2.1.3.

6.2.3 Western blot

EXO1 polyclonal primary antibody specificity (PA5-86470, Fisher Scientific, UK) was determined using western blot in breast cancer cell line lysates MCF-7, MDA-MB-436, MDA-MB-468, ZR-751, MDA-MB-231 and HCC1500 (American Type Culture Collection; Rockville, MD, USA) at a dilution of 1:2000, further description in chapter 2 section 2.4.

6.2.4 Tissue array and Immunohistochemistry analysis

Details of the immunohistochemistry (IHC) staining and evaluation were performed as described in Chapter 2, section 2.2.

Briefly, EXO1 protein expression in the Nottingham cohort was analysed using immunohistochemistry (IHC), which was performed on a 4 µm breast cancer tissue microarray (TMA). The Novolink Max Polymer Detection System (RE7280-K, Leica Biosystems, UK) was used to stain protein expression. Heat-induced antigen epitope retrieval was performed in citrate buffer (ph 6.0) for 30 minutes in a water bath at 100°C temperature. The TMAs were incubated with EXO1 primary antibody at a 1:100 dilution in antibody diluent (RE AR9352, Leica Biosystems, Newcastle upon Tyne, UK) overnight at 4°C.

EXO1 protein expression was dichotomised into high and low expression groups using the median H-score value of 0. The Interclass Correlation Coefficient (ICC) analysis showed good reliability between the observers (Ali Fakroun and Ruths Park) (ICC=0.856; P=3.1x10⁻¹⁰).

Breast cancer tissue sections demonstrated a homogenous nuclear staining pattern indicating the suitability of TMA to evaluate the expression of EXO1. The protein expression of EXO1 was dichotomised into low (H-score=0) and high (H-score>0) based on the median.

6.2.5 Statistical analysis

Statistical Package for the Social Sciences (SPSS) software Version 28.0.0.0 (SPSS Inc., Chicago, IL, USA) was used for statistical tests. Pearson's correlation coefficient was used to find the correlation between SLC7A5 mRNA and the other DNA repair mRNAs. The Chi-squared test was used to evaluate the association between clinicopathological parameters and the singular EXO1 expression and the expression of SLC7A5/EXO1 at the mRNA and protein levels. Kaplan-Meier and log-rank tests were used to assess the clinical outcome. A multivariate Cox regression analysis was used to identify the independent prognostic factors. The P-value of <0.05 was considered significant.

6.3 Results

6.3.1 EXO1 Expression in breast cancer.

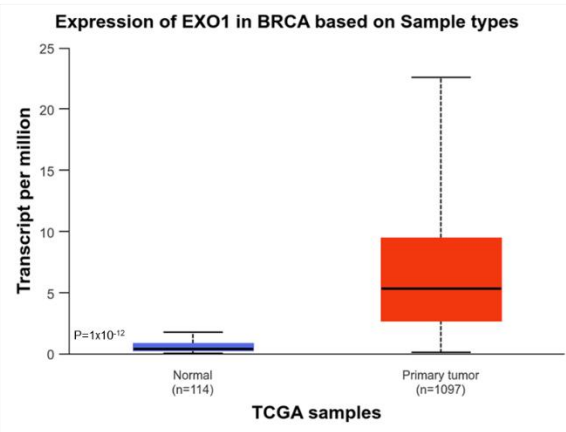
The expression of EXO1 mRNA in breast cancer was significantly higher than in normal tissue (Figure 6.1A; $P=1 \times 10^{-12}$). In breast tumours, the promoter methylation of EXO1 was slightly lower than normal tissue (Figure 6.1B; $P=4.2 \times 10^{-6}$). Suggesting that Methylation of EXO1 in breast cancer was seen in 13 different CpG sites across TSS1500:TSS200body, body and 3'UTR (Figure 6.2).

Within the METABRIC dataset, SLC7A5 were weakly negatively correlated with PMS1, PMS2, MLH1 and MSH3 ($r=-0.13$, -0.16 , -0.24 and -0.27 , respectively) (Table 6.1; all $P<0.0001$). Moderate positive correlation was found between SLC7A5 and EXO1 ($r=0.62$) (Table 6.1; $P<0.0001$), while weak positive correlation was observed with MSH2 and MSH6 ($r=0.05$ and 0.32 ; $P=0.02$ and $P<0.0001$, respectively), however, there was no significant correlation between SLC7A5 and MLH3 (Table 6.1; $P>0.05$). Similar results were observed in the bc-GenExMiner dataset, which was used to further validate the correlation between SLC7A5 and the DNA mismatch repair genes (Table 6.1).

Western blot was used to determine the protein expression of EXO1 in several breast cancer cell lines (Figure 6.3). EXO1 bands were observed in MCF-7, MDA-MB-436, MDA-MB-468 and ZR-751 cell line at around 115 kilodalton (kDa), while there were faint bands found in MDA-MB-231 and HCC-1500 cell line.

EXO1 protein expression was found in the nucleus of invasive breast cancer cells (Figure 6.4A and B). The protein expression ranged from low to high, and a total of 472 cases had low nuclear EXO1 expression, while 243 cases showed high nuclear EXO1 expression.

A



B

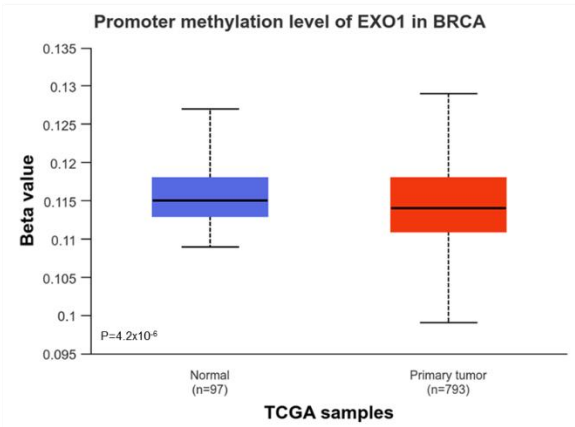


Figure 6.1. Differential expression and promoter methylation of EXO1 in breast cancer (A) comparison of EXO1 expression based on sample types between normal breast and breast cancer. **(B)** Promoter methylation level of EXO1 in normal breast and breast cancer.

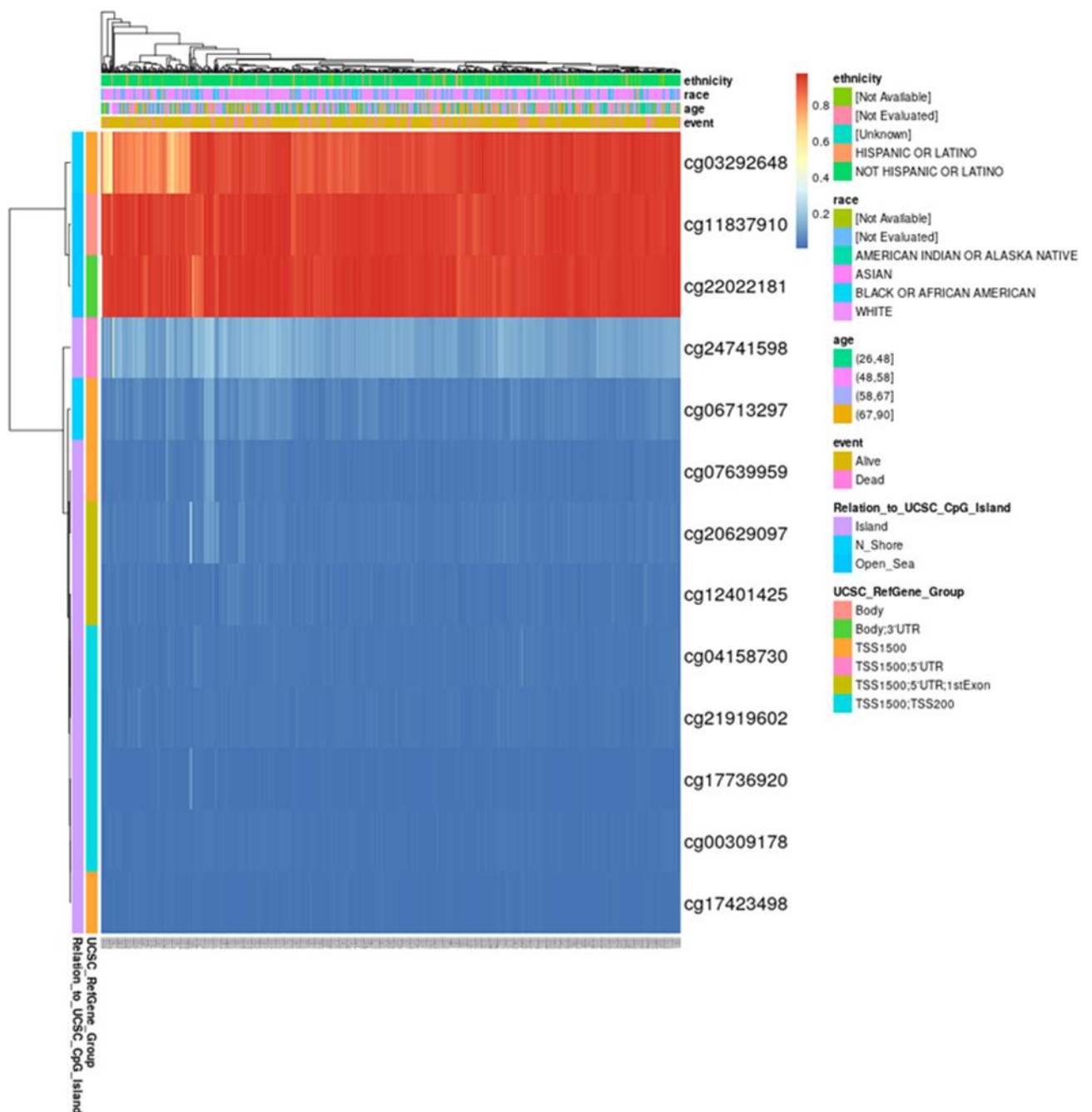


Figure 6.2. EXO1 methylation landscape in breast cancer samples analysed using MethSurv. Heatmap showing the DNA methylation levels (beta-values) of multiple CpG sites within the EXO1 gene across breast cancer samples. Methylation levels range from low (blue) to high (red). Rows represent individual CpG sites, while columns represent patient samples. Associated clinical variables, including ethnicity, race, age, and event status, are indicated in the annotation bars above the heatmap. CpG site genomic contexts (e.g., gene body, 3'UTR, and CpG islands) are also indicated in the side legend.

Table 6.1. SLC7A5 mRNA correlation with different mismatch mRNA genes using METABRIC and bc-GenExMiner.

SLC7A5 mRNA vs	METABRIC r (p-value)	GeneMiner r (p-value)
PMS1	-0.13 (< 0.0001)	0.02 (0.2)
PMS2	-0.16 (< 0.0001)	-0.05 (0.002)
MLH1	-0.24 (< 0.0001)	-0.16 (< 0.0001)
MLH3	-0.01 (0.6)	-0.31 (< 0.0001)
MSH2	0.05 (0.04)	0.31 (< 0.0001)
MSH3	-0.27 (< 0.0001)	-0.33 (< 0.0001)
MSH6	0.32 (< 0.0001)	0.37 (< 0.0001)
EXO1	0.62 (< 0.0001)	0.55 (< 0.0001)

P values in bold mean statistically significant.

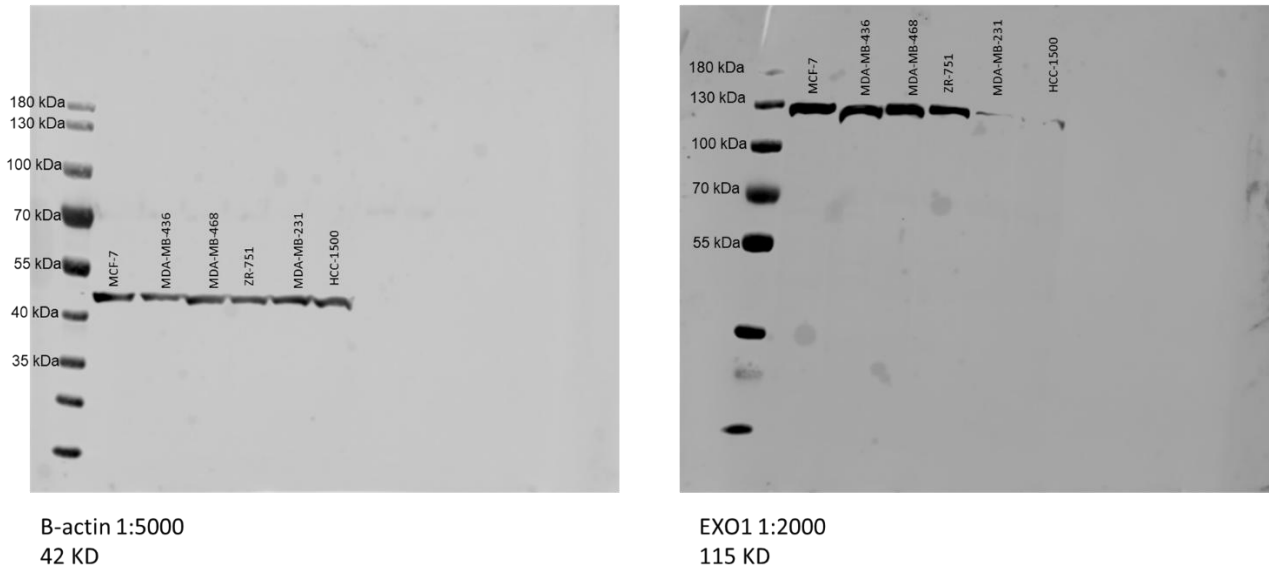


Figure 6.3. EXO1 protein expression in breast cancer cell lines. Western blot analysis of EXO1 protein expression across six breast cancer cell lines: MCF-7, MDA-MB-436, MDA-MB-468, ZR-751, MDA-MB-231 and HCC-1500. β -actin (42 kDa) was used as a loading control (left panel), and EXO1 protein (115 kDa) was detected using a 1:2000 dilution of the primary antibody (right panel).

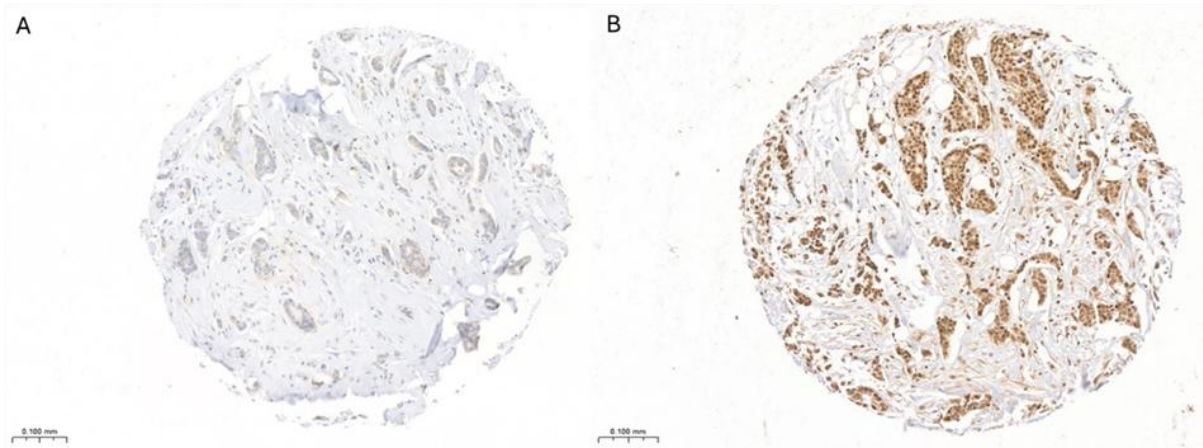


Figure 6.4: EXO1 protein expression in invasive breast cancer using immunohistochemistry. (A) Representative image showing Low EXO1 protein expression. (B) High EXO1 protein expression. immunohistochemistry was performed using rabbit polyclonal primary antibody against EXO1, diluted at 1:100, with overnight incubation at 4 °C. Positive immunoreactivity is detected in the nucleus and cytoplasm of the invasive breast cancer cells. Magnification x20.

6.3.2 Association of EXO1 with clinicopathological parameters

Within the METABRIC dataset, high EXO1 mRNA expression was associated with larger tumour size, higher tumour grade and lymph node stage (Figure 6.5A-C; all $P < 0.0001$). Furthermore, high EXO1 mRNA expression was associated with negative ER and PR status, positive HER2 status and triple negative tumours (Figure 6.5D-G; $P < 0.0001$). The Breast Cancer Gene-Expression Miner dataset was used to confirm these associations, were possible (Figure 6.6A-F; all $P < 0.01$).

At the protein level, high EXO1 protein expression was significantly associated with high lymph node stage (Table 6.2; $P = 0.03$), however, it was associated with smaller tumour size and intermediate tumour grade (Table 6.2; $P = 0.02$ and $P = 0.00003$, respectively). Unlike the mRNA expression of EXO1, the protein expression showed an association with positive ER and PR expression (Table. 6.2; $P = 0.00009$ and $P = 0.007$, respectively), and negative HER2 expression (Table. 6.2; $P = 0.0008$), moreover, it was associated with non-triple negative expression (Table. 6.2; $P = 0.005$).

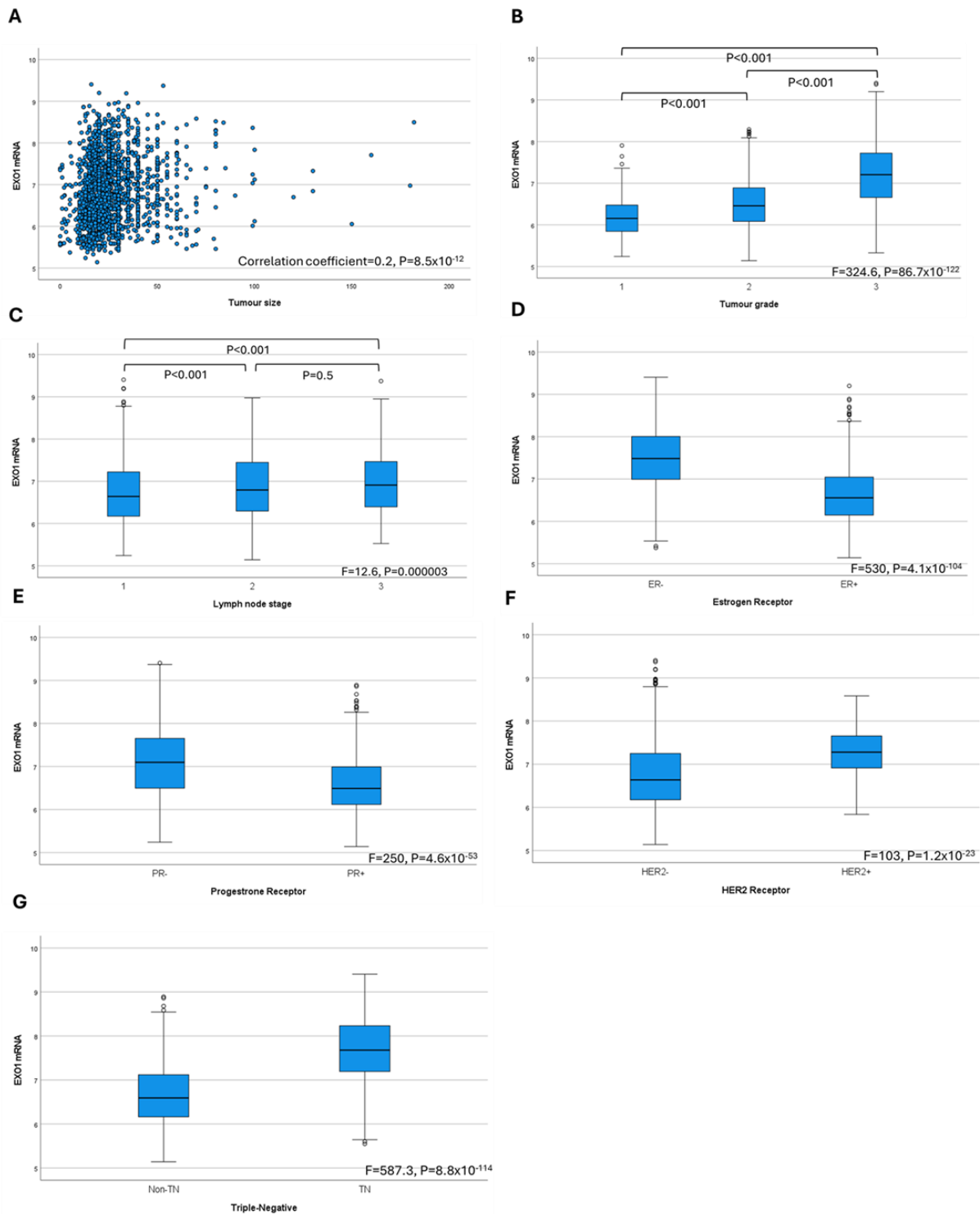


Figure 6.5. EXO1 mRNA expression and its association with: (A) Tumour size, (B) Tumour grade, (C) Lymph node status, (D) ER status, (E) PR status, (F) HER2 status, (G) Triple negative status, using the METABRIC cohort dataset. One-way ANOVA with post-hoc Tukey test was used.

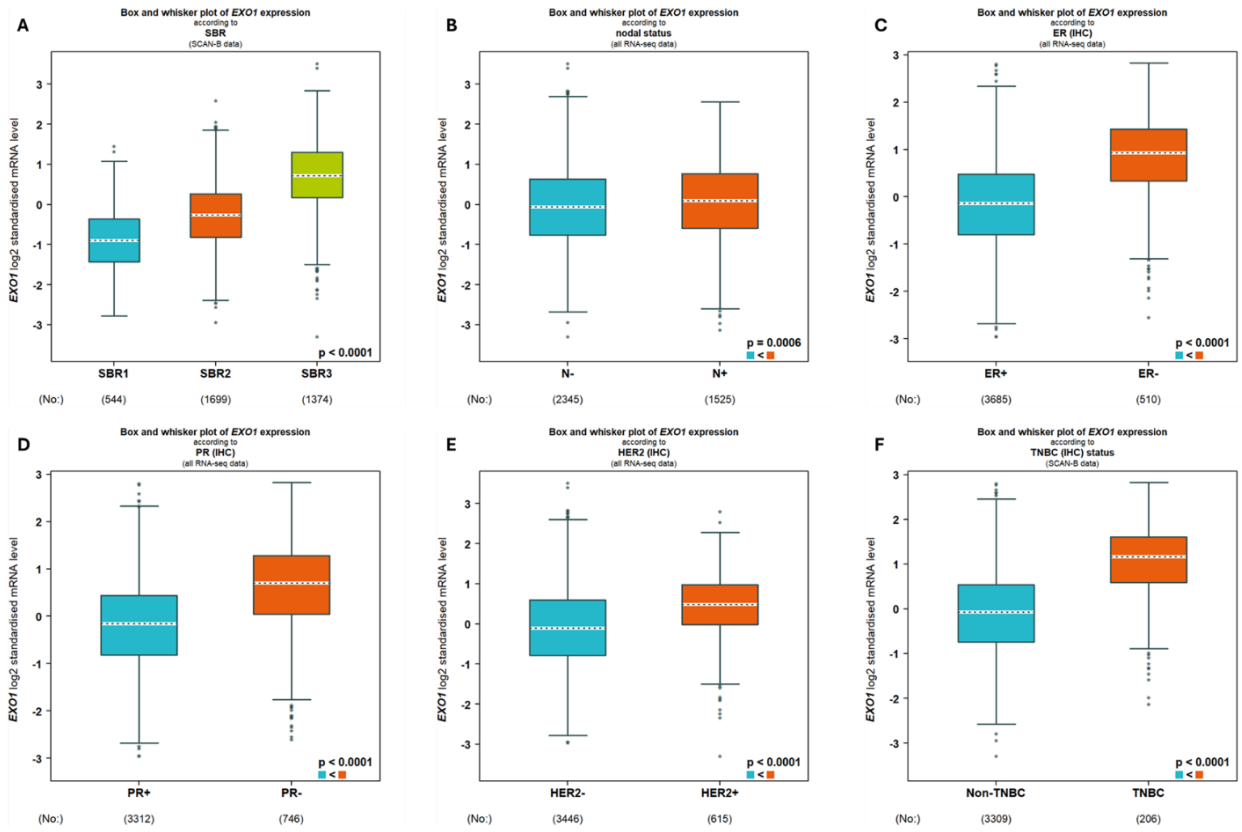


Figure 6.6. EXO1 gene expression and its association with: (A) tumour grade, (B) Lymph node status, (C) ER status, (D) PR status, (E) HER2 status, (F) Triple negative status, using the Breast Cancer Gene-Expression Miner dataset.

Table 6.2. Clinicopathological association of EXO protein in breast cancer.

	EXO1 protein		<i>P</i> -value
	Low n (%)	High n (%)	
Tumour size			0.02
< 2.0cm	233 (62)	138 (38)	
≥ 2.0cm	249 (70)	105 (30)	
Grade			0.00003
1	71 (56)	55 (44)	
2	151 (60)	103 (41)	
3	250 (75)	85 (25)	
Lymph Node Stage			0.03
1	274 (63)	159 (37)	
2	163 (73)	61 (27)	
3	35 (60)	23 (40)	
ER			0.00009
Positive	320 (62)	197 (38)	
Negative	149 (78)	43 (22)	
PR			0.007
Positive	248 (62)	151 (38)	
Negative	206 (72)	80 (28)	
HER2			0.0008
Positive	75 (82)	17 (19)	
Negative	375 (64)	213 (36)	
Triple Negative			0.005
No	355 (63)	206 (37)	
Yes	94 (76)	29 (24)	

P values in bold means statistically significant.

6.3.3 Association of EXO1 with patient outcome

Survival analysis showed that high EXO1 mRNA expression was associated with poor overall survival patient outcome in all cases (Figure 6.7A; $P=5.3 \times 10^{-18}$), and irrespective of ER (Figure 6.7B and C; $P=0.0026$ and $P=6.9 \times 10^{-12}$, respectively), or PR status (Figure 6.7D and E; $P=0.0003$ and $P=2.3 \times 10^{-11}$, respectively), in HER2 negative tumours and non-triple negative tumours (Figure 6.7F and G; $P=3.2 \times 10^{-13}$ and $P=3.3 \times 10^{-16}$, respectively). This was further validated using Kaplan-Meier Plotter, where EXO1 mRNA expression was significantly associated with poor patient outcome (Figure 6.8A; $P=1.6 \times 10^{-5}$).

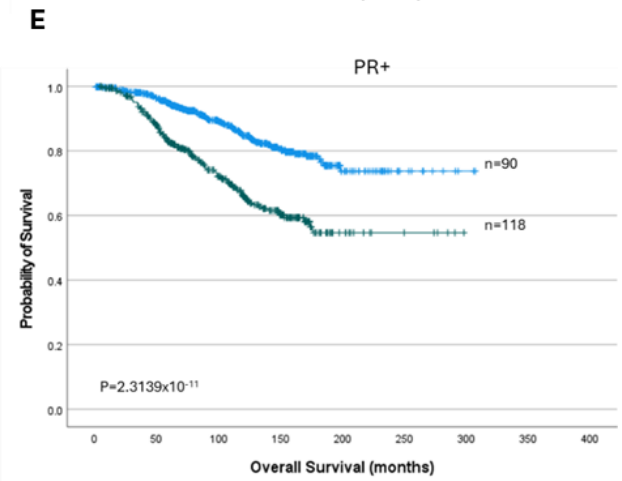
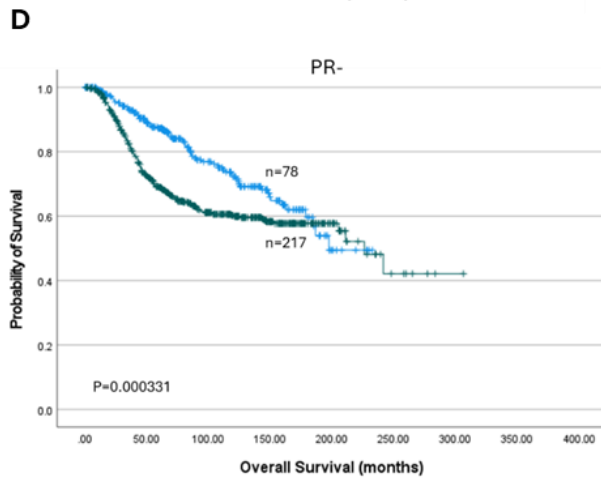
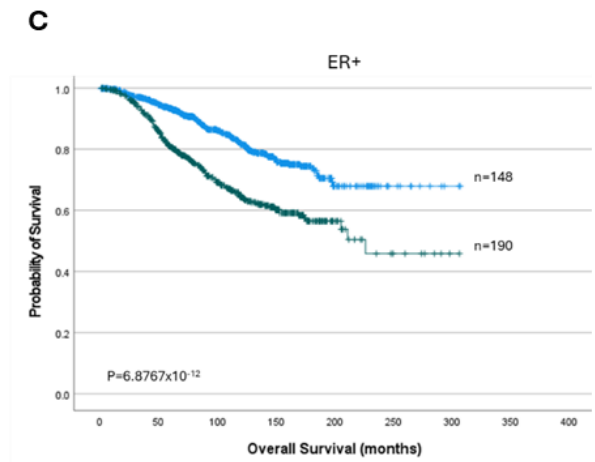
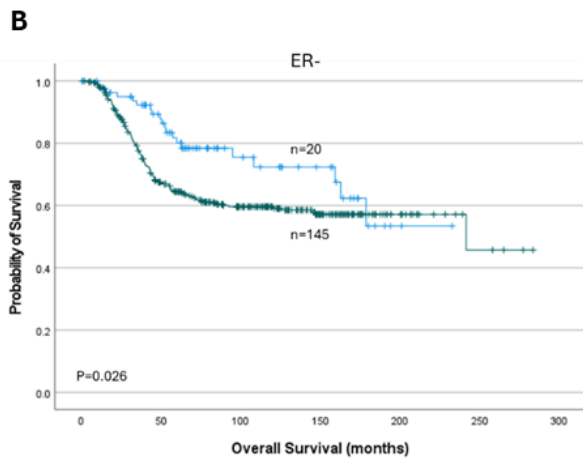
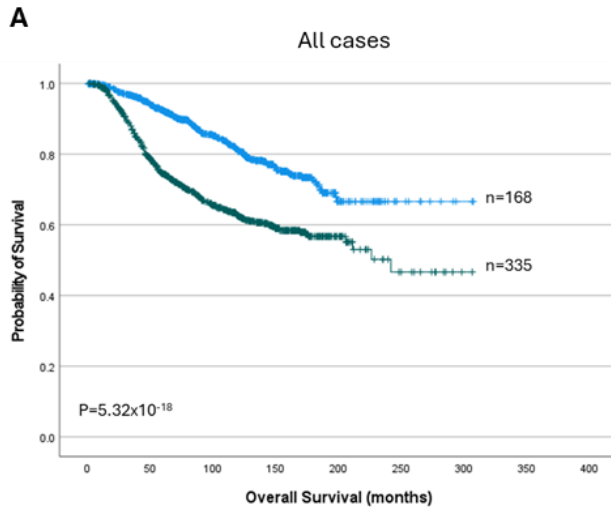
Multivariable Cox-regression analysis showed that EXO1 mRNA expression was an independent poor prognostic factor regardless of the other variables, tumour grade, tumour size, and lymph node stage, in all breast cancer cases and in ER-positive (ER+) tumours, but not in ER-negative (ER-) tumours ($P=1.6 \times 10^{-7}$ and $P=4.0 \times 10^{-7}$, respectively) (Table 6.3).

Kaplan-Meier survival analysis showed that higher methylation at cg11837910 and cg11837910 in the 3'UTR of EXO1 was not associated with better survival in breast cancer patients (Figure 6.9A and B; $P=0.07$ and $P=0.05$, respectively).

High EXO1 protein expression was associated with the worst patient outcome in BCSS in ER- tumours (Figure. 6.10B; $P=0.03$). No significant association was observed with all cases and other molecular breast cancer subtypes (Figure 6.10A and 6.4C-I; $P>0.05$).

Furthermore, high EXO1 protein expression was associated with DMFS in tumours characterised with ER- (Figure 6.11B; $P=0.02$), HER2+ (Figure 6.11G; $P=0.055$) and triple negative tumours (Figure 6.11I; $P=0.04$), however, no significant association was observed in all cases and the other molecular subtypes (Figure 6.11A, 6.11C-F and 6.11H; all $P>0.05$). Similarly, high EXO1 expression was associated with RFS in ER- (Figure 6.12B; $P=0.04$) and triple negative tumours (Figure 6.12I; $P=0.02$). No significant association was found in all cases and the other molecular breast cancer subtypes (Figure 6.12A and 6.12C-H; $P>0.05$). For multivariable cox-regression analysis, results demonstrated that EXO1 protein expression

was a predictor of poor distant metastasis and disease recurrence in ER- tumours (Table 6.4: P<0.05). EXO1 protein expression showed no significant association with patient outcome when using Kaplan-Meier Plotter (Figure 6.8B).



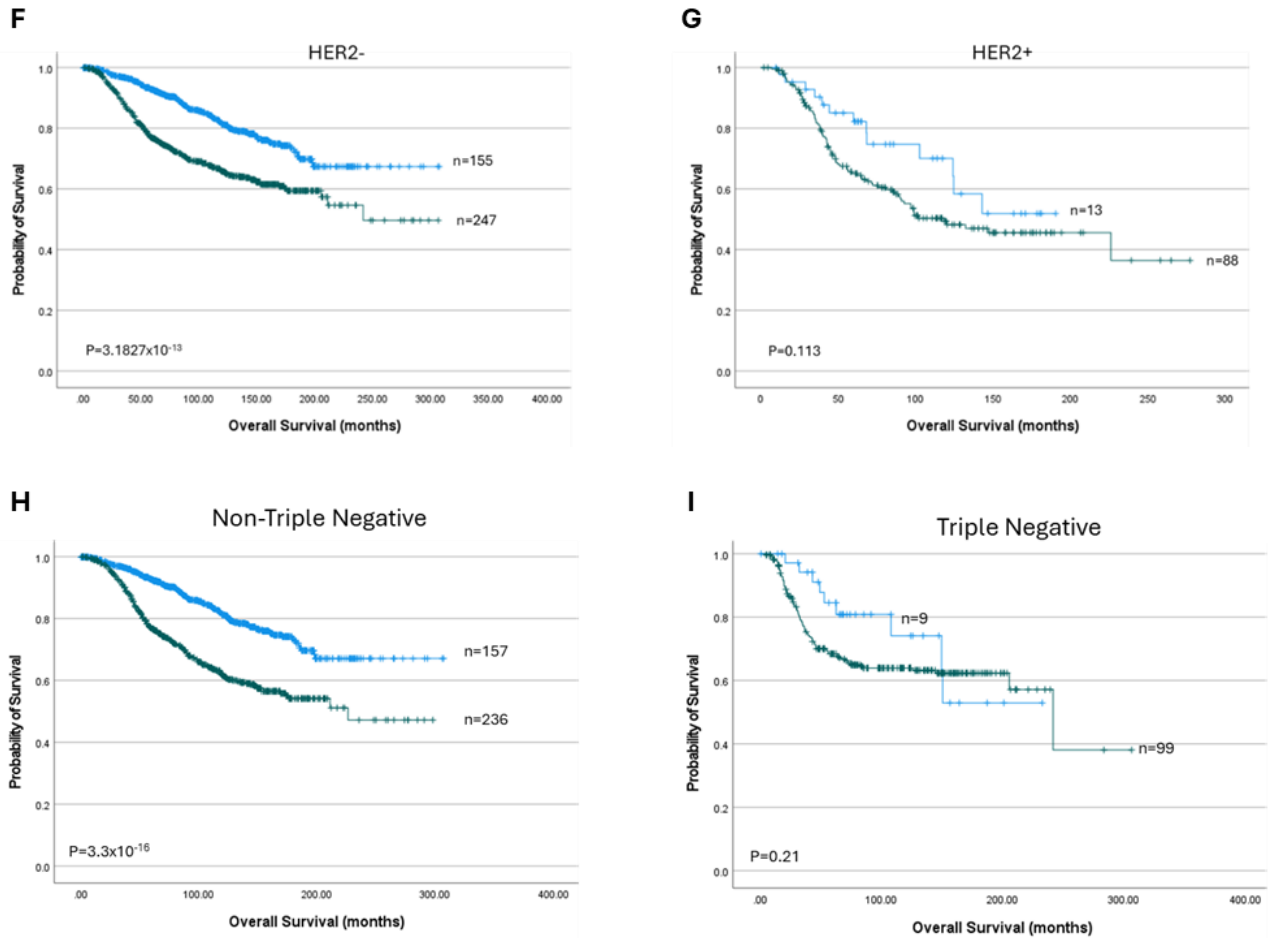


Figure 6.7. EXO1 mRNA expression and its association with overall survival (OS) in invasive breast cancer (METABRIC): a) EXO1 in all cases, b) EXO1 in ER-, c) EXO1 in ER+, d) EXO1 in PR-, e) EXO1 in PR+, F) EXO1 in HER2- and G) EXO1 in HER2+, H) EXO1 in Non-Triple Negative and I) EXO1 in Triple Negative in breast cancer. The blue line represents low expression of EXO1, and the green line represents high expression of EXO1.

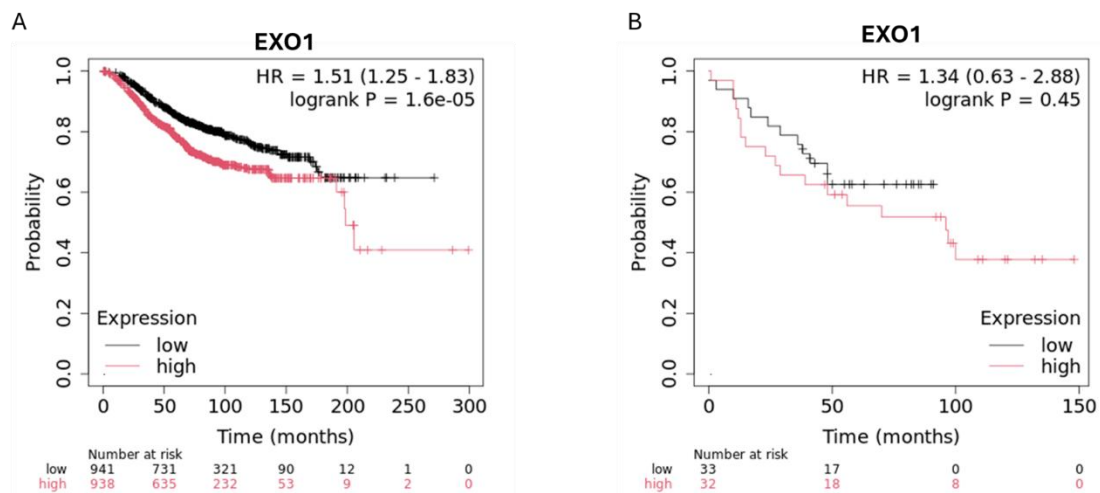


Figure 6.8: Using the Kaplan-Meier Plotter to find the association of EXO1 mRNA and protein expression with patient outcome. (A) Analysis of EXO1 mRNA expression using the Kaplan-Meier Plotter showed that high EXO1 expression was significantly associated with reduced overall survival in breast cancer patient ($P=1.6 \times 10^{-5}$). (B) Analysis of EXO1 protein expression showed no statistically significant association with survival in breast cancer patient ($P=0.45$).

Table 6.3. Multivariate Cox analysis of associations between EXO1 mRNA expression and clinicopathological parameters in all cases, ER+ and ER- breast cancer.

Parameters	EXO1 mRNA					
	All Cases		ER+		ER-	
	HR (95% CI)	<i>p</i> -value	HR (95% CI)	<i>p</i> -value	HR (95% CI)	<i>p</i> -value
EXO1-	Reference		Reference		Reference	
EXO1+	1.7 (1.4-2.1)	1.6x10⁻⁷	1.7 (1.4-2.2)	4.0x10⁻⁷	1.3 (0.8-2.2)	0.3
Grade	1.2 (1.0-1.4)	0.03	1.2 (1.0-1.4)	0.1	0.9 (0.6-1.4)	0.6
Size	1.7 (1.4-2.1)	1.2x10⁻⁷	1.7 (1.4-2.2)	4.0x10⁻⁷	1.7 (1.2-2.4)	0.03
Lymph Node Stage	1.9 (1.7-2.1)	3.4x10⁻²⁵	1.8 (1.6-2.1)	2.1x10⁻¹⁶	1.9 (1.6-2.4)	3.7x10⁻¹⁰

P values in bold mean statistically significant.

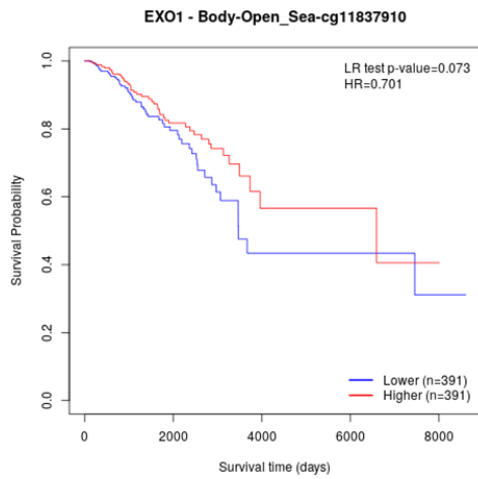
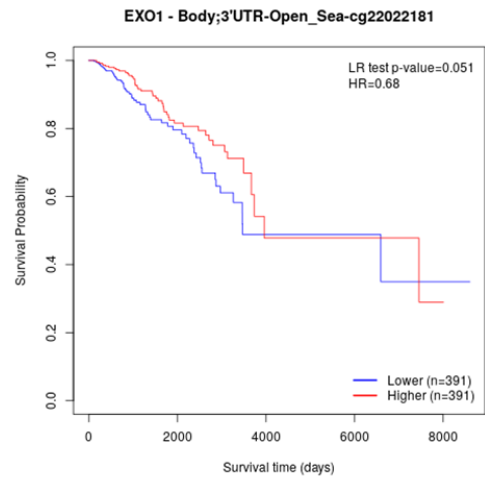
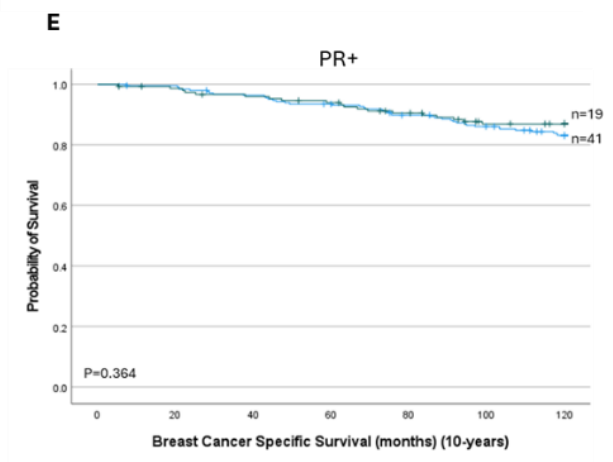
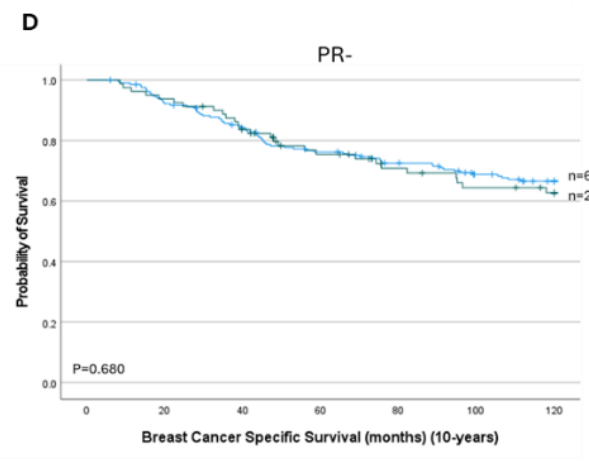
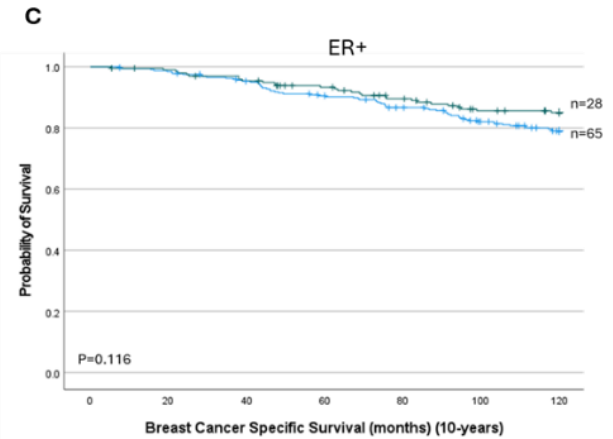
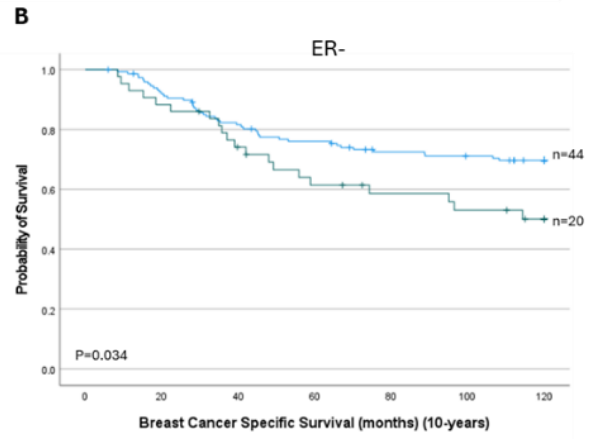
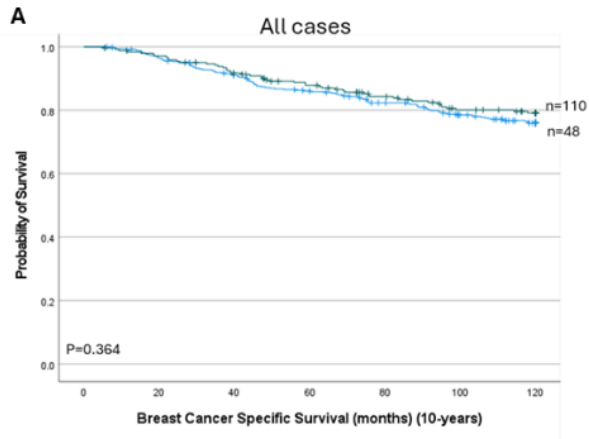
A**B**

Figure 6.9. Kaplan-Meier survival analysis based on the methylation status of EXO1 CpG sites in breast cancer patients. (A) Survival curve comparing patients with higher vs. lower methylation at CpG site cg11837910 located in the body region of EXO1. (B) Survival curve comparing patients with higher vs. lower methylation at CpG site cg22022181 located in the 3'UTR region of EXO1.



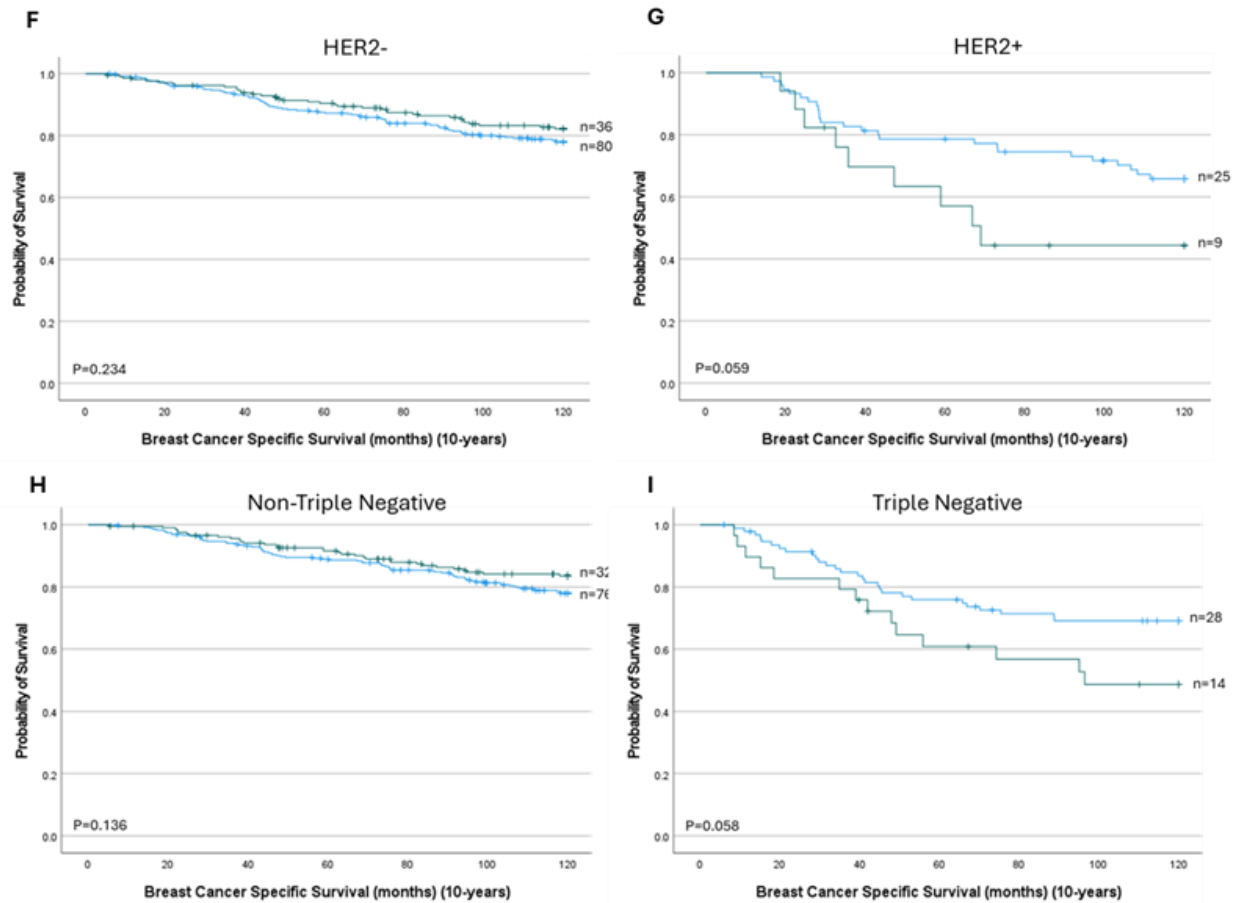
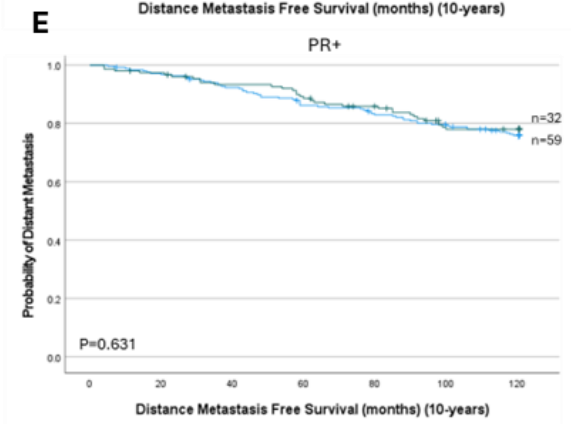
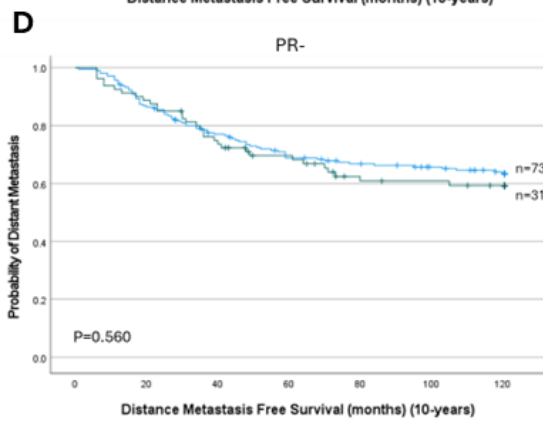
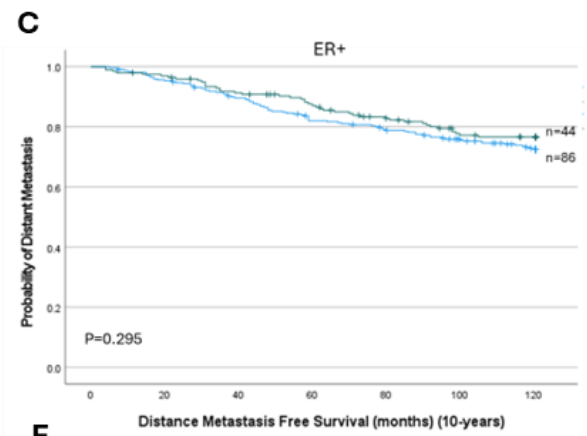
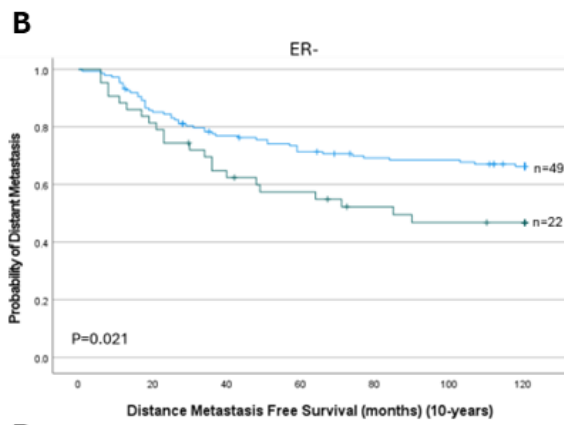
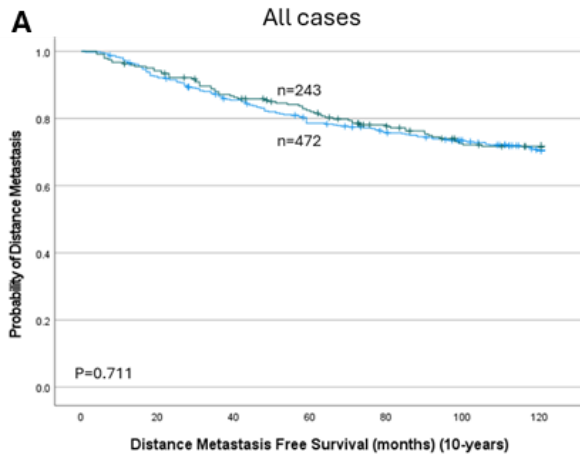


Figure 6.10. EXO1 protein expression and its association with breast cancer specific survival (BCSS) in invasive breast cancer: A) EXO1 in all cases, B) EXO1 in ER-, C) EXO1 in ER+, D) EXO1 in PR-, E) EXO1 in PR+, F) EXO1 in HER2-, G) EXO1 in HER2+, H) EXO1 in non-Triple Negative, and I) EXO1 in Triple Negative in breast cancer. The blue line represents low expression of EXO1, and the green line represents high expression of EXO1.



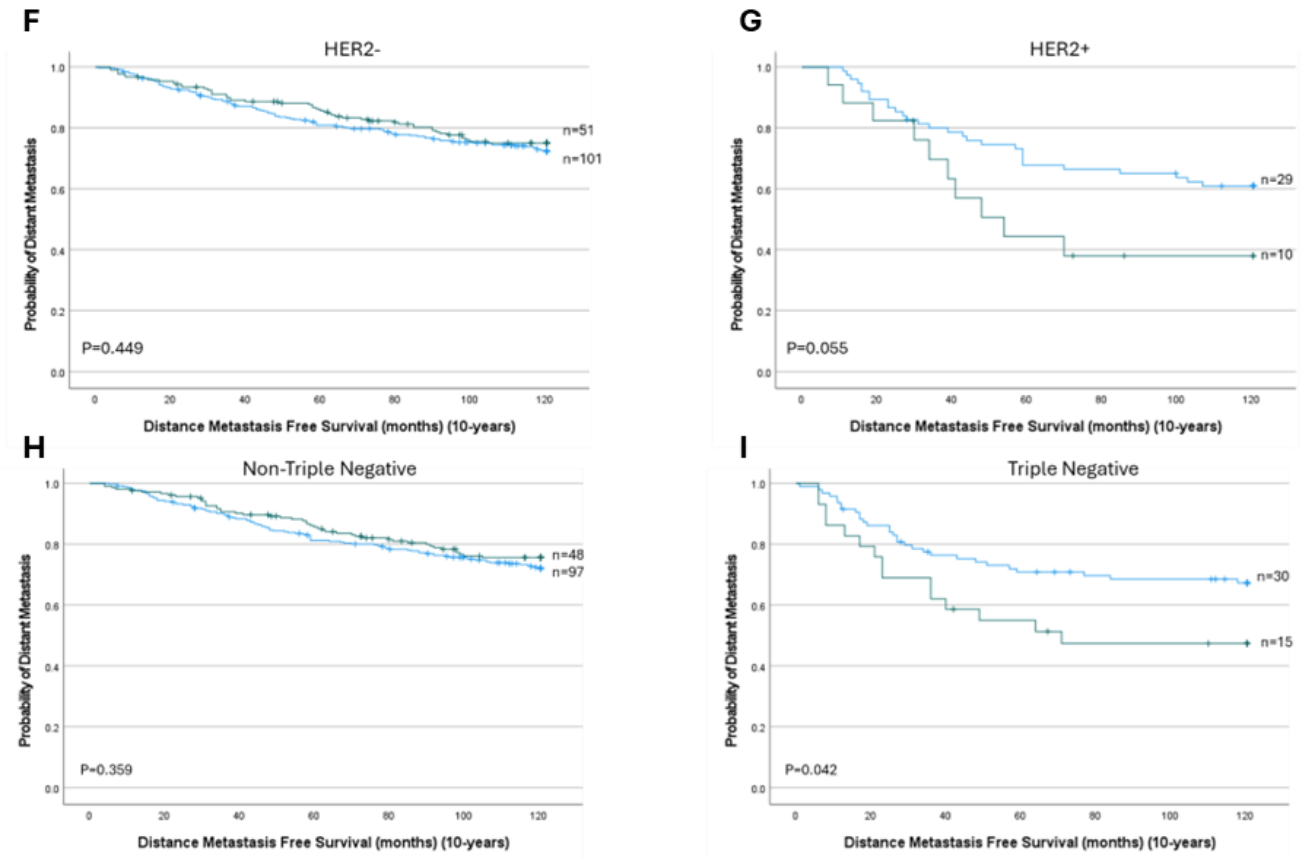
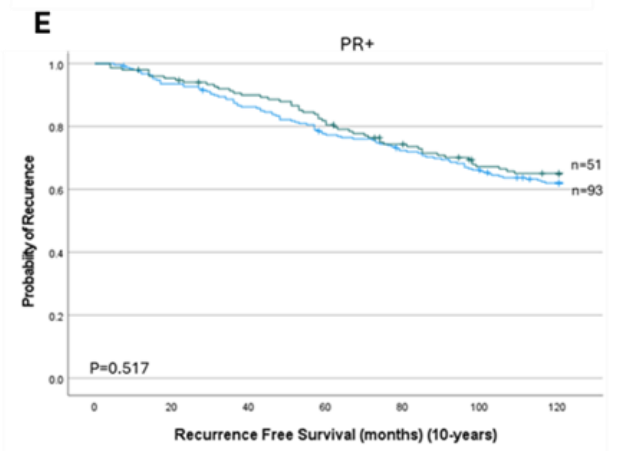
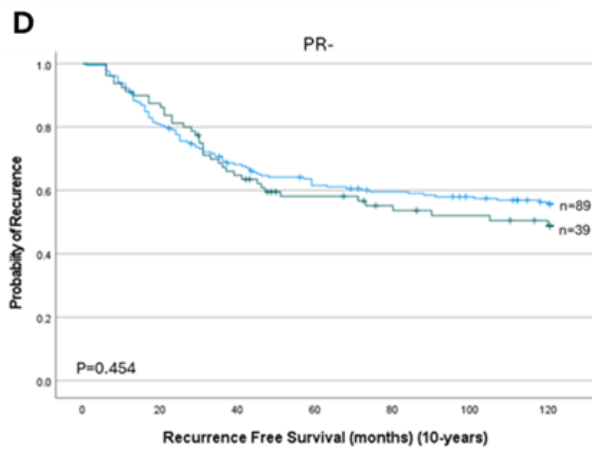
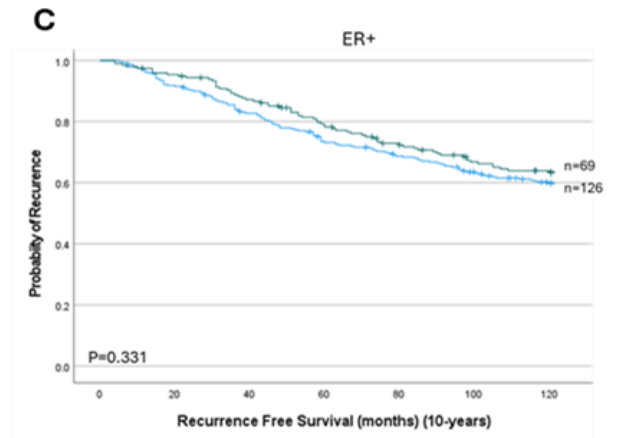
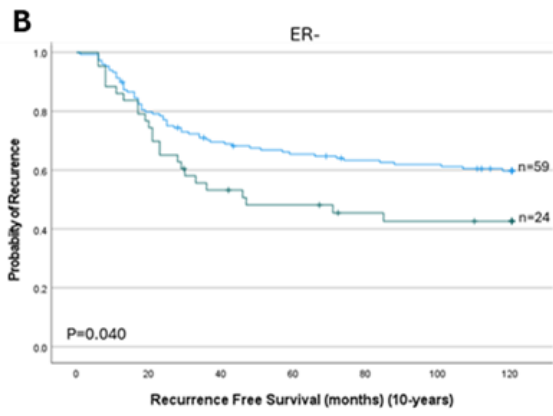
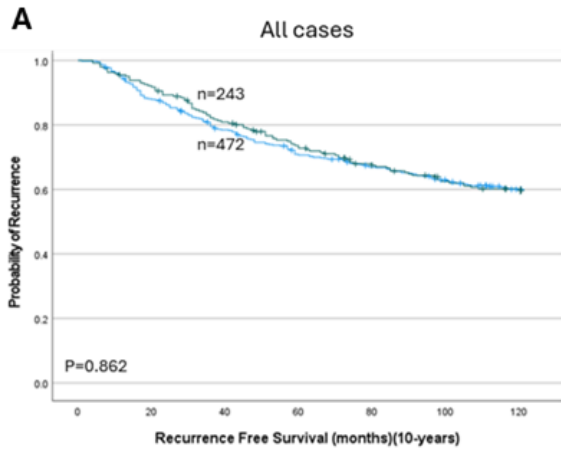


Figure 6.11. EXO1 protein expression and its association with distance metastasis free survival (DMFS) in invasive breast cancer: A) EXO1 in all cases, B) EXO1 in ER-, C) EXO1 in ER+, D) EXO1 in PR-, E) EXO1 in PR+, F) EXO1 in HER2-, G) EXO1 in HER2+, H) EXO1 in non-Triple Negative, and I) EXO1 in Triple Negative in breast cancer. The blue line represents low expression of EXO1, and the green line represents high expression of EXO1.



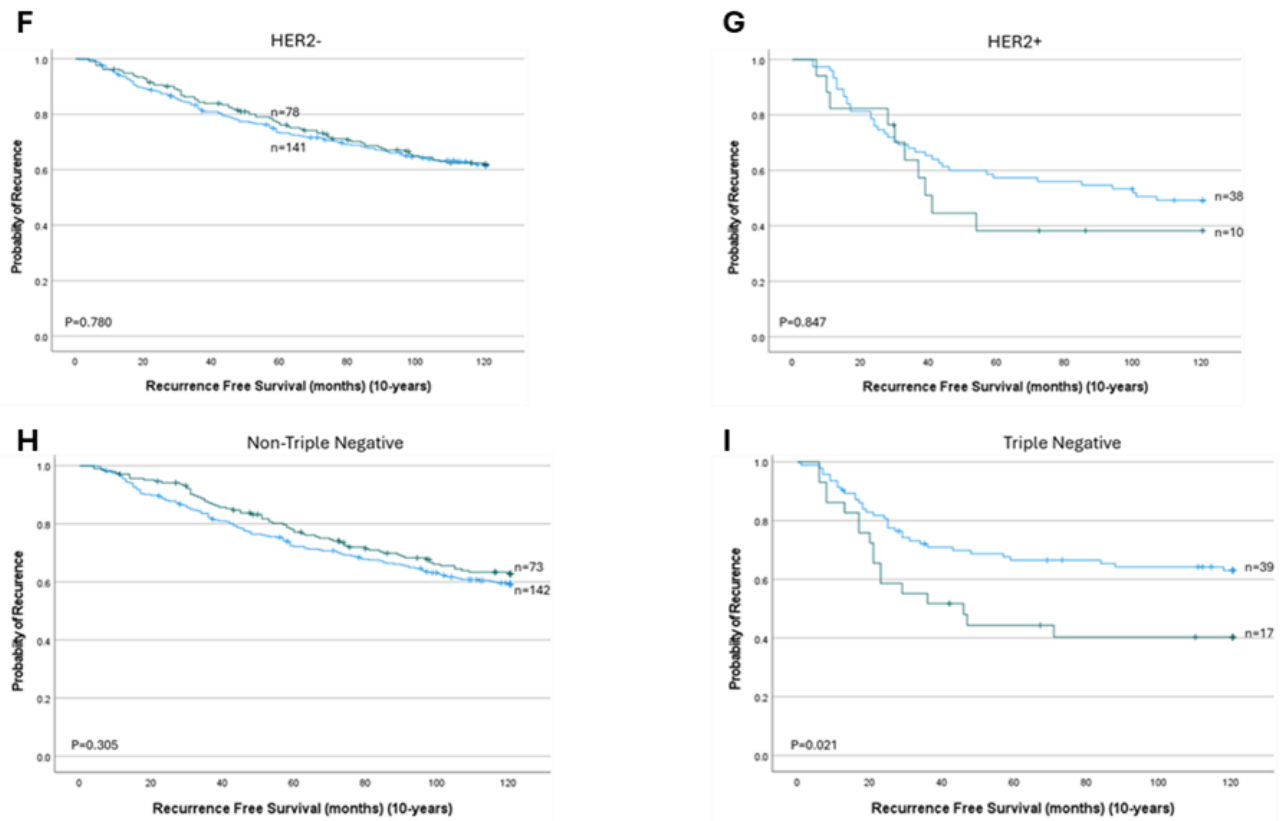


Figure 6.12. EXO1 protein expression and its association with recurrence free survival (RFS) in invasive breast cancer: A) EXO1 in all cases, B) EXO1 in ER-, C) EXO1 in ER+, D) EXO1 in PR-, E) EXO1 in PR+, F) EXO1 in HER2-, G) EXO1 in HER2+, H) EXO1 in non-Triple Negative, and I) EXO1 in Triple Negative in breast cancer. The blue line represents low expression of EXO1, and the green line represents high expression of EXO1.

Table 6.4. Multivariate Cox analysis of associations between EXO1 protein expression and clinicopathological parameters in all cases, ER+ and ER- breast cancer.

<i>Breast Cancer Specific Survival</i>						
	All Cases		ER+		ER-	
Parameters	HR (95% CI)	<i>p</i> -value	HR (95% CI)	<i>p</i> -value	HR (95% CI)	<i>p</i> -value
EXO1-	Reference		Reference		Reference	
EXO1+	1.0 (0.7-1.4)	0.908	0.9 (0.5-1.3)	0.5	1.7 (1.0-2.9)	0.06
Grade	2.1 (1.6-2.7)	2.7 x10⁻⁷	2.0 (1.4-2.8)	5.0 x10⁻⁵	1.4 (0.7-2.5)	0.3
Size	1.5 (1.1-2.2)	0.02	1.9 (1.2-2.9)	0.01	1.1 (0.6-1.9)	0.7
Lymph Node Stage	2.4 (1.9-3.0)	2.0x10⁻¹⁴	2.4 (1.8-3.2)	2.5 x10⁻⁸	2.2 (1.6-3.1)	4.0x10⁻⁷
<i>Distance Metastasis Free Survival</i>						
Parameters	HR (95% CI)	<i>p</i> -value	HR (95% CI)	<i>p</i> -value	HR (95% CI)	<i>p</i> -value
EXO1-	Reference		Reference		Reference	
EXO1+	1.2 (0.9-1.5)	0.4	1.0 (0.7-1.5)	0.9	1.8 (1.1-3.0)	0.02
Grade	1.7 (1.4-2.2)	2.0 x10⁻⁷	1.8(1.4-2.4)	0.00002	1.1 (0.7-1.9)	0.6
Size	1.6 (1.2-2.1)	0.004	2.1(1.4-3.0)	0.0002	1.0 (0.6-1.6)	0.004
Lymph Node Stage	2.1 (1.7-2.6)	8.0x10⁻¹⁴	1.9 (1.5-2.5)	7.5x10⁻⁷	2.3 (1.7-3.0)	8.5x10⁻⁸
<i>Recurrence Free Survival</i>						
Parameters	HR (95% CI)	<i>p</i> -value	HR (95% CI)	<i>p</i> -value	HR (95% CI)	<i>p</i> -value
EXO1-	Reference		Reference		Reference	
EXO1+	1.1 (0.8-1.4)	0.6	0.9 (0.7-1.2)	0.7	1.6 (1.0-2.6)	0.04
Grade	1.2 (1.0-1.4)	0.05	1.2 (1.0-1.5)	0.01	1.0 (0.7-1.6)	0.9
Size	1.3 (1.0-1.6)	0.07	1.5 (1.1-2.0)	0.1	0.9 (0.6-1.4)	0.6
Lymph Node Stage	1.9 (1.6-2.2)	2.9x10⁻¹²	1.8 (1.4-2.2)	5.3x10⁻⁷	1.9 (1.6-2.2)	4x10⁻⁶

P values in bold mean statistically significant.

6.3.4 Association of SLC7A5/EXO1 with clinicopathological parameters

The METABRIC dataset was used to determine the association between the expression of SLC7A5/EXO1 mRNA and clinicopathological parameters. SLC7A5+EXO1+ mRNA expression was associated with poor prognostic parameters, including larger tumour size, higher tumour grade and lymph node stage (Table 6.5; $P < 0.0001$), alternatively SLC7A5-EXO1- mRNA expression was associated with better prognostic parameters, smaller tumour size and lower tumour grade and lymph node stage (Table 6.5; $P < 0.0001$). SLC7A5+EXO1+ mRNA expression was significantly associated with negative ER and PR status, HER2 positive and triple negative tumours (Table 6.5; $P < 0.0001$), while SLC7A5-EXO1- mRNA expression was associated with hormone receptor (ER and PR) positive, HER2 negative and non-triple negative tumours (Table 6.5; $P < 0.0001$).

The analysis of protein expression showed that SLC7A5+EXO1+ was significantly associated with larger tumour grade (Table 6.6; $P = 8.9 \times 10^{-17}$), but there was no significant association with tumour size and lymph node stage (Table 6.6; $P > 0.05$). Similar to mRNA analysis, the protein expression of SLC7A5+EXO1+ was associated with negative ER and PR status (Table 6.6; $P = 1.1 \times 10^{-22}$ and $P = 2.1 \times 10^{-12}$, respectively), however, it was also associated with HER2 negative tumours (Table 6.6; $P = 0.006$) and triple negative tumours (Table 6.6; $P = 8.2 \times 10^{-17}$).

Table 6.5. Clinicopathological association of SLC7A5/EXO1 mRNA in breast cancer.

Parameters	SLC7A5/EXO1 mRNA				<i>p</i> -value
	SLC7A5- EXO1- n (%)	SLC7A5- EXO1+ n (%)	SLC7A5+ EXO1- n (%)	SLC7A5+ EXO1+ n (%)	
Tumour size					2.3x10⁻¹¹
< 2.0cm	413 (43)	103 (11)	151 (16)	304 (31)	
≥ 2.0cm	290 (30)	149 (15)	118 (12)	420 (43)	
Grade					7.9x10⁻¹⁰²
1	132 (78)	10 (6)	16 (10)	11 (7)	
2	390 (51)	115 (15)	116 (15)	145 (19)	
3	147 (16)	119 (13)	120 (13)	561 (59)	
Lymph Node Stage					0.000005
1	423 (41)	134 (13)	142 (14)	330 (32)	
2	198 (32)	75 (12)	85 (14)	260 (42)	
3	84 (27)	44 (14)	44 (14)	142 (45)	
ER					6.5x10⁻¹⁰⁴
Positive	671 (45)	240 (16)	223 (15)	360 (24)	
Negative	37 (8)	14 (3)	49 (10)	374 (79)	
PR					5.1x10⁻⁵⁹
Positive	506 (49)	169 (16)	139 (14)	219 (21)	
Negative	202 (22)	85 (9)	133 (14)	515 (55)	
HER2					2.1x10⁻³⁵
Positive	19 (8)	22 (9)	26 (11)	180 (73)	
Negative	689 (40)	232 (14)	246 (14)	554 (32)	
Triple Negative					1.1x10⁻⁸⁴
No	690 (42)	244 (15)	246 (15)	453 (28)	
Yes	15 (5)	9 (3)	25 (8)	280 (85)	

P values in bold mean statistically significant.

Table 6.6. Clinicopathological association of SLC7A5/EXO1 Protein in breast cancer.

Parameters	SLC7A5/EXO1 Protein				P-value
	SLC7A5- EXO1- n (%)	SLC7A5- EXO1+ n (%)	SLC7A5+ EXO1- n (%)	SLC7A5+ EXO1+ n (%)	
Tumour size					0.3
< 2.0cm	149 (54)	89 (32)	27 (10)	10 (4)	
≥ 2.0cm	148 (52)	76 (27)	53 (19)	9 (3)	
Grade					8.9x10⁻¹⁷
1	60 (62)	36 (37)	1 (1)	0 (0)	
2	111 (56)	76 (39)	8 (4)	2 (1)	
3	126 (47)	53 (20)	71 (27)	17 (6)	
Lymph Node Stage					0.3
1	178 (53)	105 (31)	41 (12)	12 (4)	
2	99 (55)	45 (2)	32 (18)	4 (2)	
3	20 (44)	16 (35)	7 (15)	3 (7)	
ER					1.1x10⁻²²
Positive	230 (57)	142 (35)	24 (6)	7 (2)	
Negative	64 (42)	22 (14)	56 (36)	12 (8)	
PR					2.1x10⁻¹²
Positive	179 (58)	108 (35)	15 (5)	7 (2)	
Negative	107 (47)	51 (22)	62 (27)	10 (4)	
HER2					0.006
Positive	45 (59)	12 (16)	18 (24)	1 (1)	
Negative	240 (52)	145 (32)	59 (13)	17 (4)	
Triple Negative					8.2x10⁻¹⁷
No	246 (56)	147 (34)	38 (9)	8 (2)	
Yes	36 (36)	16 (16)	38 (38)	9 (9)	

P values in bold mean statistically significant.

6.3.5 Association of SLC7A5/EXO1 with patient outcome

The METABRIC cohort was used to assess the prognostic value of SLC7A5/EXO1 mRNA expression in breast cancer. Results showed that the expression of SLC7A5+EXO1+ mRNA subgroup was associated with poor patient outcome in all cases (Figure 6.13A; $P=7.5 \times 10^{-18}$). Furthermore, the SLC7A5+EXO1+ subgroup of tumours was significantly associated with worse survival outcomes in patients with ER+ (Figure 6.13C; $P=1.8 \times 10^{-11}$), PR+ (Figure 6.13E; $P=3.2 \times 10^{-11}$), HER2- (Figure 6.13F; $P=3.5 \times 10^{-13}$) and non-triple negative (Figure 6.13H; $P=7.1 \times 10^{-17}$) in comparison with the other subgroups. The expression SLC7A5-EXO1+ was associated with worse patient outcome in ER-tumours (Figure 6.13B; $P=0.05$), PR- (Figure 6.13D; $P=0.006$).

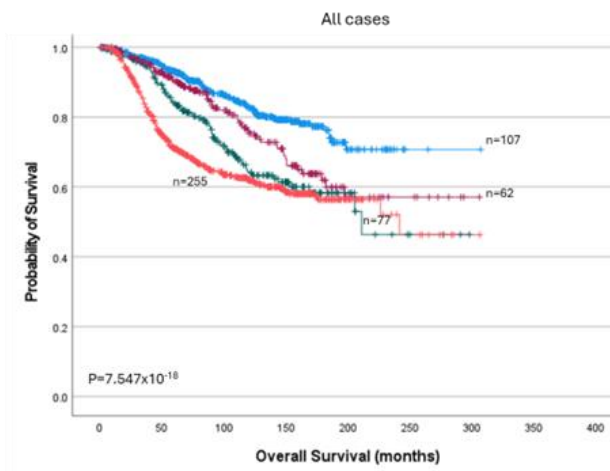
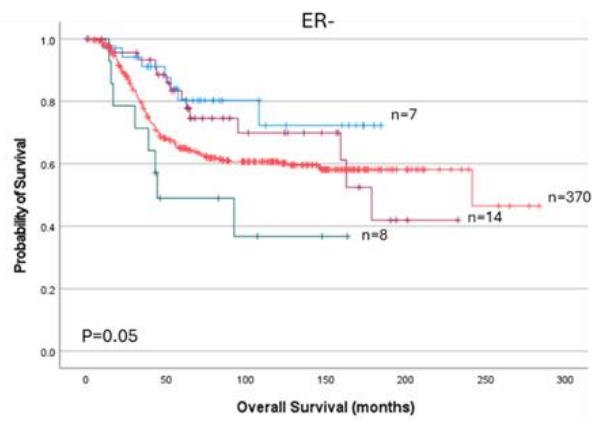
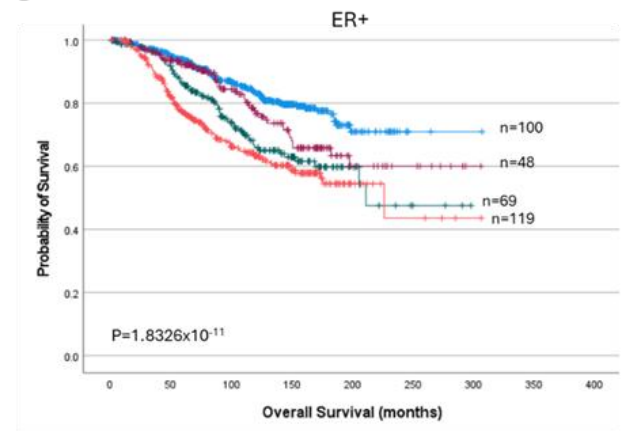
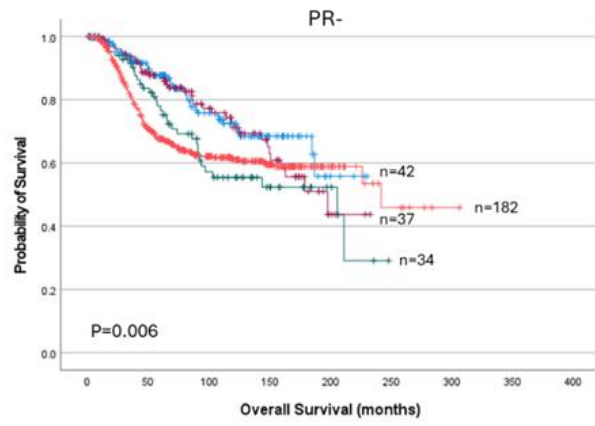
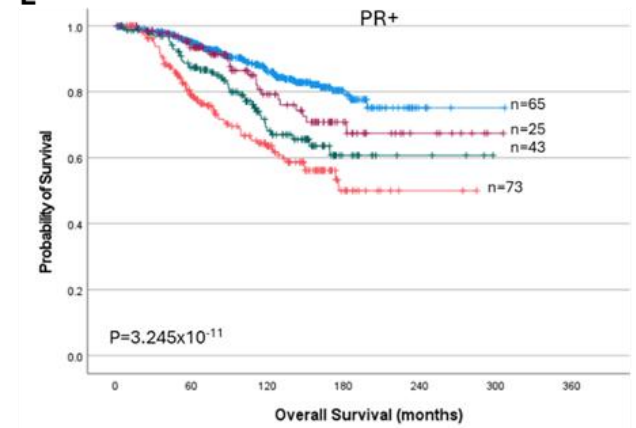
Next, Multivariable Cox-regression showed that SLC7A5+EXO1+ mRNA expression was a predictor of shorter overall survival independent of tumour size and lymph node stage in all cases and ER+ tumours (Table 6.7; $P<0.05$).

SLC7A5+EXO1+ protein expression showed the worst patient outcome in terms of BCSS in all cases and HER2- tumours (Figure 6.14A and F; $P=0.0003$ and $P=0.0004$, respectively). The protein expression of SLC7A5+EXO1- was associated with poor BCSS in ER+ and non-triple negative tumours (Figure 6.14C and H; $P=0.0002$ and $P=0.004$, respectively), SLC7A5-EXO1+ protein expression was associated with poor patient outcome in terms of BCSS in HER2+ tumours (Figure 6.14G; $P=0.001$). No significant association was observed in PR-, PR+ and triple negative tumours (Figure 6.14D-E and I; all $P>0.05$).

Protein expression of SLC7A5+EXO1+ was associated with distant metastasis in all cases (Figure 6.15A; $P=0.02$), and in ER- and HER2- (Figure 6.15B and F; $P=0.056$ and $P=0.005$, respectively). The protein expression of SLC7A5+EXO1- was associated with worse survival outcome in terms of distant metastasis in ER+ (Figure 6.15C; $P=0.002$), and non-triple negative tumours (Figure 6.15H; $P=0.002$), while SLC7A5-EXO1+ was associated with HER2+ tumours (Figure 6.15G; $P=0.01$). No significant association was observed in PR-, PR+

and triple negative tumours (Figure 6.15D-E and I; all $P > 0.05$). Moreover, SLC7A5+EXO1-protein expression was significantly associated with disease recurrence in non-triple negative tumours (Figure 6.16H; $P = 0.04$). However, there was no significant association observed in the other biological subtypes (Figure 6.16A-G and I; all $P > 0.05$).

Multivariable Cox-regression analysis showed that SLC7A5+EXO1+ protein expression is a predictor of breast cancer death and high risk of distant metastasis in all cases and ER-tumours (Table 6.8; $P < 0.05$).

A**B****C****D****E**

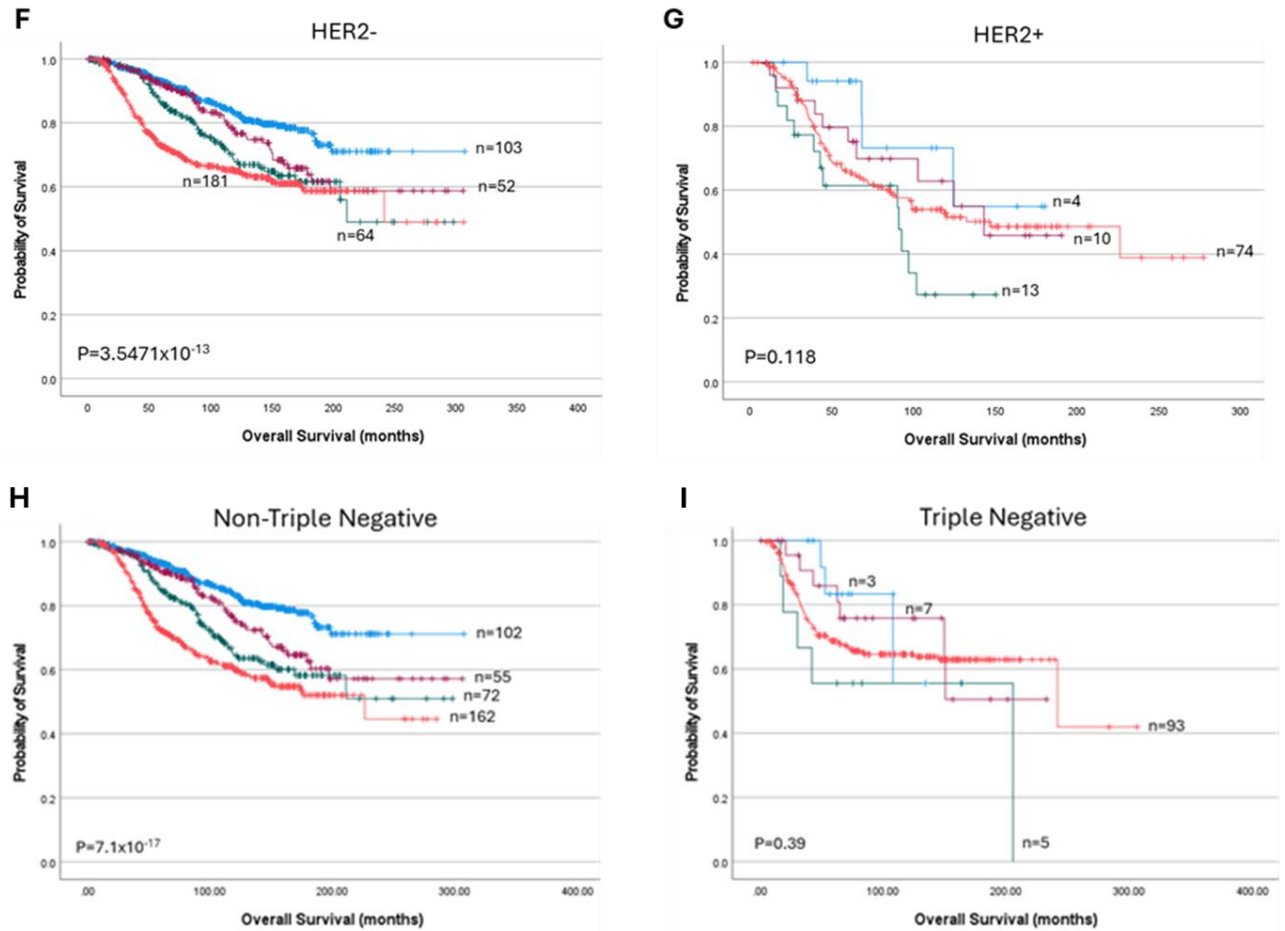
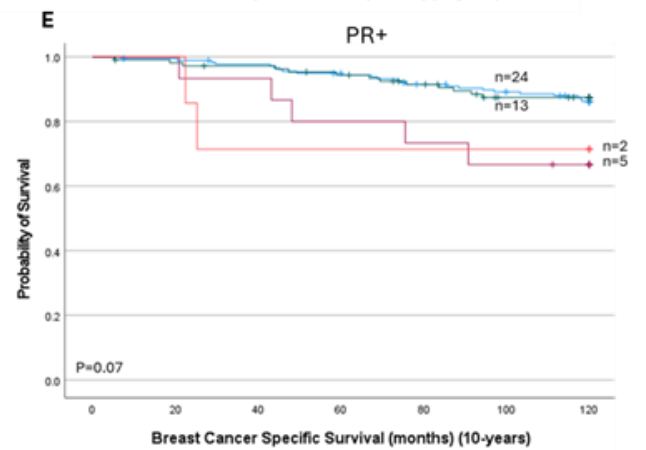
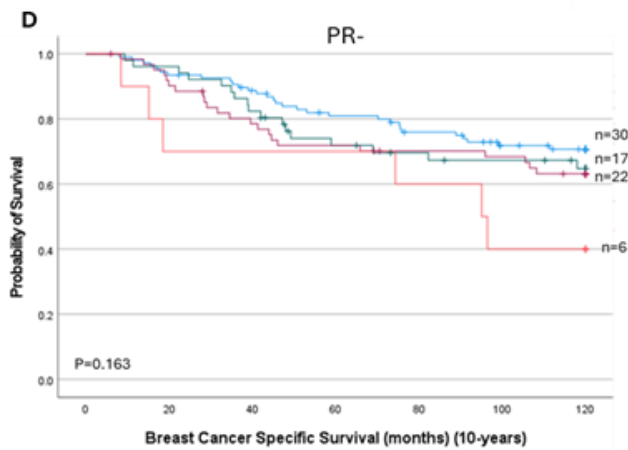
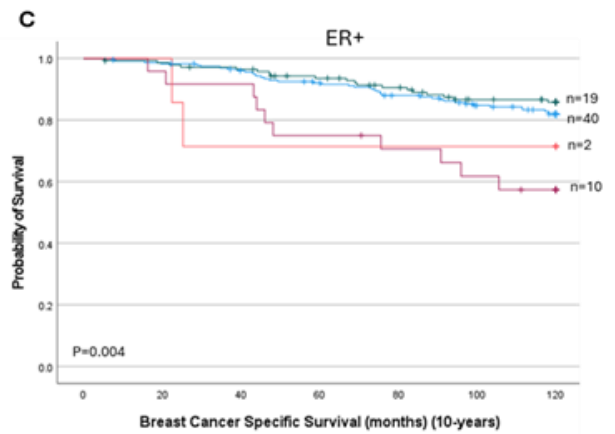
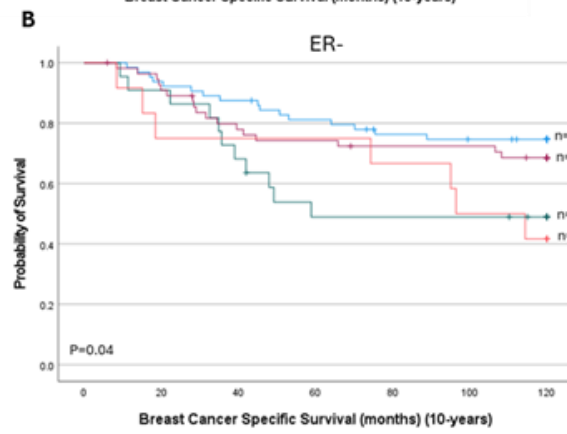
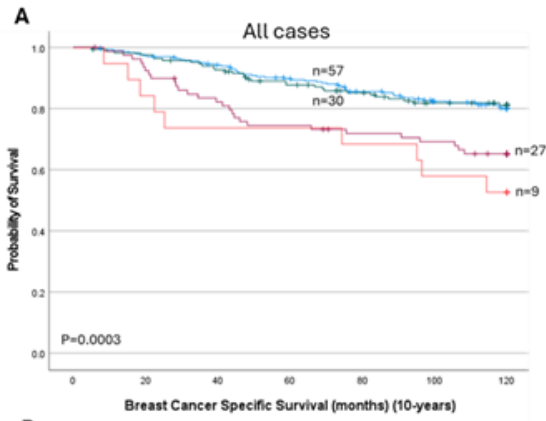


Figure 6.13. EXO1/SLC7A5 mRNA expression and its association with overall survival (OS) in invasive breast cancer (METABRIC): A) EXO1/SLC7A5 in all cases, B) EXO1/SLC7A5 in ER-, C) EXO1/SLC7A5 in ER+, D) EXO1/SLC7A5 in PR-, E) PR+, F) EXO1/SLC7A5 in HER2- and G) EXO1/SLC7A5 in HER2+ in breast cancer. Blue line represents low EXO1 and low SLC7A5, Green line represents high EXO1 and low SLC7A5, purple line represents low EXO1 and high SLC7A5, and orange line represents high EXO1 and high SLC7A5.

Table 6.7. Multivariate Cox analysis of associations between EXO1/SLC7A5 mRNA expression and clinicopathological parameters in all cases, ER+ and ER-.

Parameters	EXO1/SLC7A5 mRNA					
	All Cases		ER+		ER-	
	HR (95% CI)	<i>p</i> -value	HR (95% CI)	<i>p</i> -value	HR (95% CI)	<i>p</i> -value
SLC7A5-EXO1-	Reference		Reference		Reference	
SLC7A5-EXO1+	1.7 (1.2-2.3)	0.001	1.6 (1.2-2.3)	0.003	2.2 (0.8-6.1)	0.2
SLC7A5+EXO1-	1.3 (1.0-1.9)	0.08	1.3 (0.9-1.8)	0.205	1.4 (0.5-3.4)	0.5
SLC7A5+EXO1+	2.0 (1.6-2.6)	1.3x10⁻⁷	2.0 (1.5-2.7)	3.0x10⁻⁷	1.5 (0.7-3.3)	0.3
Grade	1.2 (1.0-1.4)	0.07	1.2 (1.0-1.4)	0.1	0.9 (0.6-1.5)	0.7
Size	1.7 (1.4-2.1)	1.2x10⁻⁷	1.7 (1.4-2.2)	5.0 x10⁻⁷	1.7 (1.2-2.4)	0.002
Lymph Node Stage	1.9 (1.7-2.1)	4.9x10⁻²⁵	1.8 (1.6-2.1)	2.7x10⁻¹⁶	1.9 (1.6-2.4)	7.6x10⁻¹⁰

P values in bold mean statistically significant.



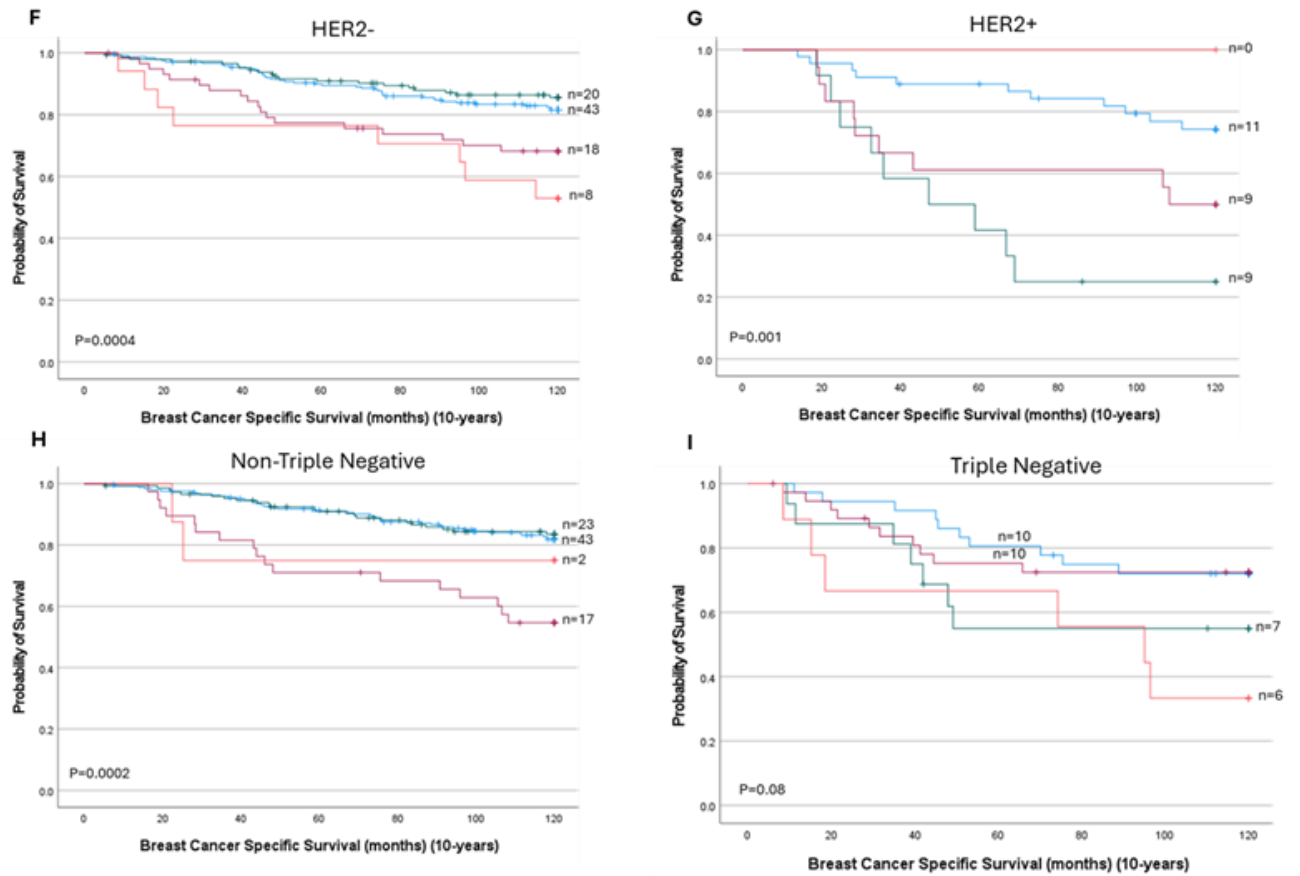
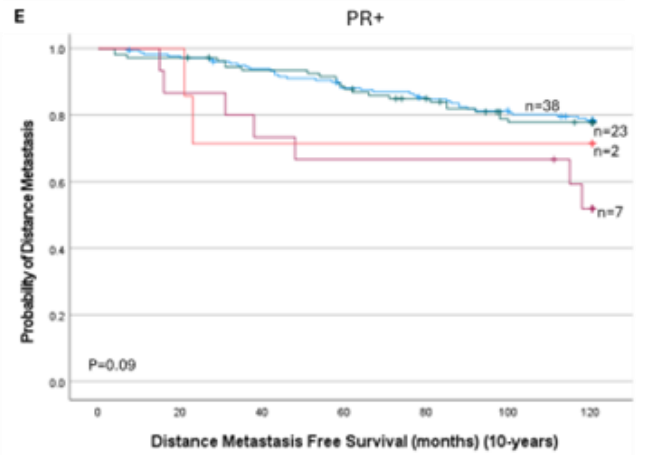
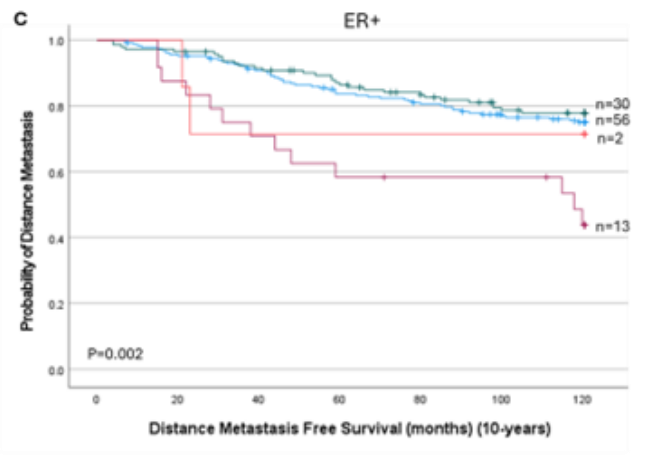
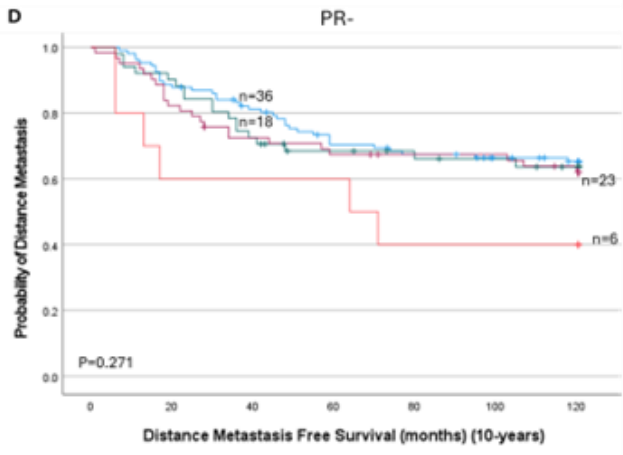
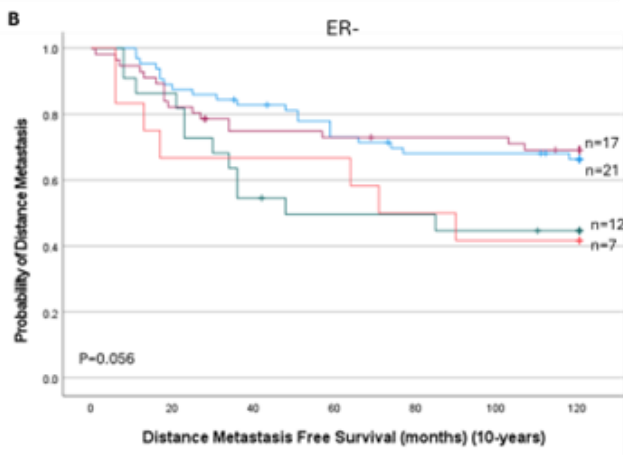
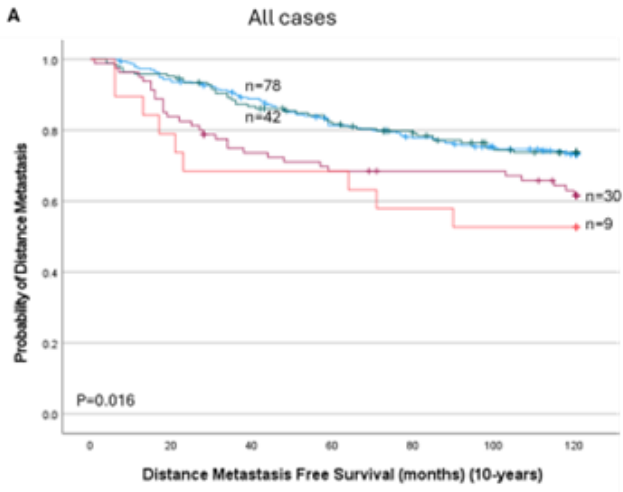


Figure 6.14. EXO1 protein expression and its association with Breast Cancer Specific Survival (BCSS) in invasive breast cancer: A) EXO1/SLC7A5 in all cases, B) EXO1/SLC7A5 in ER-, C) EXO1/SLC7A5 in ER+, D) EXO1/SLC7A5 in PR-, E) EXO1/SLC7A5 in PR+, F) EXO1/SLC7A5 in HER2-, G) EXO1/SLC7A5 in HER2+, H) EXO1/SLC7A5 in Non-Triple Negative (Non-TN) and I) EXO1/SLC7A5 in Triple Negative (TN) in breast cancer. Blue line represents low EXO1 and low SLC7A5, Green line represents high EXO1 and low SLC7A5, purple line represents low EXO1 and high SLC7A5, and orange line represents high EXO1 and high SLC7A5.



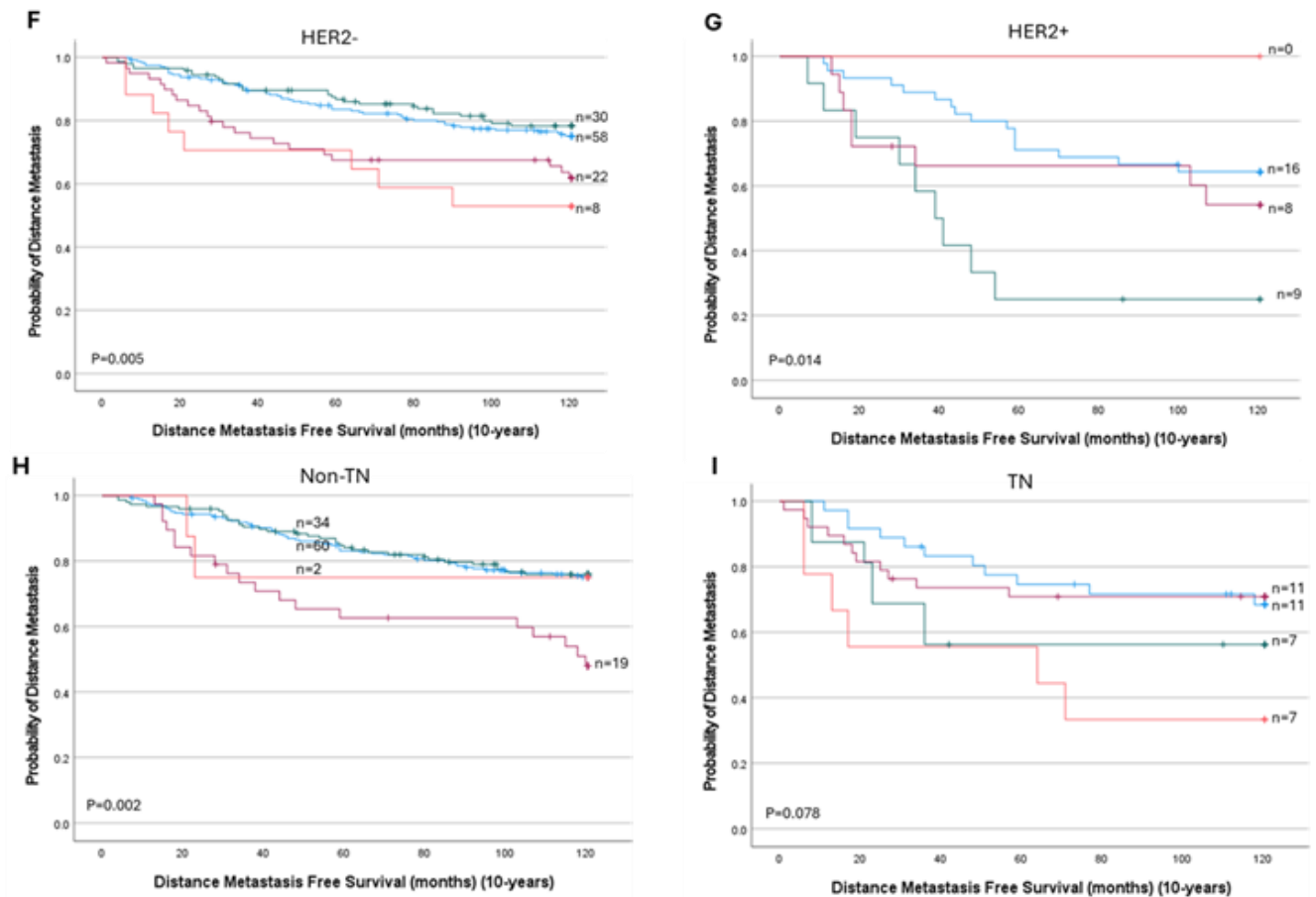
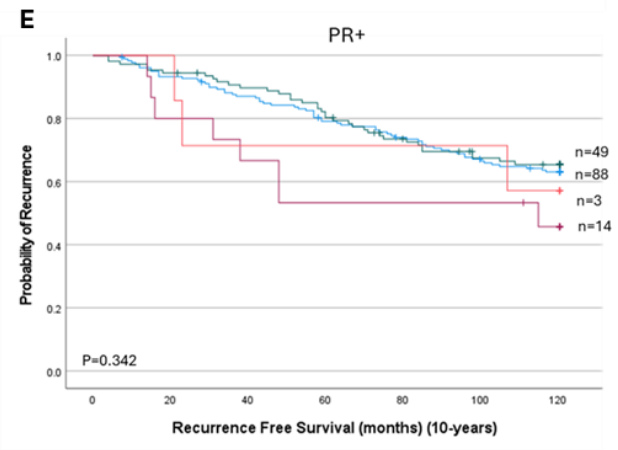
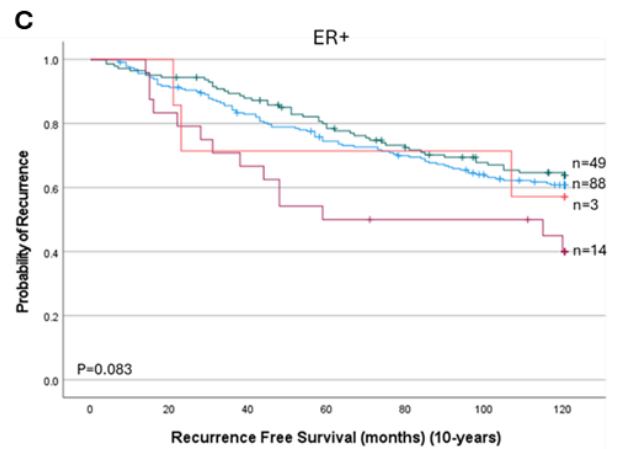
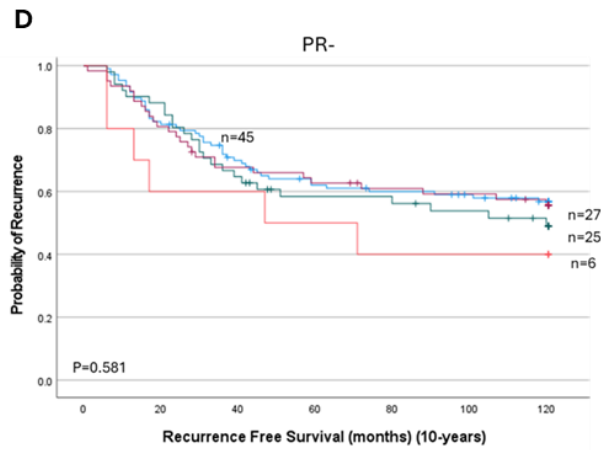
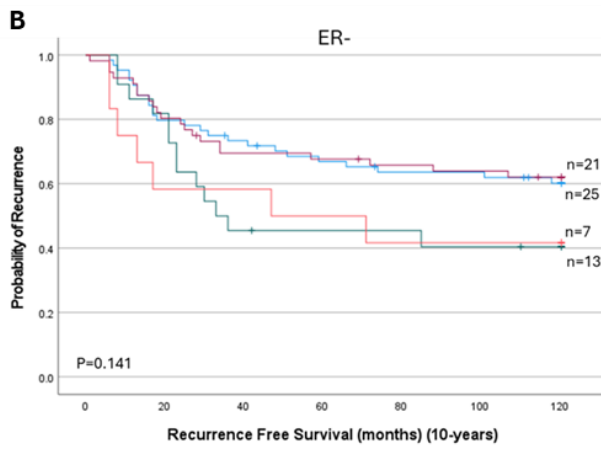
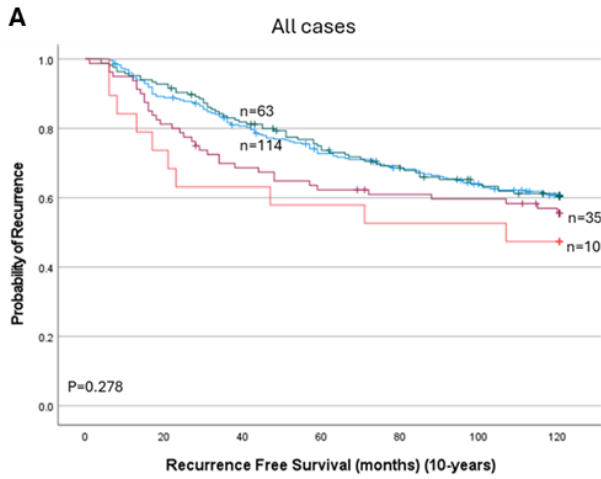


Figure 6.15. EXO1 protein expression and its association with distance metastasis free survival (DMFS) in invasive breast cancer: A) EXO1/SLC7A5 in all cases, B) EXO1/SLC7A5 in ER-, C) EXO1/SLC7A5 in ER+, D) EXO1/SLC7A5 in PR-, E) PR+, F) EXO1/SLC7A5 in HER2-, G) EXO1/SLC7A5 in HER2+, H) EXO1/SLC7A5 in Non-Triple Negative (Non-TN) and I) EXO1/SLC7A5 in Triple Negative (TN) in breast cancer. Blue line represents low EXO1 and low SLC7A5, Green line represents high EXO1 and low SLC7A5, purple line represents low EXO1 and high SLC7A5, and orange line represents high EXO1 and high SLC7A5.



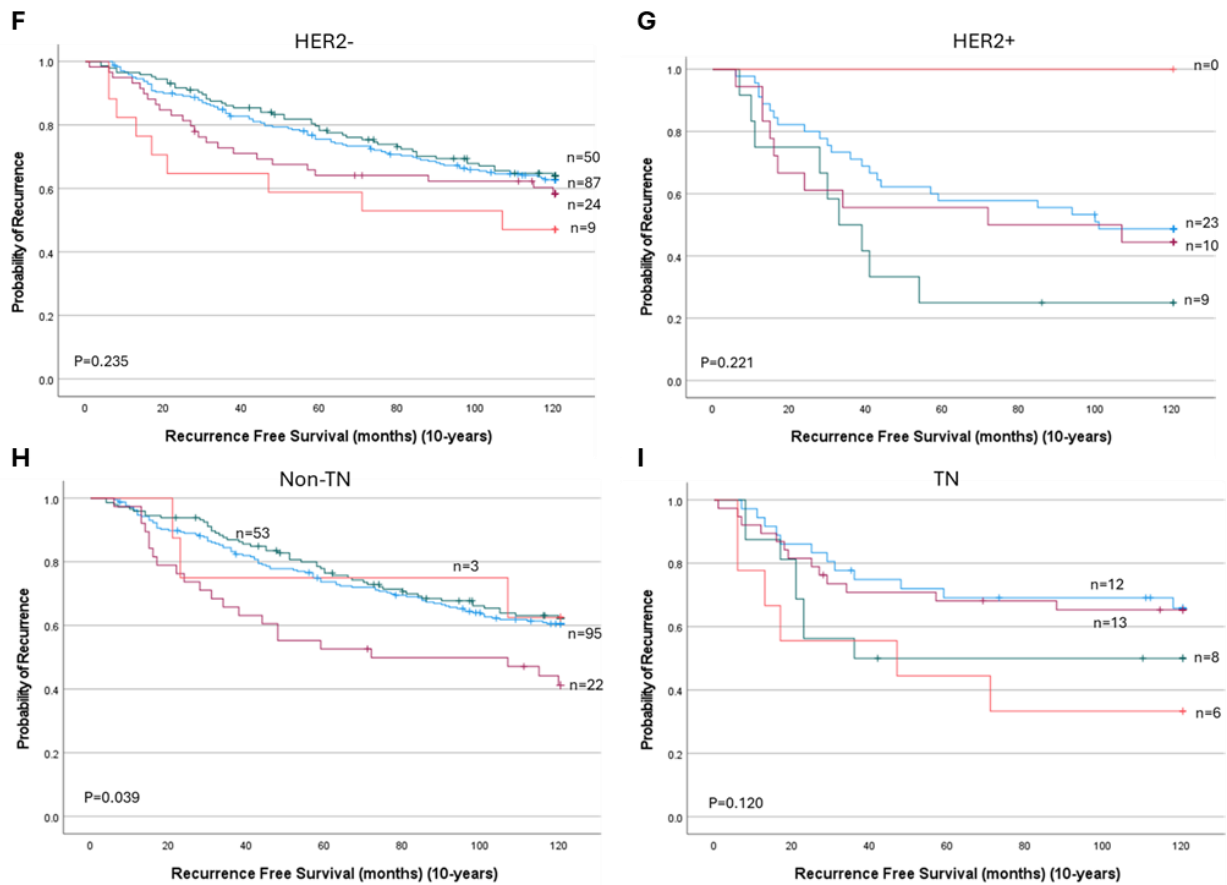


Figure 6.16. EXO1 protein expression and its association with recurrence free survival (RFS) in invasive breast cancer: A) EXO1/SLC7A5 in all cases, B) EXO1/SLC7A5 in ER-, C) EXO1/SLC7A5 in ER+, D) EXO1/SLC7A5 in PR-, E) EXO1/SLC7A5 in PR+, F) EXO1/SLC7A5 in HER2-, G) EXO1/SLC7A5 in HER2+, H) EXO1/SLC7A5 in Non-Triple Negative (Non-TN) and I) EXO1/SLC7A5 in Triple Negative (TN) in breast cancer. Blue line represents low EXO1 and low SLC7A5, Green line represents high EXO1 and low SLC7A5, purple line represents low EXO1 and high SLC7A5, and orange line represents high EXO1 and high SLC7A5.

Table 6.8. Multivariate Cox analysis of associations between EXO1/SLC7A5 protein expression and clinicopathological parameters in all cases, ER+ and ER- breast cancer.

<i>Breast Cancer Specific Survival</i>						
Parameters	All Cases		ER+		ER-	
	HR (95% CI)	p-value	HR (95% CI)	p-value	HR (95% CI)	p-value
SLC7A5-EXO1-	Reference		Reference		Reference	
SLC7A5-EXO1+	1.0 (0.6-1.5)	0.9	0.8 (0.5-1.4)	0.5	1.9 (0.8-4.1)	0.1
SLC7A5+EXO1-	1.5 (0.9-2.4)	0.1	1.9 (0.9-3.8)	0.09	1.3 (0.6-2.5)	0.5
SLC7A5+EXO1+	2.7 (1.3-5.6)	0.01	2.1 (0.5-8.9)	0.3	2.8 (1.1-7.2)	0.03
Grade	1.7 (1.3-2.4)	0.0009	1.8 (1.2-2.6)	0.004	1.2 (0.6-2.5)	0.5
Size	1.8 (1.2-2.7)	0.005	1.8 (1.1-3.1)	0.03	1.5 (0.8-2.9)	0.2
Lymph Node Stage	2.6 (2.0-3.3)	7.4x10⁻¹⁴	2.6 (1.9-3.7)	3.5x10⁻⁸	2.3 (1.6-3.3)	5.0x10⁻⁶
<i>Distance Metastasis Free Survival</i>						
Parameters	HR	p-value	HR	p-value	HR	p-value
	(95% CI)		(95% CI)		(95% CI)	
SLC7A5-EXO1-	Reference		Reference		Reference	
SLC7A5-EXO1+	1.1 (0.8-1.6)	0.6	1.0 (0.6-1.5)	0.8	1.6 (0.8-3.4)	0.2
SLC7A5+EXO1-	1.2 (0.8-1.9)	0.4	2.1 (1.1-3.8)	0.02	0.9 (0.5-1.8)	0.8
SLC7A5+EXO1+	2.3 (1.1-4.7)	0.02	1.4 (0.3-5.9)	0.6	2.7 (1.1-6.7)	0.03
Grade	1.5 (1.2-2.0)	0.002	1.6 (1.2-2.2)	0.004	1.0 (0.6-1.9)	0.9
Size	1.8 (1.2-2.5)	0.001	2.0 (1.3-3.0)	0.002	1.1 (0.6-2.0)	0.7
Lymph Node Stage	2.5 (1.8-3.4)	2.4x10⁻⁸	2.0 (1.5-2.7)	3.5x10⁻⁸	2.5 (1.7-3.5)	6.4x10⁻⁷
<i>Recurrence Free Survival</i>						
Parameters	HR	p-value	HR	p-value	HR	p-value
	(95% CI)		(95% CI)		(95% CI)	
SLC7A5-EXO1-	Reference		Reference		Reference	
SLC7A5-EXO1+	(0.8-1.4)	0.8	0.9 (0.6-1.3)	0.5	(0.8-3.1)	0.2
SLC7A5+EXO1-	1.1 (0.8-1.7)	0.5	1.7 (0.9-3.0)	0.08	0.9 (0.5-1.7)	0.8
SLC7A5+EXO1+	1.8 (0.9-3.5)	0.08	1.3 (0.4-4.1)	0.7	2.1 (0.9-5.1)	0.09
Grade	1.1 (0.9-1.3)	0.4	1.1 (0.9-1.4)	0.5	1.0 (0.6-1.7)	1.0
Size	1.3 (1.0-1.8)	0.04	1.4 (1.0-1.9)	0.08	1.0 (0.6-1.8)	0.9
Lymph Node Stage	2.0 (1.5-2.6)	3.0x10⁻⁷	1.8 (1.4-2.3)	2.0x10⁻⁷	2.1 (1.5-2.9)	8.0x10⁻⁶

P values in bold mean statistically significant.

6.4 Discussion

Glutamine metabolism and DNA repair pathways are important to maintain cellular homeostasis in normal cells. Alterations in the expression and function of these pathways in cancer cells promote rapid growth, genetic heterogeneity and survival [37]. EXO1 is a protein with 5' to 3' exonuclease activity, it is involved in the replication fork maintenance, cell cycle checkpoints and mismatch repair pathway as it interacts with MSH2 [243]. These two pathways remain relatively distinct, but there is accumulating evidence that the pathways are interdependent and intrinsically linked [244].

EXO1 is an evolutionarily conserved enzyme that belongs to the RAD2/XPG nuclease family, which consists of EXO1, FEN1, RAD2/XPG and GEN1. This family plays a critical role in repair, replication and recombination [250]. EXO1 plays an important role in cell cycle, telomere maintenance, DNA double-strand break repair, DNA mismatch repair and nucleotide excision repair, it is also involved in processing the Okazaki fragment flaps among other DNA nucleases, including FEN1 and DNA2 [251]. Overexpression of EXO1 is associated with tumour progression in several types of cancer, including prostate, lung and ovarian [250].

This Chapter has demonstrated that EXO1 was overexpressed in breast cancer compared to normal tissue, and the promoter region in the tumour was hypomethylated, which contributed to its upregulation. This was supported by a previous study, where the expression of EXO1 was higher in breast cancer tissue in comparison to normal tissues, the study further validated the overexpression through real-time quantitative polymerase chain reaction (RT-qPCR) in breast cancer cell line MDA-MB-231, indicating a potential role for EXO1 in breast carcinogenesis [243]. Furthermore, EXO1 was upregulated in breast cancer due to its hypomethylation, which suggests that promoter hypomethylation plays a role in the increased expression of EXO1 in breast cancer [252].

The study investigated the clinicopathological and prognostic utility of the singular expression of EXO1 and the high expression of both SLC7A5/EXO1. The results showed that high EXO1 expression at the mRNA level in breast cancer was associated with poor clinicopathological parameters, including larger tumour size and higher tumour grade. At the protein level, elevated EXO1 expression was specifically associated with advanced lymph node stage. In this present study, the high expression of EXO1 at mRNA level was associated with poor clinical outcome. Moreover, at the protein level, the high expression of EXO1 was associated with worse patient outcome in terms of BCSS, DMFS and RFS in ER- tumours. Breast tumours that are characterised with ER- tend to be more aggressive and have higher proliferation indices such as Ki-67 levels [253], in addition to EXO1 role in DNA repair pathway, EXO1 overexpression activates RAS/AKT/MYC/E2F1 signalling pathways, which are known to be dysregulated in ER- tumours [254].

In terms of the high expression of SLC7A5 and EXO1, this study showed that there was a positive moderate correlation between SLC7A5 and EXO1, which was the highest among the other mismatch DNA repair genes. Furthermore, the results indicated that high expression of SLC7A5/EXO1 was correlated with poor clinicopathological parameters, including higher tumour grade and lymph node stage, and it was highly expressed in ER- and triple-negative tumours at both mRNA and protein levels. Overexpression of both SLC7A5 and EXO1 was implicated in breast cancer progression, though their roles are distinct. SLC7A5 is an amino acid transporter that facilitates the uptake of large neutral amino acids, such as leucine, in exchange for glutamine [70]. Leucine is known to play a role in activating the mTORC1 signalling pathway, which enhances the biosynthesis of nucleotides, protein translation and cell proliferation [70]. On the other hand, EXO1 mainly functions in DNA mismatch repair, hence the maintenance of genomic stability [243]. While there is no evidence of direct interaction between SLC7A5 and EXO1 in breast cancer, the study hypothesises that their roles intersect through the modulation of nucleotide pools.

In this study, the high expression of SLC7A5/EXO1 at both mRNA and protein levels was associated with poor patient outcome in breast cancer patients. Specifically, this high expression was associated with worse patient outcome in terms of BCSS and DMFS, particularly in ER- and HER2- tumours, but not in triple negative, as the sample number was too small to get a significant outcome, therefore it is suggested to explore the effect of EXO1 in larger triple negative tumour cohorts.

It is reported that c-MYC expression is elevated in ER- and triple negative tumours [255], which can induce the expression of SLC7A5 [70]. In addition its expression is associated with other pathways, such as Ras/Raf/MAPK pathway [256] and PI3K-AKT pathway which plays a critical role in activating mTORC1 [257]. SLC7A5 is also involved in activating the mTORC1 signalling pathway via maintaining the intracellular levels of leucine, which is the master regulator of mTORC1 signalling pathway [164]. This pathway is known to promote the synthesis of nucleotides required for DNA repair and replication [258]. This suggests the association between glutamine metabolism and DNA repair, hence the association between SLC7A5 and EXO1 in breast cancer.

In summary, this study revealed that the overexpression of EXO1 was associated with poor prognostic characteristics and poor patient outcome in ER- tumours. The study further showed that the high expression of SLC7A5/EXO1 resulted in aggressive clinicopathological features and poor survival outcome, particularly in ER- and HER2- tumours. However, further pathway enrichment analysis and laboratory-based experiments are needed to investigate the effect of high SLC7A5/EXO1 expression in breast cancer. Exploring the association between glutamine metabolism and the DNA repair pathway will lead to finding more prognostic and predictive markers that help in improving the current therapeutic approaches for breast cancer patients.

Chapter 7 General discussion

7.1 Background

Breast cancer is a biologically complex and clinically diverse disease, comprising multiple molecular subtypes with distinct patterns of gene expression, therapeutic response, and prognosis [259]. There is increasing evidence that highlights the importance of integrating metabolic reprogramming and genomic instability, two established hallmarks of cancer, to better understand tumour progression and therapeutic resistance [1]. In particular, the interplay between amino acid metabolism, notably glutamine utilisation, and DNA repair mechanisms is emerging as a crucial axis supporting cancer cell survival under stress [260].

Metabolism is crucial for many important processes, including biosynthesis, maintaining energy production and redox balance. SLC7A5 is a glutamine-leucine transporter that is frequently upregulated in aggressive breast cancers and plays a crucial role in activating mammalian target of rapamycin complex 1 (mTORC1), which is a nutrient-sensitive kinase that controls cell growth, protein synthesis, and de novo nucleotide biosynthesis [70, 261]. On the other hand, DNA replication and repair proteins such as FEN1 and Exonuclease 1 EXO1 are essential for maintaining genomic integrity, particularly under high proliferation and oxidative stress conditions common in tumour environments [262, 263]. FEN1 and EXO1 are both members of the RAD2 family of structure-specific nucleases [264]. While FEN1 is involved in base excision and flap endonuclease activity during DNA replication, EXO1 functions primarily in mismatch repair and resection during homologous recombination [262, 263]. Despite their distinct functions, they share complementary roles, particularly in Okazaki fragment maturation during lagging-strand DNA synthesis, where both contribute to maintaining replication accuracy and genomic stability [265].

The integration of both glutamine metabolism and DNA repair becomes particularly important in tumour cells, which rely on a steady nucleotide supply not only for genome replication but

also for efficient DNA repair. The mTORC1 signalling is known to coordinate nutrient sensing with nucleotide production, while glutamine availability supports both energy metabolism and anaplerotic inputs to nucleotide pathways [206]. In this context, co-expression of SLC7A5 with DNA repair genes like FEN1 and EXO1 represents a coordinated survival strategy, particularly in metabolically active and genomically unstable tumours.

This thesis investigated the potential association between glutamine metabolism and DNA repair in breast cancer. Through clinical analysis, in vitro assay experiments, and proteomic investigations, the project examined the expression and functional roles of SLC7A5 and FEN1, aiming to determine their prognostic significance and underlying mechanistic associations. In addition, the expression of both SLC7A5 and EXO1 was explored solely through clinical data analysis to assess their prognostic value. The following discussion brings together these findings across molecular subtypes, providing new insights into breast cancer biology and highlighting potential avenues for future therapeutic strategies.

7.2 Main findings of the study

From a clinical perspective (chapter 3), analysis of large breast cancer datasets revealed that high expression of SLC7A5 and FEN1 at both the mRNA and protein levels was significantly associated with adverse clinicopathological features, such as larger tumour size, higher tumour grade, and elevated Nottingham Prognostic Index (NPI) scores. These associations suggest that co-expression of these genes characterises more biologically aggressive tumours, consistent with other studies that demonstrated the poor prognostic singular effect of SLC7A5 [171, 175, 266, 267], and FEN1 overexpression in different human cancers [268-273].

Importantly, SLC7A5/FEN1 high expression was also enriched in tumours with negative ER and PR status and triple-negative (TN) breast cancer subtypes known for limited treatment options and poorer prognosis. In addition, PAM50 analysis demonstrated that co-expression

was elevated in luminal B, HER2-enriched, and basal-like subtypes, further supporting their involvement in aggressive breast cancer phenotypes.

Regarding patient outcome, the high expression of SLC7A5/FEN1 was consistently correlated with poor survival. Multivariate Cox regression analysis demonstrated that high mRNA expression predicted shorter overall survival (OS) independently of tumour size and nodal stage in all cases and ER-positive (ER+) patients. At the protein level, this high expression was similarly associated with reduced breast cancer-specific survival (BCSS) and distant metastasis-free survival (DMFS) in all cases and ER+ patients. These findings are in line with previous studies that identified SLC7A5 and FEN1 as prognostic markers in ER+ breast cancer subtypes [70, 208].

Together, these findings reinforce the prognostic value of SLC7A5/FEN1 high expression, particularly in ER+ breast cancer, where it was also associated with distant metastasis. Collectively, these data position SLC7A5/FEN1 as a clinically relevant prognostic biomarker across multiple breast cancer subtypes.

To further validate and mechanistically understand the clinical observations, assay experiments were performed in multiple breast cancer cell lines (MCF-7, MDA-MB-436, and MDA-MB-231) (chapter 4). Double knockdown of SLC7A5 and FEN1 significantly impaired cancer cell behaviours, including proliferation, migration, and invasion, suggesting their cooperative role in promoting tumour progression. Additionally, combined silencing led to S-phase arrest, prevention of G2 phase entry, and a significant increase in apoptotic cells. These findings indicate that SLC7A5 and FEN1 not only contribute to the metabolic and replicative advantage of cancer cells but are also essential for cell cycle progression and survival under stress. The combined effect of dual knockdown further strengthens the hypothesis that their high expression supports tumour fitness and adaptability.

The mitochondrial assay experiments in Chapter 5 demonstrated that knockdown of FEN1 and SLC7A5, either alone or in combination, resulted in a significant reduction in basal

respiration, ATP production, proton leak, and spare respiratory capacity, particularly in the MCF-7 cell line. These findings indicate a marked impairment in mitochondrial membrane integrity and bioenergetic function, which is vital for cell survival and proliferation. Importantly, mitochondrial dysfunction is tightly linked to cell cycle arrest and apoptosis in cancer cells. The loss of ATP production and increased oxidative stress, caused by impaired mitochondrial respiration, can activate checkpoints leading to S-phase arrest and initiation of apoptotic pathways [274, 275].

This aligns with the functional data in Chapter 4, where dual knockdown of FEN1 and SLC7A5 not only reduced proliferation and migration but also induced cell cycle arrest in S phase and significantly increased apoptotic cell populations. Mechanistically, this was a consequence of both nucleotide depletion due to suppressed mTORC1 activity, which resulted from loss of SLC7A5-mediated leucine uptake, and accumulated unrepaired DNA lesions due to FEN1 deficiency [70, 151]. Together, this led to replication stress and activation of DNA damage response pathways, which in turn triggered mitochondria-mediated apoptosis [276, 277].

Moreover, the mitochondrial impairment observed in Chapter 5 further explains the poor prognostic implications seen in Chapter 3 for tumours with high levels of SLC7A5 and FEN1, particularly in ER+ tumours. Notably, the MCF-7 cell line demonstrated a more pronounced reciprocal downregulation of FEN1 and SLC7A5 protein levels, following the knockdown of either of them in comparison to the MDA-MB-436 cell line (Chapter 5).

Finally, the functional enrichment analysis of proteins shared between SLC7A5 and FEN1 pulldowns further reinforced the biological interplay between these two molecules (Chapter 5). In MCF-7 cells, mutual proteins were significantly enriched in pathways related to nuclear transport, DNA repair via nonhomologous end joining (NHEJ), membrane repair, and pyrimidine ribonucleotide biosynthesis, which is a finding that aligns with earlier data showing SLC7A5/FEN1 high expression being associated with poor prognosis in ER+ breast cancer (Chapter 3). These enriched pathways mirror the cellular phenotypes observed in Chapters 4 and 5, where dual knockdown of SLC7A5 and FEN1 led to reduced proliferation, G2 transition

blockade, and mitochondrial dysfunction, likely due to impaired nucleotide availability and membrane integrity.

In MDA-MB-436 cells, shared proteins also enriched pathways including mitochondrial function, RNA metabolism, and nuclear transport, providing a molecular explanation for the partial mitochondrial impairment and moderate protein interdependence observed in this triple-negative breast cancer model. These results highlight how SLC7A5 and FEN1 converge on fundamental processes such as nucleotide biosynthesis, oxidative phosphorylation, and RNA processing, with stronger phenotypic consequences in ER+ cells. Together, the pathway analysis underscores the functional cooperation of SLC7A5 and FEN1 in sustaining metabolic and DNA repair networks, which are critical for breast cancer cell survival and aggressiveness.

To expand upon the DNA repair aspect, EXO1, a mismatch repair enzyme moderately correlated with SLC7A5, was investigated. High EXO1 expression was associated with larger tumour size, higher grade, and poor patient outcome. Interestingly, mRNA and protein levels of EXO1 showed different association patterns: mRNA expression aligned with more aggressive features, including negative ER/PR and positive HER2 status, while protein expression correlated with positive ER/PR and negative HER2 status. Nonetheless, both levels were consistently associated with shorter survival and distant metastasis, especially in ER-negative (ER-) tumours. This aligns with a previous study, which indicated that EXO1 expression was elevated in ER- subgroups in comparison to ER+ subgroups of breast tumours [254].

Furthermore, the high expression of SLC7A5 and EXO1 revealed that their mRNA and protein co-expression strongly mirrored the patterns observed with FEN1. The SLC7A5+EXO1+ subgroup was consistently linked with worse prognosis, shorter overall survival, poor patient outcome in terms of BCSS and higher risk of metastasis, particularly in ER- and HER2- tumours.

Further analysis of SLC7A5 and EXO1 high expression revealed that their mRNA and protein profiles were both associated with aggressive breast cancer characteristics; however, they did not completely mirror each other in terms of prognostic value. Multivariable Cox-regression analysis showed that SLC7A5+EXO1+ mRNA high expression was a significant independent predictor of shorter overall survival, regardless of tumour size and lymph node stage, particularly in ER+ tumours. Conversely, the SLC7A5+EXO1+ protein subgroup was more strongly associated with breast cancer-specific mortality and distant metastasis, especially in ER- tumours. This discrepancy between mRNA and protein-level associations may be attributed to post-transcriptional regulation, protein stability, and tumour microenvironment influences [278, 279]. While mRNA levels often reflect transcriptional activity, they do not always translate directly to protein abundance due to factors such as mRNA degradation, translation efficiency, and differential protein turnover [280].

As it was mentioned in Chapter 6, the strong association between high SLC7A5 and EXO1 protein co-expression and poor prognosis in ER- breast cancer may be explained, in part, by the upregulation of c-MYC, a transcription factor frequently overexpressed in ER- tumours [281]. c-MYC is known to directly bind to the promoter of SLC7A5 [282], which drives its transcription leading to the increase of the uptake of large neutral amino acids, particularly leucine, which in turn causes the upregulation of mTORC1 signalling [283], leading to the promotion of anabolic processes including protein translation, nucleotide biosynthesis, and mitochondrial metabolism [284].

7.3 Final Conclusion

The current study supports the central hypothesis that glutamine metabolism and the DNA repair pathway are associated in breast cancer. Through a comprehensive investigation, the thesis examined this association with a specific focus on the glutamine transporter SLC7A5 and two DNA repair proteins, FEN1 and EXO1. Clinical analysis revealed that the high expression of SLC7A5 and FEN1 was significantly associated with aggressive tumour features and poor prognosis, especially in ER-positive breast cancer, whereas EXO1 expression was more strongly linked to poor outcome in ER-negative subtypes. These subtype-specific patterns support the notion that distinct DNA repair mechanisms may dominate in different molecular contexts, but share common metabolic pathways mediated by SLC7A5 and mTORC1 activation, which links amino acid availability to nucleotide biosynthesis and DNA repair.

The findings of this study also demonstrate that SLC7A5 and FEN1 are not only highly expressed in aggressive breast cancer subtypes, but are also functionally interdependent in supporting tumour cell growth, metabolic fitness and survival. assay experiments, including Seahorse analysis, confirmed that simultaneous knockdown of both genes impaired mitochondrial respiration and ATP production, reinforcing their role in maintaining cellular energy and biosynthetic demands. Additionally, proteomic analysis identified a subset of proteins enriched in both SLC7A5 and FEN1 pulldowns, many of which were involved in mitochondrial function, DNA repair, and RNA metabolism, highlighting the molecular crosstalk between these pathways. These findings suggest that context-dependent high expression of metabolic and DNA repair genes contributes to tumour aggressiveness, and exploring this association will provide tailored prognostic markers and therapeutic targets across breast cancer subtypes.

7.4 Limitations of the study

1. The limited number of cases available using the Nottingham cohort (such as ER- and triple negative cases), affects the results of the clinical study.
2. Further validation of the experimental assay findings is required, specifically through Western blot analysis to evaluate downstream molecular changes related to the observed phenotype, for example, assessing cell cycle regulators (such as, cyclins) or apoptosis-related proteins (such as, cleaved caspase 3).
3. Western blot validation for the double knockdown of both SLC7A5 and FEN1 was not performed.
4. The co-immunoprecipitant experiment was limited by the number of biological replicates, which affects the robustness and reproducibility of the proteomic analysis.
5. No common interactors were identified between MCF-7 and MDA-MB-436 cell lines, which highlight cell-line specificity but also limits generalisability of the results across different breast cancer subtypes.
6. No direct functional assays were performed to validate the potential mitochondrial involvement, suggested by enrichment analysis (such as JC-1 staining for membrane potential, or MitoSOX for mitochondrial reactive oxygen species).

7.5 Future directions

1. Validation of the shared proteins between SLC7A5 and FEN1, by using western blot.
2. Evaluation of the validated shared proteins at both the mRNA and protein levels to determine their prognostic significance in breast cancer.
3. Investigation of the predictive significance of the co-expression of SLC7A5 and FEN1/EXO1 in breast cancer patients.
4. In vitro assay experiments, to find the significance of SLC7A5/EXO1 on breast cancer cell lines.
5. In vivo validation of functional interdependence of SLC7A5, FEN1 and EXO1.
6. Investigation of another glutamine metabolism and other DNA repair proteins, further exploring their prognostic significance.

References

1. Hanahan, D., *Hallmarks of Cancer: New Dimensions*. Cancer Discov, 2022. **12**(1): p. 31-46.
2. Saha, T., et al., *Invasion and Metastasis as a Central Hallmark of Breast Cancer*. J Clin Med, 2021. **10**(16).
3. Hudis, C.A., *Trastuzumab--mechanism of action and use in clinical practice*. N Engl J Med, 2007. **357**(1): p. 39-51.
4. Cancer Genome Atlas Research, N., et al., *Integrated genomic characterization of endometrial carcinoma*. Nature, 2013. **497**(7447): p. 67-73.
5. Wang, H., et al., *Targeting p53 pathways: mechanisms, structures, and advances in therapy*. Signal Transduct Target Ther, 2023. **8**(1): p. 92.
6. Carbognin, L., et al., *Prognostic and Predictive Implications of PTEN in Breast Cancer: Unfulfilled Promises but Intriguing Perspectives*. Cancers (Basel), 2019. **11**(9).
7. Lee, E., et al., *Regulated cell death pathways and their roles in homeostasis, infection, inflammation, and tumorigenesis*. Exp Mol Med, 2023. **55**(8): p. 1632-1643.
8. Castillo Ferrer, C., K. Berthenet, and G. Ichim, *Apoptosis - Fueling the oncogenic fire*. FEBS J, 2021. **288**(15): p. 4445-4463.
9. Galluzzi, L., et al., *Molecular definitions of cell death subroutines: recommendations of the Nomenclature Committee on Cell Death 2012*. Cell Death Differ, 2012. **19**(1): p. 107-20.
10. Shay, J.W. and W.E. Wright, *Telomeres and telomerase: three decades of progress*. Nat Rev Genet, 2019. **20**(5): p. 299-309.
11. Kulic, A., et al., *Telomerase activity in breast cancer patients: association with poor prognosis and more aggressive phenotype*. Med Oncol, 2016. **33**(3): p. 23.
12. Sharma, P., et al., *VEGFA Gene Expression in Breast Cancer Is Associated With Worse Prognosis, but Better Response to Chemotherapy and Immunotherapy*. World J Oncol, 2025. **16**(1): p. 120-130.
13. Carstens, J.L. and S. Lovisa, *Epithelial-to-mesenchymal transition drives cancer genomic instability*. J Exp Clin Cancer Res, 2025. **44**(1): p. 135.
14. Dong, H., et al., *Overexpression of matrix metalloproteinase-9 in breast cancer cell lines remarkably increases the cell malignancy largely via activation of transforming growth factor beta/SMAD signalling*. Cell Prolif, 2019. **52**(5): p. e12633.
15. Baranwal, S. and S.K. Alahari, *Molecular mechanisms controlling E-cadherin expression in breast cancer*. Biochem Biophys Res Commun, 2009. **384**(1): p. 6-11.
16. Yang, Y., et al., *Circulating tumour cell clusters: isolation, biological significance and therapeutic implications*. BMJ Oncol, 2024. **3**(1): p. e000437.
17. Lozar, T., et al., *The biology and clinical potential of circulating tumor cells*. Radiol Oncol, 2024. **58**(3): p. 458.
18. Akhmetkaliyev, A., et al., *EMT/MET plasticity in cancer and Go-or-Grow decisions in quiescence: the two sides of the same coin?* Mol Cancer, 2023. **22**(1): p. 90.
19. Potter, M., E. Newport, and K.J. Morten, *The Warburg effect: 80 years on*. Biochem Soc Trans, 2016. **44**(5): p. 1499-1505.
20. Wang, B., et al., *A glutamine tug-of-war between cancer and immune cells: recent advances in unraveling the ongoing battle*. J Exp Clin Cancer Res, 2024. **43**(1): p. 74.
21. Schmid, P., et al., *Pembrolizumab for Early Triple-Negative Breast Cancer*. N Engl J Med, 2020. **382**(9): p. 810-821.

22. Huang, R. and P.K. Zhou, *DNA damage repair: historical perspectives, mechanistic pathways and clinical translation for targeted cancer therapy*. Signal Transduct Target Ther, 2021. **6**(1): p. 254.
23. Mohamed, R.I., et al., *The overexpression of DNA repair genes in invasive ductal and lobular breast carcinomas: Insights on individual variations and precision medicine*. PLoS One, 2021. **16**(3): p. e0247837.
24. Jiang, X., et al., *The role of microenvironment in tumor angiogenesis*. J Exp Clin Cancer Res, 2020. **39**(1): p. 204.
25. Goldberg, J.E. and K.L. Schwertfeger, *Proinflammatory cytokines in breast cancer: mechanisms of action and potential targets for therapeutics*. Curr Drug Targets, 2010. **11**(9): p. 1133-46.
26. Allison, K.H., *Prognostic and predictive parameters in breast pathology: a pathologist's primer*. Mod Pathol, 2021. **34**(Suppl 1): p. 94-106.
27. Harbeck, N., et al., *Breast cancer*. Nat Rev Dis Primers, 2019. **5**(1): p. 66.
28. Hammond, M.E., et al., *American Society of Clinical Oncology/College Of American Pathologists guideline recommendations for immunohistochemical testing of estrogen and progesterone receptors in breast cancer*. J Clin Oncol, 2010. **28**(16): p. 2784-95.
29. Rossi, S., et al., *Prognostic and predictive factors of eribulin efficacy in heavily pretreated patients affected by metastatic breast cancer: correlation with tumor biology and previous therapies*. Drugs Context, 2017. **6**: p. 212506.
30. Duffy, M.J., et al., *Validated biomarkers: The key to precision treatment in patients with breast cancer*. Breast, 2016. **29**: p. 192-201.
31. Mosly, D., et al., *Predictive markers of endocrine response in breast cancer*. World J Exp Med, 2018. **8**(1): p. 1-7.
32. Mohanty, S.S., C.R. Sahoo, and R.N. Padhy, *Role of hormone receptors and HER2 as prospective molecular markers for breast cancer: An update*. Genes Dis, 2022. **9**(3): p. 648-658.
33. Elston, C.W. and I.O. Ellis, *Pathological prognostic factors in breast cancer. I. The value of histological grade in breast cancer: experience from a large study with long-term follow-up*. Histopathology, 1991. **19**(5): p. 403-10.
34. Rakha, E.A., et al., *Prognostic significance of Nottingham histologic grade in invasive breast carcinoma*. J Clin Oncol, 2008. **26**(19): p. 3153-8.
35. Liu, Y., et al., *Tumor Size Still Impacts Prognosis in Breast Cancer With Extensive Nodal Involvement*. Front Oncol, 2021. **11**: p. 585613.
36. Kim, J.Y., et al., *The prognostic significance of the lymph node ratio in axillary lymph node positive breast cancer*. J Breast Cancer, 2011. **14**(3): p. 204-12.
37. Yang, Z.J., et al., *The prognostic value of node status in different breast cancer subtypes*. Oncotarget, 2017. **8**(3): p. 4563-4571.
38. Nemoto, T., et al., *Breast cancer in the medial half. Results of 1978 National Survey of the American College of Surgeons*. Cancer, 1983. **51**(8): p. 1333-8.
39. Fitzgibbons, P.L., et al., *Prognostic factors in breast cancer. College of American Pathologists Consensus Statement 1999*. Arch Pathol Lab Med, 2000. **124**(7): p. 966-78.
40. Hammond, M.E., et al., *American Society of Clinical Oncology/College of American Pathologists guideline recommendations for immunohistochemical testing of estrogen and progesterone receptors in breast cancer (unabridged version)*. Arch Pathol Lab Med, 2010. **134**(7): p. e48-72.
41. Derakhshan, F. and J.S. Reis-Filho, *Pathogenesis of Triple-Negative Breast Cancer*. Annu Rev Pathol, 2022. **17**: p. 181-204.

42. Chivukula, M., et al., *Clinical importance of HER2 immunohistologic heterogeneous expression in core-needle biopsies vs resection specimens for equivocal (immunohistochemical score 2+) cases*. Mod Pathol, 2008. **21**(4): p. 363-8.
43. Calhoun, B.C. and L.C. Collins, *Predictive markers in breast cancer: An update on ER and HER2 testing and reporting*. Semin Diagn Pathol, 2015. **32**(5): p. 362-9.
44. Heldring, N., et al., *Estrogen receptors: how do they signal and what are their targets*. Physiol Rev, 2007. **87**(3): p. 905-31.
45. Klinge, C.M., *Estrogen receptor interaction with estrogen response elements*. Nucleic Acids Res, 2001. **29**(14): p. 2905-19.
46. Schiff, R., et al., *Cross-talk between estrogen receptor and growth factor pathways as a molecular target for overcoming endocrine resistance*. Clin Cancer Res, 2004. **10**(1 Pt 2): p. 331S-6S.
47. Moasser, M.M., *The oncogene HER2: its signaling and transforming functions and its role in human cancer pathogenesis*. Oncogene, 2007. **26**(45): p. 6469-87.
48. Pegram, M., C. Jackisch, and S.R.D. Johnston, *Estrogen/HER2 receptor crosstalk in breast cancer: combination therapies to improve outcomes for patients with hormone receptor-positive/HER2-positive breast cancer*. NPJ Breast Cancer, 2023. **9**(1): p. 45.
49. Baselga, J. and S.M. Swain, *Novel anticancer targets: revisiting ERBB2 and discovering ERBB3*. Nat Rev Cancer, 2009. **9**(7): p. 463-75.
50. Early Breast Cancer Trialists' Collaborative, G., et al., *Relevance of breast cancer hormone receptors and other factors to the efficacy of adjuvant tamoxifen: patient-level meta-analysis of randomised trials*. Lancet, 2011. **378**(9793): p. 771-84.
51. Smith, I.E. and M. Dowsett, *Aromatase inhibitors in breast cancer*. N Engl J Med, 2003. **348**(24): p. 2431-42.
52. Josefsson, M.L. and S.J. Leinster, *Aromatase inhibitors versus tamoxifen as adjuvant hormonal therapy for oestrogen sensitive early breast cancer in post-menopausal women: meta-analyses of monotherapy, sequenced therapy and extended therapy*. Breast, 2010. **19**(2): p. 76-83.
53. Slamon, D.J., et al., *Use of chemotherapy plus a monoclonal antibody against HER2 for metastatic breast cancer that overexpresses HER2*. N Engl J Med, 2001. **344**(11): p. 783-92.
54. Swain, S.M., et al., *Pertuzumab, trastuzumab, and docetaxel in HER2-positive metastatic breast cancer*. N Engl J Med, 2015. **372**(8): p. 724-34.
55. Verma, S., et al., *Trastuzumab emtansine for HER2-positive advanced breast cancer*. N Engl J Med, 2012. **367**(19): p. 1783-91.
56. Yang, X., et al., *Endocrine treatment mechanisms in triple-positive breast cancer: from targeted therapies to advances in precision medicine*. Front Oncol, 2024. **14**: p. 1467033.
57. Bianchini, G., et al., *Triple-negative breast cancer: challenges and opportunities of a heterogeneous disease*. Nat Rev Clin Oncol, 2016. **13**(11): p. 674-690.
58. Hartkopf, A.D., et al., *PD-1 and PD-L1 Immune Checkpoint Blockade to Treat Breast Cancer*. Breast Care (Basel), 2016. **11**(6): p. 385-390.
59. Robson, M., et al., *Olaparib for Metastatic Breast Cancer in Patients with a Germline BRCA Mutation*. N Engl J Med, 2017. **377**(6): p. 523-533.
60. Litton, J.K., et al., *Talazoparib in Patients with Advanced Breast Cancer and a Germline BRCA Mutation*. N Engl J Med, 2018. **379**(8): p. 753-763.
61. Johnson, K.S., E.F. Conant, and M.S. Soo, *Molecular Subtypes of Breast Cancer: A Review for Breast Radiologists*. J Breast Imaging, 2021. **3**(1): p. 12-24.

62. Iqbal, N. and N. Iqbal, *Human Epidermal Growth Factor Receptor 2 (HER2) in Cancers: Overexpression and Therapeutic Implications*. Mol Biol Int, 2014. **2014**: p. 852748.
63. Mercogliano, M.F., et al., *Emerging Targeted Therapies for HER2-Positive Breast Cancer*. Cancers (Basel), 2023. **15**(7).
64. Zagami, P. and L.A. Carey, *Triple negative breast cancer: Pitfalls and progress*. NPJ Breast Cancer, 2022. **8**(1): p. 95.
65. Szymiczek, A., A. Lone, and M.R. Akbari, *Molecular intrinsic versus clinical subtyping in breast cancer: A comprehensive review*. Clin Genet, 2021. **99**(5): p. 613-637.
66. Yersal, O. and S. Barutca, *Biological subtypes of breast cancer: Prognostic and therapeutic implications*. World J Clin Oncol, 2014. **5**(3): p. 412-24.
67. Godoy-Ortiz, A., et al., *Deciphering HER2 Breast Cancer Disease: Biological and Clinical Implications*. Front Oncol, 2019. **9**: p. 1124.
68. Bhutia, Y.D. and V. Ganapathy, *Glutamine transporters in mammalian cells and their functions in physiology and cancer*. Biochim Biophys Acta, 2016. **1863**(10): p. 2531-9.
69. El Ansari, R., et al., *Altered glutamine metabolism in breast cancer; subtype dependencies and alternative adaptations*. Histopathology, 2018. **72**(2): p. 183-190.
70. El Ansari, R., et al., *The amino acid transporter SLC7A5 confers a poor prognosis in the highly proliferative breast cancer subtypes and is a key therapeutic target in luminal B tumours*. Breast Cancer Res, 2018. **20**(1): p. 21.
71. Yoo, H.C., et al., *Glutamine reliance in cell metabolism*. Exp Mol Med, 2020. **52**(9): p. 1496-1516.
72. Lima, Z.S., et al., *Recent advances of therapeutic targets based on the molecular signature in breast cancer: genetic mutations and implications for current treatment paradigms*. J Hematol Oncol, 2019. **12**(1): p. 38.
73. Ferguson, L.R., et al., *Genomic instability in human cancer: Molecular insights and opportunities for therapeutic attack and prevention through diet and nutrition*. Semin Cancer Biol, 2015. **35 Suppl**(Suppl): p. S5-S24.
74. Gaillard, H., T. Garcia-Muse, and A. Aguilera, *Replication stress and cancer*. Nat Rev Cancer, 2015. **15**(5): p. 276-89.
75. Ray, P.D., B.W. Huang, and Y. Tsuji, *Reactive oxygen species (ROS) homeostasis and redox regulation in cellular signaling*. Cell Signal, 2012. **24**(5): p. 981-90.
76. Sies, H., C. Berndt, and D.P. Jones, *Oxidative Stress*. Annu Rev Biochem, 2017. **86**: p. 715-748.
77. Moloney, J.N. and T.G. Cotter, *ROS signalling in the biology of cancer*. Semin Cell Dev Biol, 2018. **80**: p. 50-64.
78. Murphy, M.P., *How mitochondria produce reactive oxygen species*. Biochem J, 2009. **417**(1): p. 1-13.
79. Wallace, D.C., *Mitochondria and cancer*. Nat Rev Cancer, 2012. **12**(10): p. 685-98.
80. Pelicano, H., et al., *Mitochondrial dysfunction in some triple-negative breast cancer cell lines: role of mTOR pathway and therapeutic potential*. Breast Cancer Res, 2014. **16**(5): p. 434.
81. Perez-Amado, C.J., et al., *Mitochondrial DNA Mutation Analysis in Breast Cancer: Shifting From Germline Heteroplasmy Toward Homoplasmy in Tumors*. Front Oncol, 2020. **10**: p. 572954.
82. Oliveira, R.C., G.C. Cavalcante, and G.B. Soares-Souza, *Exploring Aerobic Energy Metabolism in Breast Cancer: A Mutational Profile of Glycolysis and Oxidative Phosphorylation*. Int J Mol Sci, 2024. **25**(23).

83. Bukato, K., et al., *Endogenous estrogen metabolites as oxidative stress mediators and endometrial cancer biomarkers*. Cell Commun Signal, 2024. **22**(1): p. 205.
84. Samavat, H. and M.S. Kurzer, *Estrogen metabolism and breast cancer*. Cancer Lett, 2015. **356**(2 Pt A): p. 231-43.
85. Huang, R., et al., *Dual Role of Reactive Oxygen Species and their Application in Cancer Therapy*. J Cancer, 2021. **12**(18): p. 5543-5561.
86. Obi, N., et al., *Estrogen metabolite ratio: Is the 2-hydroxyestrone to 16alpha-hydroxyestrone ratio predictive for breast cancer?* Int J Womens Health, 2011. **3**: p. 37-51.
87. You, Q., et al., *Decoding the enigmatic estrogen paradox in pulmonary hypertension: delving into estrogen metabolites and metabolic enzymes*. Cell Mol Biol Lett, 2024. **29**(1): p. 155.
88. Jiang, Y., et al., *Association of sulfotransferase *SULT1A1* with breast cancer risk: a meta-analysis of case-control studies with subgroups of ethnic and menopausal status*. J Exp Clin Cancer Res, 2010. **29**(1): p. 101.
89. Ji, X.W., et al., *Intratumoral estrogen sulfotransferase induction contributes to the anti-breast cancer effects of the dithiocarbamate derivative TM208*. Acta Pharmacol Sin, 2015. **36**(10): p. 1246-55.
90. Liu, W., et al., *The Uridine diphosphate (UDP)-glycosyltransferases (UGTs) superfamily: the role in tumor cell metabolism*. Front Oncol, 2022. **12**: p. 1088458.
91. Stading, R., et al., *Molecular role of cytochrome P4501A enzymes in oxidative stress*. Curr Opin Toxicol, 2020. **20-21**: p. 77-84.
92. Luo, B., et al., *Cytochrome P450: Implications for human breast cancer*. Oncol Lett, 2021. **22**(1): p. 548.
93. Sarkar, S., et al., *Cadmium-induced lipid peroxidation and the status of the antioxidant system in rat tissues*. J Trace Elem Med Biol, 1995. **9**(3): p. 144-9.
94. Bloomfield, M. and M.C. Louie, *Chronic cadmium exposure decreases the dependency of MCF7 breast cancer cells on ERalpha*. Sci Rep, 2019. **9**(1): p. 12135.
95. Albano, E., *Alcohol, oxidative stress and free radical damage*. Proc Nutr Soc, 2006. **65**(3): p. 278-90.
96. Manna, P. and S.K. Jain, *Obesity, Oxidative Stress, Adipose Tissue Dysfunction, and the Associated Health Risks: Causes and Therapeutic Strategies*. Metab Syndr Relat Disord, 2015. **13**(10): p. 423-44.
97. Jomova, K., et al., *Reactive oxygen species, toxicity, oxidative stress, and antioxidants: chronic diseases and aging*. Arch Toxicol, 2023. **97**(10): p. 2499-2574.
98. Scoccianti, C., et al., *Female breast cancer and alcohol consumption: a review of the literature*. Am J Prev Med, 2014. **46**(3 Suppl 1): p. S16-25.
99. Glassman, I., et al., *The Role of Obesity in Breast Cancer Pathogenesis*. Cells, 2023. **12**(16).
100. Braakhuis, A.J., P. Campion, and K.S. Bishop, *Reducing Breast Cancer Recurrence: The Role of Dietary Polyphenolics*. Nutrients, 2016. **8**(9).
101. Saxena, S. and L. Zou, *Hallmarks of DNA replication stress*. Mol Cell, 2022. **82**(12): p. 2298-2314.
102. Leman, A.R. and E. Noguchi, *The replication fork: understanding the eukaryotic replication machinery and the challenges to genome duplication*. Genes (Basel), 2013. **4**(1): p. 1-32.
103. Ekundayo, B. and F. Bleichert, *Origins of DNA replication*. PLoS Genet, 2019. **15**(9): p. e1008320.
104. Chapados, B.R., et al., *Structural basis for FEN-1 substrate specificity and PCNA-mediated activation in DNA replication and repair*. Cell, 2004. **116**(1): p. 39-50.

105. Dewar, J.M. and J.C. Walter, *Mechanisms of DNA replication termination*. Nat Rev Mol Cell Biol, 2017. **18**(8): p. 507-516.
106. Primo, L.M.F. and L.K. Teixeira, *DNA replication stress: oncogenes in the spotlight*. Genet Mol Biol, 2019. **43**(1 suppl 1): p. e20190138.
107. Marechal, A. and L. Zou, *RPA-coated single-stranded DNA as a platform for post-translational modifications in the DNA damage response*. Cell Res, 2015. **25**(1): p. 9-23.
108. Gralewska, P., et al., *Participation of the ATR/CHK1 pathway in replicative stress targeted therapy of high-grade ovarian cancer*. J Hematol Oncol, 2020. **13**(1): p. 39.
109. Blanco, M.G., et al., *Functional overlap between the structure-specific nucleases Yen1 and Mus81-Mms4 for DNA-damage repair in S. cerevisiae*. DNA Repair (Amst), 2010. **9**(4): p. 394-402.
110. Lalonde, M., et al., *Consequences and Resolution of Transcription-Replication Conflicts*. Life (Basel), 2021. **11**(7).
111. Hamperl, S., et al., *Transcription-Replication Conflict Orientation Modulates R-Loop Levels and Activates Distinct DNA Damage Responses*. Cell, 2017. **170**(4): p. 774-786 e19.
112. Kim, S., et al., *ATAD5 restricts R-loop formation through PCNA unloading and RNA helicase maintenance at the replication fork*. Nucleic Acids Res, 2020. **48**(13): p. 7218-7238.
113. Gu, L., et al., *Small molecule targeting of transcription-replication conflict for selective chemotherapy*. Cell Chem Biol, 2023. **30**(10): p. 1235-1247 e6.
114. Liu, W., et al., *A Selective Small Molecule DNA2 Inhibitor for Sensitization of Human Cancer Cells to Chemotherapy*. EBioMedicine, 2016. **6**: p. 73-86.
115. Wu, H.L., et al., *Targeting nucleotide metabolism: a promising approach to enhance cancer immunotherapy*. J Hematol Oncol, 2022. **15**(1): p. 45.
116. Lv, Y., et al., *Nucleotide de novo synthesis increases breast cancer stemness and metastasis via cGMP-PKG-MAPK signaling pathway*. PLoS Biol, 2020. **18**(11): p. e3000872.
117. Chen, J., et al., *De novo nucleotide biosynthetic pathway and cancer*. Genes Dis, 2023. **10**(6): p. 2331-2338.
118. Walter, M. and P. Herr, *Re-Discovery of Pyrimidine Salvage as Target in Cancer Therapy*. Cells, 2022. **11**(4).
119. Sun, X., et al., *Metabolic Reprogramming in Triple-Negative Breast Cancer*. Front Oncol, 2020. **10**: p. 428.
120. Mullen, N.J. and P.K. Singh, *Nucleotide metabolism: a pan-cancer metabolic dependency*. Nat Rev Cancer, 2023. **23**(5): p. 275-294.
121. Roberts, C., et al., *Results of a phase II clinical trial of 6-mercaptopurine (6MP) and methotrexate in patients with BRCA-defective tumours*. Br J Cancer, 2020. **122**(4): p. 483-490.
122. Hsieh, Y. and J.J. Tseng, *Azidothymidine (AZT) Inhibits Proliferation of Human Ovarian Cancer Cells by Regulating Cell Cycle Progression*. Anticancer Res, 2020. **40**(10): p. 5517-5527.
123. Melana, S.M., J.F. Holland, and B.G. Pogo, *Inhibition of cell growth and telomerase activity of breast cancer cells in vitro by 3'-azido-3'-deoxythymidine*. Clin Cancer Res, 1998. **4**(3): p. 693-6.
124. Mattson, D.M., et al., *Cisplatin combined with zidovudine enhances cytotoxicity and oxidative stress in human head and neck cancer cells via a thiol-dependent mechanism*. Free Radic Biol Med, 2009. **46**(2): p. 232-7.

125. Savaraj, N., et al., *Overexpression of mutated MRP4 in cisplatin resistant small cell lung cancer cell line: collateral sensitivity to azidothymidine*. Int J Oncol, 2003. **23**(1): p. 173-9.
126. Brown, T., et al., *Telomerase inhibition using azidothymidine in the HT-29 colon cancer cell line*. Ann Surg Oncol, 2003. **10**(8): p. 910-5.
127. Alhmoud, J.F., et al., *DNA Damage/Repair Management in Cancers*. Cancers (Basel), 2020. **12**(4).
128. Grundy, G.J. and J.L. Parsons, *Base excision repair and its implications to cancer therapy*. Essays Biochem, 2020. **64**(5): p. 831-843.
129. Dianov, G.L. and J.L. Parsons, *Co-ordination of DNA single strand break repair*. DNA Repair (Amst), 2007. **6**(4): p. 454-60.
130. Friker, L.L., et al., *MSH2, MSH6, MLH1, and PMS2 immunohistochemistry as highly sensitive screening method for DNA mismatch repair deficiency syndromes in pediatric high-grade glioma*. Acta Neuropathol, 2025. **149**(1): p. 11.
131. Sajjadi, E., et al., *Mismatch repair-deficient hormone receptor-positive breast cancers: Biology and pathological characterization*. Cancer Cell Int, 2021. **21**(1): p. 266.
132. Marteijn, J.A., et al., *Understanding nucleotide excision repair and its roles in cancer and ageing*. Nat Rev Mol Cell Biol, 2014. **15**(7): p. 465-81.
133. Cannan, W.J. and D.S. Pederson, *Mechanisms and Consequences of Double-Strand DNA Break Formation in Chromatin*. J Cell Physiol, 2016. **231**(1): p. 3-14.
134. Mathiasen, D.P. and M. Lisby, *Cell cycle regulation of homologous recombination in Saccharomyces cerevisiae*. FEMS Microbiol Rev, 2014. **38**(2): p. 172-84.
135. Takaya, H., et al., *Homologous recombination deficiency status-based classification of high-grade serous ovarian carcinoma*. Sci Rep, 2020. **10**(1): p. 2757.
136. Rassool, F.V., *DNA double strand breaks (DSB) and non-homologous end joining (NHEJ) pathways in human leukemia*. Cancer Lett, 2003. **193**(1): p. 1-9.
137. Li, L.Y., et al., *DNA Repair Pathways in Cancer Therapy and Resistance*. Front Pharmacol, 2020. **11**: p. 629266.
138. Sobanski, T., et al., *Cell Metabolism and DNA Repair Pathways: Implications for Cancer Therapy*. Front Cell Dev Biol, 2021. **9**: p. 633305.
139. Klein, H.L., *The consequences of Rad51 overexpression for normal and tumor cells*. DNA Repair (Amst), 2008. **7**(5): p. 686-93.
140. Yin, L., et al., *Triple-negative breast cancer molecular subtyping and treatment progress*. Breast Cancer Res, 2020. **22**(1): p. 61.
141. Malfatti, M.C., et al., *Revisiting Two Decades of Research Focused on Targeting APE1 for Cancer Therapy: The Pros and Cons*. Cells, 2023. **12**(14).
142. Malfatti, M.C., et al., *APE1 and NPM1 protect cancer cells from platinum compounds cytotoxicity and their expression pattern has a prognostic value in TNBC*. J Exp Clin Cancer Res, 2019. **38**(1): p. 309.
143. Ma, X., et al., *Downregulation of APE1 potentiates breast cancer cells to olaparib by inhibiting PARP-1 expression*. Breast Cancer Res Treat, 2019. **176**(1): p. 109-117.
144. Ossovskaya, V., et al., *Upregulation of Poly (ADP-Ribose) Polymerase-1 (PARP1) in Triple-Negative Breast Cancer and Other Primary Human Tumor Types*. Genes Cancer, 2010. **1**(8): p. 812-21.
145. Quan, C., et al., *Upregulated PARP1 confers breast cancer resistance to CDK4/6 inhibitors via YB-1 phosphorylation*. Exp Hematol Oncol, 2023. **12**(1): p. 100.
146. Li, J., et al., *DNA damage response in breast cancer and its significant role in guiding novel precise therapies*. Biomark Res, 2024. **12**(1): p. 111.

147. Xie, T., et al., *Targeting Homologous Recombination Deficiency in Ovarian Cancer with PARP Inhibitors: Synthetic Lethal Strategies That Impact Overall Survival*. *Cancers (Basel)*, 2022. **14**(19).
148. Janysek, D.C., et al., *Clinical use and mechanisms of resistance for PARP inhibitors in homologous recombination-deficient cancers*. *Transl Oncol*, 2021. **14**(3): p. 101012.
149. Narayan, S., et al., *Interaction between APC and Fen1 during breast carcinogenesis*. *DNA Repair (Amst)*, 2016. **41**: p. 54-62.
150. Schultz-Norton, J.R., Y.S. Ziegler, and A.M. Nardulli, *ERalpha-associated protein networks*. *Trends Endocrinol Metab*, 2011. **22**(4): p. 124-9.
151. Abdel-Fatah, T.M., et al., *Genomic and protein expression analysis reveals flap endonuclease 1 (FEN1) as a key biomarker in breast and ovarian cancer*. *Mol Oncol*, 2014. **8**(7): p. 1326-38.
152. Saito, Y., et al., *LLGL2 rescues nutrient stress by promoting leucine uptake in ER(+) breast cancer*. *Nature*, 2019. **569**(7755): p. 275-279.
153. Saito, Y. and T. Soga, *Amino acid transporters as emerging therapeutic targets in cancer*. *Cancer Sci*, 2021. **112**(8): p. 2958-2965.
154. Mossmann, D., S. Park, and M.N. Hall, *mTOR signalling and cellular metabolism are mutual determinants in cancer*. *Nat Rev Cancer*, 2018. **18**(12): p. 744-757.
155. Curtis, C., et al., *The genomic and transcriptomic architecture of 2,000 breast tumours reveals novel subgroups*. *Nature*, 2012. **486**(7403): p. 346-52.
156. Jezequel, P., et al., *bc-GenExMiner 3.0: new mining module computes breast cancer gene expression correlation analyses*. *Database (Oxford)*, 2013. **2013**: p. bas060.
157. Gyorffy, B., *Survival analysis across the entire transcriptome identifies biomarkers with the highest prognostic power in breast cancer*. *Comput Struct Biotechnol J*, 2021. **19**: p. 4101-4109.
158. Abd El-Rehim, D.M., et al., *High-throughput protein expression analysis using tissue microarray technology of a large well-characterised series identifies biologically distinct classes of breast cancer confirming recent cDNA expression analyses*. *Int J Cancer*, 2005. **116**(3): p. 340-50.
159. Kao, J., et al., *Molecular profiling of breast cancer cell lines defines relevant tumor models and provides a resource for cancer gene discovery*. *PLoS One*, 2009. **4**(7): p. e6146.
160. Dai, X., et al., *Breast Cancer Cell Line Classification and Its Relevance with Breast Tumor Subtyping*. *J Cancer*, 2017. **8**(16): p. 3131-3141.
161. Yang, W.H., et al., *Enhancing the Efficacy of Glutamine Metabolism Inhibitors in Cancer Therapy*. *Trends Cancer*, 2021. **7**(8): p. 790-804.
162. Dong, Y., et al., *Regulation of cancer cell metabolism: oncogenic MYC in the driver's seat*. *Signal Transduct Target Ther*, 2020. **5**(1): p. 124.
163. Turgeon, M.O., N.J.S. Perry, and G. Poulogiannis, *DNA Damage, Repair, and Cancer Metabolism*. *Front Oncol*, 2018. **8**: p. 15.
164. Li, Y., et al., *SLC7A5 serves as a prognostic factor of breast cancer and promotes cell proliferation through activating AKT/mTORC1 signaling pathway*. *Ann Transl Med*, 2021. **9**(10): p. 892.
165. Ichinoe, M., et al., *Prognostic values of L-type amino acid transporter 1 and CD98hc expression in breast cancer*. *J Clin Pathol*, 2021. **74**(9): p. 589-595.
166. Zeng, X., et al., *FEN1 knockdown improves trastuzumab sensitivity in human epidermal growth factor 2-positive breast cancer cells*. *Exp Ther Med*, 2017. **14**(4): p. 3265-3272.

167. Shindo, H., et al., *Targeting Amino Acid Metabolic Reprogramming via L-Type Amino Acid Transporter 1 (LAT1) for Endocrine-Resistant Breast Cancer*. *Cancers* (Basel), 2021. **13**(17).
168. Kaira, K., et al., *Expression of amino acid transporter (LAT1 and 4F2hc) in pulmonary pleomorphic carcinoma*. *Hum Pathol*, 2019. **84**: p. 142-149.
169. Ohshima, Y., et al., *Efficacy of system l amino acid transporter 1 inhibition as a therapeutic target in esophageal squamous cell carcinoma*. *Cancer Sci*, 2016. **107**(10): p. 1499-1505.
170. Altan, B., et al., *Relationship between LAT1 expression and resistance to chemotherapy in pancreatic ductal adenocarcinoma*. *Cancer Chemother Pharmacol*, 2018. **81**(1): p. 141-153.
171. Kurozumi, S., et al., *Association of L-type amino acid transporter 1 (LAT1) with the immune system and prognosis in invasive breast cancer*. *Sci Rep*, 2022. **12**(1): p. 2742.
172. Canhasi, L., E. Tina, and A.G. Eremo, *Hypoxia-mimetic by CoCl₂ increases SLC7A5 expression in breast cancer cells in vitro*. *BMC Res Notes*, 2023. **16**(1): p. 366.
173. Wang, Q., et al., *Targeting glutamine transport to suppress melanoma cell growth*. *Int J Cancer*, 2014. **135**(5): p. 1060-71.
174. Shi, L., et al., *Downregulation of L-type amino acid transporter 1 expression inhibits the growth, migration and invasion of gastric cancer cells*. *Oncol Lett*, 2013. **6**(1): p. 106-112.
175. Zhang, C., et al., *SLC7A5 correlated with malignancies and immunotherapy response in bladder cancer*. *Cancer Cell Int*, 2024. **24**(1): p. 182.
176. Nikolova, T., M. Christmann, and B. Kaina, *FEN1 is overexpressed in testis, lung and brain tumors*. *Anticancer Res*, 2009. **29**(7): p. 2453-9.
177. Xie, W., et al., *Androgen receptor knockdown enhances prostate cancer chemosensitivity by down-regulating FEN1 through the ERK/ELK1 signalling pathway*. *Cancer Med*, 2023. **12**(14): p. 15317-15336.
178. Al-Kawaz, A., et al., *The prognostic significance of Flap Endonuclease 1 (FEN1) in breast ductal carcinoma in situ*. *Breast Cancer Res Treat*, 2021. **188**(1): p. 53-63.
179. Wang, S., et al., *Down-regulation of DNA key protein-FEN1 inhibits OSCC growth by affecting immunosuppressive phenotypes via IFN-gamma/JAK/STAT-1*. *Int J Oral Sci*, 2023. **15**(1): p. 17.
180. He, L., et al., *FEN1 promotes tumor progression and confers cisplatin resistance in non-small-cell lung cancer*. *Mol Oncol*, 2017. **11**(9): p. 1302-1303.
181. Kauanova, S., A. Urazbayev, and I. Vorobjev, *The Frequent Sampling of Wound Scratch Assay Reveals the "Opportunity" Window for Quantitative Evaluation of Cell Motility-Impeding Drugs*. *Front Cell Dev Biol*, 2021. **9**: p. 640972.
182. Elmore, S., *Apoptosis: a review of programmed cell death*. *Toxicol Pathol*, 2007. **35**(4): p. 495-516.
183. Vermes, I., et al., *A novel assay for apoptosis. Flow cytometric detection of phosphatidylserine expression on early apoptotic cells using fluorescein labelled Annexin V*. *J Immunol Methods*, 1995. **184**(1): p. 39-51.
184. Najumudeen, A.K., et al., *The amino acid transporter SLC7A5 is required for efficient growth of KRAS-mutant colorectal cancer*. *Nat Genet*, 2021. **53**(1): p. 16-26.
185. Tang, S., Q. Liu, and M. Xu, *LINC00857 promotes cell proliferation and migration in colorectal cancer by interacting with YTHDC1 and stabilizing SLC7A5*. *Oncol Lett*, 2021. **22**(2): p. 578.

186. Yuwei, X., et al., *FEN1 promotes cancer progression of cholangiocarcinoma by regulating the Wnt/beta-catenin signaling pathway*. *Dig Liver Dis*, 2024. **56**(4): p. 695-704.
187. Wang, R., et al., *FEN1 Promotes Hepatocellular Carcinoma Progression by Activating Cell Cycle Transition from G2 To M Phase*. *J Cancer*, 2024. **15**(4): p. 981-989.
188. Jia, D., et al., *ZNF24 regulates the progression of KRAS mutant lung adenocarcinoma by promoting SLC7A5 translation*. *Front Oncol*, 2022. **12**: p. 1043177.
189. Shi, Z., et al., *Inhibition of cancer-type amino acid transporter LAT1 suppresses B16-F10 melanoma metastasis in mouse models*. *Sci Rep*, 2023. **13**(1): p. 13943.
190. Quan, L., et al., *Amino acid transporter LAT1 in tumor-associated vascular endothelium promotes angiogenesis by regulating cell proliferation and VEGF-A-dependent mTORC1 activation*. *J Exp Clin Cancer Res*, 2020. **39**(1): p. 266.
191. Zhou, X., et al., *Inhibition of amino acid transporter LAT1 in cancer cells suppresses G0/G1-S transition by downregulating cyclin D1 via p38 MAPK activation*. *J Pharmacol Sci*, 2024. **154**(3): p. 182-191.
192. Yothaisong, S., et al., *Inhibition of l-type amino acid transporter 1 activity as a new therapeutic target for cholangiocarcinoma treatment*. *Tumour Biol*, 2017. **39**(3): p. 1010428317694545.
193. Peng, C., et al., *Cyclin-dependent kinase 2 (CDK2) is a key mediator for EGF-induced cell transformation mediated through the ELK4/c-Fos signaling pathway*. *Oncogene*, 2016. **35**(9): p. 1170-9.
194. Hou, W., J. Chen, and Y. Wang, *MRPL35 Induces Proliferation, Invasion, and Glutamine Metabolism in NSCLC Cells by Upregulating SLC7A5 Expression*. *Clin Respir J*, 2024. **18**(7): p. e13799.
195. Mesquita, K.A., et al., *FEN1 Blockade for Platinum Chemo-Sensitization and Synthetic Lethality in Epithelial Ovarian Cancers*. *Cancers (Basel)*, 2021. **13**(8).
196. de la Cruz Lopez, K.G., et al., *mTORC1 as a Regulator of Mitochondrial Functions and a Therapeutic Target in Cancer*. *Front Oncol*, 2019. **9**: p. 1373.
197. Popova, N.V. and M. Jucker, *The Role of mTOR Signaling as a Therapeutic Target in Cancer*. *Int J Mol Sci*, 2021. **22**(4).
198. Beaudry, A.G. and M.L. Law, *Leucine Supplementation in Cancer Cachexia: Mechanisms and a Review of the Pre-Clinical Literature*. *Nutrients*, 2022. **14**(14).
199. Zhang, J., et al., *Requirement for flap endonuclease 1 (FEN1) to maintain genomic stability and transcriptional gene silencing in Arabidopsis*. *Plant J*, 2016. **87**(6): p. 629-40.
200. Mencialha, A., et al., *Mapping oxidative changes in breast cancer: understanding the basic to reach the clinics*. *Anticancer Res*, 2014. **34**(3): p. 1127-40.
201. Liu, P., et al., *Removal of oxidative DNA damage via FEN1-dependent long-patch base excision repair in human cell mitochondria*. *Mol Cell Biol*, 2008. **28**(16): p. 4975-87.
202. Didusch, S., et al., *amica: an interactive and user-friendly web-platform for the analysis of proteomics data*. *BMC Genomics*, 2022. **23**(1): p. 817.
203. Heberle, H., et al., *InteractiVenn: a web-based tool for the analysis of sets through Venn diagrams*. *BMC Bioinformatics*, 2015. **16**(1): p. 169.
204. Szklarczyk, D., et al., *STRING v11: protein-protein association networks with increased coverage, supporting functional discovery in genome-wide experimental datasets*. *Nucleic Acids Res*, 2019. **47**(D1): p. D607-D613.
205. Xie, Z., et al., *Gene Set Knowledge Discovery with Enrichr*. *Curr Protoc*, 2021. **1**(3): p. e90.

206. Ben-Sahra, I., et al., *mTORC1 induces purine synthesis through control of the mitochondrial tetrahydrofolate cycle*. *Science*, 2016. **351**(6274): p. 728-733.
207. Fukano, M., M. Park, and G. Deblois, *Metabolic Flexibility Is a Determinant of Breast Cancer Heterogeneity and Progression*. *Cancers (Basel)*, 2021. **13**(18).
208. Xu, L., et al., *FEN1 is a prognostic biomarker for ER+ breast cancer and associated with tamoxifen resistance through the ERalpha/cyclin D1/Rb axis*. *Ann Transl Med*, 2021. **9**(3): p. 258.
209. Flach, K.D., et al., *Endonuclease FEN1 Coregulates ERalpha Activity and Provides a Novel Drug Interface in Tamoxifen-Resistant Breast Cancer*. *Cancer Res*, 2020. **80**(10): p. 1914-1926.
210. Tornroos, R., E. Tina, and A. Gothlin Eremo, *SLC7A5 is linked to increased expression of genes related to proliferation and hypoxia in estrogen-receptor-positive breast cancer*. *Oncol Rep*, 2022. **47**(1).
211. Saxton, R.A., et al., *Mechanism of arginine sensing by CASTOR1 upstream of mTORC1*. *Nature*, 2016. **536**(7615): p. 229-33.
212. Morita, M., et al., *mTORC1 controls mitochondrial activity and biogenesis through 4E-BP-dependent translational regulation*. *Cell Metab*, 2013. **18**(5): p. 698-711.
213. Sarmiento-Salinas, F.L., et al., *Breast Cancer Subtypes Present a Differential Production of Reactive Oxygen Species (ROS) and Susceptibility to Antioxidant Treatment*. *Front Oncol*, 2019. **9**: p. 480.
214. Adinew, G.M., et al., *Anticancer Effects of Thymoquinone through the Antioxidant Activity, Upregulation of Nrf2, and Downregulation of PD-L1 in Triple-Negative Breast Cancer Cells*. *Nutrients*, 2022. **14**(22).
215. Beatty, A., et al., *Metabolite Profiling Reveals the Glutathione Biosynthetic Pathway as a Therapeutic Target in Triple-Negative Breast Cancer*. *Mol Cancer Ther*, 2018. **17**(1): p. 264-275.
216. Qin, S., et al., *Nrf2 inhibition sensitizes breast cancer stem cells to ionizing radiation via suppressing DNA repair*. *Free Radic Biol Med*, 2021. **169**: p. 238-247.
217. Feng, J., et al., *Emerging roles and the regulation of aerobic glycolysis in hepatocellular carcinoma*. *J Exp Clin Cancer Res*, 2020. **39**(1): p. 126.
218. Beaver, J.A., et al., *PIK3CA and AKT1 mutations have distinct effects on sensitivity to targeted pathway inhibitors in an isogenic luminal breast cancer model system*. *Clin Cancer Res*, 2013. **19**(19): p. 5413-22.
219. Pascual, J. and N.C. Turner, *Targeting the PI3-kinase pathway in triple-negative breast cancer*. *Ann Oncol*, 2019. **30**(7): p. 1051-1060.
220. Fu, V., T. Moroishi, and K.L. Guan, *Glycolitics Anonymous: Cancer Sobers Up with mTORC1*. *Cancer Cell*, 2016. **29**(4): p. 432-434.
221. Sulaiman, A., et al., *Co-inhibition of mTORC1, HDAC and ESR1alpha retards the growth of triple-negative breast cancer and suppresses cancer stem cells*. *Cell Death Dis*, 2018. **9**(8): p. 815.
222. Lee, H., et al., *Energy-stress-mediated AMPK activation inhibits ferroptosis*. *Nat Cell Biol*, 2020. **22**(2): p. 225-234.
223. Gounou, C., et al., *Inhibition of the membrane repair protein annexin-A2 prevents tumor invasion and metastasis*. *Cell Mol Life Sci*, 2023. **81**(1): p. 7.
224. Wang, Y., et al., *TIM-4 orchestrates mitochondrial homeostasis to promote lung cancer progression via ANXA2/PI3K/AKT/OPAI axis*. *Cell Death Dis*, 2023. **14**(2): p. 141.
225. Lee, H., et al., *The short variant of optic atrophy 1 (OPAI) improves cell survival under oxidative stress*. *J Biol Chem*, 2020. **295**(19): p. 6543-6560.

226. Thangadurai, S., et al., *CTP synthase: the hissing of the cellular serpent*. *Histochem Cell Biol*, 2022. **158**(6): p. 517-534.
227. Durand, R., et al., *Selective pharmacologic targeting of CTPS1 shows single-agent activity and synergizes with BCL2 inhibition in aggressive mantle cell lymphoma*. *Haematologica*, 2024. **109**(8): p. 2574-2584.
228. Ranganathan, R., et al., *Recent developments in the role of DNA damage response and understanding its implications for new therapeutic approaches in Alzheimer's disease*. *Translational Medicine of Aging*, 2023. **7**: p. 52-65.
229. Liu, Q., et al., *X-ray cross-complementing family: the bridge linking DNA damage repair and cancer*. *J Transl Med*, 2023. **21**(1): p. 602.
230. Liang, W., et al., *Exploring the relationship between abnormally high expression of NUP205 and the clinicopathological characteristics, immune microenvironment, and prognostic value of lower-grade glioma*. *Front Oncol*, 2023. **13**: p. 1007198.
231. Sakuma, S., et al., *Inhibition of Nuclear Pore Complex Formation Selectively Induces Cancer Cell Death*. *Cancer Discov*, 2021. **11**(1): p. 176-193.
232. Fumagalli, S. and M. Pende, *S6 kinase 1 at the central node of cell size and ageing*. *Front Cell Dev Biol*, 2022. **10**: p. 949196.
233. Wanders, R.J., et al., *Measurement of dihydroxyacetone-phosphate acyltransferase (DHAPAT) in chorionic villous samples, blood cells and cultured cells*. *J Inherit Metab Dis*, 1995. **18 Suppl 1**: p. 90-100.
234. Orozco, J.M., et al., *Dihydroxyacetone phosphate signals glucose availability to mTORC1*. *Nat Metab*, 2020. **2**(9): p. 893-901.
235. Jourdain, A.A., et al., *The FASTK family of proteins: emerging regulators of mitochondrial RNA biology*. *Nucleic Acids Res*, 2017. **45**(19): p. 10941-10947.
236. Magraner-Pardo, L., et al., *Systematic Analysis of FASTK Gene Family Alterations in Cancer*. *Int J Mol Sci*, 2021. **22**(21).
237. Ohkubo, A., et al., *The FASTK family proteins fine-tune mitochondrial RNA processing*. *PLoS Genet*, 2021. **17**(11): p. e1009873.
238. Gallo, M., et al., *Metabolic Profiling of Breast Cancer Cell Lines: Unique and Shared Metabolites*. *Int J Mol Sci*, 2025. **26**(3).
239. Baretta, M. and D.T. Le, *DNA mismatch repair in cancer*. *Pharmacol Ther*, 2018. **189**: p. 45-62.
240. Kasi, P.M., *Mutational burden on circulating cell-free tumor-DNA testing as a surrogate marker of mismatch repair deficiency or microsatellite instability in patients with colorectal cancers*. *J Gastrointest Oncol*, 2017. **8**(4): p. 747-748.
241. Backes, F.J., et al., *Mismatch repair deficiency identifies patients with high-intermediate-risk (HIR) endometrioid endometrial cancer at the highest risk of recurrence: A prognostic biomarker*. *Cancer*, 2019. **125**(3): p. 398-405.
242. Kim, H., et al., *Sporadic and Lynch syndrome-associated mismatch repair-deficient brain tumors*. *Lab Invest*, 2022. **102**(2): p. 160-171.
243. Liu, J. and J. Zhang, *Elevated EXO1 expression is associated with breast carcinogenesis and poor prognosis*. *Ann Transl Med*, 2021. **9**(2): p. 135.
244. Kang, T.H., *DNA Damage, Repair, and Cancer Metabolism*. *Int J Mol Sci*, 2023. **24**(22).
245. Kozonoe, M.M., et al., *Mismatch repair deficiency in bilateral breast cancer*. *Surgical and Experimental Pathology*, 2024. **7**(1): p. 13.
246. Conde, J., et al., *Association of common variants in mismatch repair genes and breast cancer susceptibility: a multigene study*. *BMC Cancer*, 2009. **9**: p. 344.
247. Modhukur, V., et al., *MethSurv: a web tool to perform multivariable survival analysis using DNA methylation data*. *Epigenomics*, 2018. **10**(3): p. 277-288.

248. Chandrashekar, D.S., et al., *UALCAN: A Portal for Facilitating Tumor Subgroup Gene Expression and Survival Analyses*. *Neoplasia*, 2017. **19**(8): p. 649-658.
249. Li, T., et al., *TIMER: A Web Server for Comprehensive Analysis of Tumor-Infiltrating Immune Cells*. *Cancer Res*, 2017. **77**(21): p. e108-e110.
250. Zhou, C.S., et al., *Exonuclease 1 (EXO1) is a Potential Prognostic Biomarker and Correlates with Immune Infiltrates in Lung Adenocarcinoma*. *Onco Targets Ther*, 2021. **14**: p. 1033-1048.
251. Kahli, M., et al., *Processing of eukaryotic Okazaki fragments by redundant nucleases can be uncoupled from ongoing DNA replication in vivo*. *Nucleic Acids Res*, 2019. **47**(4): p. 1814-1822.
252. Qi, L., et al., *Significant prognostic values of differentially expressed-aberrantly methylated hub genes in breast cancer*. *J Cancer*, 2019. **10**(26): p. 6618-6634.
253. Inwald, E.C., et al., *Ki-67 is a prognostic parameter in breast cancer patients: results of a large population-based cohort of a cancer registry*. *Breast Cancer Res Treat*, 2013. **139**(2): p. 539-52.
254. Muthuswami, M., et al., *Breast tumors with elevated expression of 1q candidate genes confer poor clinical outcome and sensitivity to Ras/PI3K inhibition*. *PLoS One*, 2013. **8**(10): p. e77553.
255. Green, A.R., et al., *MYC functions are specific in biological subtypes of breast cancer and confers resistance to endocrine therapy in luminal tumours*. *Br J Cancer*, 2016. **114**(8): p. 917-28.
256. Mahauad-Fernandez, W.D. and D.W. Felsher, *The Myc and Ras Partnership in Cancer: Indistinguishable Alliance or Contextual Relationship?* *Cancer Res*, 2020. **80**(18): p. 3799-3802.
257. Hoxhaj, G. and B.D. Manning, *The PI3K-AKT network at the interface of oncogenic signalling and cancer metabolism*. *Nat Rev Cancer*, 2020. **20**(2): p. 74-88.
258. Lamm, N., S. Rogers, and A.J. Cesare, *The mTOR pathway: Implications for DNA replication*. *Prog Biophys Mol Biol*, 2019. **147**: p. 17-25.
259. Perou, C.M., et al., *Molecular portraits of human breast tumours*. *Nature*, 2000. **406**(6797): p. 747-52.
260. Pavlova, N.N. and C.B. Thompson, *The Emerging Hallmarks of Cancer Metabolism*. *Cell Metab*, 2016. **23**(1): p. 27-47.
261. Saxton, R.A. and D.M. Sabatini, *mTOR Signaling in Growth, Metabolism, and Disease*. *Cell*, 2017. **169**(2): p. 361-371.
262. Rahman, M.R., R. Kawasumi, and K. Hirota, *The flap endonuclease-1 mediated maturation of Okazaki fragments is critical for the cellular tolerance to remdesivir*. *DNA Repair (Amst)*, 2024. **144**: p. 103773.
263. Keijzers, G., et al., *Human Exonuclease 1 (EXO1) Regulatory Functions in DNA Replication with Putative Roles in Cancer*. *Int J Mol Sci*, 2018. **20**(1).
264. Vallur, A.C. and N. Maizels, *Distinct activities of exonuclease 1 and flap endonuclease 1 at telomeric g4 DNA*. *PLoS One*, 2010. **5**(1): p. e8908.
265. Ma, L., et al., *Structure-specific nucleases: role in Okazaki fragment maturation*. *Trends Genet*, 2022. **38**(8): p. 793-796.
266. Branchi, V., et al., *Expression of the large amino acid transporter SLC7A5/LAT1 on immune cells is enhanced in primary sclerosing cholangitis-associated cholangiocarcinoma and correlates with poor prognosis in cholangiocarcinoma*. *Hum Pathol*, 2024. **153**: p. 105670.
267. Liu, Y., et al., *SLC7A5 is a lung adenocarcinoma-specific prognostic biomarker and participates in forming immunosuppressive tumor microenvironment*. *Heliyon*, 2022. **8**(10): p. e10866.

268. Zhao, E., C. Zhou, and S. Chen, *Flap endonuclease 1 (FEN1) as a novel diagnostic and prognostic biomarker for gastric cancer*. Clin Res Hepatol Gastroenterol, 2021. **45**(1): p. 101455.
269. Zhang, K., et al., *Overexpression of Flap Endonuclease 1 Correlates with Enhanced Proliferation and Poor Prognosis of Non-Small-Cell Lung Cancer*. Am J Pathol, 2018. **188**(1): p. 242-251.
270. Zhong, G., et al., *The Clinical Significance of the Expression of FEN1 in Primary Osteosarcoma*. Int J Gen Med, 2021. **14**: p. 6477-6485.
271. Mahboubi, S., et al., *Flap endonuclease 1 (FEN1) biomarker as a new diagnostic target for the biosensing of cancer*. Sensors and Actuators Reports, 2025. **9**: p. 100270.
272. Wu, M., et al., *Identification of Flap Endonuclease 1 With Diagnostic and Prognostic Value in Breast Cancer*. Front Oncol, 2021. **11**: p. 603114.
273. Bian, S., et al., *Flap endonuclease 1 Facilitated Hepatocellular Carcinoma Progression by Enhancing USP7/MDM2-mediated P53 Inactivation*. Int J Biol Sci, 2022. **18**(3): p. 1022-1038.
274. Mason, E.F. and J.C. Rathmell, *Cell metabolism: an essential link between cell growth and apoptosis*. Biochim Biophys Acta, 2011. **1813**(4): p. 645-54.
275. An, X., et al., *Oxidative cell death in cancer: mechanisms and therapeutic opportunities*. Cell Death Dis, 2024. **15**(8): p. 556.
276. Zheng, L., et al., *Polyploid cells rewire DNA damage response networks to overcome replication stress-induced barriers for tumour progression*. Nat Commun, 2012. **3**: p. 815.
277. Poncet, N., et al., *Wnt regulates amino acid transporter Slc7a5 and so constrains the integrated stress response in mouse embryos*. EMBO Rep, 2020. **21**(1): p. e48469.
278. Liu, Y., A. Beyer, and R. Aebersold, *On the Dependency of Cellular Protein Levels on mRNA Abundance*. Cell, 2016. **165**(3): p. 535-50.
279. Quail, D.F. and J.A. Joyce, *Microenvironmental regulation of tumor progression and metastasis*. Nat Med, 2013. **19**(11): p. 1423-37.
280. Vogel, C. and E.M. Marcotte, *Insights into the regulation of protein abundance from proteomic and transcriptomic analyses*. Nat Rev Genet, 2012. **13**(4): p. 227-32.
281. Stipp, M.C. and A. Acco, *c-Myc-targeted therapy in breast cancer: A review of fundamentals and pharmacological Insights*. Gene, 2025. **941**: p. 149209.
282. Yue, M., et al., *Oncogenic MYC Activates a Feedforward Regulatory Loop Promoting Essential Amino Acid Metabolism and Tumorigenesis*. Cell Rep, 2017. **21**(13): p. 3819-3832.
283. Nachev, M., et al., *Targeting SLC1A5 and SLC3A2/SLC7A5 as a Potential Strategy to Strengthen Anti-Tumor Immunity in the Tumor Microenvironment*. Front Immunol, 2021. **12**: p. 624324.
284. Ben-Sahra, I. and B.D. Manning, *mTORC1 signaling and the metabolic control of cell growth*. Curr Opin Cell Biol, 2017. **45**: p. 72-82.